GENETICALLY-ENCODED PHOTOSWITCHES FOR CONTROLLING APOPTOSIS

Dilruba Meah

A Thesis Submitted to
Cardiff University
for the Degree of
DOCTOR OF PHILOSOPHY

School of Chemistry
Cardiff University
February 2015

DECLARATION

This work has not been submitted in substance for any other degree or award at this or any other university or place of learning, nor is being submitted concurrently in candidature for any degree or other award.

Signed …… (candidate) Date: 24/02/15

STATEMENT 1

This thesis is being submitted in partial fulfillment of the requirements for the degree of PhD

Signed …… (candidate) Date: 24/02/15

STATEMENT 2

This thesis is the result of my own independent work/investigation, except where otherwise stated.
Other sources are acknowledged by explicit references. The views expressed are my own.

Signed …… (candidate) Date: 24/02/15

STATEMENT 3

I hereby give consent for my thesis, if accepted, to be available online in the University's Open Access repository and for inter-library loan, and for the title and summary to be made available to outside organisations.

Signed …… (candidate) Date: 24/02/15

STATEMENT 4: PREVIOUSLY APPROVED BAR ON ACCESS

I hereby give consent for my thesis, if accepted, to be available online in the University's Open Access repository and for inter-library loans **after expiry of a bar on access previously approved by the Academic Standards & Quality Committee.**

Signed …… (candidate) Date: 24/02/15

Acknowledgements

I would like to thank my supervisor, Prof. Rudolf Allemann for giving me the opportunity to join his group and work on this interesting project. I wish to express my sincere gratitude to Dr. Robert Mart for his excellent scientific guidance, assistance and proof reading of this thesis. I thank Prof. Gerald Richter, Dr. Mahmoud Akhtar, Dr. Thomas Fricke, Dr. Veronica Gonzalez, Dr. Amang Li, Dr. Piotr Wysoczanski, Dr. Joel Loveridge, Dr. Enas Behiry, Dr. Mihaela Dorin, Dr. Rebecca Salter and Dr. Andrew Wood for their helpful discussions and advice. Special thanks go to all the members of the Allemann group especially, Zulfa Yoosuf Aly and Dr. Seni Chanapai for their friendship and support throughout the good and bad times.

I wish to share this work with my siblings and my parents who have been the foundation throughout my life and long studies. Finally, I can't thank my husband Mohammed Rizwan Shams enough for his patience and support. I couldn't have written this thesis and completed my studies without your encouragement.

Abstract

Light-Oxygen-Voltage (LOV) domains are flavoproteins that are part of photoreceptors found in plants, prokaryotes and algae. LOV domains act as biological switches in response sensors to oxygen, redox potential or light, making them ideal for use as an optogenetics tool. The protein-switch is activated by formation of a covalent adduct between the flavin cofactor and an internal cysteine residue, causing changes in the hydrogen bonding network in the core of the protein. This results in a conformational change in the LOV domain leading to undocking of an amphiphilic helix that is generally coupled to a catalytic or transcriptional activation domain.

In this investigation the LOV2 domain of phototropin 1 from *Avena sativa* has been modified to control protein-protein interactions in apoptosis by incorporating the Bcl homology region 3 (BH3) of a key pro-apoptotic protein (Bid) to the mobile helix of *As*LOV2 (Jα). The design, cloning, production and structure of these hybrid proteins (*As*LOV-Bid1-4) are discussed and their photo-switching characteristics are examined using UV/Vis and CD spectroscopy. Half-lives of the proteins varied between 13 min and 7.5 min, with small deviation between UV/Vis and CD half-life measurements for each protein. A further investigation on the binding of *As*LOV2-Bid proteins to Bcl-xL, the natural binding partner of Bid, has been conducted in the dark and light states using fluorescence anisotropy measurements. The results verified that *As*LOV-Bid1-4 bound to Bcl-xL effectively in the light state with K_D values at less than 300 nM. However, *As*LOV-Bid2 also bound in the dark state with K_D at 1 mM.

A second LOV domain, YtvA from *Bacillus subtilis* is characterised using UV/Vis and CD spectroscopy. YtvA is a homodimeric photo-switch, with a longer relaxation half-life than *Avena sativa* LOV2, making it more suitable for use as an optogenetics tool. Here, investigations on amino acid residues key for the dimerisation of this protein were performed, before any hybrid proteins could be engineered. Residues V27 and I113, were replaced with aspartate residues by site-directed mutagenesis to explore the effects on the protein quaternary structure using size-exclusion chromatography. Comparing against standards mutant I113D is considered as monomeric, however further experiments need to be conducted to verify this.

Contents

List of Figures

List of tables

Abbreviations

AIF	Apoptosis inducing factor
Apaf1	Apoptosis protease activating factor
APS	Ammonium persulfate
As	*Avena sativa*
At	*Arabidopsis thaliana*
ATP	Adenosine triphosphate
ADP	Adenosine diphosphate
Bak	Bcl-2 homology antagonist/killer
Bcl-2	B-cell lymphoma-2
Bcl-x_L	B-cell lymphoma extra large
Bid	BH3 interacting domain death antagonist
BME	Beta-mercaptoethanol
Boc	t-butoxycarbonyl
Bp	Base pair
Bs	*Bacillus subtilis*
CARD	Caspase recruitment domain
CD	Circular dichroism
Chl	Chlorophyll
Cyt	Cytochrome
dATP	Deoxyadenosine triphosphate

dCTP	Deoxycytosine triphosphate
DCM	Dichloromethane
DD	Death domain
DED	Death effector domain
DEPC	Diethylpyrocarbonate
dGTP	Deoxyguanosine triphosphate
DIABLO	Direct IAP binding protein of low pI
DIEA	Diisopropylethylamine
DIPCDI	*N,N*-diisopropylcarbodiimide
DISC	Death inducing signalling complex
DMF	*N,N*-dimethylformamide
DMSO	Dimethylsulfoxide
DNA	deoxyribonucleic acid
DTT	Dithiothreitol
dTTP	deoxythymidine triphosphate
EDTA	ethylenediaminetetraacetic acid
ESI MS	Electrospray ionisation mass spectrometry
FAD	Flavin adenine dinucleotide
FAM	Carboxyfluorescein
FMN	Flavin mononucleotide
Fmoc	9-Fluorenylmethoxycarbonyl
FPLC	Fast protein liquid chromatography

HBTU	2-(1H-benzotriazole-1-yl)-1-piperazineethanesulfonic acid
HEPES	4-(2-hydroxyethyl)-1,1,3,3-tetramethyluronium
HPLC	High pressure liquid chromatography
HoBt	N-hydroxybenzotriazole
IAP	Inhibitor of apoptosis protein
ISC	Intersystem crossing
IPTG	Isopropyl-β-D-thiogalactopyranoside
ICT	Isothermal titration calorimetry
K_D	Dissociation constant
Kbp	Kilo base pair
LB	Luria-Bertani
LOV	Light-oxygen-voltage
MALDI	Matrix-assisted laser desorption/ionisation
MS	Mass spectrometry
MOMP	Mitochondrial outer membrane permeabilisation
MRE	Mean residue ellipticity
MWCO	Molecular weight cut off
NADP(H)	Nicotinamide adenine dinucleotide phosphate
NMR	Nuclear magnetic resonance
OD	Optical density
PAGE	Polyacrylamide gel electrophoresis
PBS	Phosphate buffer saline

PC	Plastocyanin
Phot	Phototropin
PMSF	Phenylmethylsulfonyl fluoride
PSI	Photosystem I
PSII	Photosystem II
p53	Tumour suppressor protein p53
$Q(H_2)$	quinone
SDS	Sodium dodecyl sulfate
STAS	Sulfate transporter anti-sigma factor antagonist
TB	Terrific broth
TCEP	Tris(2-chloroethyl) phosphate
TEMED	*N,N,N',N'*- Tetramethylethan-1,2-diamine
TFA	Trifluoroacetic acid
TFE	2,2,2-trifluoroethanol
TIPS	Triisopropylsilane
TMR	Tetramethylrhodamine
TNF	Tumour necrosis factor
TOF	Time-of-flight
tRNA	Transfer ribonucleic acid
Tris	Tris(hydroxymethyl)-aminomethane
Wt	Wild-type
UV	Ultra violet

Vis	Visible

Chapter 1:

Introduction

1.1 Light energy

Light from the sun is the Earth's most important source of energy. Directly or indirectly, light is essential for most living organisms, from photosynthesis, movement and growth in plants, gene-expression responses in micro-organisms to vision in animals. This energy reaches the earth as photons of electromagnetic radiation. Photons are absorbed by light sensing molecules, often by co-factor chromophores within protein complexes, which allow the absorption of photons of wavelengths beyond the UV spectrum of proteins alone.[1] Energy form the photon, promotes an electron in the chromophore to excited states (S_n) from the ground state (S_0, Figure 1.1). The host protein must then interact somehow with the excited state of the chromophore to transduce the absorption of a photon into a chemical or physical response. Energy is dissipated to the surrounding environment by non-radiative transitions through vibrational-relaxation between vibrational spin levels, and internal-conversion occurring between two overlapping vibrational spin levels from different electronic states. The electrons can then return to the ground state from the first excited state (S_1-S_0) by emission of photons through a radiative transition (fluorescence). An alternative pathway is through intersystem-crossing, a non-radiative transition that involves changes in spin multiplicity from singlet to triplet state (S_1-T_1), finally returning to ground state from the first excited triplet state (T_1-S_0, Figure 1.1) by emission of radiative phosphorescence or by delayed fluorescence, thermally obtaining enough energy to return to the first excited singlet state then to ground state (T_1-S_1-S_0).

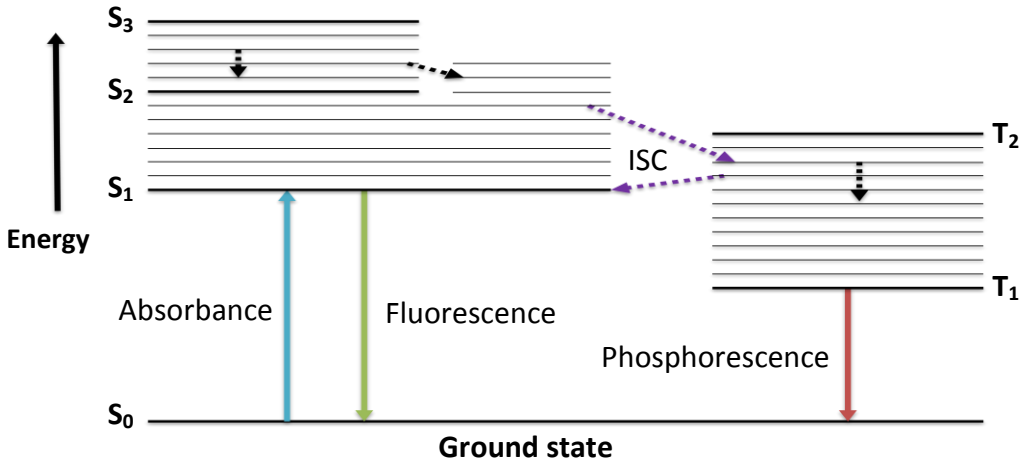

Figure 1.1: *Jablonski diagram[2] illustrating electronic states at different energy levels (bold lines) and vibrational spin levels (thin lines). Absorption and emission radiation are shown by straight arrows, and non-radiative relaxation, conversion and inter-system crossing are shown by dotted arrows.*

Although light is vital for existence on earth, certain wavelengths of light can also damage living organisms; ultra-violet (UV) radiation (UV-C: 200-280 nm, UV-B: 280-330 nm, and UV-A: 320-400 nm) is absorbed by proteins and nucleic acids, from which high exposure can cause DNA lesions.[64] Failure to repair these mutagenic DNA lesions can lead to genetic diseases[65] and predisposition to various cancers,[80] most notably skin melanoma.[3,4,67] A major form of DNA lesion is the covalent link between adjacent pyrimidine bases[68,69] forming cyclobutane-pyrimidine dimers (Figure 1.2), that cause distortion of the DNA structure and therefore prevent replication and gene expression,[70] The *p53* oncogene is commonly mutated due to UV induced DNA damage.[64,66,71]

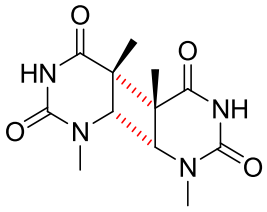

Figure 1.2: *Pyrimidine dimer of two thymine bases showing covalent cross-links in red.*

On the contrary, visible-light (400-700 nm) radiation (Figure 1.3) is known not to cause direct damage; rather it has paved the way for further investigation on photo-sensory systems that utilise light at these wavelengths. There are various classes of chromophores that absorb light at different wavelengths according to their chemical structure (Sections 1.2 and 1.3). These chromophores are usually part of larger photo-sensory protein complexes that use light energy for biological processes, such as photosynthesis.

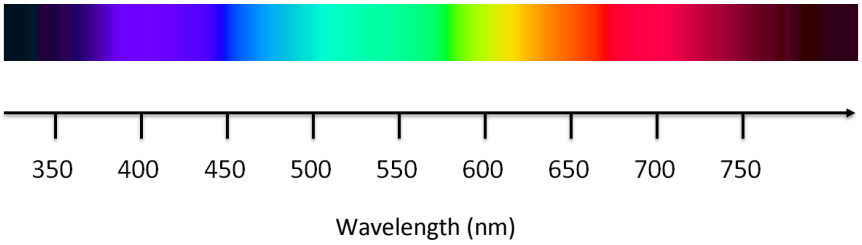

Figure 1.3*: Illustration of the visible region of the electromagnetic spectrum.*

1.2 Photosynthesis

Photosensitive proteins in photosynthetic organisms use light as a source of energy to drive endergonic chemical processes or as a signal for morphological changes. Photosynthesis in plants, many bacteria and algae converts light energy to chemical energy in the form of ATP and NADPH. This complex procedure is mediated by the chloroplast reaction centres that bind pigments such as chlorophyll molecules that absorb energy from photons in the blue-green region (400-700 nm) of the electromagnetic spectrum. Chlorophyll-a (Figures 1.4 and 1.5A), absorbs at wavelengths between 400-450 nm and 650-700 nm, and chlorophyll-b (Figures 1.4 and 1.5B) at 450-500 nm and 600-650 nm.[5] Chlorophylls vary in chemical structures and differ from bacteriochlorophylls (Figure 1.5A-D). Light-harvesting antenna complexes envelop the reaction centres and aid the capture and transfer of energy through additional pigments such as pheophytin (Figure 1.5 E) and β-carotene (Figures 1.4 and 1.5F).

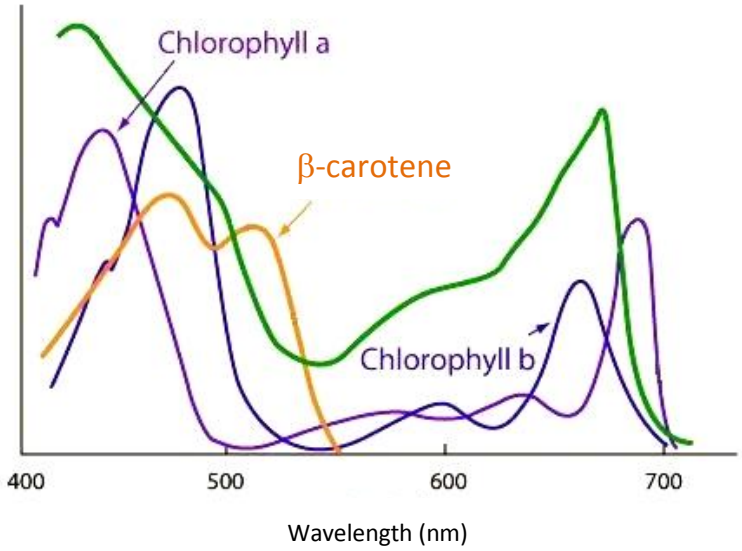

Figure 1.4: *Absorption spectra of chlorophyll a (purple), chlorophyll b (blue), β-carotene (xanthophyll) (orange) individually and together (dotted green), including the photochemical efficiency (solid green) as a measure of the amount of oxygen released by leaves.*[63]

A

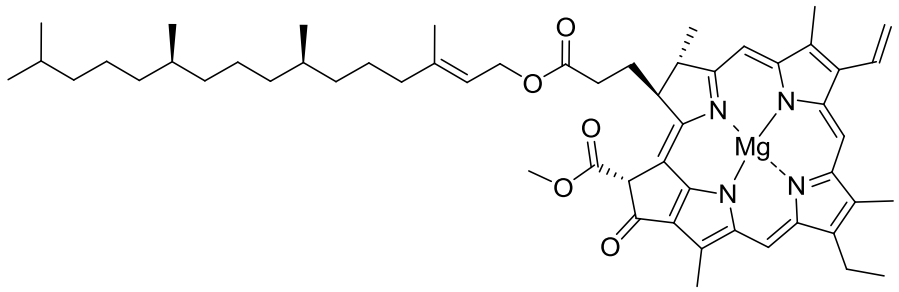

B

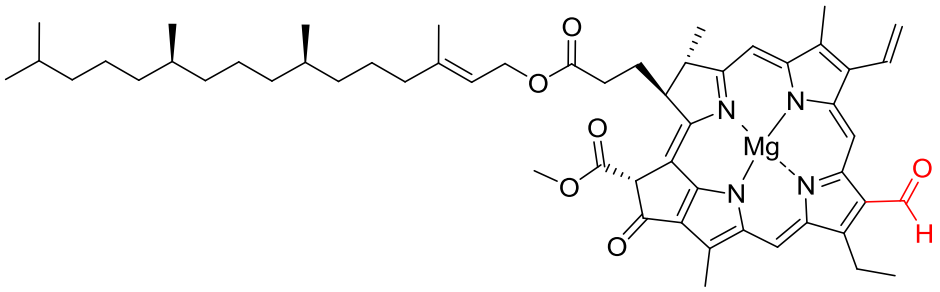

C

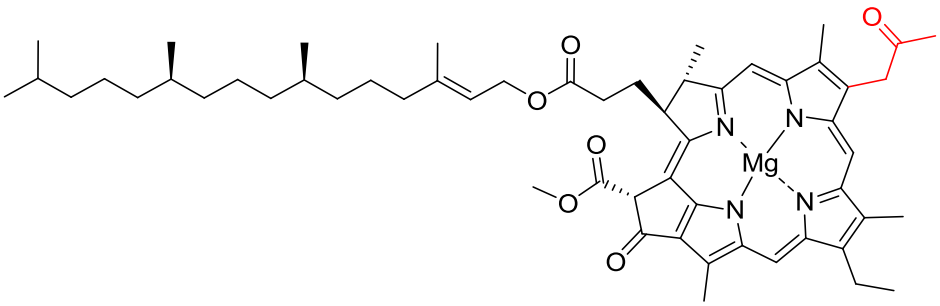

D

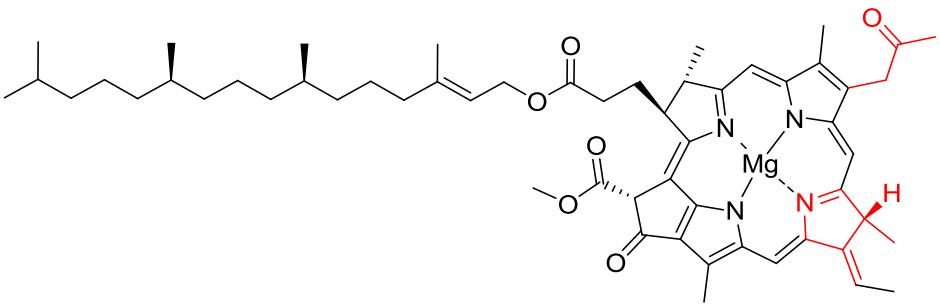

E

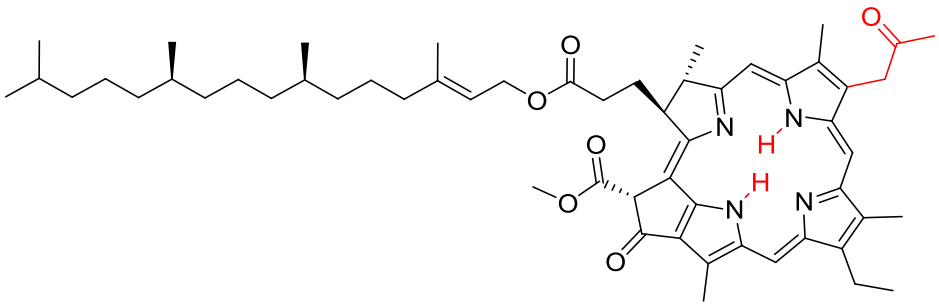

F

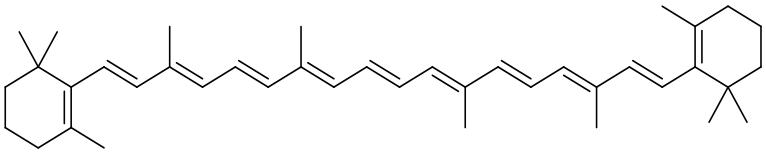

Figure 1.5: *Structure of: A) chlorophyll-a, B) chlorophyll-b, C) bacteriochlorophyll-a, D) bacteriochlorophyll-b, E) bacteriopheophytin and F) β-carotene.*

In plants and many bacteria chlorophyll dimers (often called the ''special pair'') are present in the reaction centres[6] (Figure 1.6). They form lower energy states than single chlorophyll molecules present in the antenna complexes leading to a resonance energy transfer from excited states of single chlorophyll molecules to the special-pair (electron acceptor). The special pair in bacterial cells absorb light maximally at 960 nm wavelength, it is therefore often referred to as *pigment* 960 (*P*960) when excited and is quickly converted to $P960^{+}$ following the transfer of electrons through single chlorophyll-b molecules to neighbouring quinone (plastoquinone in plants, Figure 1.7) electron acceptors (Q_A then Q_B) that are present in the cell membrane (Figure 1.9). Q_B is part of the electron-transport chain and its close proximity to the cytoplasm (bacteria) results in the uptake of protons, which in turn is reduced from Q to QH_2 once a second electron is accepted. This results in the formation of a proton gradient (electrochemical gradient) in the cell membrane (thylakoid membrane in plants) that drives the synthesis of ATP[6] through the ATP Synthase complex. Photosynthetic archaea use bacteriorhodopsin (Figure 1.8) to generate ATP also using an electrochemical gradient.[7]

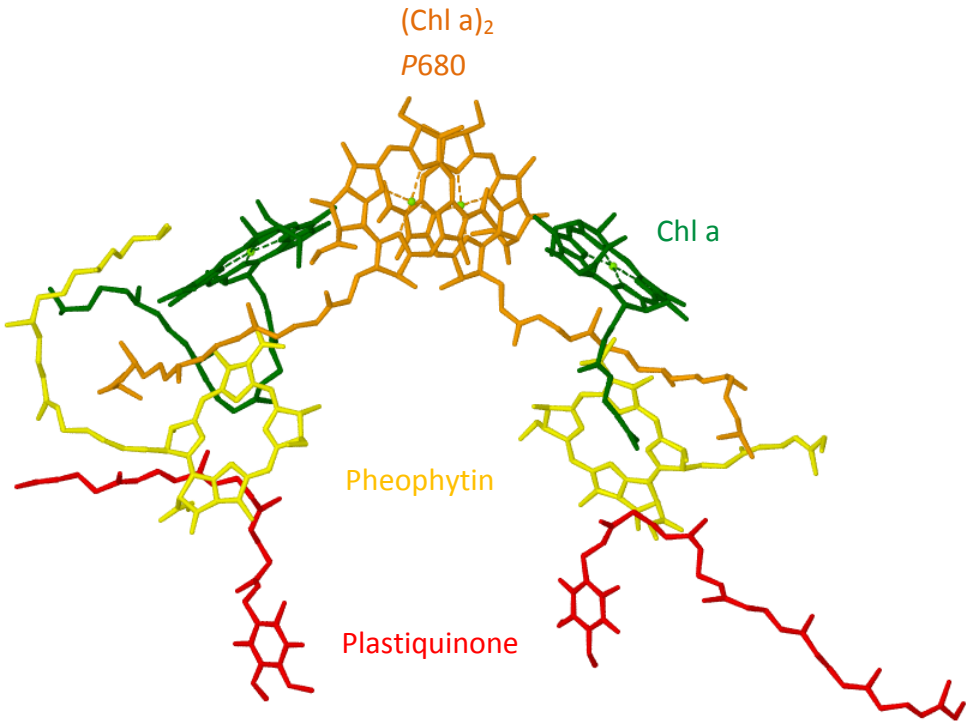

Figure 1.6: *Plant photosystem II reaction center showing the ''special-pair'' chlorophyll dimer (P680) in orange.*[156]

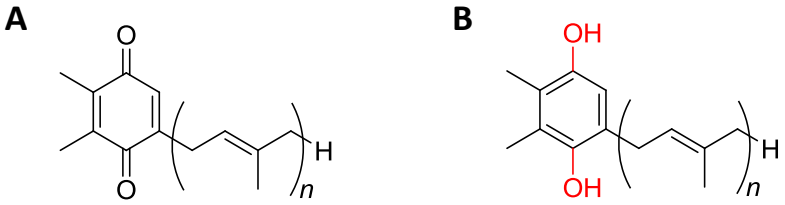

Figure 1.7: *A) Plastoquinone (oxidized form, Q) and B) plastoquinol (reduced form, QH_2). The change is highlighted in red and n = 6 to 10 isoprene units.*

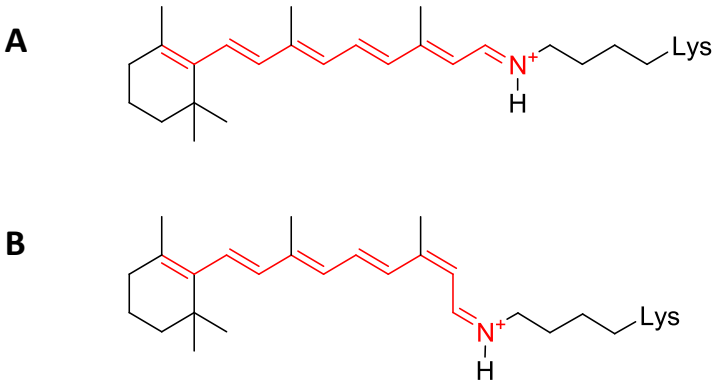

Figure 1.8: *Bacteriorhodopsin in red: A) All trans retinal and B) 13-cis retinal.*

In green plants electron transfer occurs by charge separation through photosystem I (PSI) and photosystem II (PSII) (Figure 1.9). These photosystems closely resemble the reactions in the bacterial reaction centers in that it cycles a quinone from its oxidised form (plastoquinone) to its reduced form of (plastoquinol, Figure 1.7). The special-pair in plants (Figure 1.6) differs from that of bacteria in that it absorbs at 680 nm and is referred to P680 and $P680^+$. $P680^+$ is a strong oxidant which is neutralised by electrons from two water molecules bound to a manganese cluster (Mn_4Ca, contains multiple oxidation states Mn^{2+}, Mn^{3+}, Mn^{4+}, Mn^{5+}) forming a single oxygen molecule (Figure 1.9). Initially the electrons are donated from a tyrosine residue of PSII, forming a radical that removes electrons from the manganese ions, in bacteria cytochromes are responsible for the transfer of electrons. Another important pigment in plant photosynthesis is the cytochrome (*bf*) complex which links PSI with PSII and transfers the flow of electrons to from plastiquinol (QH_2) to the Q-cycle in the thylakoid lumen *via* a copper binding protein called plastocyanin (Pc). Similarly to bacterial cells, the ATP Synthase complex uses the electrochemical gradient to generate ATP (Figure 1.9).[6]

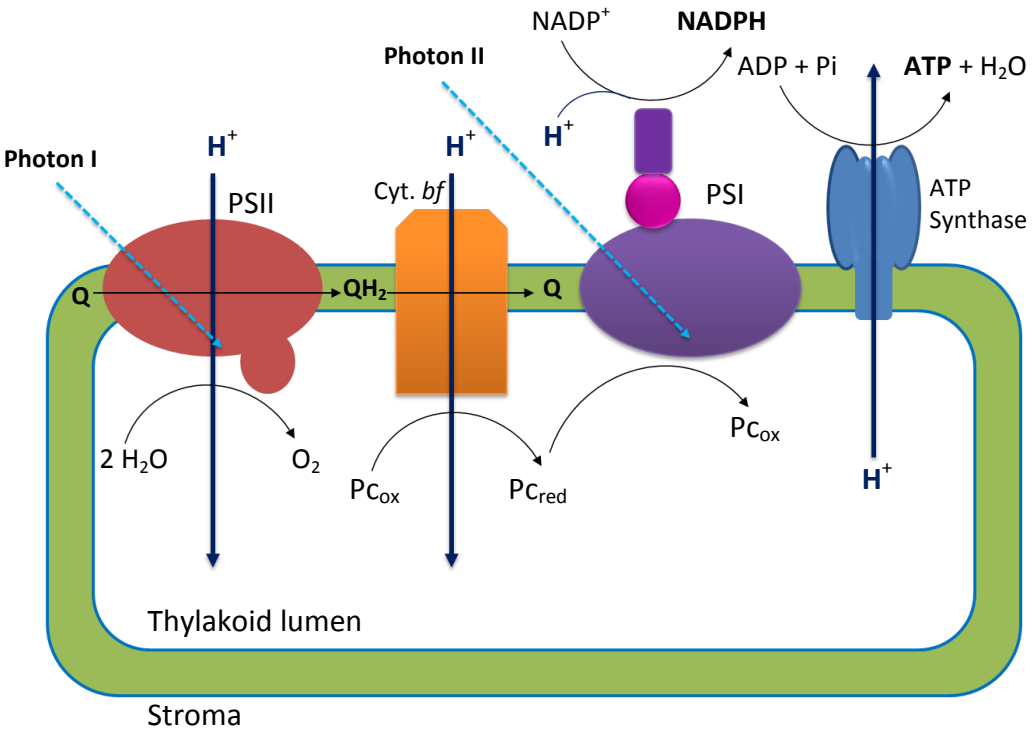

Figure 1.9: *The electron transport-chain in plants, illustrating the transfer of electrons (e^-), the Q-cycle ($Q \rightarrow QH_2 \rightarrow Q$), the proton gradient ($H^+$) and the generation of NADPH (PSI and ferredoxin) and ATP through the ATP Synthase complex.*

1.3 Photosensing

Rhodopsins, phytochromes,[8] xanthopsins[9] and phototropins are all examples of photoreceptors that control activation of biological pathways. For example, rhodopsins are a group of retinal (Figure 1.8) binding photoreceptors that are the basis for visual perception in animals. The retinal chromophore is covalently linked by a Schiff base to a lysine residue of opsin, a protein component of rhodopsin. Retinal in its protonated state absorbs at wavelengths between 440-500 nm. The energy from a photon causes a *cis-trans* isomerisation of 11-*cis* retinal (Figure 1.10) and triggers conformational changes within rhodopsin.[6] This results in the activation of a series of signalling cascades[10] leading to the regeneration of 11-*cis* retinal in the visual photo-transduction pathway (visual cycle).

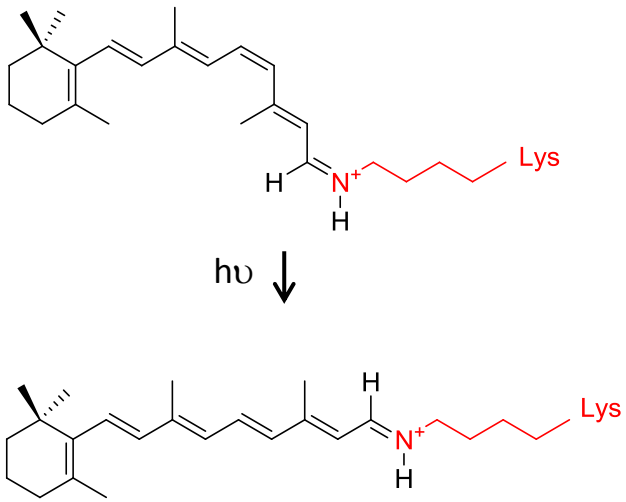

Figure 1.10: *Photoisomerisation of retinal chromophore from 11-cis-retinal to all-trans retinal.*

Both phytochromes and xanthopsins contain chromophores that follow a similar *cis-trans* activation process, where phytochromes absorb in the red/far-red region (620-740 nm), and xanthopsins such as photoactive yellow protein (PYP)[9] absorb at the blue region (420-475 nm). Phytochromes consist of light-sensing tetra-pyrrole chromophores (Figure 1.11A) that forms a thio-ether linkage to a conserved cysteine residue. Phytochromes regulate plant responses, such as photoperiodism (flowering) and are also involved in regulating root development[72] and other responses like chloroplast movement, cytoplasmic motility,

germination of seeds and the synthesis of chlorophyll molecules.[73] Xanthophylls are yellow pigmented carotenoids that are mainly long-chain hydrocarbons containing hydroxyl groups (Figure 1.11B). They mainly absorb light for photosynthesis in plants[6] although, β-cryptoxanthine has been found to have provitamin-A activity and was determined to stimulate osteoblastic bone formation *in vitro* and also prevent bone loss in human models.[71]

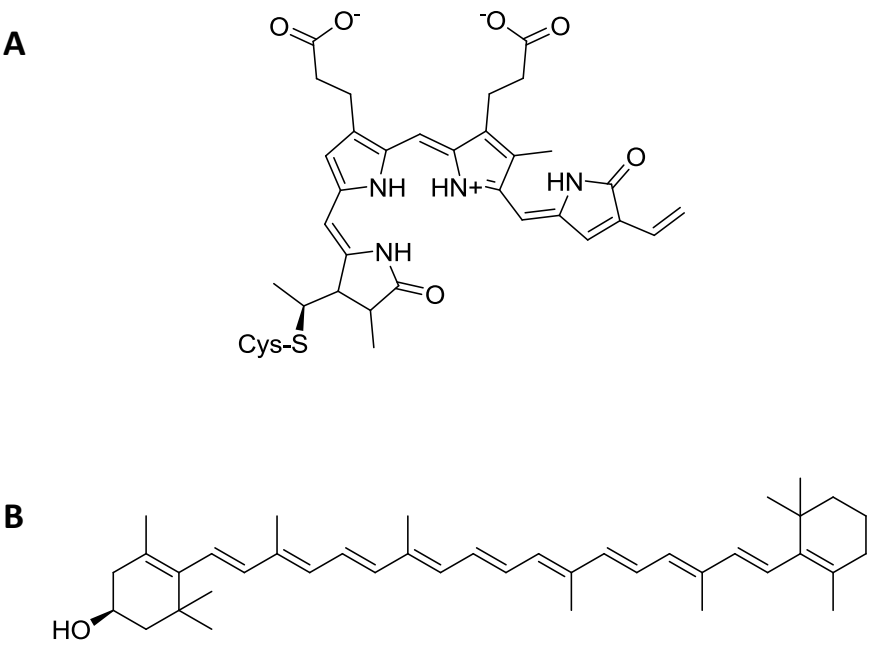

Figure 1.11: *A) Phytochromobilin, a phytochrome tetra-pyrrole and B) cryptoxanthine, a xanthophyll.*

Phototropins are another type of blue-light photo-receptors that regulate directional growth in plants, a process known as phototropism.[11] Phototropins are serine/threonine protein kinases that mediate phototropism through light-activated autophosphorylation, which is initiated by two light-oxygen-voltage (LOV) domains. These are flavoproteins, containing a flavin mononucleotide (FMN, Figure 1.12A) or flavin adenine dinucleotide (FAD, Figure 1.12B) cofactor, which sensitise phototropins to blue light.

1.4 LOV Domains

1.4.1 Morphological features of LOV domains

Light-Oxygen-Voltage (LOV) domains belong to the per-ARNT-sim (PAS) family[34] of molecular switches that act as internal sensors of oxygen, redox potential and light[18] using covalently bound flavin cofactors (FMN or FAD).[19] They are found in plants, fungi and bacteria and function as light sensitive component of kinases,[20-22] DNA binding domains,[23,24] STAS (sulfate transporter anti-sigma factor antagonist) domains[25] and as single LOV domains[26] that function as DNA-binding proteins (such as EL222)[74,75] or are usually coupled to other effector domains such as, the VVD LOV domain and white collar-1 (WC-1) protein complex (WCC), which regulates circadian clock function in fungus *Neurospora crassa*. [27] These LOV domains function as reversible photo-switches[30] to regulate a range of blue light responses such as phototropism,[11,20] chloroplast mobility,[28] stomatal opening[29] and bacterial cell-cell attachment.[21] LOV domains comprise of five alpha helices (Cα, Dα, Eα, Fα and Jα) and five beta sheets (Aβ, Bβ, Gβ, Hβ and Iβ) forming an anti-parallel beta sheet ($\beta_2\ \alpha_4\ \beta_3$) which is coupled to the kinase domain through an amphipathic helix[18] also referred to as the Jα linker (Figure 1.13).

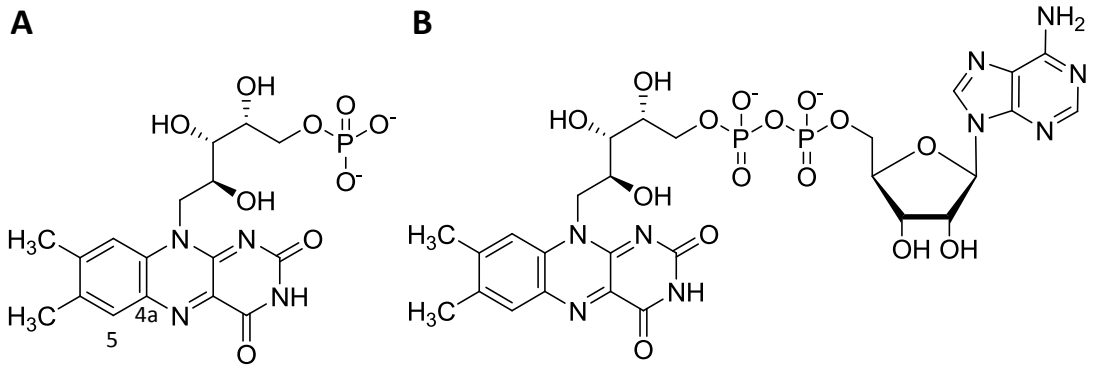

Figure 1.12: *Structure of A) FMN and B) FAD.*

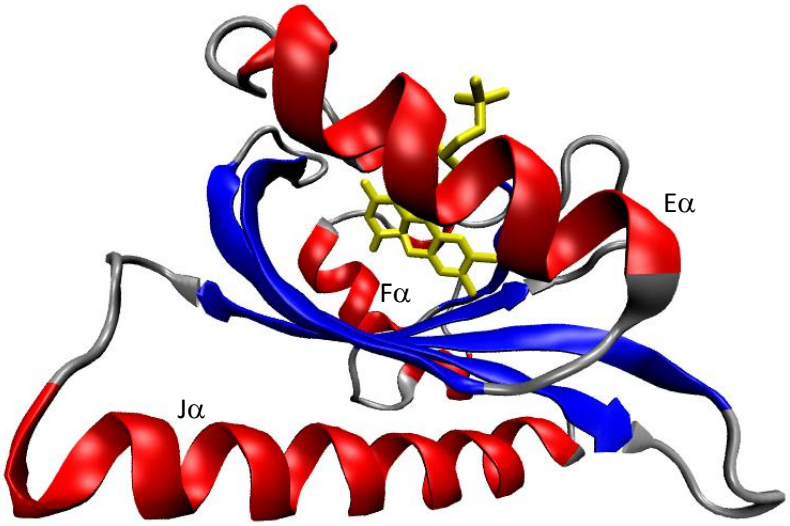

Figure 1.13: *The structure of Avena sativa phot1 LOV2 (dark state) showing the position of the FMN (yellow) between helices Eα and Fα. Model generated using VMD 1.8.7. (PDB: 2V1B).*

1.4.2 FMN-cysteine adduct

Studies on the photochemistry of the FMN-C4a-cysteine adduct were first performed on phot1 *As*LOV2[32,35] and later followed by other LOV domains, which also demonstrated photoreactions with comparable mechanisms.[36] The mechanism of the primary photoreaction has been the subject of considerable debate with three possible mechanisms proposed for the formation of FMN-C4a-cysteine adduct. Crosson and Moffat, suggested that a concerted mechanism takes place, the S-C adduct forming from a triplet state generated by the direct transfer of a proton from the cysteine thiol to the N5 position of the FMN. They used X-ray crystallographic studies to show that the cysteine residue 450 is located a short distance (4.2 Å) from the FMN (C4a) position, therefore favouring the transfer of a proton which would eliminate the electronic-charge on the isoalloxazine ring formed from photo-excitation.[37] An alternative pathway involves a putative ionic mechanism, where the FMN triplet state triggers protonation and formation of a reactive carbocation at the C4a position, due to the increased electronegativity at the N5 position of the isoalloxazine ring.[35,37] The reactive carbocation at the C4a position then undergoes nucleophilic attack by the thiol of cysteine.[38] A third possibility was described by Kay *et al.,* who proposed that the FMN-cysteine adduct formation occurs *via* a radical pair mechanism

(Figure 1.14)[39] that involves the transfer of a hydrogen atom[39-42] from the cysteine to the N5 of the isoalloxazine of the flavin resulting in a radical pair ($FMNH^{\bullet}$ - $H_2C\text{-}S^{\bullet}$) in the triplet state. The cysteine radical ($\text{-}CH_2\text{-}S^{\bullet}$) proximity to the isoalloxazine ring initiates spin-orbital coupling, followed by inter-system crossing between triplet and singlet states resulting in an FMN-C4a-cysteine adduct formation. Although semiquinone formation cannot be directly detected by spectroscopy, various studies using mutants of *As*LOV2 where the key cysteine is replaced by other residues[39-42]have supported the radical-pair mechanism.

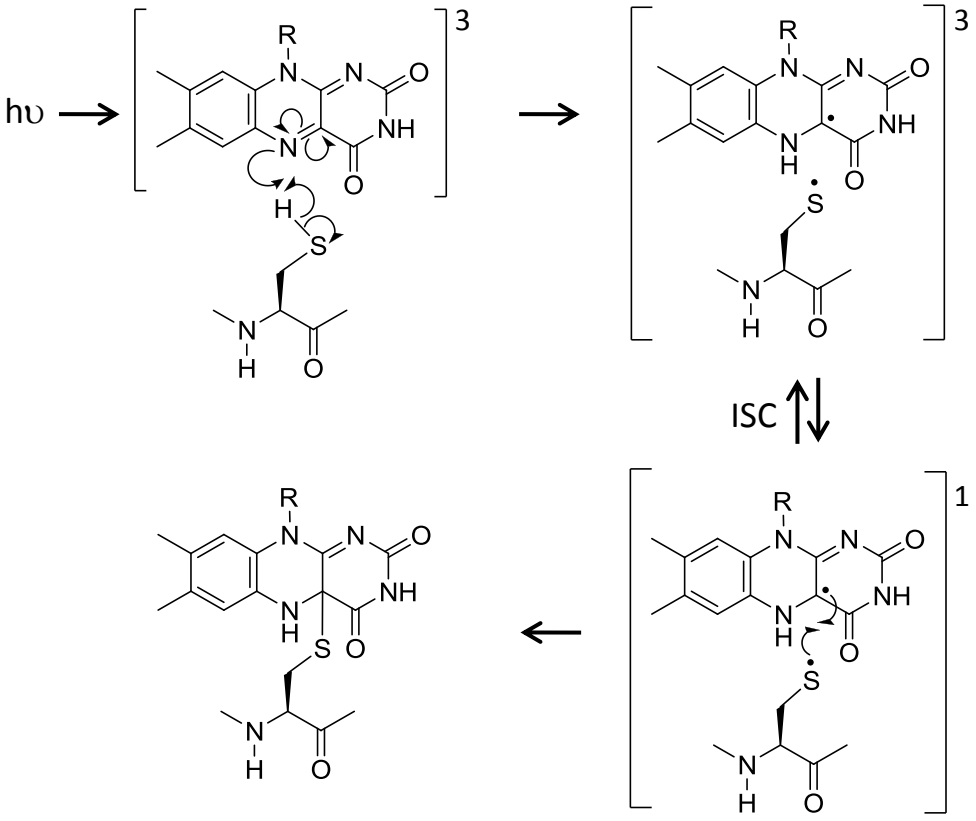

Figure 1.14: *Radical pair mechanism, showing the triplet (3), singlet (1) states and the intersystem crossing (ISC) between both states.*

1.4.3 Arabidopsis thaliana Phot1/2

In *Arabidopsis thaliana* (*At*), two phototropins (phot1 and phot2) have been discovered comprising two light sensing light-oxygen-voltage domains (LOV1 and LOV2) situated at the N-terminal region and a serine/threonine protein kinase domain (Figure 1.15).[11,12]

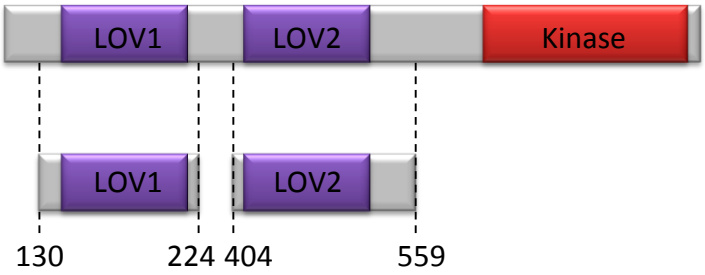

Figure 1.15: *Diagram of Arabidopsis thaliana phototropin structure annotated with residue numbers.*

In *At* phot1 and phot2, LOV1 and LOV2 are almost structurally identical comprising the common five alpha helices and five beta strands.[11,12] The isolated LOV1 domain relaxes with a half-life of 11.5 sec. whereas LOV2 relaxes with a half-life of 27 seconds.[32] The LOV2 domain, mediates light-dependent autophosphorylation[20] and is coupled to the kinase domain through the Jα helix.[18] LOV1 however is unable to elicit autophosphorylation in the absence of LOV2.[20] Although the exact function of LOV1 is unclear, studies suggest that it may have a role in receptor dimerisation.[33]

1.4.4 Avena sativa LOV2

Avena sativa (*As*) LOV2 is similar to *At*LOV2 with 91.6 % sequence similarity,[62] with the FMN cofactor positioned at the N-terminal half of the LOV domain, between helices Eα and Fα (Figure 1.13). *As*LOV2 was one of the first LOV domains discovered for regulating phototropism and has been used in a wide range of studies including the studies on photo-switching dynamics. The Jα helix was first identified by Gardner and co-workers and the NMR structure of *As*LOV2 (Figure 1.13) revealed that in the dark state the Jα helix is docked to the β-sheet of the LOV core,[48,18] suggesting that the monomeric nature of *As*LOV2 is primarily due to the flexibility of the Jα, which prevents the formation of LOV dimers through β-sheet interactions.[43] Harper *et al.* using NMR spectroscopy and limited proteolysis demonstrated kinase-activity in the dark-state of full length phototropin in absence of the Jα helix,[18] indicating that dimerisation through β-sheet interactions between the LOV-core and the kinase domain takes place in the absence of Jα. Light induced covalent adduct formation between the FMN and an internal cysteine (C450), displaces the amino acid residues of the Jα from the central β-sheet, which leads to the undocking of the Jα which then regulates the activity of the kinase domain.[49]

1.4.4.1 AsLOV2 as an Optogenetics tool

1.4.4.1.1 *Introduction to Optogenetics*

Interactions between intracellular proteins regulate signalling processes and pathways vital to the function of cells. These signalling pathways can often be observed by directly tagging proteins using fluorescent proteins. Optogenetics is derived from the Greek word for *visible* (*optos*) and it is the technique of introducing genetically engineered light-sensitive proteins into a live cell or an organism, to monitor its localisation and/or effect within a cell.[50] Examples of such optogenetic tools have been demonstrated with various biological protein-switches. Toettcher and co-workers, demonstrated light activated interactions between phytochrome (Phy) and phytochrome-interacting factor (PIF) to direct reversible protein translocation, in fibroblast cells.[157] Red light has also been used to control motility of fibroblast cells, which were demonstrated through fusions between phytochrome B and PIF6.[158] Optogenetics has been used to photo-control DNA-binding where, Morgan and Wolley demonstrated photo-control of DNA-binding protein GCN4 (leucine zipper bZIP) when fused with PYP. The fusion protein was found to bind 10-fold more weakly than wild-type and once light-irradiated, the DNA-binding affinity was enhanced by double in comparison to the wild-type GCN4 protein.[159] Further modification on the GCN4-PYP gene by removal of a heptad repeat from the leucine zipper to improve its packing with PYP core, resulted in a reverse action where the protein bound DNA better in its dark state than in the light.[160,161] However, this study still remains to be more widely tested and the a question remains to whether it will reach the stage of *in vivo* testing.

The most successful optogenetics tool up to date is the green-fluorescent protein (GFP) from jelly fish, *Aequorea victoria*. Its wide-scale use in science has awarded its founders the Nobel Prize in chemistry 2008. Despite its success, GFP has several disadvantages such as, its use is restricted to aerobic systems,[162] it displays pH sensitivity[163] and is a relatively large protein.[164] Recent research has been aimed at producing LOV-based fluorescent probes, and has resulted in a small (11 kDa) photo-reversible fluorescent protein called iLOV, engineered from *At* Phot2 LOV2. It has been established to perform better than GFP as a fluorescent reporter for plant viral infections.[164] Recent advances in producing LOV domain based

photo-switches has excelled, with *As*LOV2 being widely used as a basis for engineered fusions, of which a few are discussed below.

1.4.4.1.2 *LOV-TAP*

Strickland *et al.* produced and screened 12 fusions of *As*LOV2-Jα to the *Escherichia coli* tryptophan repressor protein (TrpR) to form a family of LOV-TAP (tryptophan activated protein) proteins. The fusion was conducted through the C-terminal Jα to 13 different N-terminal TrpR truncations as schematically illustrated below (Figure 1.16). The best example showed regulation of the DNA-binding activity with weak (788 nM) DNA binding in the dark state and 5-fold higher activity in the light state.[51] Subsequently the design was optimised and the dark state binding was reduced by introducing single point mutations (G528A, I532A and N538E) and double mutations (G528A and N538E) to stabilise the Jα-hybrid. This resulted in a much improved light state binding of 64-fold.[52]

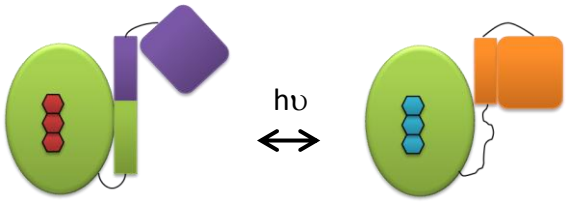

Figure 1.16: *An illustration of photo-switching of LOV-TAP (LOV domain in green) from inactive form (purple) in the dark state (FMN in red) to active form (orange) in the light state (FMN in blue).*

1.4.4.1.3 *LOV-DHFR*

Lee *et al.* produced more drastic fusions by inserting *As*LOV2 in-between the βF-βG loop and the αC-βE loop of dihydrofolate reductase (DHFR, Figure 1.17), an enzyme required for folate metabolism. They expected to use the photo-switching mechanism of *As*LOV2 to enhance the rate of hydride transfer in the reduction of 7,8-dihydrofolate (H_2F) to 5,6,7,8-tetrahydrofolate (H_4F). However, the designs led to distortions in the enzymatic function of DHFR and enzyme activity and substrate binding were reduced by more than half. No photo-activation was demonstrated *in vivo* although, photo-switching revealed an increase of 1.5-2 fold enzyme activity *in vitro*. In this case, regulation using light was not as successful.[53]

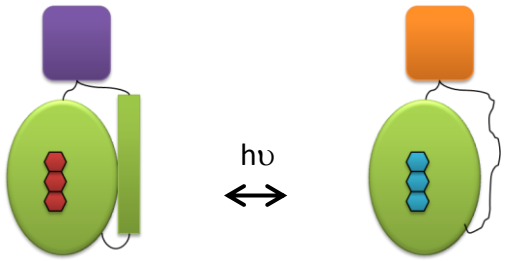

Figure 1.17: *An illustration of photo-switching of LOV-DHFR (LOV domain in green) from inactive form (purple) in the dark state (FMN in red) to active form (orange) in the light state (FMN in blue).*

1.4.4.1.4 *LOV-Rac*

Perhaps the most impressive of the *As*LOV2-derived optogenetic switches is the Rac1 GTPase fusion. Rac1 is an important GTPase responsible for regulating many cellular process through actin cytoskeletol reorganisation (motility, cell-cell adhesion and cell growth).[76] Rac1 has therefore been a useful tool for de-regulating and controlling cancer cell motility[97,78] and growth.[79] Wu *et al.* fused the N-terminus of Rac1 (Isoleucine, residue 4) to the C-terminal Jα of *As*LOV2, so that access to the active site of PA-Rac1 (Photoactivatable-Rac1) by its effector domain (Pak) is blocked (caged, Figure 1.18). X-ray crystallographic studies revealed dark state caging of the PA-Rac1 variant, whereas irradiation led to binding to Pak protein at approximately the same affinity as wild-type Rac1 which was demonstrated in mouse-embryo fibroblasts stably expressing PA-Rac1. Additionally, this mechanism of blue light activation has been sufficient to control the motility of fibroblast cells expressing PA-Rac1.[54] The success of PA-Rac1 as an optogenetic tool has been portrayed in more recent studies on controlling neutrophil motility in developing zebra fish embryos[55] and *Drosophila* ovary cells.[56]

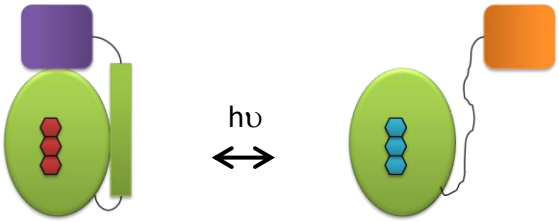

Figure 1.18: *An illustration of photo-switching of LOV-Rac (LOV domain in green) from inactive form (purple) in the dark state (FMN in red) to active form (orange) in the light state (FMN in blue).*

1.4.4.1.5 *TULIPs*

Tunable, light-controlled interacting protein tags (TULIPs), are *As*LOV2-peptide (LOVpep) fusions that function as optogenetic dimerisation tags that bind to proteins containing localisation signals to specific sites in yeast or mammalian cells. Fusions of small peptide sequences were made *via* overlapping parts of the C-terminus of Jα helix in order to adapt a docked α-helical peptide conformation in the dark state therefore, caging the peptide sequence and preventing it binding to its effector domain (PDZ). Longer fusions showed sensitivity both in the light and dark states. Studies showed that the translocation in HeLa cells was reversible in three cycles of photo-excitation and recovery, using ePDZb1-mCherry co-localised with GFP-LOVpep. Strickland and co-workers also succeeded in controlling MAPK activation and cellular growth arrest using LOVpep^{CA} (constitutively-active LOVpep variant) fused to Mid2 under the control of GAL1 promoter.[57]

1.4.4.1.6 *Photo-activated Caspase-7*

Caspase-7 is an executioner caspase (Section 1.5.3) usually present in cells in an inactive form, referred to as pro-domain (or pro-enzyme) that is activated upon internal proteolytic cleavage by caspase-8 or caspase-9. A recent study of the regulation of apoptosis used a fusion between the *As*LOV2 domain and the catalytic domain of caspase-7 which formed an auto-inhibitory pseudoprodomain (LOV2-Jα–Caspase-7 complex), where in the dark state it is presumed that the LOV2 domain is packed against the caspase cleavage site, preventing autolysis (auto-inhibition). This was activated upon light illumination, thus releasing its auto-inhibition once the unfolding of LOV2-Jα took place. They showed positive results *in vivo* by testing the mortality of transfected COS7 cells upon photoactivation.[58]

1.4.5 *Bacillus subtilis YtvA*

Bacillus subtilis (*Bs*) YtvA was the first bacterial blue-light photoreceptor found to contain an FMN binding LOV domain.[44,45] A large group of bacterial LOV domains were later discovered, which contain histidine-kinase domains.[46,22] However in YvtA, the LOV domain (Figure 1.19) is connected to a C-terminal sulfate transporter anti-sigma factor antagonist (STAS) domain (YtvA-LOV-STAS), which upon activation positively regulates the DNA-binding transcription factor SigmaB,[47] which regulates environmental stress responses[165,166,167] in *Bacillus subtilis* by transcribing over 150 genes whose products protect against threats to the cell.[25] Studies by Buttani *et al.* have shown that the STAS domain also has NTP-binding properties.[119] YtvA possessing a single LOV domain (YtvA-LOV) has been crystallised in its dark state, revealing head-to-head dimers between LOV domains. Unlike *As*LOV2,[48] the Jα helix is not docked onto the LOV core in the dark state and irradiated dark state crystals show little structural change.[45] The photo-recovery time is 10-fold longer for YtvA-LOV[45] than for *As*LOV2.[32,35]

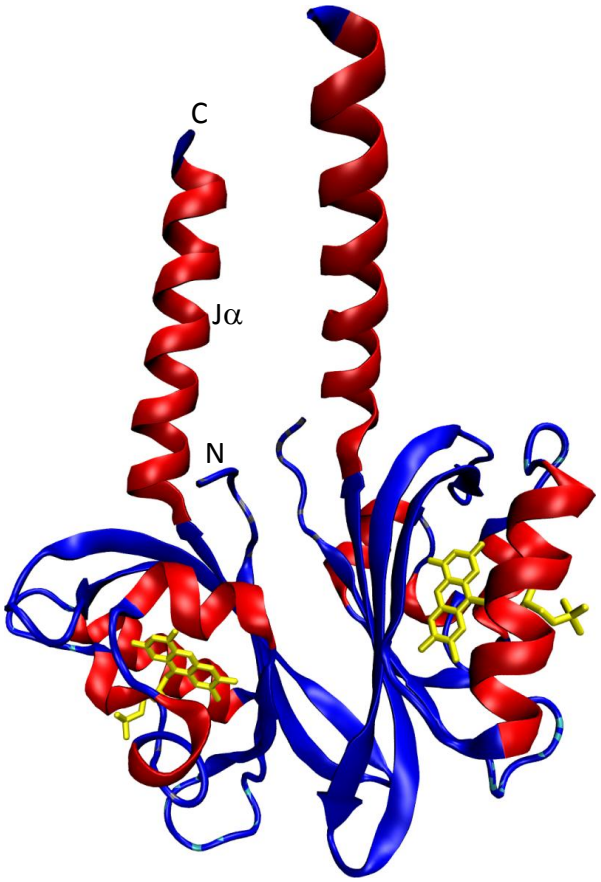

Figure 1.19: *The structure of Bacillus subtilis YtvA-LOV (dark state) showing the position of the FMN (yellow). Model generated using VMD 1.8.7. (PDB: 2PR5).*

1.4.5.1 YtvA-LOV as an Optogenetics tool

1.4.5.1.1 *YF1*

The LOV domain from *Bs* YtvA has been fused to a bacterial haem-binding PAS-histidine kinase (FixL) that is part of a two component system FixL/FixJ which regulates nitrogen metabolism in response to oxygen sensitivity. YtvA has been used to alter the signal specificity of FixL from oxygen to light by replacing its PAS domain with YtvA-LOV.[59] This YF1 fusion was active in the dark state (Figure 1.20) with irradiation leading to a 1000-fold decrease in its kinase activity. The study explored the importance of the lengths of the linker between the two domains, suggesting that amphipathic α helix linkers in dimeric fusion kinases form coiled coils.[60] Light-induced changes in the YtvA-LOV domain are passed to the histidine kinase domain *via* a small 4-5° rotational movement in the coiled-coil linker.[45] Further research resulted in dual-sensing FixL variants (YHF and HYF), that have both a light sensing YtvA-LOV domain and a oxygen sensing FixL-PAS domain fused together for stronger signal activation. Autoradiographic studies using [γ-^{32}P]ATP for detecting phosphate incorporation into FixJ, revealed reduced activity of YHF in the presence of either light or oxygen, and almost complete inhibition of activity in the presence of both.[60]

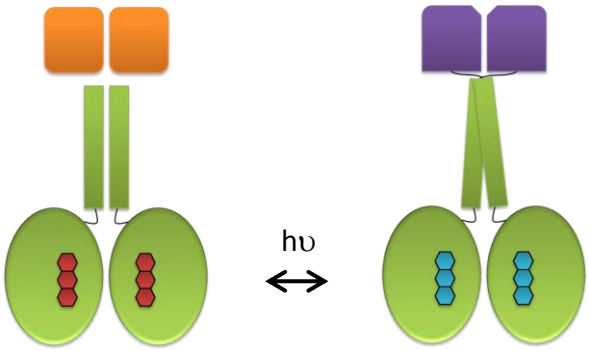

Figure 1.20: *An illustration of photo-switching of YF1/YHF (LOV domain in green) from active form (orange) in the dark state (FMN in red) to inactive form (purple) in the light state (FMN in blue).*

1.4.5.1.2 *YtvA-Lipase*

YtvA-LOV has also been fused to the N-terminus of *Bs* lipase A enzyme via the Jα helix (nLOV-BSLA). Light activated lipase activity was demonstrated using a standard assay for detecting lipase activity using *p*-nitrophenylpalmitate as a substrate that changes colour when converted to *p*-nitrophenolate. The assay therefore detects the enzymatic cleavage of the ester bond in *p*NPP in the presence of light-activated nLOV-BSLA.[61]

1.5 Apoptosis

1.5.1 Physical role and morphological features of apoptosis

Apoptosis is the vital process of non-accidental cell death, also referred to as type I 'programmed cell death' by Lockshin and Williams in 1964[80] and further reviewed by Lockshin and Zakeri in 2001.[81] Apoptosis originates from the Greek word meaning ''falling off" or "to drop off'' in similarity to falling leaves from trees.[82] It is required for tissue development[83] and homeostasis of multicellular organisms. *Caenorhabditis elegans* is an important model organism for research on apoptosis; during their development over 1000 somatic cells are generated of which, around 13% of cells are premeditatedly eliminated during the process of morphogenesis.[84-87] Apoptosis also plays an important role in mammalian development including the formation of separate digits by death of inter-digital mesenchymal tissue,[88] the development of the cranial cavity[89] and development of reproductive organs, during which the uterus is deleted in males (Müllerian duct) and the male organs are deleted in females (Wolffian duct).[83]

Apoptosis is characterised by morphological changes of which 'cell shrinkage' is a key feature, followed by chromatin condensation and nuclear fragmentation (karyorrhexis) leading to 'budding' and formation of apoptotic bodies enclosed by intact cell membrane decorated by markers which encourage phagocytosis.[82,86] Programmed necrosis (necroptosis) is another form of programmed cell death caused by cell membrane damage or depletion of energy and impairment of cell membrane ionic channels, leading to cell swelling (oncotic necrosis) then 'blebbing' and leakage of cellular contents which can stimulate strong local immune responses.[90,91] Studies on knock-out mice lacking genes for the protein Apaf-1, which binds to cytochrome c (Section 1.5.4 and Figure 1.23) resulted in

slow activation of inter-digital cell death, suggesting that an alternative cell death mechanism (necrosis) took place.[92]

Defects or dysfunction in apoptotic signalling can lead to autoimmune diseases and cancer, while excessive apoptosis can enhance ischaemic diseases and neurodegenerative disorders.[93] Researches in cancer therapy often target the "programmed cell death" pathways, such as the activation of p53 of the intrinsic pathway by ionizing radiation in radiotherapy.[94] There are three major apoptosis pathways resulting in the activation of members of a network of caspases (cysteine aspartate proteases).[95,96] Caspases 8 and 9 are key components of the extrinsic and intrinsic pathways respectively and both lead to the activation of caspases 3,6 and 7, which are known as the executioner caspases and perform the downstream functions common to apoptotic pathways.

1.5.2 Bcl-2 family of proteins

The Bcl-2 (B-cell lymphoma) family of proteins are key regulators of apoptosis. Their function depends on their ability to form hetero-dimers with anti-apoptotic members (Bcl-2, Bcl-x_L, Bcl-w, Mcl-1).[102] Full-length pro-apoptotic members of the Bcl family (Bak, Bax) are capable of homo-oligomerising to modulate the outer mitochondrial membrane permeabilisation for the release of cytochrome c.[103] Both pro-apoptotic and anti-apoptotic proteins contain up to four homologous regions in their structure, termed Bcl-2 homology domains (BH1-4).[104] The pro-apoptotic proteins can be further divided into subgroups of the multi-domain members Bak and Bax consisting BH1-BH3 domains, Bcl-x_S consisting BH3 and BH4 domains, and the BH3-only members Bid, Bik, Bim, Bad, Puma and Noxa (Figure 1.21). The anti-apoptotic Bcl-2 proteins (Bcl-x_L and Bcl-2), additionally are able to bind BH-3 domains of pro-apoptotic proteins due to a distinct hydrophobic cleft in their protein structure.[105,106] Therefore, the relative concentration of both pro-apoptotic and anti-apoptotic members determine the cells survival.

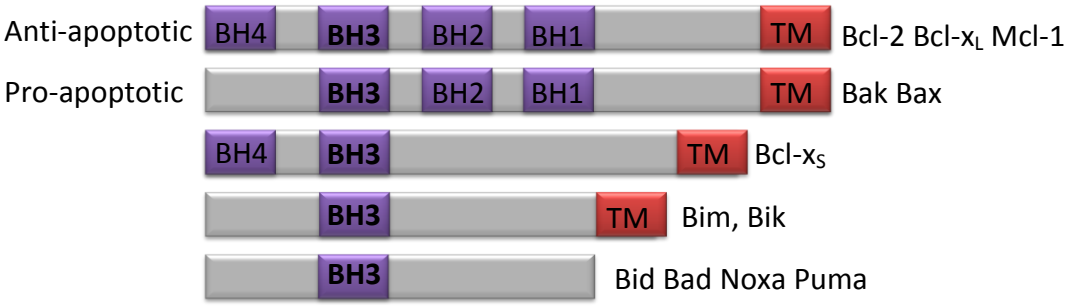

Figure 1.21: *Schematic domain structure of Bcl-2 family, also showing the trans-membrane domain(TM) at the C-terminus in red.*

1.5.3 Extrinsic pathway

The extrinsic pathway is activated by the binding of ligands (Fas, Tumour necrosis factor TNF and TNF-related apoptosis-inducing ligand TRAIL) to cell surface receptors. Once activated conformational changes occur in these signalling receptors leading to the binding of adaptor molecules such as Fas-associated death domain (FADD). In Type I cells (independent of mitochondria) the adaptor domains recruit of pro-caspase-8, resulting in the formation of the death-inducing signalling complex (DISC, Figure 1.22). DISC causes the activation of pro-caspase-8 to caspase-8 *via* auto-proteolytic cleavage. Caspase-8 directly activates casapse-3 and caspase-7 which induce the morphological changes associated with apoptosis.[18] Type II cells (mitochondria-dependent) have reduced DISC formation due to low levels of localised caspase-8, therefore activation of caspases-3 and 7 does not proceed directly, rather the BH3-interacting domain death antagonist (Bid) is cleaved to its truncated form (tBid), which then translocates to the mitochondrial outer membrane and initiates the intrinsic pathway (Figure 1.22), with executioner caspase-3 activation instead occurring through caspase-9.[98]

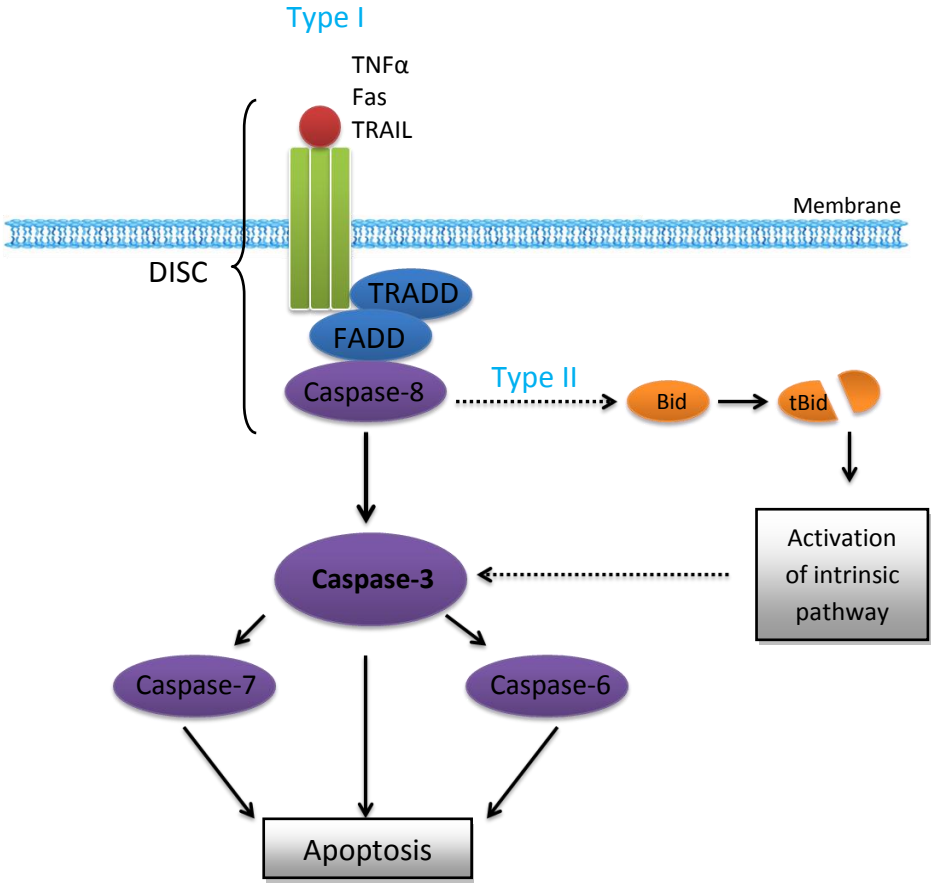

Figure 1.22: *The extrinsic pathway of apoptosis in type I cells through Caspase-8 auto-catalytic activation at the DISC. Initiation of type II cells is through proteolytic cleavage of Bid by caspase-8, which then activates the intrinsic pathway.*

1.5.4 Intrinsic pathway

The intrinsic pathway can be activated by oxidative stress, DNA damage, UV-exposure or chemo-toxic substances. It is regulated by interactions between the pro-apoptotic and anti-apoptotic Bcl-2 family of proteins. The BH3-only proteins: Bid, Bim, Bad, Bik, PUMA, Noxa can bind to the anti-apoptotic proteins, therefore an increase in their effective concentration either through up-regulation of their transcription by p53 or, as described above for Bid, cleavage of a passive to an active form can result in sequestering sufficient anti-apoptotic protein for Bak and Bax to homo-oligomerise and form pores leading to the mitochondrial outer-membrane permeabilisation (MOMP). MOMP allows the release of cytochrome c and Smac I (second mitochondria-derived activator of caspases, also known as

DIABLO) into the cytosol, the first committed step in the intrinsic apoptosis pathway (Figure 1.24). Smac I binds to IAP (apoptosis inhibitor) and inactivates it[99] whilst cytochrome c released from the mitochondria forms a complex with Apaf-1, a cytosolic protein that oligomerises in the presence of dATP and forms a protein complex known as the apoptosome (Figure 1.23), containing multiple caspase-recruitment domains (CARD) which activate caspase-9.

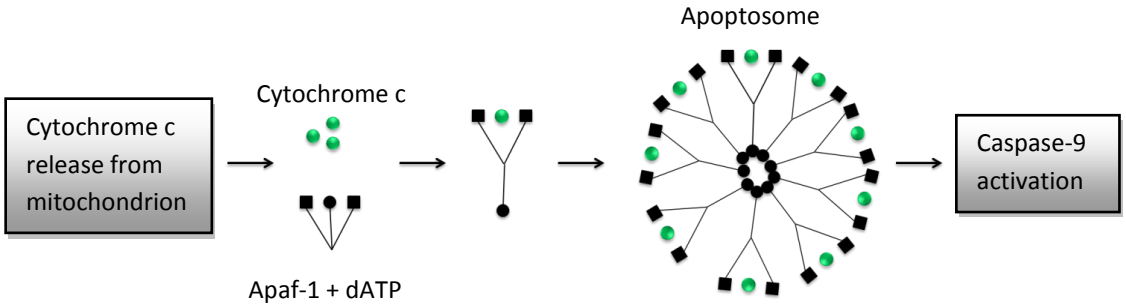

Figure 1.23: *Apoptosome assembly in the extrinsic pathway of apoptosis. Cytochrome c (green, round), CARD (black, round), and WD40 domain (black, square) are illustrated.*

1.5.5 Granzyme pathways

Cytotoxic T-cells are tasked with killing tumours or virus infected cells, for which purpose they employ Granzymes-A and -B. Granzymes are serine proteases that are delivered into target cells with the assistance of perforin, a transmembrane pore forming molecule.[100] The exact mechanism of entry into the cell is still a matter of debate with the strongest candidates being entry through the mannose-6-phosphate receptor or endocytosis during membrane repair processes triggered by calcium-loss. What is known is that their ability to induce apoptosis in human cells is strongly dependent on Bid, which granzymes truncate,[101] activating the downstream elements of the intrinsic apoptosis pathway; i.e. *via* capsase-9 (Figure 1.24).

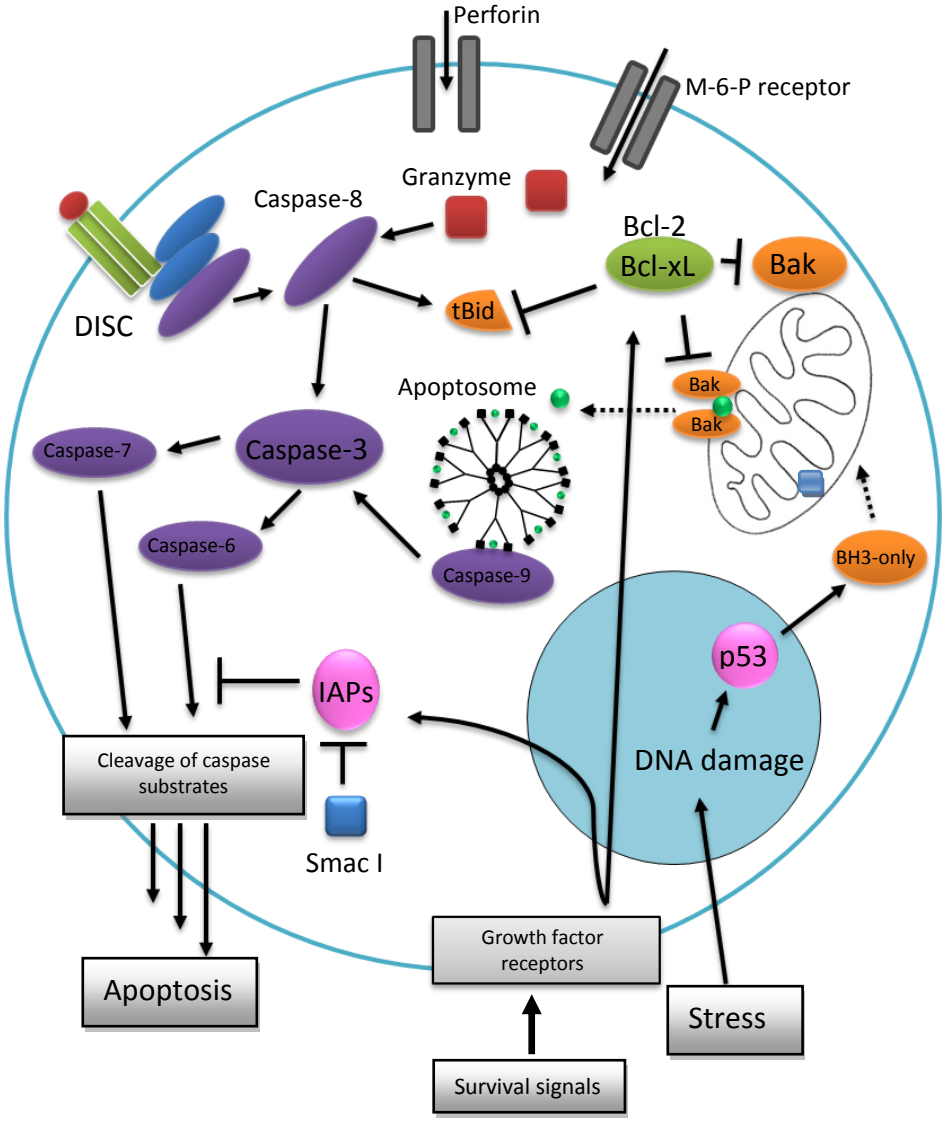

Figure 1.24: *Schematic representation of important apoptosis signalling interactions. The nucleus is in cyan and the mitochondrion above nucleus, showing the release of cytochrome c (green, round).*

1.6 Overview and Hypothesis

LOV based optogenetics tools have so far proven to be successful in controlling cellular functions as seen with LOV-Rac,[54-56] TULIPs,[57] and YF1/YHF.[59,60] As discussed earlier, Mills *et al.* have already demonstrated activation of apoptosis using an *As*LOV-Jα-caspase-7 hybrid.[58] However, executioner caspases such as caspase-7 rely on internal cleavage by upstream initiator caspases (caspase-8 and -9), which are activated allosterically on platforms such as the apoptosome, which is regulated by the Bcl-2 family of proteins. Since the Bcl-2 family consists of anti-apoptotic proteins that can inhibit executioner caspase activation, as seen with *As*LOV-Jα-caspase-7 and Bcl-2 overexpression,[58] apoptosis can be better regulated by targeting Bcl-2 proteins from further upstream of the apoptosis pathway. Limitations of optogenetics tools lay within the design concepts, as seen with LOV-DHFR.[53] This work tests the hypothesis that if various designs are produced and optimised using examples of successful LOV-based photo-switches then regulation of cellular pathways, such as apoptosis further upstream of caspase execution, can be conducted through fusions between LOV-Jα and catalytic domains such as the BH3 domain of proapoptotic Bcl-2 family of proteins.

1.7 Aim of the Investigation

The aim of this investigation is to develop and engineer a new optogenetic tool to control apoptosis. Bcl-x_L protein is a major regulator of apoptosis by binding and sequestering BH3 domains of pro-apoptotic proteins. Here we firstly aim to develop fusions of the *As*LOV2 domain to pro-apoptotic BH3 domains such that the BH3 domains are only available for interacting with anti-apoptotic proteins when illuminated with blue light. The second part of this research is to study and develop possible fusions using the YtvA-LOV domain, as this photo-receptor encompasses longer photo-recovery time and will allow longer duration for signalling *in vivo.* However, this second objective is complicated by the homodimeric form of the parent protein and therefore requires further investigation using mutational studies in order to understand the importance of specific amino acid residues on its homodimeric form.

Chapter 2:

Materials and

Methods

2.1 Materials

Chemicals were purchased from Chemodex, Fisher, Fluka, GE Healthcare, Merck, New England Biolabs, NovaBiochem, QIAGEN or Sigma-Aldrich. DNA primers (oligonucleotides) were purchased from Operon or Sigma-Aldrich.

A *p*NCO-Hisact plasmid containing the gene encoded for *Avena sativa* LOV2 fused to the C-terminus of hisactophilin was provided by from Prof. G. Richter (Cardiff University). YtvA-LOV-STAS (encoding both the single LOV domain and STAS domain) was cloned from *Bacillus subtilis.* A *p*ET 21a plasmid containing a gene encoding for loop truncated (1-209 Δ45-84, Δ210-233) Bcl-x_L was obtained from Dr. M. Crump (Bristol University)

2.1.1 Rich culture media

2.1.1.1 Luria Bertani (LB) medium

Bacto tryptone (10 g/L), yeast extracts (5 g/L) and sodium chloride (10 g/L) was dissolved in deionised water (dH_2O). The medium was transferred to bottles or flasks and autoclaved for 1 hour and 30 minutes at 15 lb/In^2.

2.1.1.2 Terrific broth (TB) medium

Bacto tryptone (12 g/L), yeast extracts (24 g/L) and glycerol (4 mL/L) was mixed in 900 mL of deionised water (dH_2O) and the medium was transferred to flasks. Monopotassium phosphate (2.31 g) and dipotassium phosphate (12.54 g) were dissolved in distilled water (100 mL) and autoclaved alongside the medium for 1 hour and 30 minutes at 15 lb/In^2. Once both solutions had cooled to room temperature they were mixed.

2.1.2 Agar plates

Agar plates were prepared using autoclaved LB medium containing agar (15 g/L) and a magnetic stirring bead. After the media had cooled to approximately 40 °C the appropriate concentration of antibiotic added and the mixture was stirred. The solution was then poured in to 90 mm Petri dishes using aseptic techniques. Once set, the agar plates were stored inverted at 4 °C. For cell growth a solution of bacterial culture was spread over the

agar plate using a sterile glass rod. The plates were then incubated inverted at 37 °C overnight (15-16 hours).

2.1.3 Preparation of antibiotic solutions

An ampicillin stock solution in distilled water (50 mg/mL) was used to create a final concentration of 100 µg/mL in media. A stock solution of kanamycin in distilled water (25 mg/mL) was used to create final concentration of 50 µg/mL.

2.1.4 Escherichia coli strains

E. coli BL21 (DE3) and BL21 (DE3) star strains were used for expression of plasmids (Table 2.14). They contain the λDE3 lysogen carrying the gene for T7 RNA polymerase under the control of *lac*UV5 promoter allowing induction of the expression of recombinant proteins with isopropyl-1-thio-β-D-galactopyranoside (IPTG). The BL21 (DE3) star cells exhibit enhanced mRNA stability due to a mutation in the RNaseE gene (*rne*131), which reduces levels of endogenous RNases and mRNA degradation, increasing the stability of mRNA transcripts and increasing protein yield. Protein expression is further enhanced by the absence of the *lon* and outer membrane (*Omp*T) proteases, which reduces degradation of heterologous proteins. The XL-1 Blue strain was used as a host for optimal propagation of plasmids and was used for cloning where high transformation efficiencies were required.

Strain	Genotype
BL21(DE3)	F– *omp*T *hsd*SB (rB- mB-) *gal dcm* (DE3)
BL21(DE3)*	F– *omp*T *hsd*SB (rB– mB–) *gal dcm rne*131 (DE3)
XL1-Blue	*end*A1 *rec*A1 *gyr*A96 *thi*-1 *hsd*R17 *sup*E44 *rel*A1 *lac* [F' *pro*AB *lacl*qZΔM15 Tn10 (Tet^r)]

Table 2.1: *Genotype of the Escherichia coli strains used in this study.*

2.1.5 Oligonucleotides (Primers)

Oligonucleotide sequences used for Bcl-x_L and in the cloning of *As*LOV-BID proteins and YtvA-LOV are listed below.

	Name	Sequence (5' – 3')
1	Hisact-*As*LOV2-V416I	*For*: GAACGTATTGAGAAGAACTTTATTATTACTGACCCACGTTTGCC *Rev*: GGCAAACGTGGGTCAGTAATAATAAAGTTCTTCTCAATACGTTC
2	Hisact-*As*LOV2-V416I-BID	*LOVBID F1:* CGAACATGTCCGTGATTGCGCCGAGGATTGGTGTCAACATCGCGCGTCATCTGGC ACAGGTGGGTGAT *LOVBID F2:* AGCATTGATAGCCGTATTCCAGATGCTAATCTGCGTCCAGAGGATTTGTGGGCTA ACTA *LOVBID R1:* AGCTTAGTTAGCCCACAAATCCTCTGGACGCAGATTAGCATCTGGAATACGGCTA TCAATGCTATCACCCACCTGTGC *LOVBID R2:* CAGATGACGCGCGATGTTGACACCAATATCCTCGGCGCAATCACGGACATGTTCG GTAC
3	Hisact-*As*LOV-V416I-BID-PD547C_	*For*: GATAGCATTGATAGCCGTATTTGCTAAGCTAATCTGCGTCCAGAGG *Rev*: CCTCTGGACGCAGATTAGCTTAGCAAATACGGCTATCAATGCTATC
4	YtvA-LOV-STAS-pET19b	*YtvA F:* ATCTCGCGCATATGGCTAGTTTTCAATCATTTGG *YtvA R:* GGAGGATCCTTACATAATCGGAAGCACTTTAACG
5	YtvA-LOV	*YtvALOV F:* CTGCACTTTCAACTTAATAACCTATTGTCCCGATTCGC *YtvALOV R:* GCGAATCGGGACAATAGGTTATTAAGTTGAAAGTGCAG
6	YtvA-LOV-V27D	*V27D F*: CACGTGCGAGTCGGTGATGTAATTACAGATCCCG *V27D R*: CGGGATCTGTAATTACATCACCGACTCGCACGTG
7	YtvA-LOV-I113D	*I113D F*: GATCCAATGGAAGATGAGGATAAAACG *I113D R*: CGTTTTATCCTCATCTTCCATTGGATC

8	*As*LOV-BID1 (pET28a)	*LB-Pet F: TATATA*CATATGTTTCTTGCTACTACACTTGAACG *LB-Pet R:* AATTAAGGATCCTTAAGCTTAGTTAGCCCACAAATC
9	*As*LOV-BID2	*For 1:* CGAACATGTCCGTGATGCGGCCGAGCGTGAGGGTGTC *LOVBID2 F2:* ATGCTGATTAAGGATATTGCACGTAATATTGATCGTGCG *LOVBID2 F3:* CTGGCGGAAGTGGGTGATAGCATTGATCGTAGCATTTA *LOVBID2 R1:* AGCTTAAATGCTACGATCAATGCTATCACCCAC *LOVBID2 R2:* TTCCGCCAGCGCACGATCAATATTACGTGCAATATCCTT *Rev 3:* AATCAGCATGACACCCTCACGCTCGGCCGCATCACGGACATGTTCGGTAC
10	*As*LOV-BID3	*For 1:* CGAACATGTCCGTGATGCGGCCGAGCGTGAGGGTGTC *LOVBID3 F2:* ATGCTGATTAAGAAAACTGCAGATATTATTGATAACGCGGCACGT *LOVBID3 F3:* GAACTTGCACAGGTGGGTGATAGCATTGATCGTAGCATTTA *LOVBID3 R1:* AGCTTAAATGCTACGATCAATGCTATCACCCAC *LOVBID3 R2:* CTGTGCAAGTTCACGTGCCGCGTTATCAATAATATCTGCAGTTTTCTT *Rev 3:* AATCAGCATGACACCCTCACGCTCGGCCGCATCACGGACATGTTCGGTAC
11	*As*LOV-BID4	*For 1:* CGAACATGTCCGTGATGCGGCCGAGCGTGAGGGTGTC *LOVBID4 F2:* ATGCTGATTAAGAAAACTGCAGAAAATGATATTGCGCGTAATATC *LOVBID4 F3:* GCGCGTCATCTGGCACAGGTGGGTGATAGCATTGATCGTAGCATTTA *LOVBID4 R1:* *AGCTTAAATGCTACGATCAATGCTATCACCCACCTGTGC* *LOVBID4 R2:* CAGATGACGCGCGATATTACGCGCAATATCATTTTCTGCAGTTTTCTT *Rev 3:* AATCAGCATGACACCCTCACGCTCGGCCGCATCACGGACATGTTCGGTAC
12	*As*LOV-BID5	*For 1:* CGAACATGTCCGTGATGCGGCCGAGCGTGAGGGTGTC *LOVBID5 F2:* ATGCTGATTAAGAAAACTGCAGAAAATATTGATGAGGCG *LOVBID5 F2.5:* GCAAAAGAACTTGATATTATTCGTAATATCGCGCGTCATCTG *LOVBID5 F3:* GCACAGGTGGGTGATAGCATTGATCGTAGCATTTA *LOVBID5 R1:* AGCTTAAATGCTACGATCAATGCTATC *LOVBID5 R2:* ACCCACCTGTGCCAGATGACGCGCGATATTACGAATAATATCAAG *LOVBID5 R2.5:* TTCTTTTGCCGCCTCATCAATATTTTCTGCAGTTTTCTT

		Rev 3: AATCAGCATGACACCCTCACGCTCGGCCGCATCACGGACATGTTCGGTAC
13	Bcl-x_L-S2C	*For:* GGAGATATACATATGTGCCAGTCTAACCGTG
		Rev: CACGGTTAGACTGGCACATATGTATATCTCC

Table 2.2: *DNA sequences of oligonucleotides used for cloning and site-directed mutagenesis of engineered proteins.*

2.1.6 Preparation of reagents and buffers

2.1.6.1 TFB I buffer for super-competent cells

30 mM Potassium acetate

100 mM Rubidium chloride

10 mM Calcium chloride

50 mM Manganese chloride

15 % (v/v) Glycerol

The solids were dissolved in distilled water and the pH was adjusted to 5.8 using acetic acid. The resulting solution was stored at 4 °C.

2.1.6.2 TFB II buffer for super-competent cells

10 mM 3-(N-morpholino)propanesulfonic acid (MOPS)

75 mM Calcium chloride

10 mM Rubidium chloride

15 % (v/v) Glycerol

The solids were dissolved in distilled water and the pH was adjusted to 6.5 using sodium hydroxide. The solution was stored at 4 °C.

2.1.6.3 P1 buffer for QIA DNA isolation protocol

50 mM Tris(hydroxymethyl)aminomethane hydrochloride (Tris HCl)

10 mM Ethylene diaminotetracetic acid (EDTA)

The solids were dissolved in water and the pH was adjusted to 8.0 then 50 µg/ml RNase A was added to the buffer.

2.1.6.4 P2 buffer for QIA DNA isolation protocol

200 mM Sodium hydroxide

1 % (w/v) Sodium dodecyl sulfate (SDS)

2.1.6.5 N3 buffer for QIA DNA isolation protocol

4 M Guanidine hydrochloride

500 mM Potassium acetate

Once dissolved in water, the pH was adjusted to 4.2 using acetic acid.

2.1.6.6 PB buffer for QIA DNA isolation protocol

5 M Guanidine hydrochloride

20 mM Tris HCl

38 % (v/v) Ethanol

Once the solids were dissolved in water, the pH was adjusted to 6.6 and then ethanol was added to the final volume.

2.1.6.7 PE buffer for QIA DNA isolation protocol

20 mM Sodium chloride

2 mM Tris(hydroxymethyl)aminomethane (Tris base)

80 % (v/v) Ethanol

Once the solids were dissolved in water, the pH was adjusted to 7.5 and then ethanol was added.

2.1.6.8 TAE 50x (Tris-acetate/EDTA) agarose gel electrophoresis buffer

2 M Tris base

6 % (v/v) Glacial acetic acid

0.5 M EDTA

Once the solids were dissolved in water, the pH was adjusted to pH 8.0.

2.1.6.9 Gel loading buffer for agarose gel electrophoresis

0.25 % (w/v) Bromophenol blue

15 % (v/v) Glycerol

2.1.6.10 Resolving-gel buffer for SDS-PAGE

1.5 M Tris base

The solution was adjusted to pH 8.8 using hydrochloric acid and the buffer was stored at 4 °C.

2.1.6.11 Stacking-gel buffer for SDS-PAGE

0.5 M Tris base

The solution was adjusted to pH 6.8 using hydrochloric acid and the buffer was stored at 4 °C.

2.1.6.12 10x SDS-PAGE running buffer

250 mM Tris base

1.9 M Glycine

1 % (w/v) SDS

Once the solids were dissolved in water, the pH was adjusted to pH 8.3.

2.1.6.13 SDS-PAGE gel-loading buffer

1.25 mL Stacking-gel buffer

2 mL SDS solution (10% w/v)

0.2 mL Bromophenol blue

2.5 mL Glycerol

0.5 mL β-Mercaptoethanol

Volume made up to 10 mL with distilled water.

2.1.6.14 Staining solution for SDS-PAGE

0.25 % (w/v) Comassie brilliant blue

45 % (v/v) Methanol

10 % (v/v) Glacial acetic acid

2.1.6.15 De-staining solution for SDS-PAGE

10 % (v/v) Glacial acetic acid

40 % (v/v) Ethanol

2.1.6.16 0.1 M Isopropyl β-D-1-thiogalactopyranoside

0.24 g Isopropyl β-D-1-thiogalactopyranoside (IPTG)

IPTG was dissolved in distilled water, the volume was then made up to 10 mL and the solution was sterilized by passing it through a 0.2 µm syringe filter.

2.1.6.17 0.5 M Phenylmethylsulfonyl fluoride

0.87 g Phenylmethylsulfonyl fluoride (PMSF)

1 mL Isopropanol

PMSF was dissolved in isopropanol and stored at 4 °C.

2.1.6.18 Phosphate buffered saline (1x PBS)

137 mM Sodium chloride

2.7 mM Potassium chloride

10 mM Disodium phosphate

1.8 mM Monopotassium phosphate

The solids were dissolved in distilled water; then the solution was adjusted to pH 7.4 using hydrochloric acid and made up to the required volume with distilled water..

2.1.6.19 Buffer for fluorescent labelling

50 mM Tris base

100 mM Sodium chloride

2 mM Tris(2-carboxyethyl)phosphine (TCEP)

The solids were dissolved in distilled water; then the solution was adjusted to pH 8.3 using sodium hydroxide and made up to the required volume with distilled water.

2.1.6.20 LOV protein purification buffers

1.7.1.1.1 *Cell lysis buffer*

50 mM Disodium phosphate

300 mM Sodium chloride

10 mM Imidazole

0.02 % (w/v) Sodium azide

The solids were dissolved in distilled water and the pH was adjusted to 8.0 using hydrochloric acid. PMSF from a stock solution in isopropanol was added separately to cell suspension (final concentration 0.1 M) immediately prior to lysis.

2.1.6.20.1 *Ni-NTA affinity chromatography: Ni- NTA binding buffer*

50 mM Disodium phosphate

300 mM Sodium chloride

10 mM Imidazole

0.02 % (w/v) Sodium azide

Once the solids were dissolved in distilled water the solution was adjusted to pH 8.0 using hydrochloric acid and made up to the required volume with further distilled water.

2.1.6.20.2 *Ni-NTA affinity chromatography: wash buffer*

50 mM Disodium phosphate

300 mM Sodium chloride

40 mM Imidazole

0.02 % (w/v) Sodium azide

Once the solids were dissolved in distilled water the solution was adjusted to pH 8.0 using hydrochloric acid and made up to the required volume with further distilled water.

2.1.6.20.3 *Ni-NTA affinity chromatography: Elution buffer*

50 mM Disodium phosphate

300 mM Sodium chloride

500 mM Imidazole

0.02 % (w/v) Sodium azide

Once the solids were dissolved in distilled water the solution was adjusted to pH 8.0 using hydrochloric acid and made up to the required volume with further distilled water.

2.1.6.20.4 *Size-exclusion chromatography purification buffer A*

50 mM Disodium phosphate

100 mM Sodium chloride

Once the solids were dissolved in distilled water the solution was adjusted to pH 7.5 using hydrochloric acid and made up to the required volume with further distilled water. The buffer was degassed under reduced pressure before use.

2.1.6.21 UV spectroscopy buffer

50 mM Disodium phosphate

100 mM Sodium chloride

Once the solids were dissolved in distilled water the solution was adjusted to pH 7.5 using hydrochloric acid and made up to the required volume with further distilled water.

2.1.6.22 CD spectroscopy buffer

50 mM Disodium phosphate

10 mM Sodium chloride

Once the solids were dissolved in distilled water the solution was adjusted to pH 7.5 using hydrochloric acid and made up to the required volume with further distilled water.

2.1.6.23 Fluorescence anisotropy assay buffer

50 mM Disodium phosphate

10 mM Sodium chloride

Once the solids were dissolved in distilled water the solution was adjusted to pH 7.5 using hydrochloric acid and made up to the required volume with further distilled water. The buffer was filtered before use.

2.1.6.24 Unfolding buffer

50 mM Disodium phosphate

300 mM Sodium chloride

10 mM Imidazole

0.02 % Sodium azide

4.5 M Guanidinium thiocyanate

Once the solids were dissolved in distilled water the solution was adjusted to pH 8.0 using hydrochloric acid and made up to the required volume with further distilled water.

2.1.6.25 Bcl-x_L protein purification buffers

2.1.6.25.1 *Buffer A1*

100 mM Disodium phosphate

500 mM Sodium chloride

5 mM Imidazole

1 mM PMSF (added immediately prior to use)

Once the solids were dissolved in distilled water the solution was adjusted to pH 7.5 using hydrochloric acid and made up to the required volume with further distilled water.

2.1.6.25.2 *Buffer A2*

100 mM Disodium phosphate

500 mM Sodium chloride

5 mM Imidazole

Once the solids were dissolved in distilled water the solution was adjusted to pH 7.5 using hydrochloric acid and made up to the required volume with further distilled water.

2.1.6.25.3 *Buffer B*

100 mM Disodium phosphate

500 mM Sodium chloride

50 mM Imidazole

The buffer was adjusted to pH 7.5.

2.1.6.25.4 *Buffer C1*

100 mM Disodium phosphate

500 mM Sodium chloride

100 mM Imidazole

Once the solids were dissolved in distilled water the solution was adjusted to pH 7.5 using hydrochloric acid and made up to the required volume with further distilled water.

2.1.6.25.5 *Buffer C2*

100 mM Disodium phosphate

500 mM Sodium chloride

150 mM Imidazole

Once the solids were dissolved in distilled water the solution was adjusted to pH 7.5 using hydrochloric acid and made up to the required volume with further distilled water.

2.1.6.25.6 *Buffer C3*

100 mM Disodium phosphate

500 mM Sodium chloride

200 mM Imidazole

Once the solids were dissolved in distilled water the solution was adjusted to pH 7.5 using hydrochloric acid and made up to the required volume with further distilled water.

2.1.6.25.7 *Buffer D*

100 mM Disodium phosphate

500 mM Sodium chloride

500 mM Imidazole

Once the solids were dissolved in distilled water the solution was adjusted to pH 7.5 using hydrochloric acid and made up to the required volume with further distilled water.

2.1.6.25.8 *Size-exclusion chromatography purification buffer B*

50 mM Disodium phosphate

100 mM Sodium chloride

5 mM β-Mercaptoethanol

The buffer was adjusted to pH 7.5 with hydrochloric acid and the buffer was filtered and degassed before β-mercaptoethanol addition.

2.2 Methods

2.2.1 Preparation of competent cells

The calcium chloride method was used to prepare competent cells.[111] LB medium (100 mL) was aseptically inoculated with the desired *E. coli* strain. The culture was incubated overnight at 37 °C with vigorous shaking. The following day a sample (1 mL) of the culture was used to inoculate fresh LB media (100 mL) and the flask was incubated at 37 °C with vigorous shaking. Upon reaching an OD_{600} of 0.6 the flask was cooled on ice (or 4 °C) for 20 min and then centrifuged at 4000 rpm for 10 min at 4 °C. The supernatant was discarded and the pellet was re-suspended in calcium chloride solution (20 mL, 100 mM $CaCl_2$ pH 7.0; sterilised by autoclaving or with a syringe filter) and cooled on ice for 20 min, and then centrifuged again. The pellet was re-suspended in calcium chloride solution (6 mL, 100 mM $CaCl_2$ with 15 % glycerol (w/v), pH 7.0; sterilised using syringe filter) and cooled on ice for 20 min. Aliquots (100 µL) were flash frozen in liquid nitrogen and stored at -80 °C.

2.2.2 Preparation of super-competent cells

The rubidium chloride method[111] was used to prepare super-competent cells. The desired *E. coli* strain (1 mL) was used to inoculate LB media (100 mL). The culture was incubated overnight at 37 °C with vigorous shaking. The following day a sample (1 mL) of the culture was used to inoculate fresh LB media (100 mL) and the flask was incubated at 37 °C with vigorous shaking. Upon reaching an OD_{600} of 0.6 the flask was cooled on ice (or 4 °C) for 15 min and then centrifuged at 5000 rpm for 5 min at 4 °C. The supernatant was discarded and the pellet was re-suspended in TFB I buffer (40 mL, sterilised by autoclaving or with a syringe filter) and cooled on ice for 15 min, and then centrifuged again. The pellet was re-suspended in TFB II buffer (4 mL) and cooled on ice for 15 min. Aliquots (100 µL) were flash frozen and stored at -80 °C.

2.2.3 Transformation

Plasmid DNA (1-5 µL) was mixed with competent (or super-competent) cells (100 µL) in a 1.5 mL Eppendorf tube and incubated on ice (4 °C) for 30 min. The cells were subjected to a heat shock in a 42 °C water bath for 45 sec and then placed on ice for 2 minutes. LB medium (0.75-1 mL) was added to the cells and incubated at 37 °C for 1 hr. The solution was then centrifuged at 10,000 rpm for 30 sec on a bench top microcentrifuge. The supernatant was

discarded and the pellet was re-suspended in fresh LB medium (100 µL). The solution was spread on an agar plate containing the appropriate antibiotic(s) and then incubated overnight at 37 °C.

2.2.4 DNA isolation, purification and storage

2.2.4.1 QIAprep spin miniprep kit

Plasmid DNA was prepared from overnight cultures of *E. coli* in LB medium (5 mL) according to the manufacturer's instructions.

2.2.4.2 Agarose gel electrophoresis

Agarose gels were used for analysis and isolation of DNA fragments. For 1% agarose gels 1× TAE buffer (50 mL) was used to dissolve agarose (0.5 g) by heating the suspension in a microwave oven until homogeneous. The mixture was then poured into the minigel kit and left to set. Samples were mixed with the gel-loading buffer and loaded into the gel and run in 1× TAE buffer at 100 V for 60 minutes after which time the gel was stained with ethidium bromide and DNA visualised using an UV lamp at 254 nm. DNA fragments were extracted from the agarose gel with a clean, sharp scalpel. The QIAquick Gel Extraction Kit was used according to the manufacturer's instructions (QIAGEN).

2.2.4.3 Alcohol precipitation

Alcohol precipitation was used to adjust DNA concentrations, for purification and as a method of storing DNA over long periods. The DNA sample was gently mixed with ammonium acetate (to a final concentration of 2-2.5 M), then absolute ethanol (2.5 volumes) was added and the sample was incubated at 25 °C for 10 min. The solution was then centrifuged at 13,500 rpm for 15 min on a bench top microcentrifuge. The supernatant was discarded and the pellet was gently washed with 80 % (w/v) ethanol, and then centrifuged for 10 min. The supernatant was discarded and the pellet was allowed to dry for 20 min. The sample was then stored at -20 °C or diluted to the required concentration.

2.2.4.4 Glycerol stocks

Samples from an overnight culture of XL-1 Blue cells harbouring the desired plasmid (0.6 mL) were aseptically mixed with sterile 50 % glycerol (0.6 mL). The stocks were stored at -80 °C until used to inoculate LB medium for preparation of overnight cultures.

2.2.5 Quantification of DNA and oligonucleotides in solution

The concentration of nucleic acids was determined using a Thermo Scientific NanoDrop 1000 photospectrometer, by measuring the optical density (OD) of a solution of DNA or oligonucleotide at 260 nm.

2.2.6 Digestion with restriction enzymes

Digestion reactions were performed with plasmid DNA (10 µL of 200 ng/µL DNA) and the appropriate restriction endonuclease (1 µL, 20,000 units/mL) in their recommended buffers (New England Biolabs). Reactions were incubated for 3-4 hours at 37 °C. For double digestions the buffer used was the recommended one that gave the highest digestion efficiency for both enzymes. The DNA product for the digestion was analysed by agarose gel electrophoresis.

2.2.7 Dephosphorylation of DNA fragments

Following digestion with a single restriction enzyme, the vector was dephosphorylated at the 5' end with Antarctic Phosphatase to avoid self-ligation. DNA (10 μL^{-1} from 0.5 µg stock) was suspended in 1× Antarctic Phosphatase buffer (New England Biolabs) and 5 units of Antarctic Phosphatase were added to the mixture. The solution was incubated for 15 minutes at 37 °C. The enzyme was heat inactivated (at 65 °C) for 5 minutes, and DNA purified using the QIAquick PCR purification protocol according to the manufacturer's instructions.

2.2.8 Phosphorylation of DNA fragments

Oligonucleotide stock solutions (100 pmol/ mL) were diluted to 50 pmol/ mL with deionised water. Equal volumes of all forward oligonucleotides were combined to a total of 50 pmol, prior to phosphorylation. The same procedure was also applied to reverse oligos. The phosphorylation of forward and reverse mixtures were carried out in separate Eppendorf tubes; the combined oligonucleotides were phosphorylated at the 5'-end with 0.5 µL of

20,000 units/mL of T4 polynucleotide kinase (New England Biolabs) in T4 ligase buffer (50 mM Tris pH 7.5, 10 mM magnesium chloride, 10 mM dithiothreitol, 1 mM adenosine triphosphate, 25 μg/mL bovine serum albumin). The solutions were incubated at 37 °C for 30 minutes, and subsequently purified using the QIAquick PCR purification protocol and stored at -20 °C for future use.

2.2.9 Annealing oligonucleotides

Equimolar quantities of oligonucleotides were mixed in deionised water in an Eppendorf tube that was placed in a thermal cycler at 95 °C. The temperature gradually was reduced to 15 °C over a period of 15 hours. The annealed oligonucleotides were stored at -20 °C.

2.2.10 Ligation reaction

Ligation reactions were carried out to insert desired genes into an expression vector. Digested plasmid (50 ng/μL) and the annealed oligonucleotides (50 ng/μL) or digested DNA fragments (50 ng/μL) were mixed together to a 1:3 or 1:5 ratio with 1 μL T4 DNA ligase (10 units/μL) and 1 μL 10× T4 DNA ligase buffer (400 mM Tris, pH 7.8, 100 mM magnesium chloride, 100 mM dithiothreitol, 5 mM ATP). The solution was then incubated at 4 °C overnight (in polystyrene box to allow gradual cooling) or at 16 °C for 4 hours. Ligation products were stored at -20 °C.

2.2.11 Polymerase chain reaction (PCR)

Each reaction was prepared in a 0.5 mL thin-walled PCR tube to a final volume of 50 μL containing 50 ng/μL DNA (0.3 μL, 0.5 μL or 0.8 μL), Pfu polymerase buffer (5 μL 10x), mutagenic primers (2 μL from 10 pmol/ μL stock of each forward and reverse primers), deoxynucleotide triphosphates (1 μL, 0.2 mM each of dATP, dCTP, dGTP and dTTP), magnesium sulfate (1 μL, 25 mM) and Pfu polymerase (0.5 μL, 2.5U/ μL).

The temperatures were adjusted in each case according the melting temperatures of the primers being used. A typical cycle was as follows: 1 min at 95 °C (denaturation), 1 min at 55 °C (annealing) and 1 min/1000 base-pairs at 72 °C (extension). This cycle was repeated 30 times.

Amplification of the desired DNA fragment was confirmed by agarose gel electrophoresis and PCR products were stored at -20 °C.

2.2.12 Mutagenesis

The mutagenic primers were designed using PrimerX (Web-based program: Automated design of mutagenic primers for site-directed mutagenesis) using the following parameters: 70-85 °C melting temperature, 35-60 % GC content and termination in G or C residues. PCR was carried out on the sample using temperatures considering the melting temperature of the primers being used. Once the reaction was complete *Dpn*I (1 μL, 20 units) was added to each of the samples which were then incubated for 1.5 hours at 37°C. The products were stored at -20 °C.

2.2.13 DNA Sequencing

All sequencing reactions were carried out by Cardiff University sequencing services or Eurofins MWG Operon DNA sequencing service.

2.3 General Methods for Protein Preparation and Analysis

2.3.1 Growth of bacterial cultures

Overnight cultures were grown in sterile conditions by inoculating from glycerol stock or a single colony from an agar plate into LB medium (5 mL) containing the appropriate antibiotic. The cultures were incubated overnight at 37 °C with constant shaking at 150 rpm (Innova 43/44 incubator shaker).

2.3.2 Protein expression using the T7 system

Chemically competent cells were transformed with plasmid DNA, plated onto selective media and grown overnight at 37 °C. Individual colonies were then picked and grown overnight in LB medium (100 mL) containing the appropriate antibiotic. Samples from the overnight culture were transferred to fresh LB or TB (for LOV protein expression) medium (5 mL inoculum per 500 mL) containing the appropriate antibiotic in 2 L conical flasks, and incubated until they reached an OD_{600} of 0.6-0.8. The cells were then induced by the addition of IPTG to a final concentration of 1 mM, and left to grow for 4 to 6 hours (Bcl-x_L) or overnight at 20 °C (LOV proteins). Samples (0.5 mL) were taken from each flask (including a sample prior to induction) and a SDS-PAGE was used to assess the extent of the expression of the target protein. The cells were then centrifuged at 6,000 *g* (Sorvall RC6 Plus) for 30 minutes at 4 °C and pellets were stored at -20 °C.

2.3.3 Purification of LOV proteins

2.3.3.1 Cell lysis

Frozen pellets were thawed on ice and re-suspended by vortexing in cell lysis buffer. The suspension was sonicated for 6 minutes (3 s on, 5 s off) on ice using a Sonicator W-37 (Heat Systems Ultrasonics Inc.). The resulting lysate was centrifuged at 12,000 g for 30 minutes. The supernatant was transferred to a separate tube and a sample was taken for SDS-PAGE analysis. The remainder of the supernatant was purified immediately and the pellet was kept for analysis.

2.3.3.2 Purification by Ni-NTA affinity chromatography

The supernatant containing the protein was loaded onto a Ni-NTA agarose (QIAGEN) packed column pre-washed in Ni-NTA binding buffer. After loading the protein on to the column, it was washed with 1.5 column volumes of wash buffer. The bound protein was then eluted from the column with the elution buffer and the sample was kept at 4 °C until further purification. Samples (10 μL) of each of the flow-through, washed solution and eluted protein sample were kept for analysis by SDS-PAGE.

2.3.3.3 Thrombin cleavage of LOV2 protein

The protein sample was dialysed against a large volume (4 L) of PBS buffer pH 7.4 (137 mM NaCl, 2.7 mM KCl, 10 mM Na_2HPO_4, 1.8 mM KH_2PO_4) for 4 hours. Calcium chloride (4.5 μL, 25 mM) and thrombin protease (50 μL, ~50 units = 10 NIH units) was added and the sample was incubated overnight at 20°C. The following day the protein was purified using Ni-NTA affinity chromatography. The cleaved sample was allowed to flow through the pre-washed column with *As*LOV2 protein recovered from the flow-through solution. The resin was eluted with elution buffer and each sample was analysed using SDS-PAGE.

2.3.3.4 Purification by size-exclusion chromatography (SEC)

The eluted protein sample (up to 10 mL) was loaded onto a Superdex-75 10/300 GL (GE Healthcare) column pre-equilibrated with the size-exclusion chromatography Buffer A. The column was run at 2.5 mL/min and 10 mL fractions were collected. The eluted protein

fraction was wrapped in foil and stored at 4 °C. A sample (10 µL) was retained for SDS-PAGE analysis.

2.3.4 Purification of Bcl-x_L

2.3.4.1 Cell lysis

Frozen pellets were thawed on ice and re-suspended by vortexing in buffer A1. The suspension was sonicated for 5 minutes (5 s on, 10 s off) on ice using a Sonicator W-37 (Heat Systems Ultrasonics Inc.). The resulting lysate was centrifuged at 15,000 g for 30 minutes. To the supernatant was transferred to a separate tube. A sample (10 µL) was retained for SDS-PAGE analysis and the remainder of the protein was purified immediately. The pellet was also kept for analysis.

2.1.1.1 Purification by Ni-NTA affinity chromatography

The supernatant containing the protein was loaded onto a Ni-NTA agarose (QIAGEN) packed column pre-washed in buffer A2. After passing the solubilised protein through the column, it was washed with 1.5 column volumes of buffer B. The bound protein was then eluted using a step gradient elution using buffers C1-C3 (3 mL of each) collecting fractions (1.5 mL) then finally buffer D (10 mL). The sample was kept at 4 °C until further use.

2.3.4.2 Purification by size-exclusion chromatography (SEC)

Protein samples (up to 10 mL) were loaded onto a Superdex 75 10/300 GL (GE Healthcare) column pre-equilibrated with buffer B. The column was run at 2.5 mL/min and fractions (10 mL) were collected. The eluted protein fraction was stored at 4 °C.

2.3.5 Dialysis of pure proteins

In order to remove undesired components, the protein was dialysed using Medicell International Ltd. dialysis membrane (12,000-14,000 MWCO) in the appropriate buffer with stirring at 4 °C. The dialysis was carried out overnight in 5 L of buffer for large volumes of protein solution, or in 500 mL to 1 L, exchanging to fresh buffer every 1 hour in 3-5 intervals for smaller volumes of protein solution.

2.3.6 Sodium dodecyl sulfate polyacrylamide gel electrophoresis

Precursor solutions for 12 % resolving gels were created by mixing degassed deionised water (3.4 mL), acrylamide/bisacrylamide (4 mL, 30 %), Tris buffer (2.5 mL, 1.5 M, pH 8.8), sodium dodecylsulfate solution (SDS, 0.1 mL, 10 % w/v) with polymerising agents ammonium persulfate (APS, 100 µL, 10 % w/v in water) and tetramethylethylenediamine (TEMED, 15 µL). The solution was immediately poured between assembled glass plates with integrated 0.75 mm spacers and left to polymerise under a layer of isopropanol at room temperature. A 5 % stacking gel was created by mixing deionised water (5.7 mL), degassed acrylamide/bisacrylamide (1.7 mL 30 %), Tris buffer (2.5 mL, 0.5 M, pH 6.8), SDS (0.1 mL, 10 % w/v) containing was mixed with APS solution (100 µL, 10 %) and TEMED (10 µL) and pipetted on top of the resolving gel. A comb was immediately inserted between the plates and the stacking gel was left to polymerise at room temperature. The comb was then removed and the wells rinsed with 1× SDS running buffer. Samples, mixed with 1× SDS gel-loading buffer, were loaded into the gel (15 µL in the 10-well gels and 8 µL in the 15-well gels) and subjected to 160 V potential for 60 minutes. After electrophoresis, the gel was stained and destained using the corresponding solutions, followed by visualisation of the protein bands on a light box equipped with a UV lamp.

2.3.7 Measurement and calculation of protein concentration

2.3.7.1 Determination of protein concentration

The concentrations of proteins were determined spectrophotometrically using a Jasco V-660 UV/Vis spectrophotometer. The measurements were taken three times for accuracy and the following equation was used to calculate the concentration:

$$C = \frac{A}{\varepsilon l}$$

Where C is the concentration in mg/mL, A is the absorbance; ε is the extinction co-efficient and *l* is the pathlength in cm.

2.3.7.1.1 *LOV proteins*

The concentration of LOV proteins was determined using an extinction co-efficient of 12,550 $M^{-1}cm^{-1}$ at 407 nm (an isosbestic point) using a clean quartz cuvette subtracting a blank measurement of buffer alone.

2.3.7.1.2 *Bcl-x_L*

The concentration of Bcl-x_L was determined using an extinction co-efficient value of 41,940 $M^{-1}cm^{-1}$ at 280 nm (isosbestic point) using a clean quartz cuvette subtracting a blank measurement of buffer alone.

2.3.7.1.3 *Labelled protein*

To determine the concentration of tetramethylrhodamine-5-maleimide labelled protein an extinction coefficient of 91,000 $M^{-1}cm^{-1}$ at 550 nm was used using a clean quartz cuvette subtracting a blank measurement of buffer alone.

2.3.8 Mass spectrometry (MS)

2.3.8.1 MALDI-TOF MS

Matrix assisted laser desorption/ionisation-time of flight (MALDI-TOF) mass spectrometry was performed to identify the purified proteins and peptides. α-Cyano-4-hydroxycinnamic acid in 1:1 MeCN/H_2O was used as the matrix.

2.3.8.2 ESI-TOF MS

Electrospray ionisation-time of flight (ESI-TOF) mass spectrometry was preformed to identify the purified proteins. The sample was prepared in deionised water and concentrated to 200-250 µM using a spin concentrator (10,000 MWCO).

2.4 General Method for Peptide Synthesis and Purification

2.4.1 Peptide synthesis

All peptides were synthesized according to standard fluorenylmethylcarbamoyl (Fmoc) solid phase synthesis protocols using a CEM Liberty microwave-assisted peptide synthesizer. The amino acids were protected with trityl (Trt), tert-butyl (tBu), butoxycarbonyl (Boc) or 2,2,4,6,7- pentamethyldihydrobenzofuran (Pbf) sidechain protecting groups as required, O-benzotriazole-N,N,N',N'-tetramethyl-uronium-hexa-fluorophosphate (HBTU), hydroxyl-benzotriazole (HOBt), N- methylpyrrolidinone (NMP) and dimethylformamide (DMF) were purchased from AGTC Bioproducts. Dichloromethane (DCM), trifluoroacetic acid (TFA) and diethyl ether were sourced from Fisher. Piperidine, acetic anhydride, triisopropylsilane (TIS), N,N-diisopropylethylamine (DIEA), 4-(2-hydroxyethyl)-1-piperizineethanesulfonic acid (HEPES) and triscarboxyethylphosphine (TCEP) were purchased from Sigma Aldrich. Rink Amide resin (0.72 mmol/g) was purchased from NovaBioChem. The procedure used for the synthesis of all peptides was as described by Wysoczanski *et al.*[107]

Steps	Solutions
Activator	0.45 M HBTU in DMF
Deprotection mix	20% piperidine, 0.1 M HOBt in DMF
Activator base	2 M DIEA in NMP
Capping solution	20% acetic anhydride in DMF
Amino acid solutions	0.1 M solutions of Fmoc-protected amino acids in DMF: Fmoc-Ala-OH, Fmoc-Arg(Pbf)-OH, Fmoc-Asn(Trt)-OH, Fmoc-Asp(tBu)-OH, Fmoc-Cys(Trt)-OH, Fmoc-Gln(Trt)-OH, Fmoc-Gly-OH, Fmoc-Leu-OH, Fmoc-Ile-OH, Fmoc-Phe-OH, Fmoc-Thr(tBu)-OH, Fmoc-Val-OH
Cleavage cocktail	95% TFA, 2.5% TIPS, 2.5% water

Table 2.3: *The solutions that were used for peptide synthesis.*

Peptide	Sequence
LOVBid	DCAEDIGVNIARHLAQVGDSIDRSI-NH_2
Ac-Bak wt	Ac-GQVGRQLAIIGDDINR-NH_2
CG_Bid wt	CGDIIRNIARHLAQVGDSIDRSI-NH_2

Table 2.4: *Peptides synthesized for fluorescence anisotropy studies (Ac-Bak peptide was provided by Dr. Robert Mart from Cardiff University).*

2.4.2 Peptide purification and identification

The peptide samples were purified by reverse phase HPLC (Dionex) using a Phemonenex Gemini C18 column (10 µm, 110 A, 10×250 mm) with an water/gradient from 0 % to 100 % acetonitrile (0.1 % TFA) containing in water (0.1 % TFA) over 50 min at a flow rate of 5 mL/min (Figures 10 and 15), peaks were collected, identified by MALDI-TOF MS (Matrix: α-cyano-hydroxy-cinnamic acid in 1:1 ratio of CH_3CN/H_2O) and the samples were freeze-dried and kept at -20 °C until further use.

The purity of peptides was confirmed using analytical HPLC using an Acclaim Dionex Ultimate-3000 equipped with a Acclaim C18 column (3 µm, 120 A, 4.6×150 mm) with a gradient from 100% water (0.1% TFA) to 100% acetonitrile (0.1% TFA) over 50 minutes at a flow rate of 1 mL/minute. Peptides were identified using MALDI-TOF MS.

2.4.3 Determination of peptide concentration

The extinction coefficient of the fluorescent dye was used to determine the concentration of labelled peptides using the Thermo Scientific NanoDrop 1000 spectrophotometer. The following labelling dyes were used: Fluoresceinamide (FAM) with extinction coefficient of 72,000 M-1 cm-1 at 494 nm, Tetramethylrhodamin-5-maleimide (TMR) with extinction coefficient of 91,000 M-1 cm^{-1} at 550 nm.

2.5 Fluorescent Labelling

For fluorescent labelling, protein samples were dialysed or peptide freeze-dried samples were dissolved in Tris (50 mM, pH 8.3) buffer containing sodium chloride (100 mM) with TCEP (2 mM, added from 100 mM stock) reducing agent and incubated with maleimidofluorescein or maleimidotetramethylrhodamine at 15 °C overnight for proteins (at 300 rpm, using Eppendorf Thermo Mixer Comfort), and 4 °C overnight for peptides. The protein samples were dialysed into 50 mM disodium phosphate buffer pH 7.5 to remove excess dye, and size exclusion chromatography was carried out for further purification. The peptide samples were purified and their identities were confirmed by reverse phase HPLC and MALDI-TOF MS. Peptide samples were freeze-dried and redissolved in buffer for fluorescent anisotropy experiments.

2.6 Photoswitching

2.6.1 Dark state

Dark state measurements of LOV proteins were recorded after the sample was kept in a dark bottle, covered in foil for a minimum of 2 hours at 4 °C.

2.6.2 Light state

A royal blue (455 nm peak wavelength) Luxeon K2 LAMRT Light emitting diode (LED) was used to photoswitch proteins. For CD spectroscopy and fluorescence anisotropy measurements samples were irradiated for 30 sec before taking measurements, for all UV/Vis spectroscopic measurements samples were directly irradiated in spectrometer.

2.7 UV/ Visible Absorption Measurements

UV/Visible absorption experiments were carried out using a JASCO V-660 UV/Vis Spectrophotometer with a 1 cm path length quarts cuvette. Single wavelength kinetics measurements were carried out at 447 nm and the half-life ($t_{½}$) of LOV proteins was calculated using the following equation:

$$t_{1/2} = \frac{\ln 2}{k}$$

Where *k* is the first order rate constant for the relaxation process, which was calculated by plotting the natural logarithm of the absorbance at 447 nm versus time

2.8 Circular Dichroism (CD) Spectroscopy

CD spectra were recorded on a Applied Photophysics ChiraScan spectrometer. Measurements were recorded at 20 °C using a 0.1 cm path length quartz cuvette. Temperature dependent measurements of protein structure were carried out over a temperature range of 4–96 °C. The mean residue ellipticities [Θ]r (deg cm^2 $dmol^{-1}$) of different states of LOV2 proteins were calculated according to the equation:

$$[\Theta]_r = \frac{\Theta}{(10\ \mathrm{n\ c\ l})}$$

Where, Θ is the measured ellipticity in mdeg, *n* is the number of backbone amide bonds, *c* is the concentration and *l* is the pathlength (0.1 cm).

The percentage change in α-helical content at 222 nm of LOV2 proteins from dark to light states were calculated from the following equations:

$$\%\ difference = \frac{L[\Theta_{222}]}{D[\Theta_{222}]} \times 100$$

$$\%\ change = 100 - \%\ difference$$

2.9 Binding Assay using Fluorescence Anisotropy

Fluorescence anisotropy measurements were performed at 15 °C on a Perkin Elmer LS55 luminescence spectrometer arranged in L format (FAM: 492 nm excitation, 520 nm emission TMR: 545 nm excitation, 573 nm emission). A quartz fluorescence cuvette (4 mL) contained labelled protein or peptide (2.5-10 nM) in sodium phosphate buffer (3 mL, 50 mM, pH 7.5) containing sodium chloride (10 mM). Bak peptide, Bcl-x_L or LOV2 proteins at concentrations of 0-5000 nM were successively added to cuvette. For peptide-peptide or peptide-protein assays each anisotropy value was from twenty single measurements were taken using an

integration time of 1 sec. For protein-protein binding assays each anisotropy value was from ten single measurements taken using an integration time of 5 sec.

The *G* factor (ratio of sensitivities of the monochromator for horizontally and vertically polarised light) can be calculated using the equation:[108]

$$G = \frac{I_{HV}}{I_{HH}}$$

Where, I_{HH} and I_{HV} are the intensities of the fluorescent emissions in parallel and perpendicular planes, respectively to the excitation plane. The *G* factor value was always close to 1.16 for FAM-labelled peptides and 0.85 for TMR-labelled proteins. Values for fluorescence anisotropy (*A*) were then determined from the equation:[109]

$$A = I_{HH} - \frac{GI_{HV}}{I_{HH}} + 2GI_{HV}$$

The data were fit to the Langmuir isotherm:

$$\emptyset_{Fit} = \frac{1}{1 + \left(\frac{{K_D}^n}{[P]^n}\right)}$$

Where, $\emptyset_{Fit}$ denotes the fraction of bound labelled-ligand, K_D is the apparent dissociation constant, [P] is the concentration of protein and *n* is the number of binding sites.

All binding curves were acquired independently at least three times and the resulting K_D values averaged. Errors are the standard errors of the mean for each concentration point.

Fluorescence anisotropy data were normalised and expressed as:

$$F = \frac{(A - A_D)}{(A_{max} - A_D)}$$

Where, *A* denotes the fluorescence anisotropy in the presence of the indicated concentration of protein, A_D denotes the fluorescence anisotropy in the absence of protein, and A_{max} denotes the fluorescence anisotropy at saturation.[110]

Chapter 3:

Avena sativa

LOV2

3.1 Aim

The aim of this project was to create modified versions of the second LOV domain of phototropin 1 from the plant *Avena sativa* to improve its properties for use as a photo-switch that can be further developed to control and regulate protein-protein interactions of important regulatory proteins.

3.2 Introduction

As previously described (Section 1.4.4), *As*LOV2 contains a five stranded anti-parallel β-sheet (β_2 α_4 β_3) (Figure 3.1). Upon formation of the FMN-cysteinyl adduct, rapid structural changes take place to amino acids of the Gβ, Hβ, Iβ strands and Eα helix[18] that affect the Jα helix. The Jα is initially docked to the β-sheet of the LOV2 core (Gβ, Hβ and Iβ strands), but the conformational changes result in disruption of the hydrophobic interactions that hold the Jα in the docked position.[112,30] Harper and co-workers[18] created a series of point mutations along the Jα to disrupt its hydrophobic interface in the absence of light. Using partial proteolysis and NMR spectroscopy they demonstrated that several of these mutations caused displacement and unfolding of the Jα helix. The photo-activated undocking mechanism of the wild type LOV domain will allow protein-protein binding using modified Jα fusions in the absence of the C-terminal kinase domain.

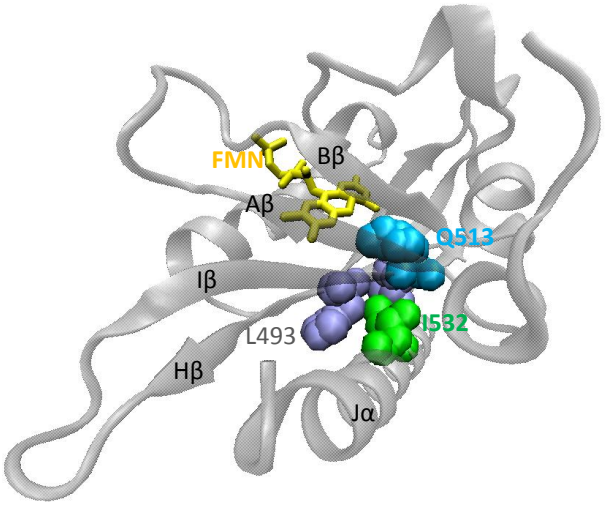

Figure 3.1: *Structure of AsLOV2 showing residue I532 (green) on the Jα helix, residue Q513 (blue) from the Iβ strand and residues L493 and H495 (gray) from the Hβ strand (PDB: 2V1B).*

A combination of crystallography and NMR spectroscopy of *As*LOV2[18,112,30] provided structural information that identified the residues responsible for the hydrophobic interaction between the β-sheet of the LOV core and the Jα helix (Figure 3.2). The side chain of I532 of the Jα helix packs between the side chains of L493 and H495 of the Hβ strand, holding the helix to the LOV core (Figures 3.1 and 3.2A). Residues K533 and T535 also anchor the Jα to the β-sheet through hydrogen bonding[112,30] with K533 forming a hydrogen bond network with E475, T477, H495 and Q497 (Figure 3.3A). The side chain of T535 forms a single hydrogen bond with K413 (Figure 3.3B). Residues I539, A542 and A543 are highly conserved hydrophobic residues at the C-terminal open-end of the Jα helix[112,30] suggesting that these are important residues for the docking of the Jα helix.

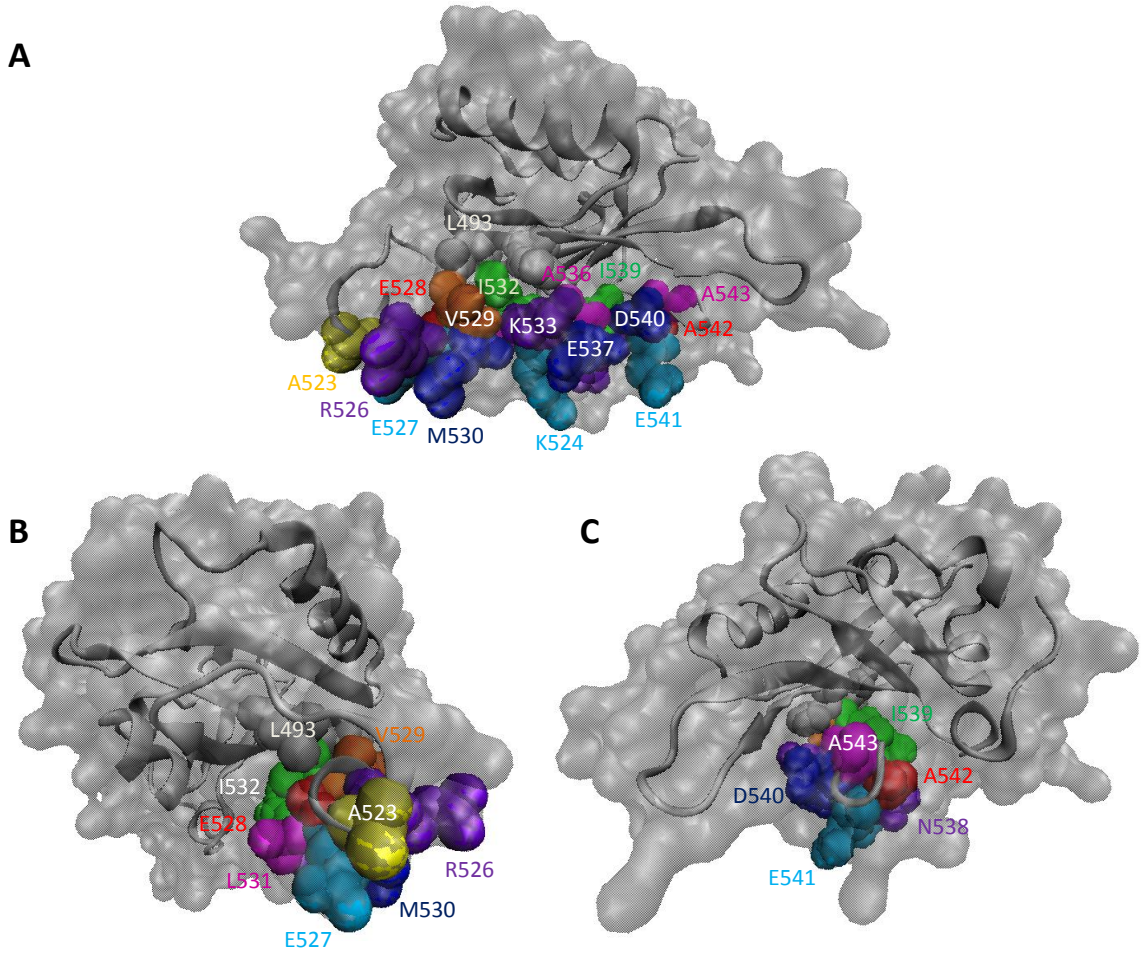

Figure 3.2: *Structures of AsLOV2 showing A) residues in the Jα helix and residues L493 and H495 from the Hβ strand (PDB: 2V1B), B) Jα helix from its N-terminal end representation C) Jα helix from C-terminal end.*

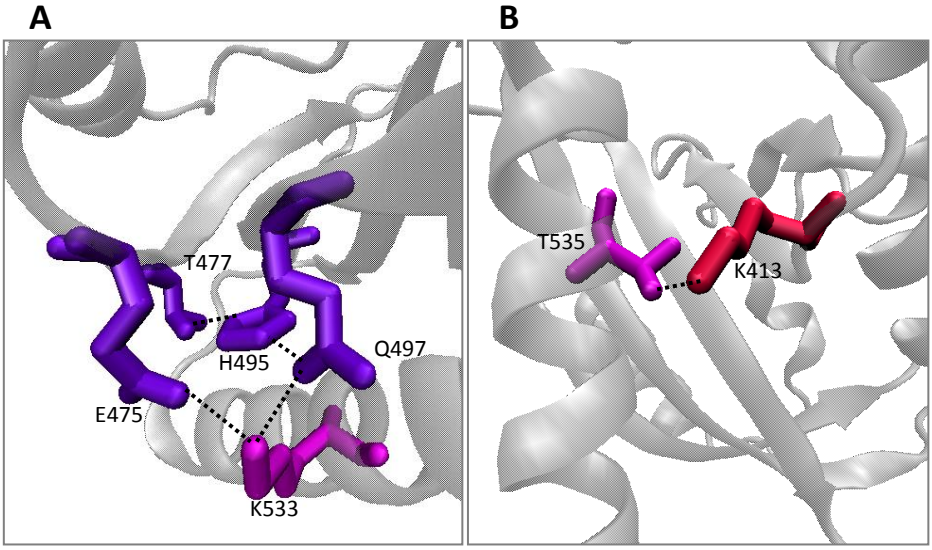

Figure 3.3: *The hydrogen bonding network between A) amino acid residues T477, H495, E475, and Q479 located in the hydrophobic core of LOV2 and K533 of the Jα helix. B) Hydrogen bond between residues K413 located in the hydrophobic core of LOV2 and T535 from the C-terminal end of Jα helix.*

The short photo-recovery time of *As*LOV2 has rendered it difficult to crystallise in the open form, therefore structural information available on the light state of *As*LOV2 is limited to irradiated crystals as opposed to a definite light state structure. The results from blue light irradiated crystals of LOV2 reveal that the FMN isoalloxazine ring is tilted towards the side chain of a highly-conserved glutamine residue (Q513) on the Iβ strand (Figure 3.4A and B) which forms hydrogen bonds with the O4 and N5 of the FMN isoalloxazine ring[30,37,113,115] (Figure 3.4C). Formation of a secondary hydrogen bond at N5 of FMN causes slight displacement of residue Q513, changing the structure of the FMN binding pocket and increasing Iβ strand dynamics and therefore disrupting the hydrophobic docking site for Jα helix as residue Q513 is located close to I532 (Figure 3.4B).[30,113]

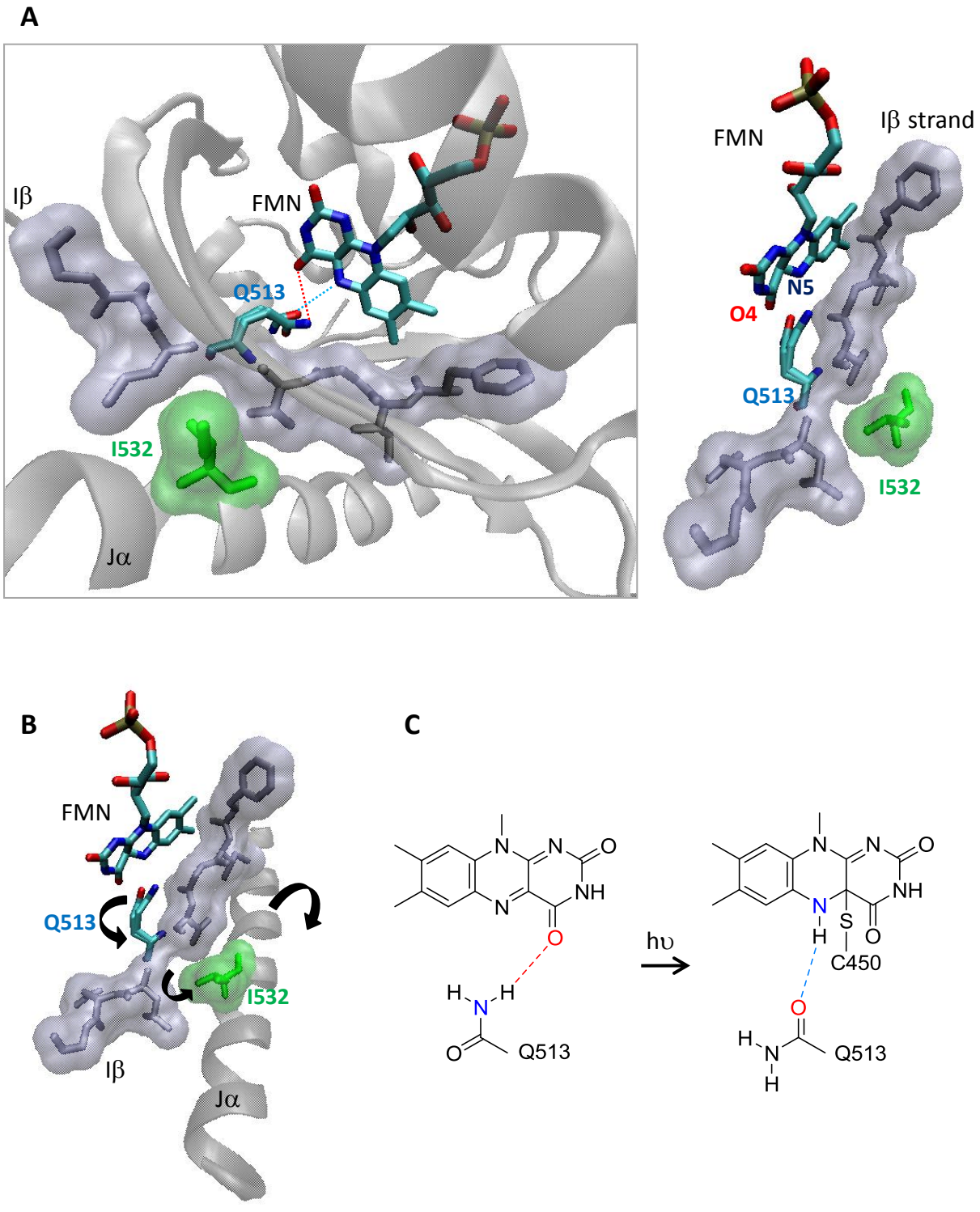

Figure 3.4: *Structures showing the connection between residue I532 (green) on the Jα helix and residue Q513 (blue) on the Iβ strand (remaining residues in gray) A) within the FMN binding pocket of AsLOV2 B) and also a schematic representation (shown by black arrows) of the possible conformational changes to the protein, C) due to formation of a secondary hydrogen bond (dashed lines) between Q513 and the N5 position of FMN upon light absorption (PDB: 2V1B).*

3.3 Results and Discussion

3.3.1 Expression and purification of AsLOV2 proteins

LOV proteins were expressed and purified by adapting the procedure of Kay *et al.*[120] (Section 2.3). *E. coli* BL21 (DE3) cells harbouring a pNCO-Hisact-*As*LOV2, containing a gene encoding the LOV2 domain of phototropin from *Avena sativa* fused to the hisactophilin protein from *Dictyostelium discoideum* were grown in LB medium. Over expression was induced by the addition of IPTG and after 5 hours SDS-PAGE showed copious amounts of the fusion protein (Figure 3.5) producing a luminous yellow protein solution. Histidine residues at the surface of the fused hisactophilin protein allowed purification by affinity chromatography using a nickel-nitrilotriacetic acid (Ni-NTA) resin and the eluted fractions were analysed using SDS-PAGE (Figure 3.6). Lane 5 of figure 3.6 shows vertical streaking of bands which may be as a result to high imidazole concentration in sample.

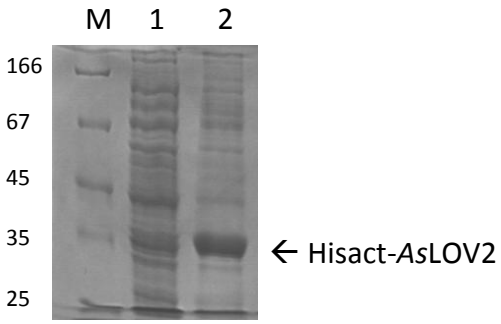

Figure 3.5: *SDS-PAGE analysis of Hisact-AsLOV2 expression. M: protein marker, lane 1: total cellular protein before induction, lane 2: total cellular protein 5 hours after induction.*

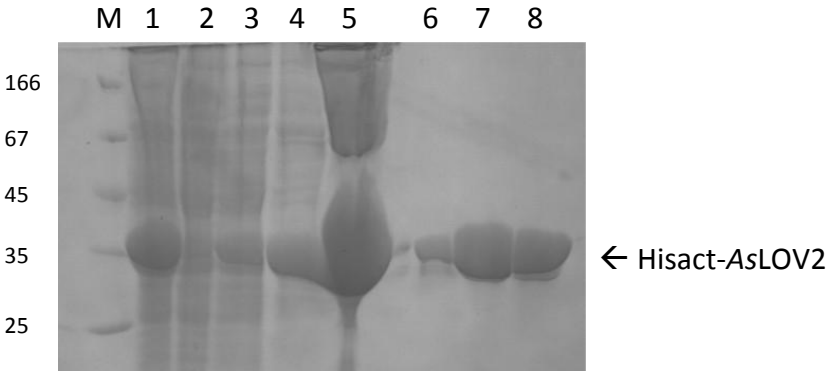

Figure 3.6: *SDS-PAGE analysis of Hisact-AsLOV2 at various stages of purification. M: protein marker, lane 1: supernatant after sonication of total cellular protein, lane 2: flow through from affinity column (10 mM imidazole), lane 3: wash (40 mM imidazole), lane 4: elution fraction 1 (200 mM imidazole), lane 5: elution fraction 2 (500 mM imidazole), lane 6-8: elution fractions after dialysis.*

Wild-type LOV2 has a relatively short lived light-state of 59.5 ± 3.2 seconds (Section 3.2.4), therefore a valine to isoleucine mutation that is known to stabilise the cysteinyl-FMN adduct[116] was introduced to generate a protein with a longer light-state half-life. Site-directed mutagenesis using Pfu polymerase to perform a V416I alteration generated the pNCO-Hisact-*As*LOV2-V416I plasmid and successful mutation of the codon was confirmed by sequencing (Appendix B). The protein was then expressed without any difficulty as before and MALDI-TOF MS was used to determine the protein mass of 32123.3 (without FMN) (Figure 3.7), this corresponded well to the calculated mass of 32700 which includes the FMN (456.34 for FMN).

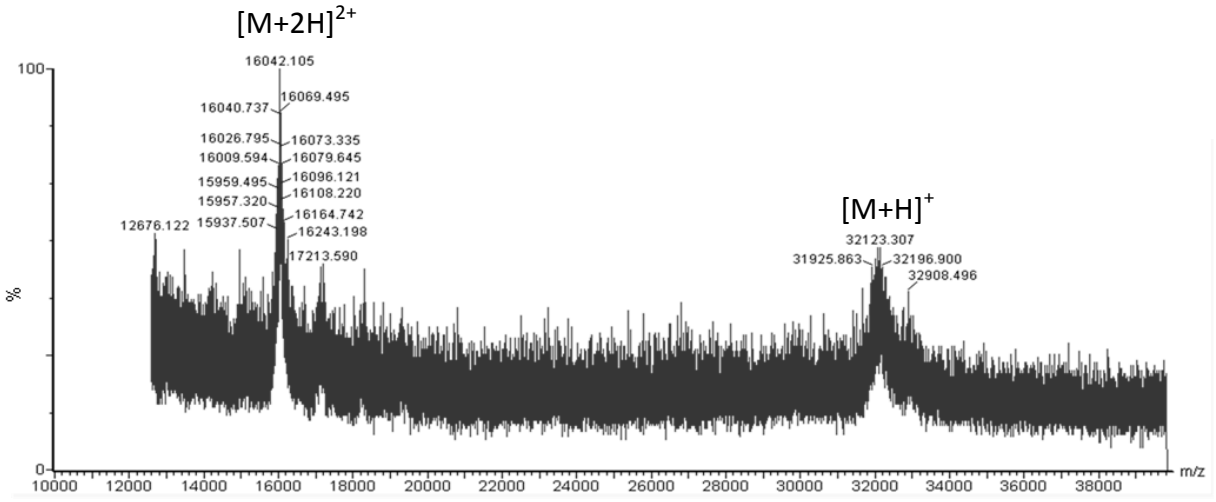

Figure 3.7: *MALDI-TOF spectrum of Hisact-AsLOV2-V416I (positive mode).*

In order to remove the fused hisactophilin, proteins were cleaved by thrombin at the target site (LVPR-GS) between the two domains. SDS-PAGE suggested incomplete cleavage by the continued presence of band at the correct size for Hisact-*As*LOV2-V416I (32.7 kDa). Bold bands at the lower region suggest that the hisactophilin (14.3 kDa) and LOV2 (18.4 kDa) have been cleaved successfully (Figure 3.8). Collection of the protein fraction that no longer bound to the Ni-NTA column was followed by size-exclusion chromatography which separated LOV2 from thrombin. The peak at approximately 110 mL is expected to be thrombin (36 kDa) as it is a colourless solution (Figure 3.9). LOV2 eluted at 190 mL (bright yellow solution), suggesting that there was mostly monomeric protein (Figure 3.9), as observed in previous studies.[33,120]

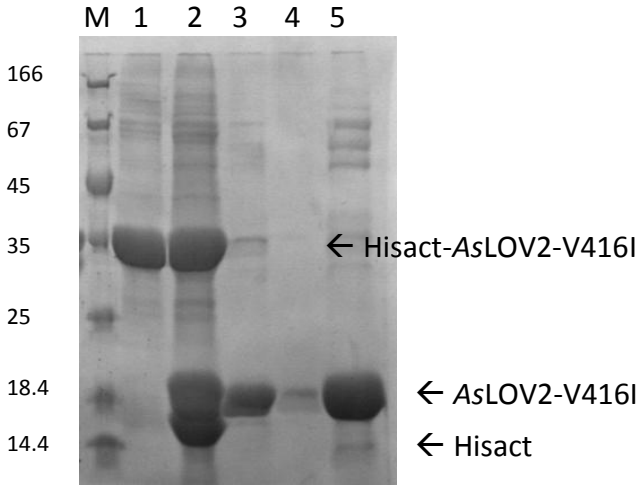

Figure 3.8: *SDS-PAGE analysis of AsLOV2-V416I through the stages of purification after thrombin cleavage. M: protein marker, lane 1: Hisact-AsLOV2-V416I before thrombin cleavage, lane 2: after overnight cleavage with thrombin, lane 3: flow through fraction after loading on Ni-NTA affinity column, lane 4: sample after dialysis, lane 5: concentrated sample.*

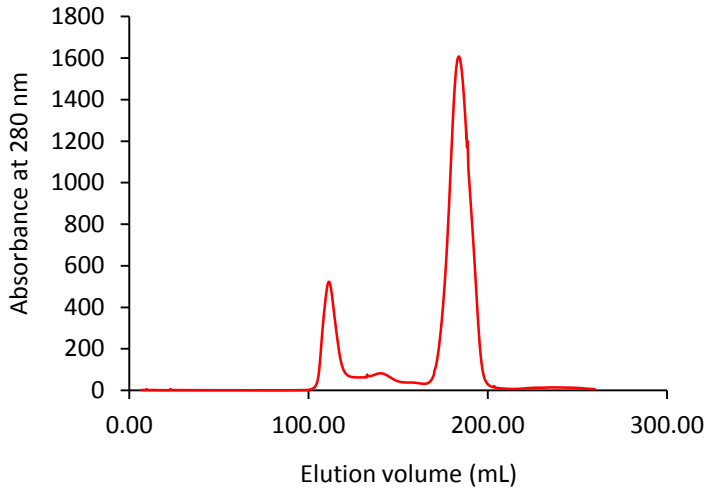

Figure 3.9: *Superdex-75 size-exclusion chromatogram of AsLOV2-V416I.*

3.3.2 UV/Vis spectroscopic characterisation of AsLOV2 proteins

As expected, UV/Vis spectra of dark adapted wild-type Hisact-*As*LOV2 showed an FMN absorption maximum at 447 nm with side bands at 427 nm and 474 nm[32,35,62] (Figure 3.10) due to vibronic coupling resulting in changes to the electronic and vibrational energy of the isoalloxazine ring within the environment of the FMN binding pocket.[125] After broad band UV irradiation using GG 455 band pass filter, the UV/Vis spectra of wild-type LOV2 reflected a photo-stationary equilibrium consisting of 80-90 % of LOV2 in the dark state, with the 447 nm maximum still clearly evident (Figure 3.10). Prolonged irradiation intervals with UV light passed through a WG 360 filter to remove < 360 nm light still did not completely diminish the 447 nm maximum, however after several hours a change in dark state spectra (red) was seen, likely due to protein degradation (Figure 3.10).

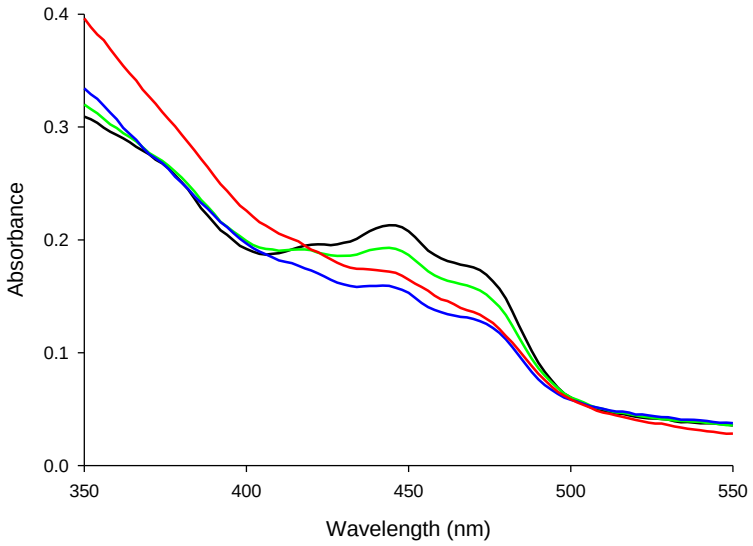

Figure 3.10: *UV/Vis absorption spectra of Hisact-AsLOV2 in the dark (black) immediately after irradiation for 1 min (green) and 10 min (blue), using UV lamp and filter WG 360. The relaxation of same sample after 6 hours is shown in red.*

Careful investigation of the cause of this lack of switching revealed a discrepancy between samples that had been purified by size exclusion chromatography and those purified by dialysis alone. Residual imidazole was speculated to be present from insufficiently stringent dialysis; imidazole, which resides in its basic form at pH 7.5-8, has previously been reported to enhance relaxation to dark state or cause incomplete conversion to light state. Alexandre *et al.* observed this effect and ascribed it to an imidazole 'base-catalysed' mechanism

(Figure 3.11) which prevents the hydrogen bond formation between Q513 and the FMN N(5)-H in the light state, thus detaching the proton from the N(5) position and therefore disrupting the FMN-cysteine covalent adduct.[30] Using a royal blue LED (Wavelength maxima at 455 nm) for irradiation did not improve switching for protein in the presence of imidazole (Figure 3.12)

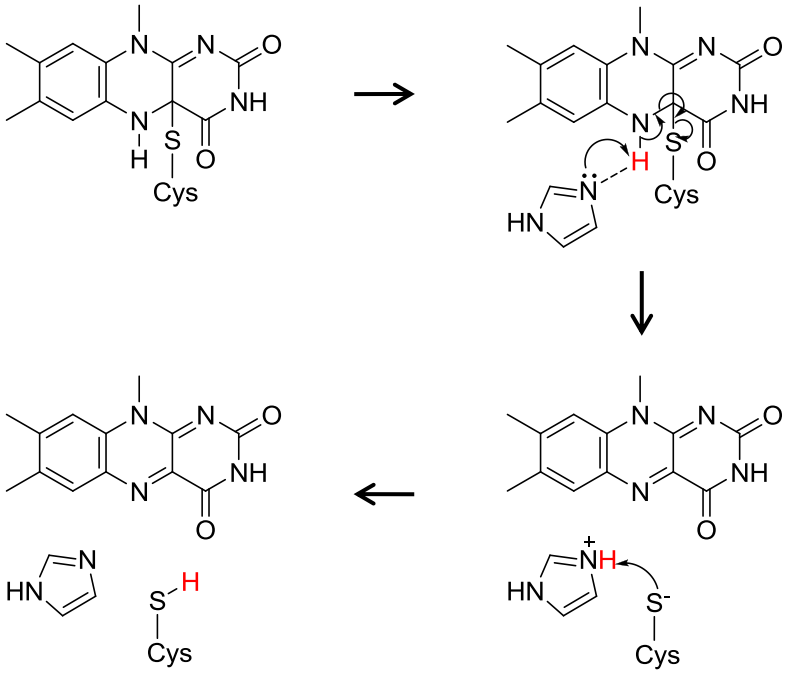

Figure 3.11: *Imidazole mediated 'base-catalysed' mechanism (ionic) of enhancing the FMN dark state relaxation.*

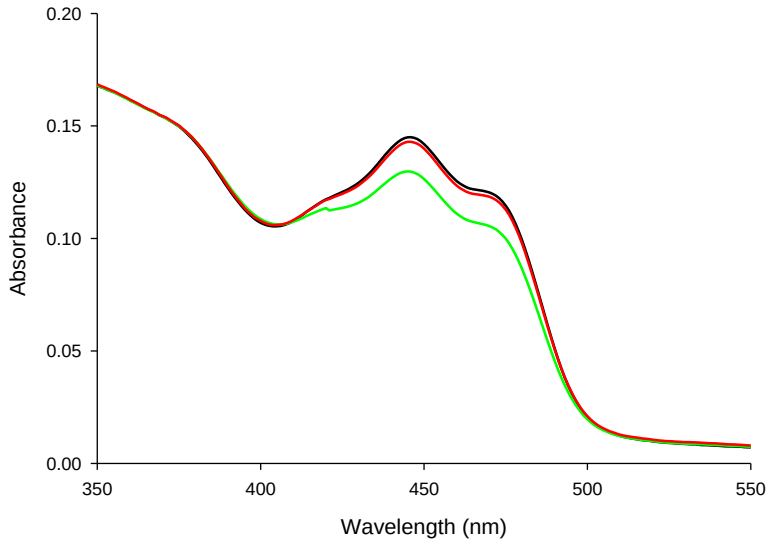

Figure 3.12: *UV/Vis absorption spectra of AsLOV2 (solution containing 500 mM imidazole) in the dark (black) immediately after irradiation for 1 min (green) and after 20 sec in the dark (red) using a Luxeon Rebel royal blue LED.*

However, LED irradiation after removing residual imidazole from the protein solution by extensive dialysis (Figure 3.6), allowed complete conversion to light state (Figure 3.13). Irradiated LOV2 domains recover to the dark state in a non-photochemical process. The sample was irradiated for 30 sec and the absorbance spectra was recorded every 2 min for 20 min (Figure 3.13). Isosbestic points for *As*LOV2-V416I at 330 nm, 380 nm and 407 nm (Figure 3.13) suggests that there is equilibrium between two chemical species. Absorbance at 407 nm was used to calculate protein concentration using an extinction-coefficient of 12,550 $M^{-1}cm^{-1}$ which was derived from the published extinction coefficient for the dark state protein of 13,800 M^{-1} cm^{-1} at 447 nm.[39]

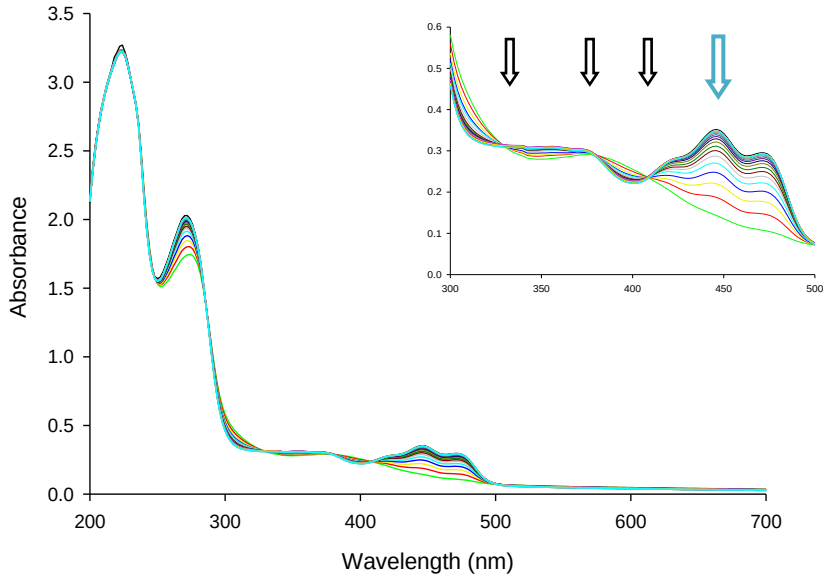

Figure 3.13: *UV/Vis absorption spectra of AsLOV2-V416I relaxation (reading at every 2 min) from light state (green) to dark state (black), the FMN absorption maximum visible at 447 nm (blue arrow) and three isosbestic points are seen at 330 nm, 380 nm and 407 nm (black arrows).*

3.3.3 Half- life measurements

UV/Vis absorption spectroscopy was used to perform time-course measurements at 447 nm, which enabled calculation of the half-life of the cysteinyl-FMN adduct in wild-type and various mutant LOV2 domains. The samples where irradiated for 30 sec and the absorbance measured every second for Hisact-*As*LOV2 and every 1 min for Hisact-*As*LOV2-V416I and *As*LOV2-V416I. The half-life of *As*LOV2 has been recorded between 27 and 81 seconds in previous studies.[32,35,116] In this study, the half-life of wild-type Hisact-*As*LOV2 at 20 °C, pH 7.5 was calculated to be 59.5 ± 3.2 seconds, whereas that of the Hisact-*As*LOV2-V416I mutant was extended to 461.3 ± 6.4 seconds and again to 684 ± 6 seconds for *As*LOV2-V416I (Figure 3.14).

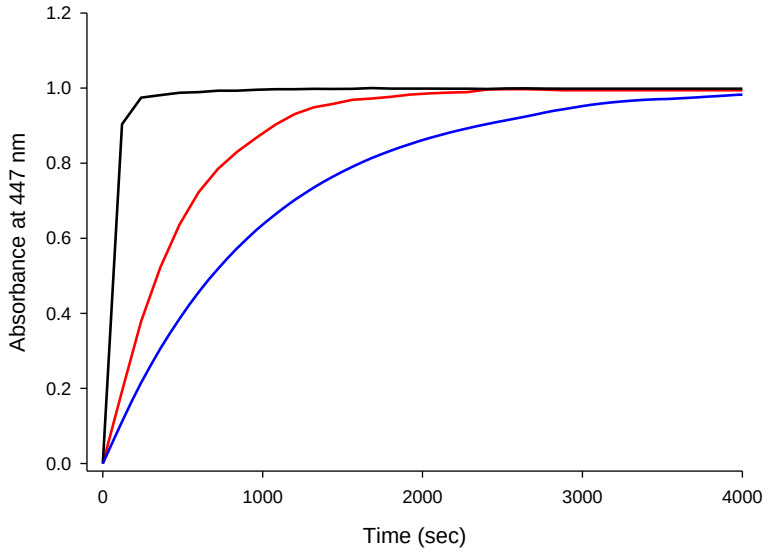

Figure 3.14: *UV/Vis absorption time-course measurements at 447 nm of Hisact-AsLOV2 (black) and Hisact-AsLOV2-V416I (red) and AsLOV2-V416I (blue).*

Valine 416 is located within the FMN pocket (Figure 3.15) and substitution to isoleucine (addition of a methyl group) sterically alters FMN dynamics and increases the light-state stability, therefore increasing the relaxation half-life. It has already been shown that imidazole (side chain in histidine residues) disrupts the FMN-cysteine adduct,[30] thus removal of the hisactophilin protein from the N-terminus of LOV2 may have altered the redox potential and light-state stability of FMN as the large numbers of histidine residues are no longer present. This would explain why *As*LOV2-V416I protein has a longer relaxation half-life than Hisact-*As*LOV2-V416I. Although, in comparison to the half-life determined by

Zoltowski, *et al.* (821 sec) *As*LOV2-V416I in this case has a faster relaxation half-life by 137 ± 6 seconds. However the half-life for V416I mutants is still significantly slower in comparison to wild-type LOV2, making it ideal to use as an optogenetics tool as prolonged irradiation periods will be illuminated and the risk of protein denaturation caused by heat from the light source will be reduced.

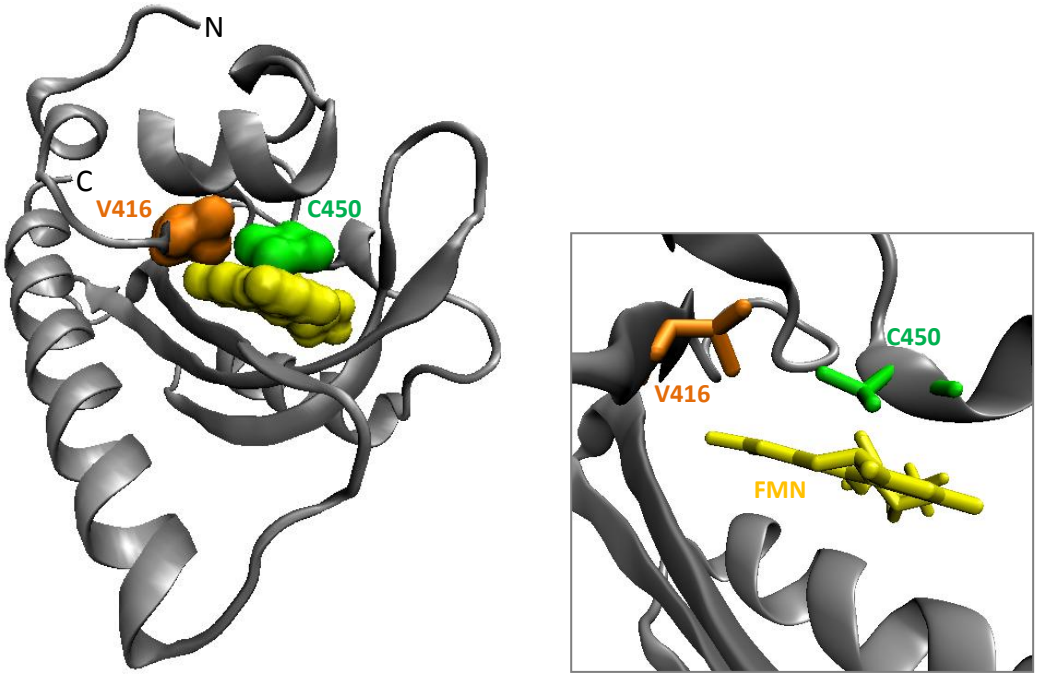

Figure 3.15: *Structure of AsLOV2 showing C450 (green), V416 (orange) and the FMN (yellow) within the FMN binding pocket.*

3.3.3.1 The effect of temperature on relaxation rates

The effect of temperature on Hisact-*As*LOV2 and Hisact- *As*LOV2-V416I was determined by repeating the time course measurements at temperatures between 10 °C and 37 °C at pH 7.5. The results show an increase in temperature causes an increase in rate of relaxation for both wild-type Hisact-*As*LOV2 (Figure 3.16) and Hisact-*As*LOV2-V416I (Figure 3.17). At 10 °C wild type LOV2 has a half-life of 142 seconds which decreases to 16 seconds as the temperature was increased to 37 °C. In contrast the mutant Hisact-*As*LOV2-V416I has a much longer half-life of 1385 seconds at 10 °C decreasing to 138 seconds as the temperature is increased to 37 °C.

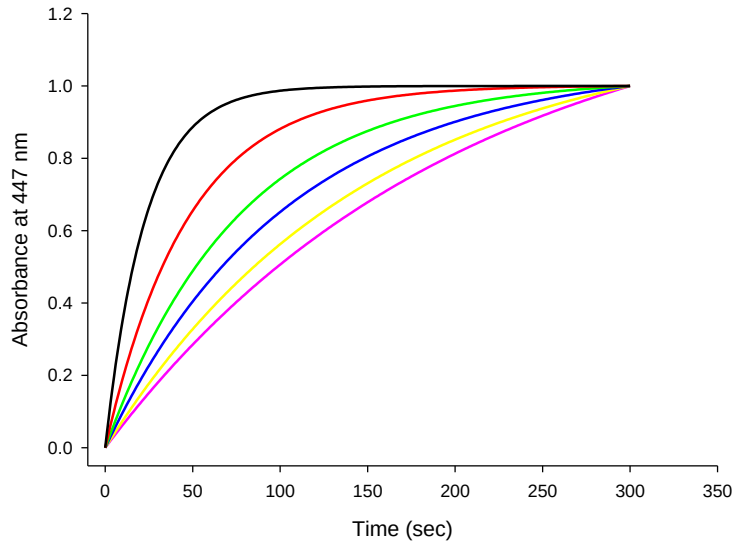

Figure 3.16: *UV/Vis absorption time-course measurements at 447 nm of irradiated Hisact-AsLOV2 at 10 °C (pink), 15 °C (yellow), 20 °C (blue), 25 °C (green), 30 °C (red) and 37 °C (black).*

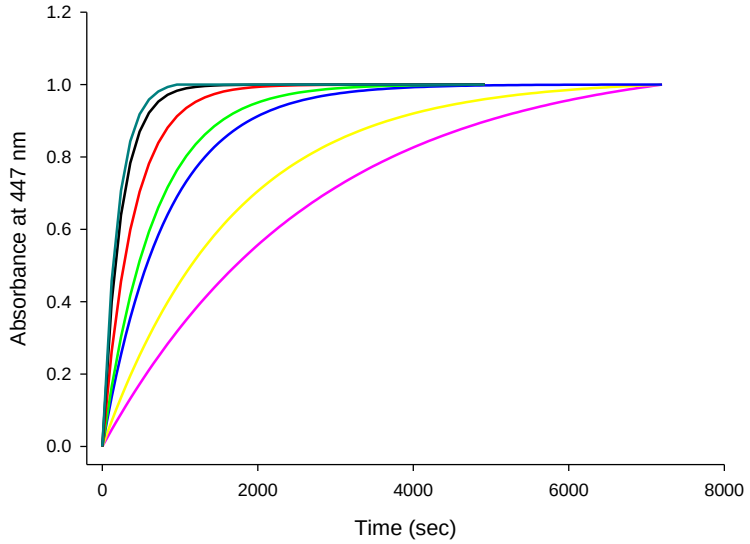

Figure 3.17: *UV/Vis absorption time-course measurements at 447 nm of irradiated Hisact-AsLOV2-V416I at 10 °C (pink), 15 °C (yellow), 18 °C (blue), 20 °C (green), 25 °C (red), 30 °C (black) and 37 °C (cyan).*

The time-course measurements were performed in triplicate for each temperature. The data was used to determine the activation energies in the thermal-relaxation of Hisact-*As*LOV2 and Hisact-*As*LOV2-V416I (Tables 3.1) using Arrhenius plots (Ln *k* versus 1/T) (Figure 3.18). Ln A is the intercept, where A is called the pre-exponential factor and the slope is equivalent to $-E_a/R$, where R is the gas constant and E_a is the activation energy. Reactions

that obey this equation show Arrhenius behaviour; LOV domains generally show linear Arrhenius behaviour for the temperature dependence for adduct relaxation.[127,129] In this case both wild type and mutant exhibited linear Arrhenius behaviour, as expected (Figure 3.18). Large activation energies signify that the rate is sensitive to the changes in temperature. The activation energies for Hisact-*As*LOV2 (57.3 kJ mol^{-1}) and Hisact-*As*LOV2-V416I (69.5 kJ mol^{-1}) differ slightly (Table 3.2), where Hisact-*As*LOV2-V416I has 12.2 kJ mol^{-1} higher activation barrier than wild type Hisact-*As*LOV2, suggesting that the mutant is slightly more sensitive to changes in temperature than wild type LOV2. This increase in activation energy has also been observed with other slow-cycling LOV mutants[128] and may be as a result of steric hindrance to the FMN-cysteine adduct formation, solvent accessibility or perturbation to the hydrogen bonding network of the isoallozaxine ring at N1, O2 and N3 positions. These factors all affect proton transfers within protein complexes; previous studies have determined that the rate limiting step for thermal recovery in LOV domains, are due to the proton transfer to the N5 of FMN,[30,35,129,130] and the activation energy barrier for the proton transfer step has been determined as 55 kJ mol^{-1}.[129]

Temperature	Hisact-*As*LOV2 Half-life (sec)	Hisact-*As*LOV2-V416I Half-life (sec)
10 °C	142.4 ± 29.9	1924.0 ± 12.5
15 °C	104.1 ± 2.4	1164.2 ± 10.6
18 °C	-	725.0 ± 37.7
20 °C	59. 5 ± 3.2	461.3 ± 6.4
25 °C	53.2 ± 3.5	273.0 ± 10.5
30 °C	32.7 ± 2.0	156.0 ± 14.1
37 °C	15.9 ± 1.3	137.6 ± 2.8

Table 3.1: *Half-life measurements of irradiated samples of Hisact-AsLOV2 and Hisact-AsLOV2-V416I; listing the average half-lives from three independent experiments and their standard deviation.*

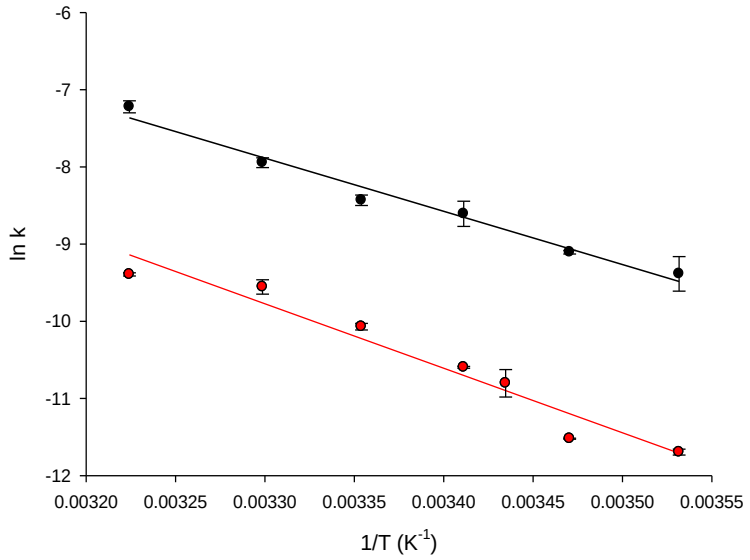

Figure 3.18: *Arrhenius plot of the relaxation rates of light state to dark state Hisact-AsLOV2 (black) and Hisact-AsLOV2-V416I (red).*

	E_A (kJ mol^{-1})	A (s^{-1})
Hisact-*As*LOV2	57.3	2.86×10^6
Hisact-*As*LOV2-V416I	69.5	5.45×10^7

Table 3.2: *Arrhenius parameters for the thermal relaxation of Hisact-AsLOV2 and Hisact-AsLOV2-V416I.*

3.3.3.2 The effect of pH on relaxation rates

The effect of pH on the relaxation of light-state Hisact-*As*LOV2-V416I was examined by recording time-courses monitoring absorbance at 447 nm over time at pH 6.5, 7.9, 7.5 and 8.0 (Figure 3.19). At each pH the average half-life differed by only a maximum of 31 sec (Table 3.4) however, all except pH 6.5 and pH 8.0 are within the errors. The protein samples at pH 6.5 showed precipitation after 8-12 hours and after 16-24 hours at pH 7.0, whereas samples at pH 7.5 and 8.0 lasted up to two weeks without precipitation of the protein. The results obtained correspond to preceding studies. Bogomolni *et al.,* used absorption difference spectroscopy to monitor proton transfers where light-induced adduct formation was found pH independent between pH 6.3 and pH 9.5.[129] Amino acid residues such as lysine, tyrosine, glutamate, aspartate and arginine have side chain groups with acid dissociation (pK) values outside the range for pH 6.3-9.5, suggesting that these groups do not interact with FMN and/ or that their ionisation energies are insignificant. Studies on the triplet state decay however was found to have a small change between pH 3.7 and pH 9.5, where slow chromophore release was monitored below pH 5,[129] this also corresponds to earlier studies that showed the same effect as the pK of cysteine in LOV2 is less than 4.[35]

The theoretical isoelectric point (pI) for Hisact-*As*LOV2-V416I is 6.41, at which there is no net electrical charge. Lowering the pH will affect the ionic bonds within the proteins, and alter their 3D structure causing protein denaturation. pH 7.5 and pH 8 were optimum for the LOV protein. pH 7.5 has a slightly higher average relaxation half-life than pH 8.0 therefore, all experiments from this point forward were conducted at pH 7.5 unless otherwise stated.

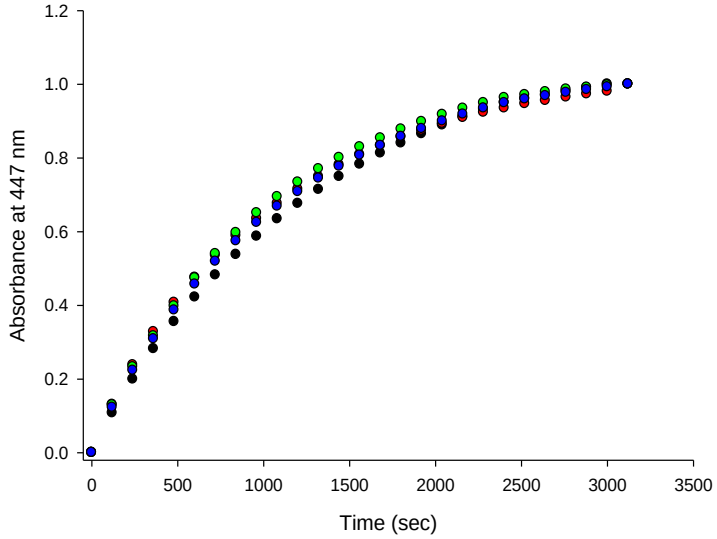

Figure 3.19: *pH dependant time course absorption measurements of Hisact-LOV2-V416I at pH 6.5 (black), pH 7.0 (red), pH 7.5 (green) and pH 8 (blue).*

pH	Half-life (sec)
6.5	730.6 ± 19.5
7.0	700.0 ± 44.2
7.5	725.0 ± 37.8
8.0	711.4 ± 11.2

Table 3.3: *Half-life measurements of Hiscat-LOV2-V416I at 18 °C* at varying pH *values showing the average half-life and the standard deviation.*

3.3.4 Circular Dichroism spectroscopy

Circular dichroism (CD) spectroscopy was carried out on purified proteins to assess the change in secondary structure upon photo-adduct formation. The rapidly relaxing Hisact-*As*LOV2 rendered it difficult to get an accurate light CD state spectra in the far UV region, however the dark spectra was recorded (Figure 3.20A), which is in agreement to existing literature[37,129] showing a CD spectrum typical of a protein containing considerable fractions of both α-helical and β-sheet structure. The maximum signal at approximately 190 nm and double minimum signal at 208 nm and 222 nm are features of α–helical secondary structure and represent the π -π^* (~190 nm and 208 nm) and *n*-π^* (222 nm) electronic transitions of peptide bonds. In β-sheet structures, a maximum signal at around 195 nm (π–π^* transitions) and a strong minimum signal at 216-218 nm (*n*-π^* transitions) is observed.[123] Hisact-*As*LOV2-V416I has a large β-sheet content due to the hisactophilin domain,[121,122] resulting in a strong negative signal between 210-220 nm (Figure 3.20B). In contrast, *As*LOV2-V416I displays distinct negative signals at 208 nm and 222 nm characteristic of high α-helical content (Figure 3.20C).[123]

Undocking and/or disordering of the Jα-helix were observed by the change in mean residue ellipticity (MRE) at 222 nm (Table: 3.4). As expected, a decrease in the α-helical content was recorded upon irradiation: a 39.2 % decrease in ellipticity in Hisact-*As*LOV2, 38.1 % in Hisact-*As*LOV2-V416I and 38.5 % in *As*LOV2-V416I. Since the Jα helix accounts for 38.5 % of α-helical residues in dark state *As*LOV2 (25 amino acids of 65) this change in α-helicity is likely due to Jα undocking and unfolding.

Protein	% Change in $[\Theta]_r$ at 222 nm
Hisact-*As*LOV2 [a]	39.2
Hisact-*As*V183I [a]	38.1
LOV2-*As*V416I [b]	38.5

Table 3.4: *Extent of photo-switching. Length of protein: [a] 288 amino acid residues [b] 160 residues.*

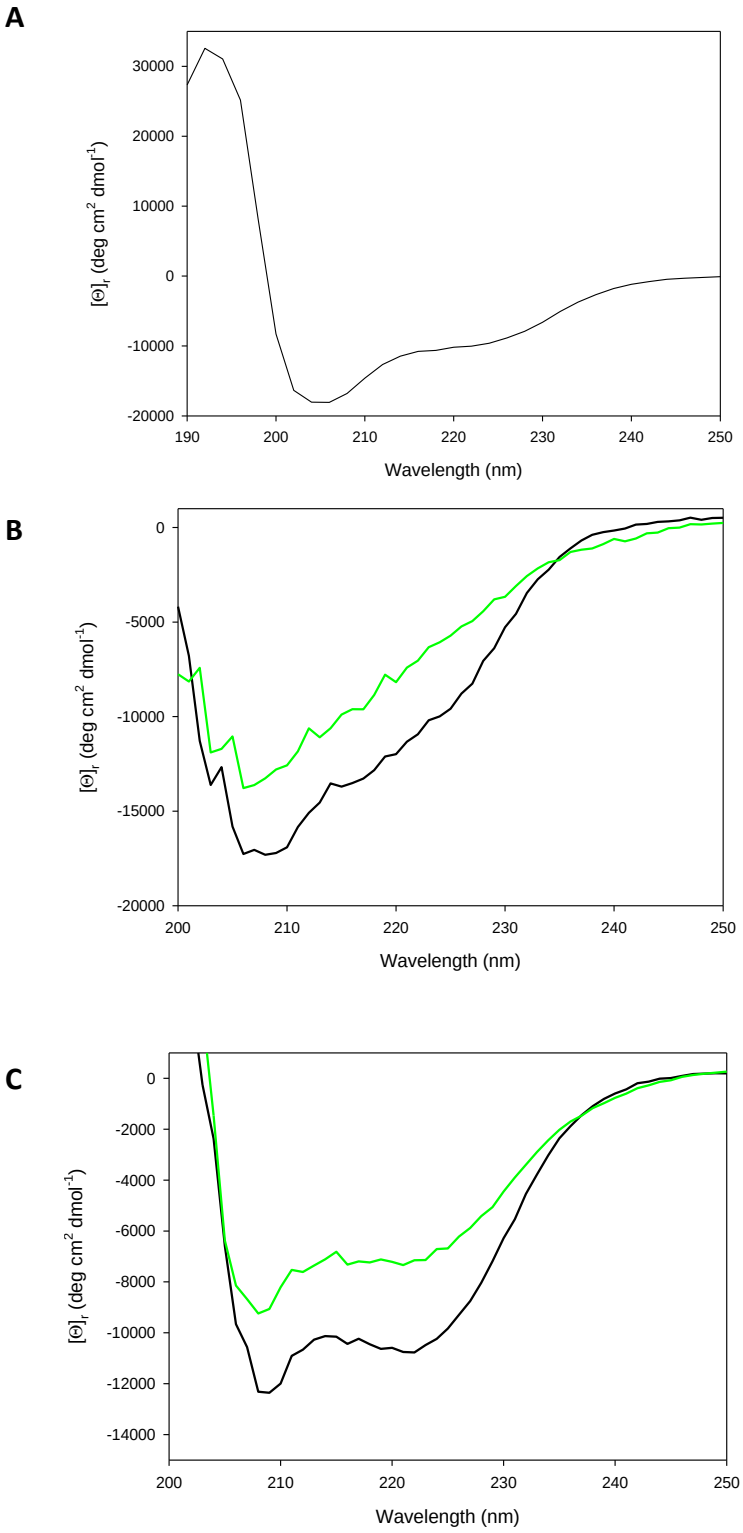

Figure 3.20: *CD Spectra of A) Hisact-AsLOV2, B) Hisact-AsLOV2-V416I and C) AsLOV2-V416I in the dark-state (black) and light state (green).*

3.3.4.1 Half-life measurements

The half-life was measured using the MRE at 222 nm (Figure 3.21) to give an estimation of the refolding time once the dark state is re-established. Compared with the half-lives of the light states measured with the UV/Vis the structural relaxation time was slightly slower than that for FMN adduct reversion except for the rapidly relaxing Hisact-*As*LOV2 (Table 3.5). It is unexpected that the protein relaxation time to be slower than that of the FMN, as decay kinetics for CD spectral changes in the far UV region was found to occur at the same rate as in the visible region.[129] In the case of Hisact-*As*LOV2, the faster protein recovery time may be due to a systematic error as a result to the short relaxation time of this protein; It is important to consider that several seconds (~ 5-10 sec) was required to transfer the sample cuvette from the LED light box to the CD sample holder. *As*LOV2-V416I relaxation kinetics fall within error and Hisact-*As*LOV2-V416I, may recover slower due to steric restraints to the protein conformation caused by fusion to hisactophilin. However, it likely that the cysteinyl-FMN adduct decay is faster than the protein relaxation in response to alterations in redox potential and light-state stability caused by the histidine residues from hisactophilin.

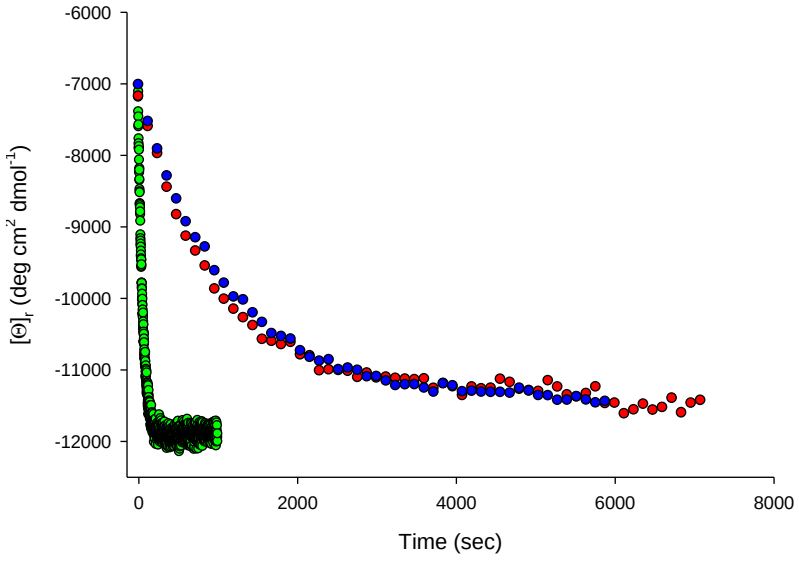

Figure 3.21: *CD relaxation curve of Hisact-AsLOV2 (green) Hisact-AsLOV2-V416I (red) and AsLOV2-V416I (blue).*

Protein	Half-life (sec)	
	UV	CD
Hisact-*As*LOV2	59.5 ± 3.2	39.7 ± 0.87
Hisact-*As*LOV2-V416I	461.3 ± 6.4	666 ± 162
LOV2-*As*V416I	684 ± 6.0	780 ± 168

Table 3.5: *Half-lives of light states of Hisact-AsLOV2, Hisact-AsLOV2-V416I and AsLOV2-V416I at 20 °C measured by UV/Vis observation of cysteinyl-FMN adduct reversion at 447 nm and CD mean residue ellipticity at 222 nm.*

3.3.4.2 The effect of temperature on AsLOV2 proteins

It is already investigated that the relaxation half-life of *As*LOV2 proteins are temperature dependent, therefore to acknowledge the temperature at which the proteins denature at will be ideal for when future optogenetics studies are conducted. The CD signal at 222 nm represents the n-π^* electronic transitions, which represents the strong hydrogen bonding environment of α-helices[123] within the protein complex, therefore increasing the temperature diminishes the hydrogen bonds and a loss in signal at 222 nm is observed. Temperature dependent measurements between 4 °C and 96 °C were conducted at 222 nm, which gave 56 °C as the melting point for Hisact-*As*LOV2, although unfolding of the protein can be seen from as low as 30 °C onwards. Hisact-*As*LOV2-V416I (melting point: 56 °C) starts to unfold at higher temperature of 48 °C and *As*LOV2-V416I (melting point: 54 °C) at 44 °C (Figure 3.22) although the melting point is within the same range of wild-type Hisact-*As*LOV2. The temperature dependent measurements, suggest that the insertion of the mutation did not affect the protein stability any great extent and the absence of the Hisact also has relatively small impact on stability.

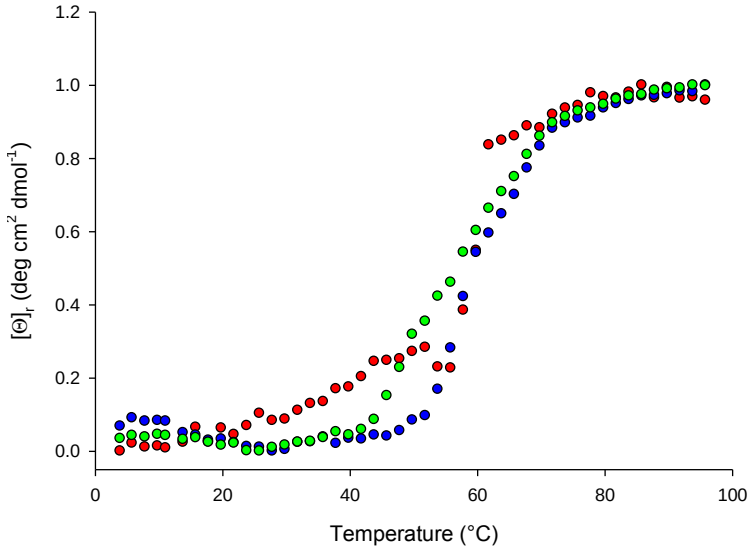

Figure 3.22: *Temperature dependent CD Spectra of Hisact-AsLOV2 (red), Hisact-AsLOV2-V416I (blue) and AsLOV2-V416I (green) at 222 nm.*

3.4 Conclusion

LOV domains are very specific to blue light irradiation as seen with the preliminary UV/Vis absorption spectroscopic studies that showed limited switching with various UV band pass filters. Confirmation on the negative effect of imidazole, known to enhance relaxation to the dark state,[30] was demonstrated through the use of a blue LED which did not improve the switching observed by UV/Vis spectroscopy in the presence of imidazole. The 'base-catalysed' effect of imidazole suggests that the FMN binding pocket is solvent accessible, this is supported by the evidence from previous studies where, deuterium (D_2O) exchange at N3 and N5 positions of FMN was observed by Fourier transform infrared spectroscopy[37] and through pH and isotope effects.[35,129] Solvent accessibility of the FMN binding pocket would implicate that a change in redox potential, caused by the removal of the histidine dominated hisactophilin protein, is a possible explanation for the slower dark state recovery for the *As*LOV-V416I in comparison to Hisact-*As*LOV2-V416I, observed by UV/Vis and CD spectroscopy. Full length proteins containing both *Arabidopsis thaliana* LOV1 and LOV2 but with non-switching LOV1 (C39A mutant)[20] showed kinetic differences to *Avena sativa* LOV2[129] in studies by Bogomolni *et al.,* suggesting that extensions at the N-terminus of LOV2 may have an impact on light induced protein behaviour. Therefore changes in the half-life kinetics caused by the presence of hisactophilin may reflect similar changes in the protein secondary structure. UV/Vis and CD half-life values for all except Hisact-*As*LOV2-V416I are within error, which follow the proceedings in the literature.[129]

It was found that *As*LOV2 proteins are sensitive to the change in temperature as the half-life values for both wild-type and mutant *As*LOV2 drastically decrease with increased temperatures from 10 °C to 37 °C, this is observed through linear Arrhenius behaviour in both this study and previous studies.[127,128] It was observed that elevated temperature also affects protein folding and stability demonstrated by CD temperature dependent measurements. Although no significant changes in protein melting point were observed between Hisact-*As*LOV2, Hisact-*As*LOV2-V416I and *As*LOV2-V416I, the slightly higher unfolding temperatures for the V416I mutants renders it ideal to use as an optogenetics tool at 37 °C for *in vivo* assays.

The effect of pH in the range of pH 6.5 to pH 8 had a minimal effect as no substantial change was observed in the relaxation half-life measured using UV/Vis absorption at 447 nm. This suggests that important residues involved in the rate-limiting step have pK_a values outside the pH range investigated. A broader range of pH was not tested due to protein precipitation that occurred at extreme pH ranges. For this reason, future experiments will be conducted between pH 7.5 and pH 8.5.

In conclusion, mutant AsLOV2-V416I has the most extended half-life and will provide a longer cysteinyl-FMN adduct yield under reduced irradiation intervals, which will reduce damage to protein samples cause by extensive heat from the light source. CD time-course measurements at 222 nm also enabled calculation of the % change in α-helical content which suggests that the change is likely due to the undocking and/or unfolding of Jα. Future hybrid proteins engineered with fusions at the Jα helix to control cellular apoptotic signalling will benefit from the longer undocked period of Jα to allow any possible binding/ interactions to regulatory proteins.

Chapter 4:

Genetically Engineered *As*LOV2 for Regulating Apoptosis

4.1 Aim

The aim is to design and develop an *As*LOV2-based photo-switch containing the BH3 domain of a pro-apoptotic protein that could be used to initiate apoptosis in response to light. The Bid/Bcl-x_L complex was selected as a model system because of the abundance of structural and functional information available on their interaction.

4.2 Introduction

Most cancer cells evade apoptosis either by inactivating mutations to p53 or as a result of aberrant over-expression of anti-apoptotic proteins, such as Bcl-x_L.[132] In either case the molecular machinery needed to conduct apoptosis remains intact, but is in a latent state. Introducing BH3 peptides or proteins in sufficient numbers to occupy all anti-apoptotic proteins in a cell leads to induction of apoptosis. This makes BH3 structure-based mimicry an interesting target for inducing apoptosis in multiple carcinomas.[133] Widespread research has produced BH3-like small molecule inhibitors and peptides including Obatoclax[134] and *R*-(-)-gossypol (AT-101)[135] which mimic the action of the BH3 region and are antagonists of Bcl-2, Bcl-x_L and Mcl-1. They disrupt the hetero-dimerisation of Bcl-2 with pro-apoptotic proteins, making them cytotoxic to drug-resistant cancer cells.[136] BH3 peptides also have high binding affinities to anti-apoptotic proteins such as, the Bak BH3/Bcl-x_L complex[105] (Figure 4.1), however isolated peptides usually show low α-helicity in aqueous solution.[138] Therefore lactam bridges,[139] hydrocarbon staples[140] or the use of photo-switchable azo-benzene staples[137] are required for helix stabilisation. Non-peptide foldamer scaffolds have also been used to mimic the BH3 α-helix side chains. These scaffolds were found to be more stable than isolated α-helices, with correspondingly high binding affinities.[141]

Currently there are limited protein-based mimics of BH3 proteins, although the downstream proteolytic activity of caspase-7 has been regulated using a LOV domain[58] (Section 1.4). However as we have discussed earlier, that the activation of executioner caspases are dependent on the activities of upstream Bcl-2 family of proteins, in this study we investigate the replacement of all or parts of the *As*LOV2 Jα-helix with BH3 helices (Table 4.1) capable of directly or indirectly inducing apoptosis.[138]

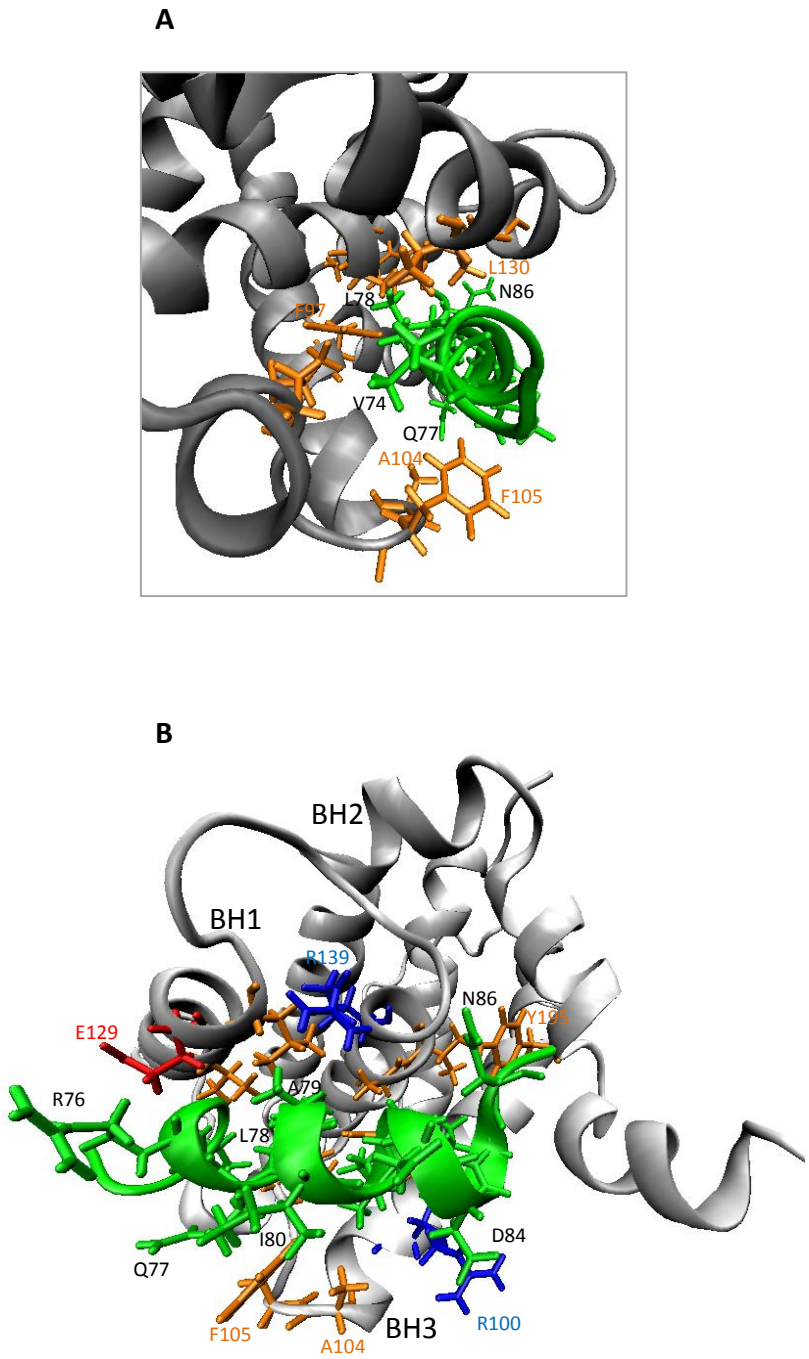

Figure 4.1: *Structure of Bcl-x_L (grey) in complex with Bak BH3 peptide (green) situated within the Bcl-x_L cleft (PDB: 1BXL). A) N-terminal view of Bak peptide showing Important interacting amino acid residues (labelled in black) with binding pocket of Bcl-x_L (hydrophobic residues in orange). B) Illustration of residues in the binding site of Bcl-x_L (hydrophobic residues in orange, positively charged residues in blue, and negatively charged residue in red).*

4.3 Results and Discussion

4.3.1 Design of Hisact-AsLOV2-V416I-BID

Previous designs of *As*LOV2 photo-switches included whole domain insertion as seen with LOV-DHFR.[53] However, most photo-switches were primarily based on introducing interacting domains after the Jα-helix, as seen with LOV-TAP.[52] More recently, sequences have been tested at different positions on the Jα-helix as seen with LOV-IpaA and LOV-SsrA.[151] Here the initial design concept was to replace or substitute key hydrophobic residues in the *As*LOV2 Jα-helix for residues key to from a BH3 region of a pro-apoptotic peptide (Table 4.1). This will allow photo-control of binding to anti-apoptotic proteins by a genetically encoded photo-switch.

Parent protein	BH3 Sequence
Bad	WAAQR**Y**GRE**L**RR**MSD**E**F**VDSF
Bak	STMGQ**V**GRQ**L**AI**IGD**D**I**NRRY
Bax	ASTKK**L**SEC**L**KR**IGD**E**L**DSNM
Bid	DIIRN**I**ARH**L**AQ**VGD**S**M**DRSI
Bim	RPEIW**I**AQE**L**RR**IGD**E**F**NAYY

Table 4.1: *BH3 regions of pro-apoptotic proteins with important binding residues in bold.*

BH3 peptides bind Bcl-x_L at the hydrophobic binding pocket formed by the BH1, BH2 and BH3 regions of Bcl-x_L.[105] Although BH3 peptides are present as random coils in solution,[138] it is in an α-helical conformation when bound to Bcl-x_L, as seen with the solution structure of Bcl-x_L/ Bak complex in Figure 4.1. The N-terminal amino acid residues of BH3 peptides are found to interact with residues from the BH1 region of Bcl-x_L (E129, A139, V126, L130 and F146) and the C-terminal residues with side chains from the BH2 (Y195) and BH3 (F97 and R100) regions of Bcl-x_L.[105,106,107] Hydrophobic residues of the BH3 peptides, such as residues V74, L78, I81 and I85 of Bak are found to stabilise the complex formation. In addition, electrostatic interactions also play an important role in complex formation as seen in figure 4.1, where residues R76, D83 and D84 of Bak BH3 are located close to oppositely charged residues (E129, R139 and R100) of Bcl-x_L.[105] Mutations of these hydrophobic and charged

residues to alanine are known to weaken there binding affinity to Bcl-x_L as the dissociation constant (K_D) of 0.34 ± 0.03 μM for Bak peptide (residue G72-R87) was found to significantly increase to 270 ± 90 μM for L78A mutant and 93 ± 20 μM for D84A mutant.[105] From this it can be understood that the changes made to BH3 sequences when fused to LOV2, have to be carefully considered to avoid completely diminishing binding affinity for Bcl-x_L.

The BH3 domain of Bid (Figure 4.2) was used in this study, since previous research in the Allemann group[137,145] and elsewhere[146,147] showed the BH3 peptide derived from Bid to bind strongly to Bcl-x_L. Bid derived peptides also bind to Mcl-1, allowing activity against both of the sub-branches of the anti-apoptotic protein family in contrast to Bad, BH3 peptides or mimics such as, the small molecule inhibitor ABT-737 which is ineffective against cells expressing Mcl-1.[124] Similar to the hydrophobic contacts of the Jα-helix to the LOV2 β-core (Section 3.2.1) the Bid BH3 region includes residues that make important hydrophobic interactions with the Bcl-x_L binding pocket (Table 4.1). It is important that these key residues are retained in the design of the hybrid protein, as well as residues G528, I532, T535, I539, D540 and A542 of *As*LOV2 which are important for the Jα helix to correctly dock back to the LOV core.[144]

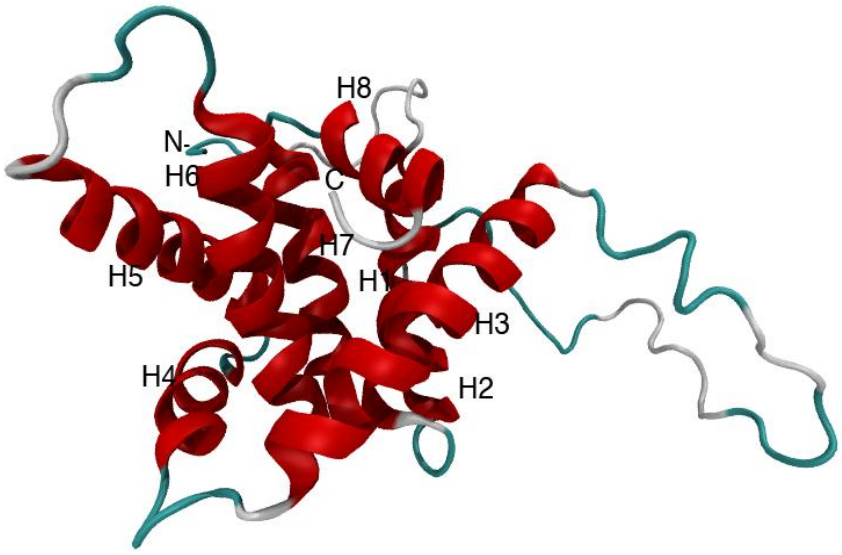

Figure 4.2: *Structure of human pro-apoptotic Bcl-2 protein, Bid (PDB: 2BID).*

In the preliminary design of LOV2-Bid (Figure 4.3), the Bid BH3 sequence (residue 81-101) is aligned with the Jα helix so that D540 and the conserved aspartate of the BH3 sequence overlap, to ensure that the hybrid protein remains able to bind to Bcl-x_L. Changes in the Jα sequence are favoured over changes of residues from Bid BH3 sequence, as minor changes in the Bid BH3 may eliminate its binding affinity to its target.

Figure 4.3: *Amino acid sequences of AsLOV2 Jα-helix (blue), Bid BH3-helix (black, residue 81-101) and LOV2-BID hybrid Jα-helix. Important residues involved in hydrophobic interactions are shown in bold. As in previous work, isoleucine replaces methionine in the LOV2-Bid sequence to avoid oxidation.* [137,145]

4.3.2 Bid BH3 and LOV2-Bid peptides

In order to ensure that the modified *As*LOV2-Bid protein (Figure 4.3) bound to Bcl-x_L, peptides corresponding to the LOV2-Bid Jα-helix sequence with a cysteine inserted in place of an alanine was synthesised by solid phase synthesis. A wild-type Bid BH3 peptide with an additional N-terminal cysteine-glycine pair of amino acids was also synthesised as a control, to allow comparison of binding affinities. The additional cysteine residues were included to allow the attachment of maleimido-fluorophores to the peptides. The peptides were purified *via* reverse phase HPLC then labelled with a fluorescent dye; LOV2-Bid was labelled with maleimido-fluoroscein (FAM) and Bid BH3 with maleimido-tetramethylrhodamine (TMR). The rhodamine dye was used for the wild type peptide so that it could be used in the presence of a green fluorescent FMN cofactor for displacement assays. Following fluorescent labelling, the samples were purified once again, freeze-dried and re-dissolved in buffer. Sample purity was assessed by analytical HPLC (Figures 4.4 and 4.5) and the masses were determined using MALDI-TOF MS (Table 4.2).

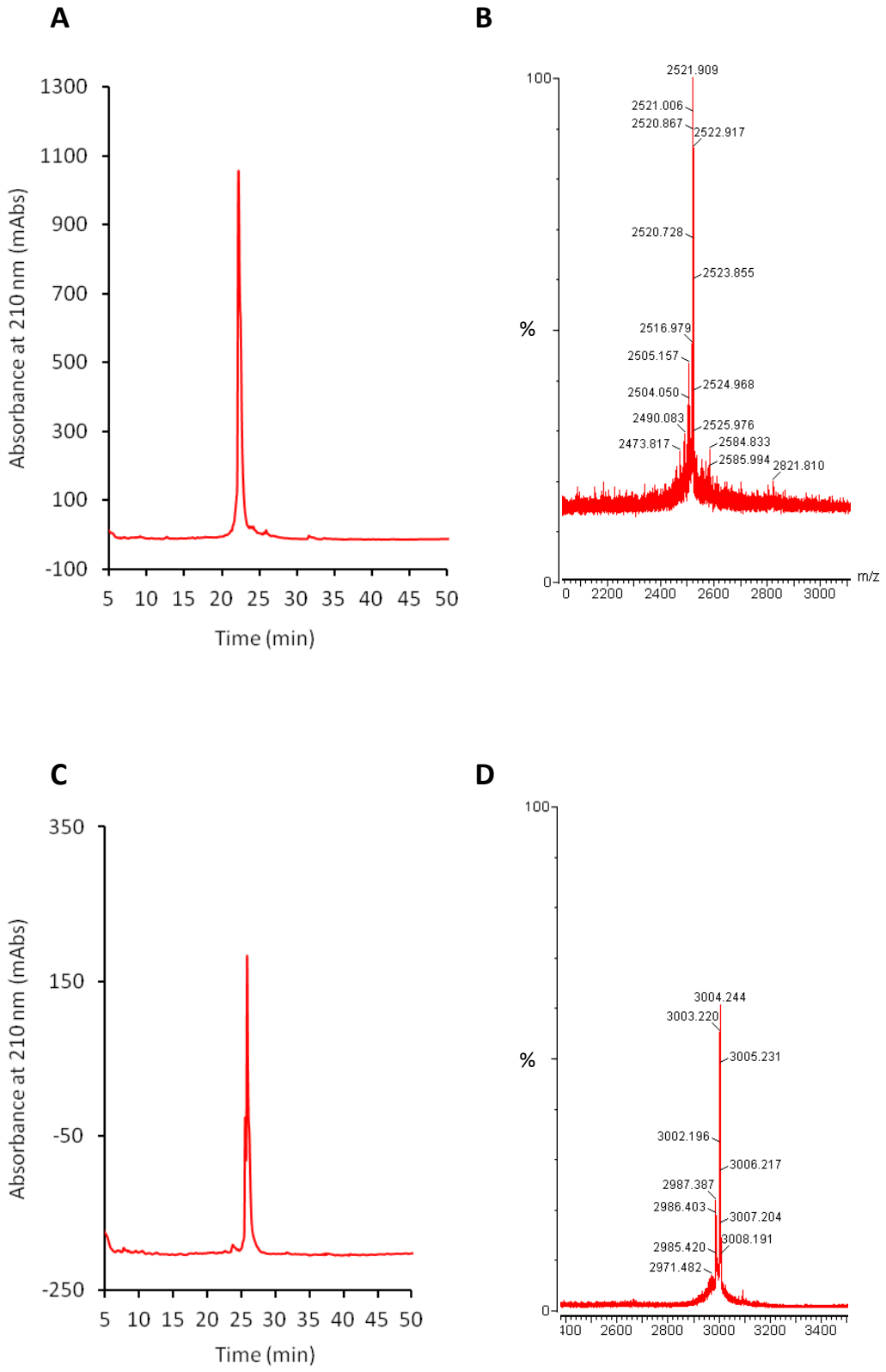

Figure 4.4: *A) Analytical HPLC of Bid-BH3 peptide. B) MALDI-TOF spectrum of Bid-BH3 peptide showing m/z 2521.9 ($[M+H]^+$). C) Analytical HPLC showing TMR-Bid BH3 peptide. D) MALDI-TOF spectrum of TMR-Bid BH3 peptide showing m/z 3004.2 ($[M+H]^+$).*

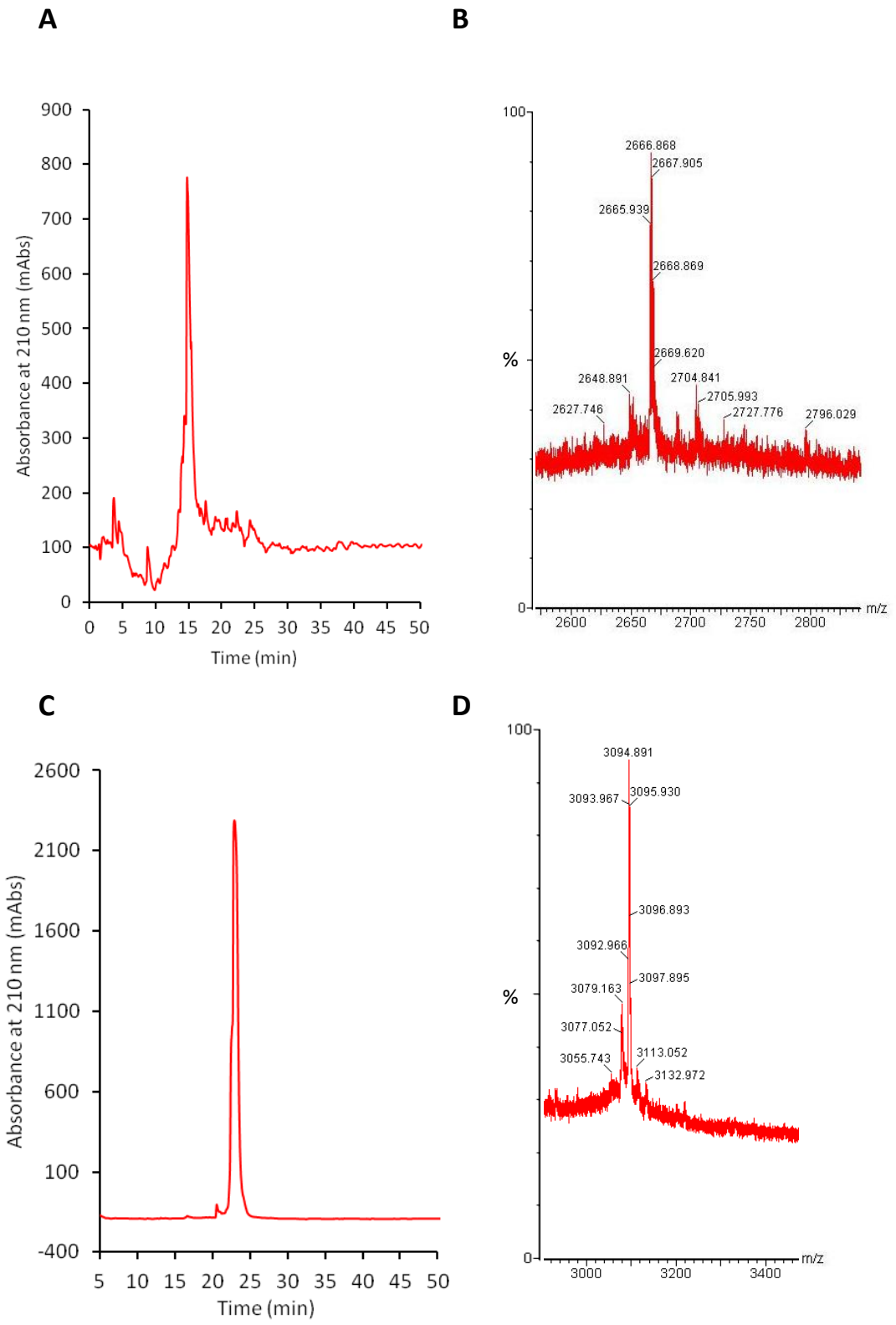

Figure 4.5: *A) Analytical HPLC of LOV2-Bid peptide B) MALDI-TOF spectrum of LOV2-Bid peptide showing a peak at m/z 2666.9 ($[M+H]^+$) C) Analytical HPLC of FAM-LOV2-Bid peptide D) MALDI-TOF spectrum of FAM-LOV2-Bid peptide at 3094.9 m/z ($[M+H]^+$).*

Peptide	Sequence	Theoretical mass	Observed mass ($[M+H]^+$)
Bid BH3	CGDIIRNIARHLAQVGDSIDRSI-NH_2	2520.3	2521.9
TMR-Bid BH3		3003.4	3004.2
LOV2-Bid	DCAEDIGVNIARHLAQVGDSIDRSI-NH_2	2665.0	2666.9
FAM-LOV2-Bid		3093.4	3094.9

Table 4.2: *Theoretical mass and observed mass of Bid-BH3 and LOV2-Bid peptides.*

4.3.2.1 Fluorescence anisotropy

Fluorescence anisotropy experiments measure differences in the plane of excited and emitted light to determine rates of rotation during the lifetime of excited dye molecules in solution. Since larger molecules tumble more slowly in solution than smaller molecules, significant changes are observed in the tumbling rates and therefore fluorescence anisotropy values of labelled peptides can be obtained when free in solution and when bound in complexes with proteins.

Bcl-x_L was expressed using the T7 expression system as described in Section 2.3 followed by purification using Ni-NTA affinity chromatography (section 2.3.4). Bound Bcl-x_L was eluted in a stepwise addition of imidazole in the same buffer up to 500 mM imidazole (Figure 4.6). The elution fractions were pooled and dialysed against 50 mM sodium phosphate buffer (pH 7.5) containing 100 mM sodium chloride and 5 mM β-mercaptoethanol. The purity of the resulting 21.4 kDa protein was analysed by SDS-PAGE (Figure 4.7) with two bands visible; one at ~ 22 kDa as expected and also one at ~ 44 kDa. Treatment with strong reducing agent dithiothreitol (DTT) diminished this band indicating that the latter corresponded to Bcl-x_L dimer complexes.

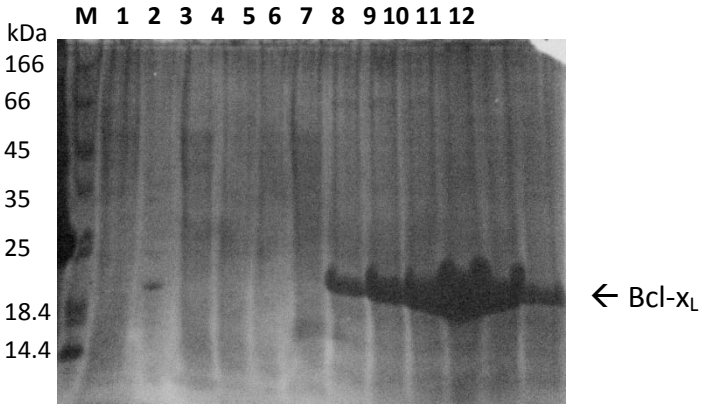

Figure 4.6: *SDS-PAGE gel showing the purification steps for Bcl-x_L using Ni-NTA resin. M: protein marker, lane 1: cell pellet, lane 2: supernatant after sonication of total cellular protein, lane 3: flow-through fraction, lane 4-6: wash fractions (50 mM imidazole) and lane 7-12: elution fractions (containing 500 mM imidazole) containing Bcl-x_L (band at ~22 kDa).*

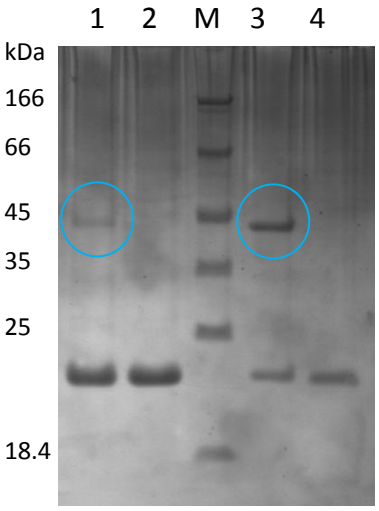

Figure 4.7: *SDS-PAGE gel of the elution fractions of Bcl-x_L: Lane 1 and 3: show visible band at ~44 kDa (circled). Lane 2 and 4: D1 and D2 after treatment with reducing agent dithiothreitol, there is no visible band at ~44 kDa.*

Fluorescence anisotropy measurements were carried out to quantify the binding affinities of TMR-Bid BH3 and FAM-LOV2-Bid peptides for Bcl-x_L protein. Solutions of TMR-Bid BH3 (2.5 nM) and FAM-LOV2-Bid (5 nM) were titrated with increasing concentrations of Bcl-x_L and the resulting anisotropy values were plotted against Bcl-x_L concentration (Figure 4.8) and fitted to a single site Langmuir binding isotherm.

$$\emptyset_{Fit} = \frac{1}{1 + \left(\frac{{K_D}^n}{[P]^n}\right)}$$

Where, $\emptyset_{Fit}$ denotes the fraction of bound labelled-ligand, K_D is the apparent dissociation constant, [P] is the concentration of protein and *n* is the number of binding sites.

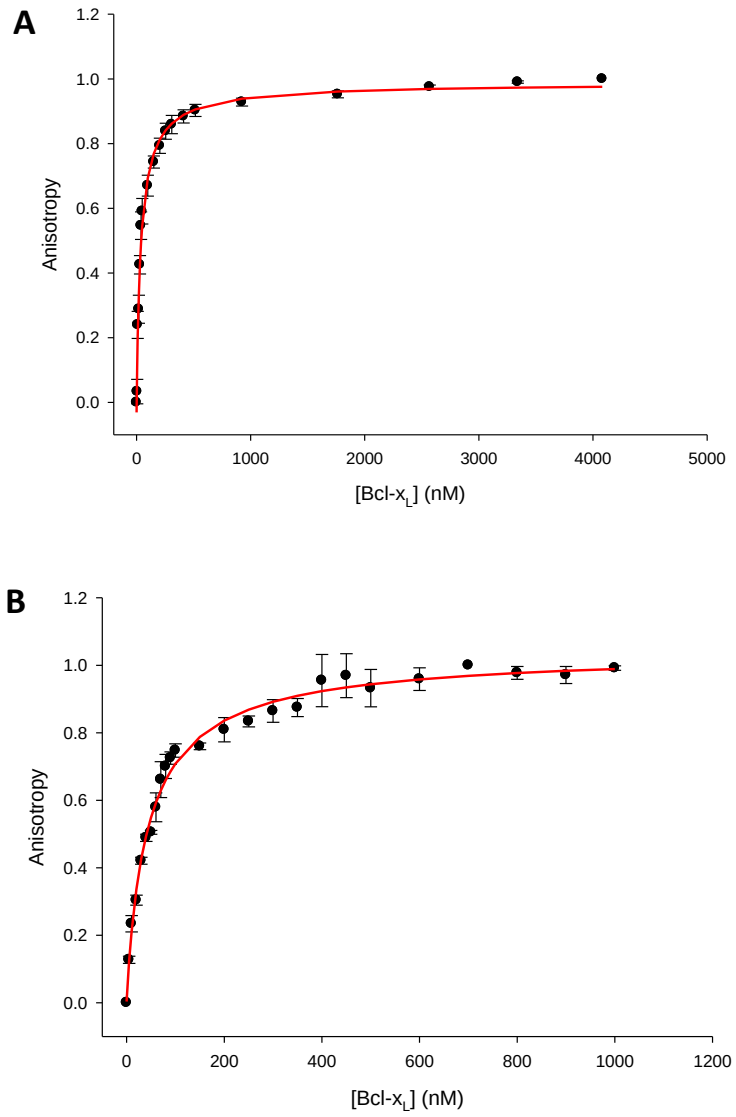

Figure 4.8: *Normalised fluorescence anisotropy binding curves of: A) TMR-Bid BH3 B) FAM-LOV2-Bid peptide.*

TMR-Bid BH3 peptide has an equilibrium dissociation constant (K_D) of 27 ± 5.1 nM in good agreement with a literature value of K_D 23 ± 7[148] and 27.2 ± 0.5[153] measured by isothermal calorimetry. The FAM-LOV2-Bid peptide gave a K_D of 46 ± 2.6 nM, a relatively small decrease in affinity (Table 4.3), therefore the LOV2-Bid hybrid Jα retained a strong enough binding affinity for Bcl-x_L, which allowed the full-length *As*LOV2-BID protein to be engineered.

Peptide	Sequence	K_D (nM)
TMR-Bid BH3[a]	CGDIIRNIARHLAQVGDSIDRSI-NH_2	27 ± 5.1
FAM-LOV2-Bid[b]	DCAEDIGVNIARHLAQVGDSIDRSI-NH_2	46 ± 2.6

Table 4.3: *Binding to Bcl-x_L: [a] 2.5 nM TMR- Bid peptide, [b] 5 nM FAM-LOV2-Bid peptide*

A strong binding affinity of LOV2-Bid peptide for Bcl-x_L was expected as minimal changes to Bid BH3 sequence was made, retaining key hydrophobic (I86, L90 and V93) and charged (D95) residues common in BH3 regions of pro-apoptotic proteins (Table 4.1). Only two substitutions to Bid BH3 sequence were made in favour of LOV2 (I83 to G and R84 to V), residues A91 and D95 are unchanged as they align in position with A536 and D540 of LOV2. However as discussed earlier with the Bcl-xL/ Bak complex formation,[105] even a single point mutation can cause dramatic change in the binding affinity of BH3 peptides.

4.3.3 Hisact-AsLOV2-V416I-Bid

The plasmid harbouring the gene encoding Hisact-*As*LOV2-V416I contains *Kpn*I and *Hin*dIII restriction sites (Figure 4.9), which were used to excise the wild-type Jα-helix. The doubly cut plasmid was purified by agarose gel electrophoresis (Figure 4.10). Annealed oligonucleotides with complementary sticky ends encoding the hybrid Jα (*As*LOV2-BID) were ligated with the purified linearised pNCO plasmid DNA. *E. coli* XL-1 Blue cells were transformed with the resulting DNA and grown overnight at 37 °C on agar plates containing ampicillin. Individual colonies were picked and the plasmid was isolated and sequenced until the intended gene was isolated.

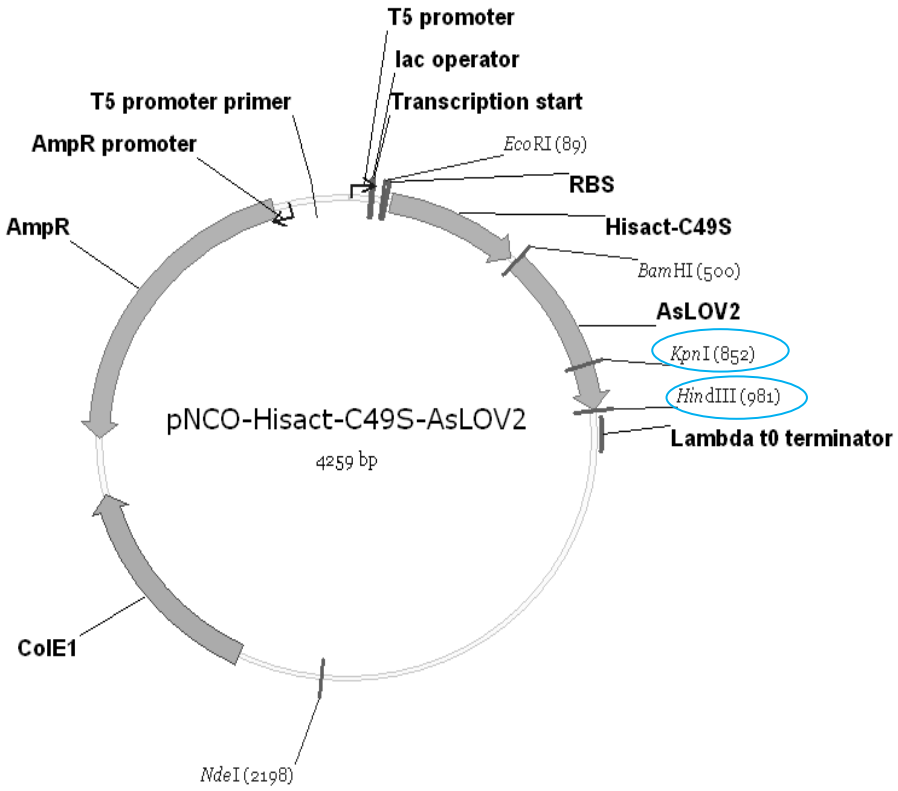

Figure 4.9: *pNCO-Hisact-AsLOV2-V416I vector map. KpnI and HindIII sites are circled in blue.*

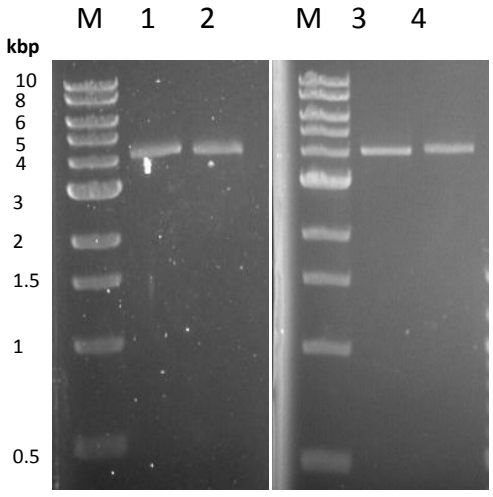

Figure 4.10: *1 % Agarose gel showing pNCO-Hisact-AsLOV2-V416I. Lane M: 1 kb DNA marker, Lane 1: cut with KpnI. Lane 2: cut with HindIII. Lane 3: cut with KpnI then HindIII. Lane 4: cut with HindIII then KpnI.*

E. coli BL21 (DE3) *Star* cells were transformed with pNCO-Hisact-*As*LOV2-V183I-Bid (Hisact-*As*LOV-Bid) and grown to OD_{600} 0.8. Protein production was induced by the addition of 1 mM IPTG and expression was allowed to continue overnight at 20 °C. Over-expression of the protein was verified by SDS-PAGE (Figure 4.11) which was expected to migrate at a speed depending on its mass. Following purification by size-exclusion chromatography the resulting protein was analysed by MALDI-TOF MS and a mass of 32497.5 (Figure 4.12), compared to the theoretical mass of 32687.3 was established.

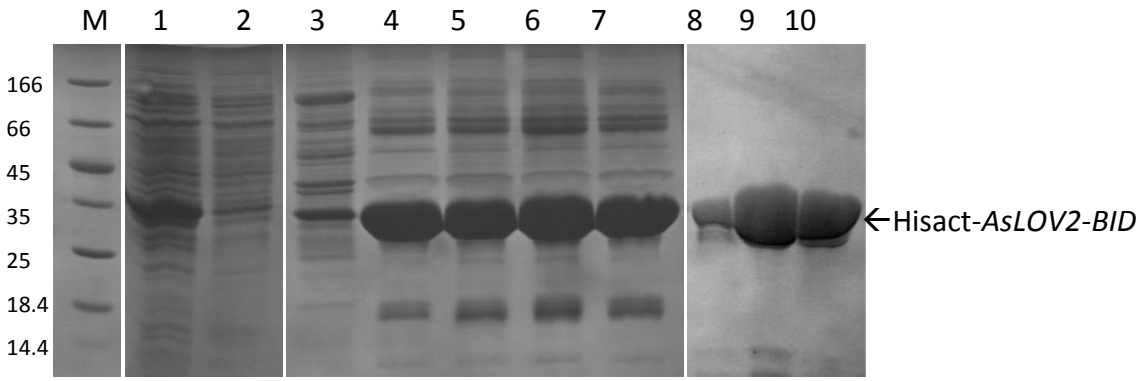

Figure 4.11: *Purification of Hisact-AsLOV2-Bid: M: protein marker, lane 1: cell lysate, lane 2: Ni-NTA column flow-through, lane 3: wash, lane 4-7: eluted fractions and lane 8-9: fractions from preparative Superdex-75 column.*

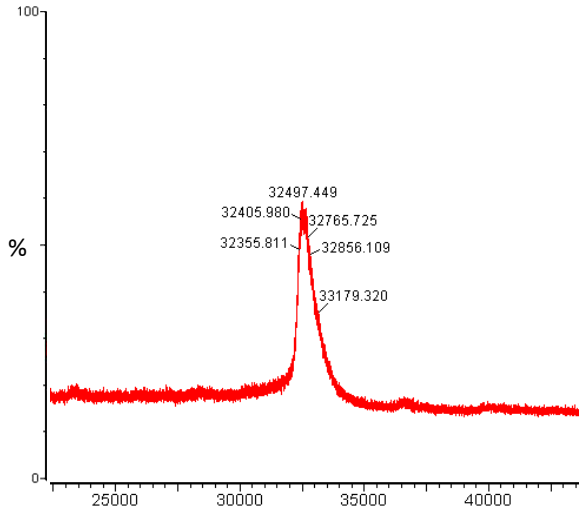

Figure 4.12: *MALDI-TOF Mass spectra of Hisact-AsLOV2-Bid; m/z 32497.5*

A cysteine and a stop codon were introduced into the Hisact-*As*LOV2-Bid sequence (PD547C_) at the C-terminal end of Jα-helix (Figure 4.13) by site-directed mutagenesis to facilitate labelling with TMR for fluorescence anisotropy binding studies.

Figure 4.13: *Sequence of the Jα-helix of Hisact-AsLOV2-V416I-Bid-Cys (Hisact-asLOV2-Bid-cys).*

Unbound TMR gives a maximum absorption at 540 nm and once bound to protein a bathochromic shift to 551 nm is observed (Figure 4.14). An approximate extinction co-efficient of 91,000 $M^{-1}cm^{-1}$ at 551 nm (according to manufacturer's instructions: Chemodex ltd customized molecules) was used to estimate the concentration of labelled protein.

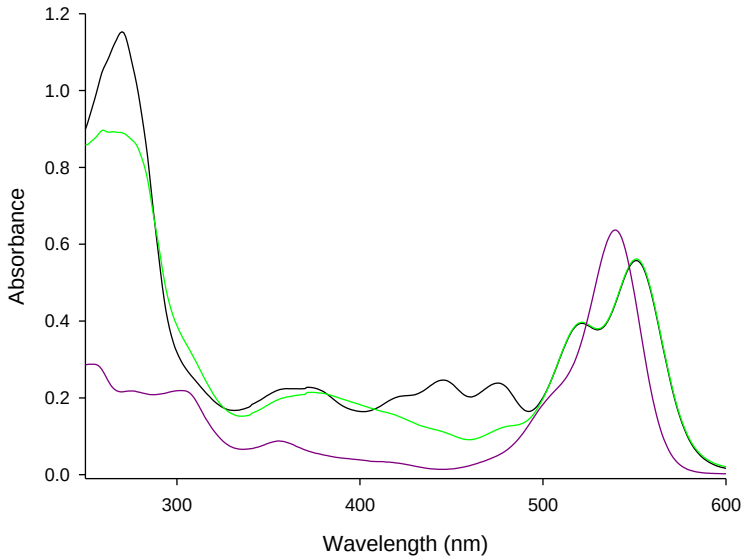

Figure 4.14: *UV/Vis spectra of free TMR (purple) and Hisact-AsLOV2-V416I-Bid-Cys(TMR) in dark (black) and light state (green).*

4.3.3.1 Fluorescence anisotropy

Fluorescent Hisact-*As*LOV2-V416I-Bid-Cys(TMR) allowed the binding of the full length photoswitch hybrid to Bcl-x_L to be examined by fluorescence anisotropy. Bcl-x_L was titrated into a Hisact-*As*LOV2-V416I-Bid-Cys(TMR) solution (10 nM) and the anisotropy was recorded. The results were fitted to a single site Langmuir binding isotherm (Figure 4.15) using the average of 3 sets of readings.

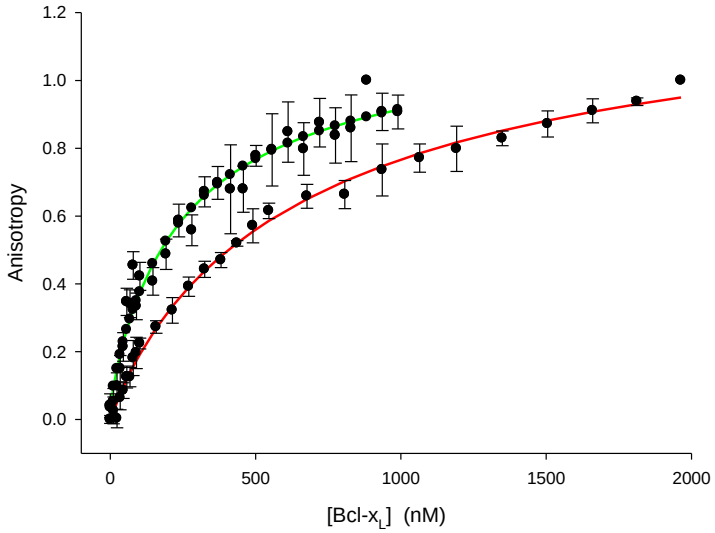

Figure 4.15: *Normalised fluorescence anisotropy curves of Hisact-AsLOV2-V416I-Bid-Cys(TMR) in the presence of increasing concentrations of Bcl-x_L: dark state (red) and light state (green).*

The expected result was that there would be no significant binding at the dark state, however Hisact-*As*LOV2-V416I-Bid-Cys(TMR) bound to Bcl-x_L with a K_D = 699 ± 65 nM in the dark and 266 ± 68 nM in the light state (Table 4.4). The protein bound far less effectively than the LOV2-Bid peptide (K_D = 46 ± 2.6 nM), which is less hindered and the BH3 domain is free to move in solution than when attached to a protein complex. It is imperative to note that in the cell, Bid protein is naturally cleaved to t-Bid to allow the BH3 domain binding accessibility to its partner.[98]

Protein	K_D (Dark state)	K_D (Light State)
Hisact-*As*LOV2-V416I-Bid-Cys(TMR)	699 ± 65 nM	266 ± 68 nM

Table 4.4: *Dissociation constants for binding of Hisact-AsLOV2-V416I-Bid-Cys(TMR) to Bcl-x_L.*

In comparison to the K_D reported in the literature, for t-Bid binding to Bcl-x_L (200 ± 20 nM) using Fluorescence correlation spectroscopy (FCCS, Bcl-x_L was labelled which fluorescent dye),[147] the K_D determined in this investigation (266 ± 68 nM) is in strong agreement. Although, this is promising in terms of binding susceptibility with our preliminary LOV2-Bid hybrid design, it failed to show a switching on/ off mechanism clearly sought after in this project.

The lack of switching can be correlated to several factors affecting the protein conformation and preventing the Jα-helix from docking properly back to the hydrophobic LOV core, therefore allowing the Bcl-x_L to effectively bind in dark adapted state. Firstly, the N-terminal fusion of hisactophilin, which was previously found to have an effect on the protein photoswitching (section 3) and possibly the secondary structure, may have sterically hindered photoswitching in addition to the changes made to the Jα-helix. An additional factor could be disruption of the re-docking process caused by the TAMRA dye attached to the C-terminus of Jα. Finally it may be that the overall design of the hybrid helix causes steric clashes with residues on the hydrophobic surface of LOV2, therefore always remaining partially undocked. In order to improve the LOV2-Bid photoswitch, changes were made to the Hisact-*As*LOV2-V416I-Bid and finally new designs were incorporated and compared (outlined in section 4.3.4).

4.3.4 Improving the AsLOV2-Bid photoswitch

4.3.4.1 Cloning AsLOV2-Bid1

In order to more conveniently isolate the *As*LOV2-Bid1 from the hisactophilin domain, *Nde*I and *Bam*HI restriction sites were incorporated at the start and end of the *As*LOV-Bid sequence *via* site-directed mutagenesis and then confirmed by sequencing. The gene encoding LOV2-Bid (474 bp) was then cut at these sites (Figure 4.16) and the resulting sticky-ends were ligated to multiple cloning site of pET28a (previously containing a 2.1 kbp calpain gene) singly and doubly cut using the same restriction enzymes and purified by the same procedure as Hisact-*As*LOV2-V416I-Bid (Figure 4.17). The resulting DNA was used to transform super-competent *E. coli* XL1-Blue cells and incubated overnight on an agar plate containing kanamycin. Overnight cultures were inoculated with single colonies from the plate, harvested and DNA extracted until a digestion test was performed in order to determine whether the insert had been ligated into the vector (Figure 4.18). The pET28a vector does not contain a *Kpn*I restriction site whereas the *As*LOV2-BID sequence (LDG-TEH) does, between the LOV core and the Jα-helix. As a result, samples that cut with *Kpn*I (5.4 kbp vector plus 474 bp insert) were sequenced to confirm the identity of the desired plasmid containing a gene encoding *A. sativa* Phot1-LOV2-V183I (residue V183 is V416 in full length protein containing hisactophilin) with an N-terminal hexa-histidine tag for affinity purification (*As*LOV2-Bid1, all *As*LOV2-Bid proteins described from here onwards incorporate the V183I mutation to stabilise their light-state).

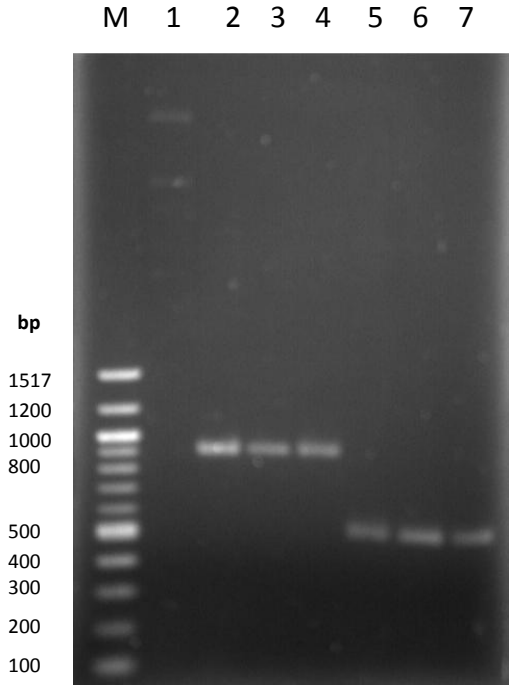

Figure 4.16: *2 % Agarose gel showing pNCO-Hisact-AsLOV2-Bid (858 bp) and AsLOV2-Bid1 (474 bp). Lane M: 100 bp DNA marker. Lane 1: uncut (4259 bp). Lane 2-3: cut with NdeI. Lane 4: cut with BamHI. Lane 5-7: cut with both NdeI and BamHI.*

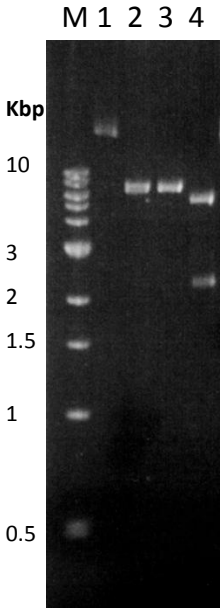

Figure 4.17: *1.5 % Agarose gel showing pET28a vector (5.37 kbp). Lane M: 1 kb DNA marker. Lane 1: uncut. Lane 2: cut with BamHI. Lane 3: cut with NdeI. Lane 4: cut with both NdeI and BamHI.*

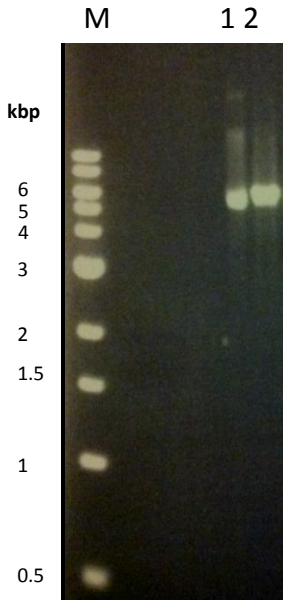

Figure 4.18: *Digestion test: 1 % agarose gel of pET28a-AsLOV2-Bid1 (~5.85 kbp). M: 1 kb DNA marker. Lane 1: Uncut. Lane 2: cut with KpnI.*

4.3.5 Design of AsLOV2-Bid2-4

Previous studies by Lungu *et al.* made conservative changes to the *As*LOV2 Jα-helix, varying at a maximum of seven residues[151] in order not to disturb photo-switching. In contrast, in this investigation the *As*LOV2-Bid1 was designed for effective BH3 mimicry where extensive changes in the Jα-helix were made by replacement of residues with hydrophobic side-chains from the four separate turns of Bid BH3 (Table 4.14). Inspired by the strategy of Lungu *et al*. who tried embedding their peptide sequence at different positions of equivalent helical register within the Jα-helix, in order to optimise the dynamic range of their interaction,[151] here a series of *As*LOV2-Bid proteins were designed where the Bid BH3 is steadily displaced towards the end of the Jα (Figure 4.19). This was designed to create a series of compromises between dark state caging (of the BH3 residues required for protein-protein interaction) and light state steric accessibility.

Residues I532, A536 and I539 of LOV2 are located along the three consecutive turns of the Jα-helix that face the hydrophobic LOV2 core (Figure 4.20); these residues have been retained in all 4 designs. Residue D540 of LOV2 makes an important electrostatic interaction to the hydrophobic core[18] and was therefore retained in the *As*LOV2-Bid2 and *As*LOV2-Bid3 sequences. In *As*LOV2-Bid4 D540 aligns with residue D81 of Bid BH3 helix. Residues A536,

A542 and E545 are highly conserved in LOV domains. Where possible, the fusion designs retained these residues but were otherwise constructed so that the key hydrophobic interactions of one helix were replaced with those of another to retain the hydrophobic stripe that docks the Jα-helix. Residues I86, L90, V93 and M97 occupy these positions in Bid and are vital for interactions with pro-survival proteins.[153] Residue I86 is overlapped with Jα-helix in *As*LOV2-Bid1-4, to prevent dark state binding through 'caging'.[51,57] All 25 residues on the Jα-helix of LOV2 are identical in *As*LOV2-Bid5; the Bid BH3 residues overhang from the end of the Jα-helix with only the proximity of the LOV domain to sterically constrain their accessibility.

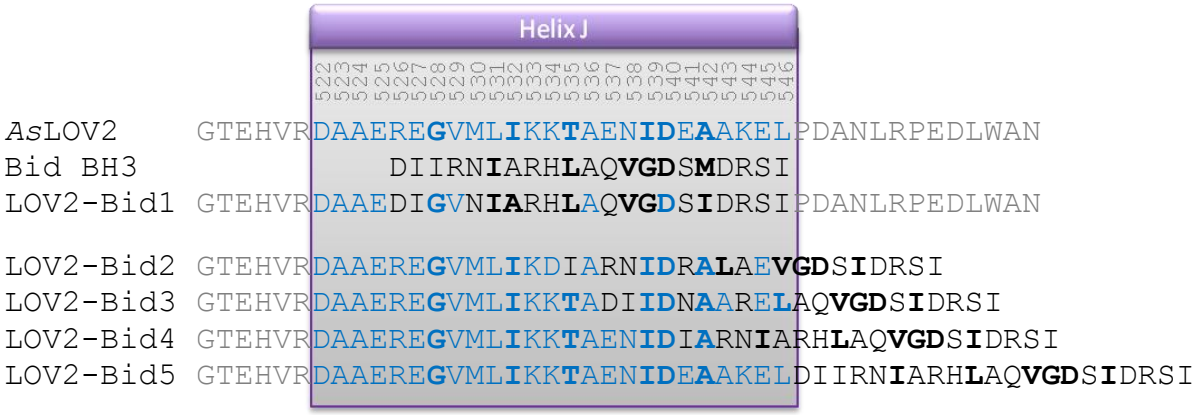

Figure 4.19: *Amino acid sequences of AsLOV2 Jα-helix (blue), Bid BH3-helix (black) and AsLOV2-Bid1-5 hybrid Jα-helices. Important residues involved in hydrophobic interactions are shown in bold.*

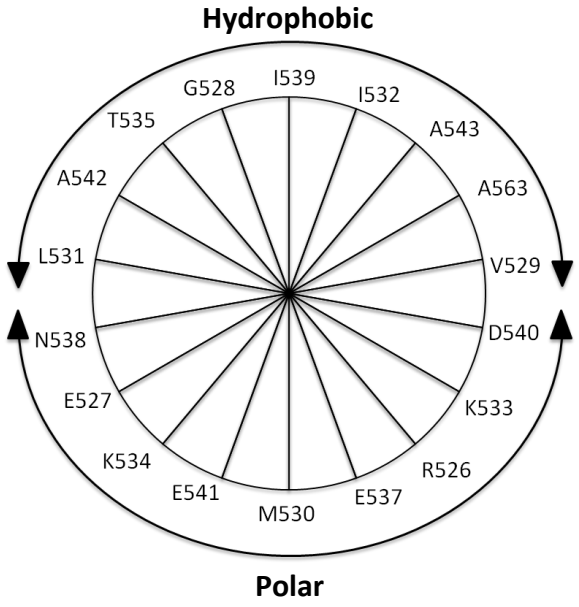

Figure 4.20: *Helical wheel projection of Jα helix showing the residues associated with hydrophobic and polar face.*

4.3.5.1 Construction of AsLOV2-Bid2-4

The pET28a plasmid harbouring the gene encoding *As*LOV2-Bid1 retains the *Kpn*I and *Hin*dIII restriction sites used to insert the original Bid sequence and these were used once again to excise the *As*LOV2-Bid1 Jα-helix (Figure 4.21) in order to insert annealed oligonucleotides (Figure 4.22) encoding further the hybrid Jα sequences (*As*LOV2-BID2-4, multiple strategies aimed at producing an insert to create DNA encoding *As*LOV2-Bid5 proved unsuccessful). The *As*LOV2-Bid1 Jα-helix is 44 base pairs (bp) and therefore cannot be seen on the agarose gel (Figure 4.21: lane 5), however single digests using both enzymes indicate that both enzymes cut appropriately (Figure 4.21: lane 2 and 3). A digestion test was performed using *Kpn*I as done with *As*LOV2-Bid1, in order to test whether the insert had been ligated into the vector (Figure 4.23-4.25), as a result positive clones were also verified by DNA sequencing.

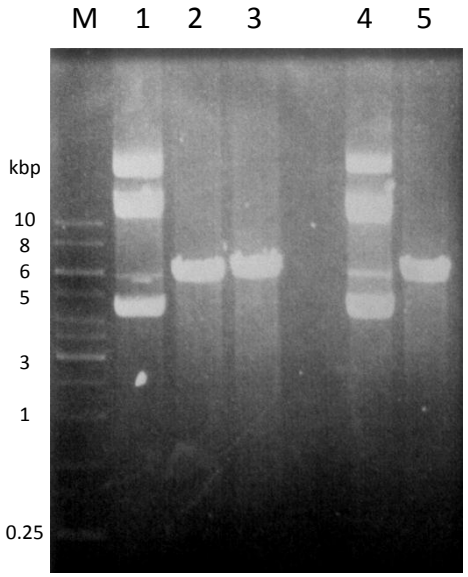

Figure 4.21: *1 % Agarose gel showing pET28a-AsLOV2-Bid1 (~5.85 kbp). Lane M: 250 bp DNA marker. Lane 1: uncut. Lane 2: cut with KpnI. Lane 3: cut with HindIII. Lane 4: uncut. Lane 5: cut with both KpnI and HindIII.*

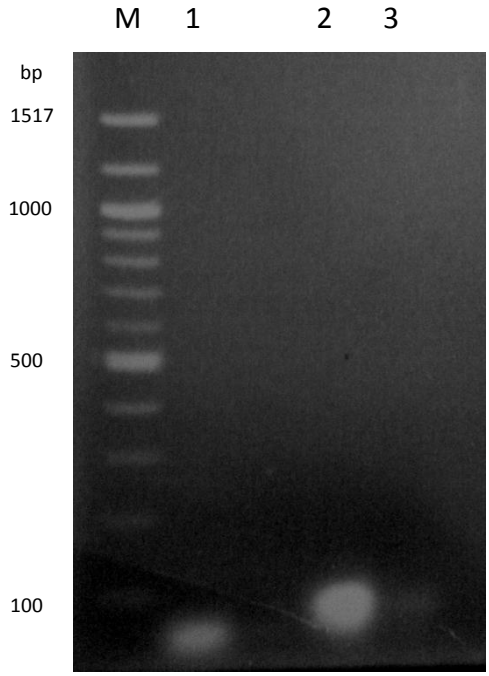

Figure 4.22: *2 % Agarose gel showing pET28a-AsLOV2-Bid2-4 annealed oligonucleotides: lane M: 100 bp DNA marker, lane 1: AsLOV2-Bid2, lane 2: AsLOV2-Bid3, lane 3: AsLOV2-Bid4.*

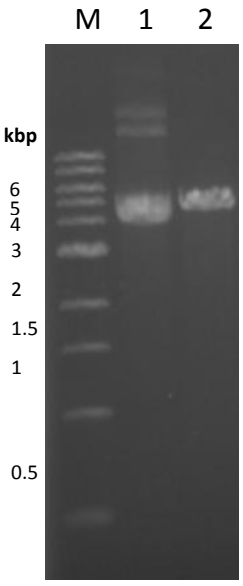

Figure 4.23: *Digestion test: 1 % agarose gel of pET28a-AsLOV2-Bid2 (~5.85 kbp). M: 1 kb DNA marker. Lane 1: uncut. Lane 2: cut with KpnI.*

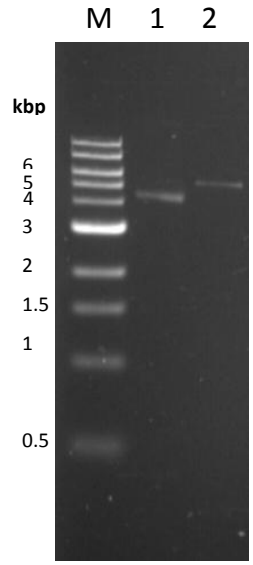

Figure 4.24: *Digestion test: 1.5 % agarose gel of pET28a-AsLOV2-Bid3 (~5.85 kbp). M: 1 kb DNA marker. Lane 1: uncut. Lane 2: cut with KpnI.*

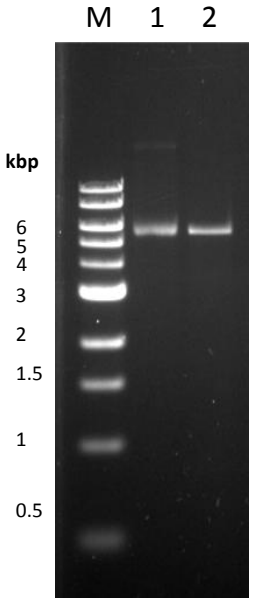

Figure 4.25: *Digestion test: 1.5 % agarose gel of pET28a-AsLOV2-Bid4 (~5.85 kbp). M: 1 kb DNA marker. Lane 1: uncut. Lane 2: cut with KpnI.*

4.3.6 Expression and purification of AsLOV2-Bid1-4

Expression and purification of all proteins was achieved as previously stated for wild-type *As*LOV2. *As*LOV2-Bid1-4 over-expressed after induction (Figures: 4.26 and 4.28) using IPTG. The cells were harvested and lysed using an ultrasonicator (3 seconds on and 5 seconds off for 6 minutes), the resulting lysate was centrifuged and the lysate and pellet were analysed by SDS-PAGE. All the proteins were present in the supernatant of the cell lysate, additionally *As*LOV2-Bid1 and *As*LOV2-Bid2 contained large amounts of protein in the debris pellet (Figures: 4.27 and 4.29). Ni-NTA affinity chromatography was carried out to purify the proteins (Figures: 4.27, 4.29 and 4.30). Figures: 4.29 and 4.30 both show that eluted fractions for *As*LOV2-Bid2-4 are almost pure, however the SDS-PAGE for *As*LOV2-Bid1 showed several other bands in the eluted fraction (Figure 4.27), and therefore required further purification.

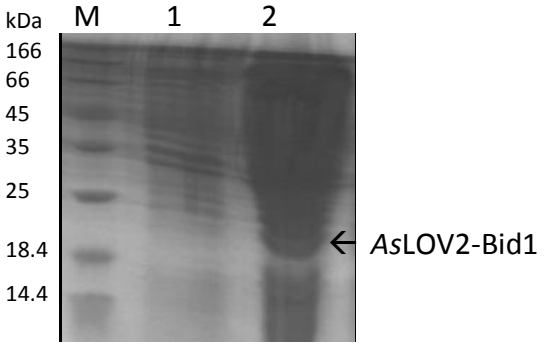

Figure 4.26: *SDS-PAGE analysis of crude cells of: AsLOV2-Bid1 before induction (lane 1) and after induction (lane 2).*

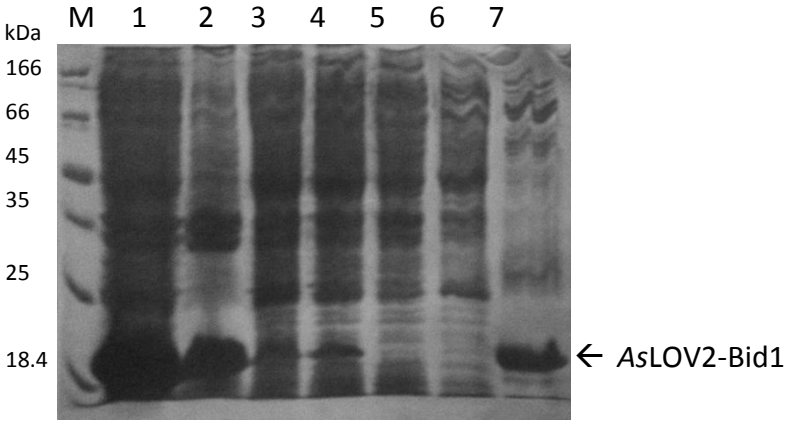

Figure 4.27: *Purification of AsLOV2-Bid1. M: protein marker, lane 1: cell lysate, lane 2: cell pellet, lane 3: Ni-NTA column flow-through, lane 4-6: wash and lane 7: eluted fraction.*

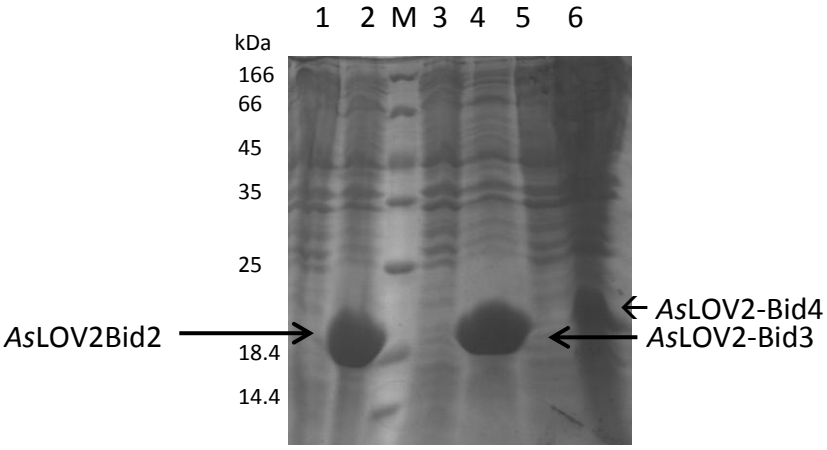

Figure 4.28: *SDS-PAGE analysis of crude cells of: AsLOV2-Bid2 before induction (lane 1) and after induction (lane 2), AsLOV2-Bid3 before induction (lane 3) and after induction (lane 4), and AsLOV2-Bid4 before induction (lane 5) and after induction (lane 6). M: protein marker.*

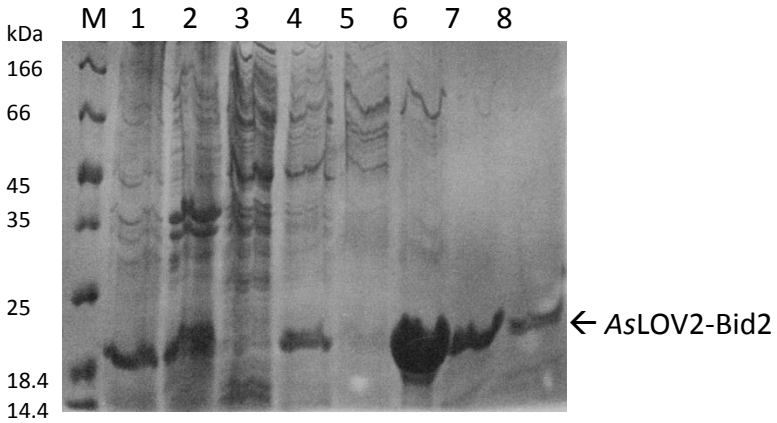

Figure 4.29: *Purification of AsLOV2-Bid2: M: protein marker, lane 1: cell lysate, lane 2: cell pellet, lane 3: Ni-NTA column flow-through, lane 4-5: wash, lane 6-8: eluted fractions.*

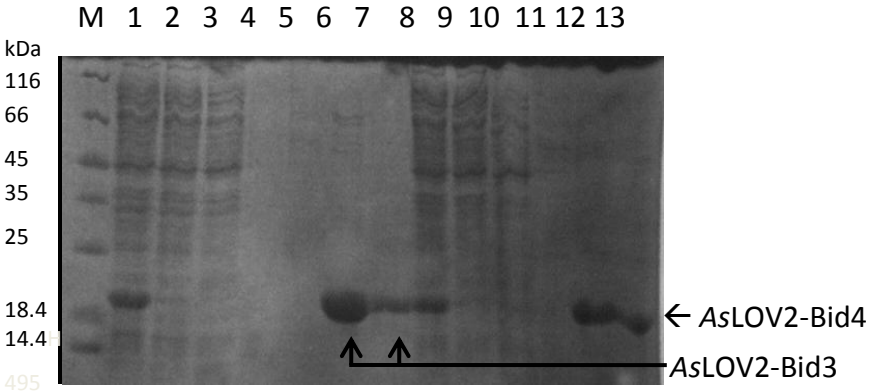

Figure 4.30: *Purification of AsLOV2-Bid3: M: protein marker, Lane 1: cell lysate, lane 2: cell pellet, lane 3: Ni-NTA column flow-through, lane 4-5: wash, lane 6-7: eluted fractions. Purification of AsLOVBid4: lane 8: cell lysate, lane 9: cell pellet, lane 10: Ni-NTA column flow-through, lane 11: wash, and lane 12-13: eluted fractions.*

*As*LOV2-Bid1-4 were further purified to remove impurities by size-exclusion chromatography (Figure: 4.31) and the masses were determined by ESI-TOF MS (Figures: 4.33-4.36). SDS-PAGE analysis of eluted fractions from preparative Superdex-200 column, show single bands for *As*LOV2-Bid1-4 at the approximately the correct protein mass (Figure: 4.32). Molecular masses of proteins were calculated from their ESI mass spectra (Tables: 4.5-4.8), where *As*LOV2-Bid2 (including FMN at 456.34) has the lowest calculated mass at 20438 and *As*LOV2-Bid4 (including FMN at 456.34) obtains the highest at 20940. All four observed protein masses deviate from the theoretical masses (including FMN at 456.34) by less than 0.5 %.

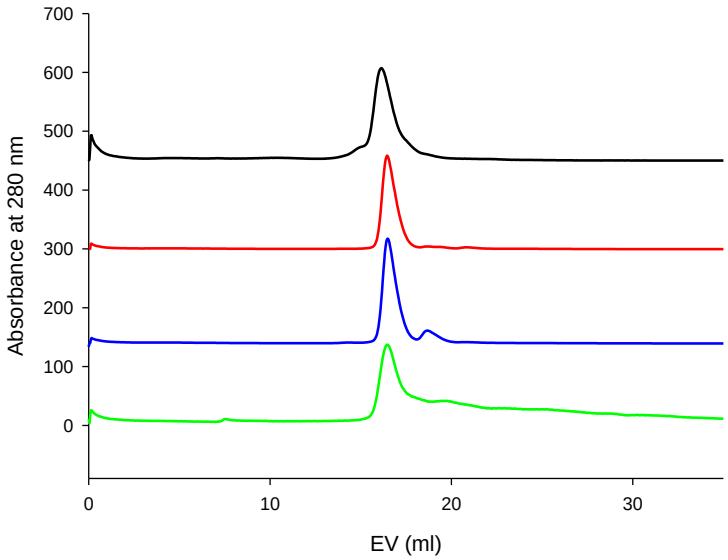

Figure 4.31: *Size-exclusion chromatograms of AsLOV2-Bid1 (black), AsLOV2-Bid2 (red), AsLOV2-Bid3 (blue) and AsLOV2-Bid4 (green) run on an analytical Superdex-200 column. Smaller peaks are due to impurities that are referred to in text.*

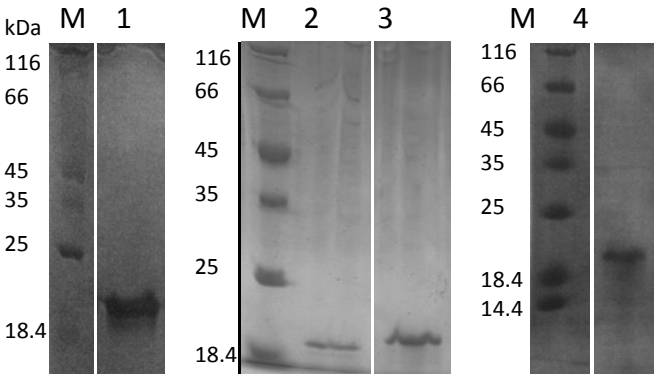

Figure 4.32: SDS-PAGE analysis of fractions from size-exclusion chromatography *purification of AsLOV2-Bid1-4 using preparative Superdex-200 column: Lane 1: AsLOV2-Bid1, Lane 2: AsLOV2-Bid2, Lane 3: AsLOV2-Bid 3, and Lane 4: AsLOV2-Bid4.*

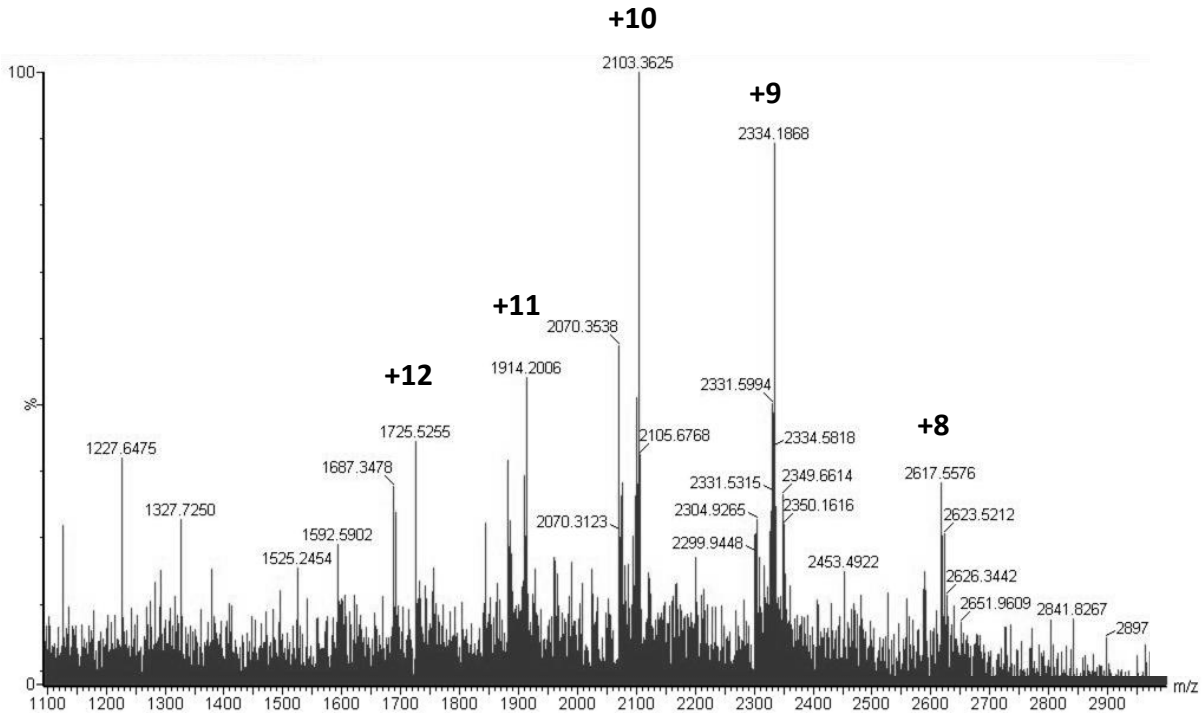

Figure 4.33: *ESI-TOF Mass spectrum of AsLOV2-Bid1. Illustrating the net charges in bold.*

m/z	net charge	Mass		Mass
1725.5255	12	20694.306	Calculated	20938.856
1914.2006	11	21045.2066	Theoretical	20812.569
2103.3625	10	21023.625	Difference	126.287
2334.1868	9	20998.6812	% Difference	0.60
2617.5576	8	20932.4608		

Table 4.5: *ESI-TOF MS data for AsLOV2-Bid1.*

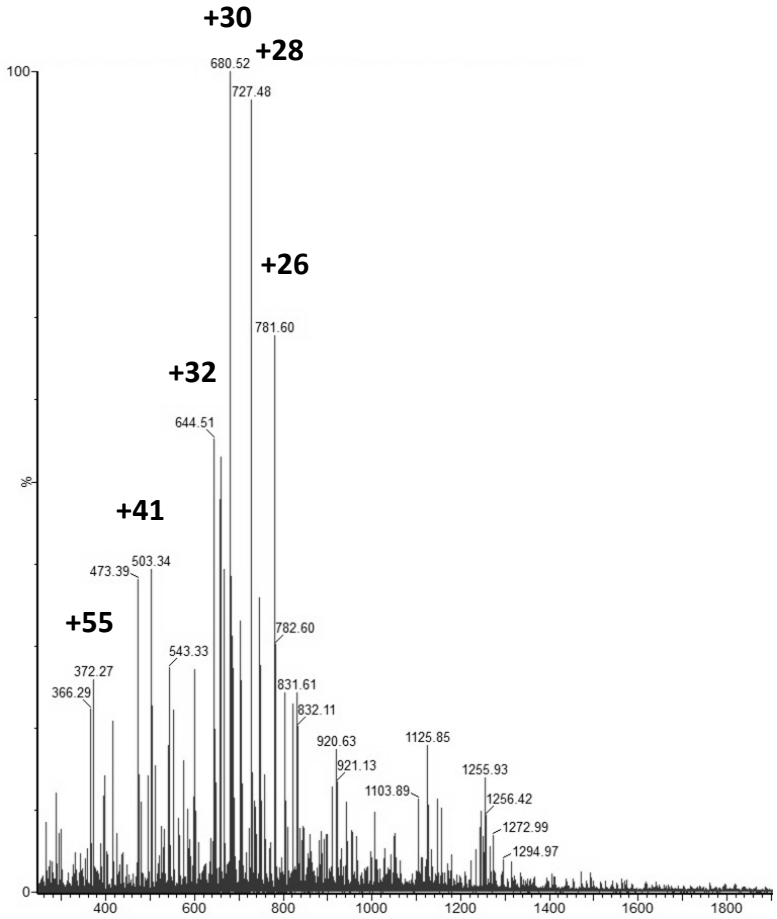

Figure 4.34: *ESI-TOF mass spectrum of AsLOV2-Bid2. Illustrating the net charges in bold.*

m/z	net charge	Mass		Mass
372.27	55	20419.85	Calculated	20438.458
503.34	41	20595.94	Theoretical	20523.535
644.51	32	20592.32	Difference	85.077
680.52	30	20385.6	% Difference	0.41
727.48	28	20341.44		
781.6	26	20295.6		

Table 4.6: *ESI-TOF MS data of AsLOV2-Bid2.*

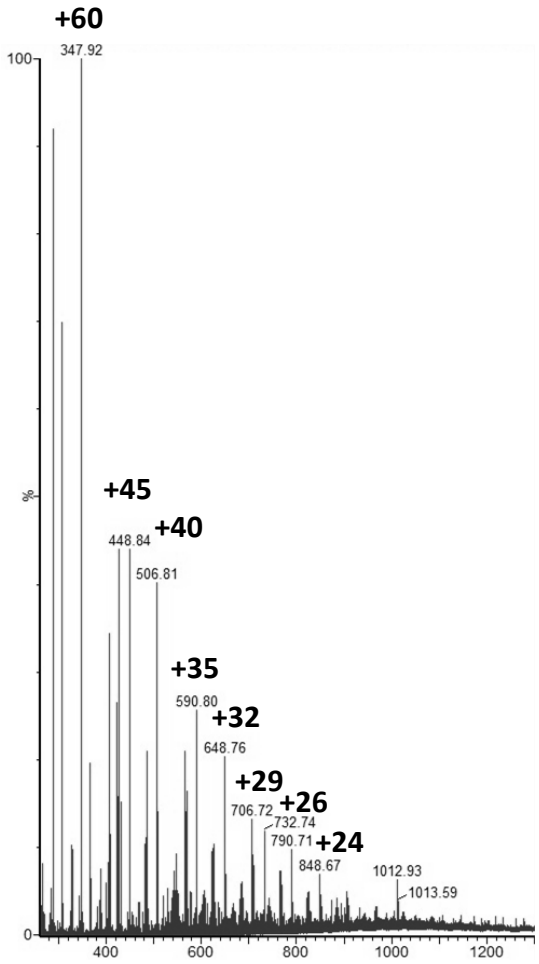

Figure 4.35: *ESI-TOF mass spectrum of AsLOV2-Bid3. Illustrating the net charges in bold.*

m/z	net charge	Mass		Mass
347.92	60	20815.2	Calculated	20489.27
448.84	45	20152.8	Theoretical	20523.55
506.81	40	20232.4	Difference	34.2825
590.8	35	20643	% Difference	0.167
648.76	32	20728.32		
706.72	29	20465.88		
790.71	26	20532.46		
848.67	24	20344.08		

Table 4.7: *ESI-TOF MS data of AsLOV2-Bid3.*

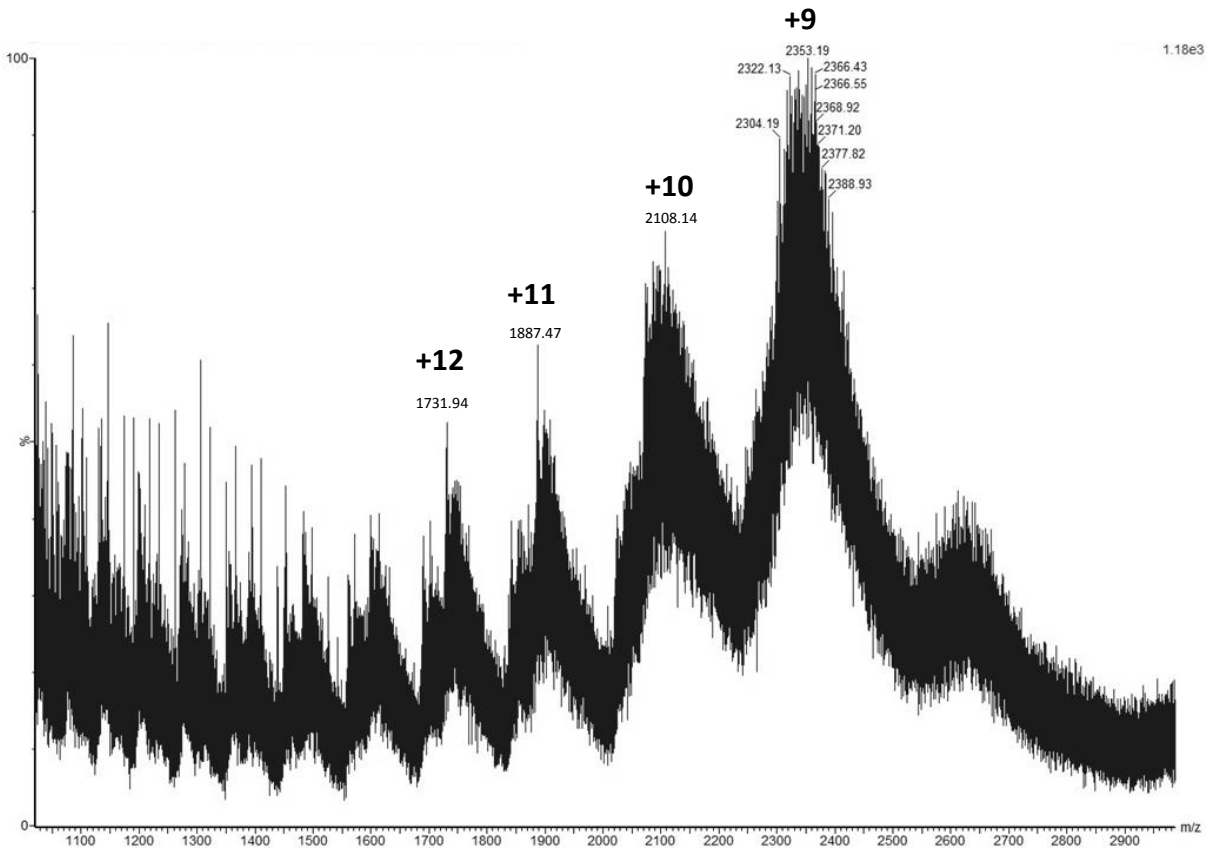

Figure 4.36: *ESI-TOF mass spectrum of AsLOV2-Bid4. Illustrating the net charges in bold.*

m/z	net charge	Mass		Mass
1731.94	12	20771.28	Calculated	20940.89
1887.47	11	20751.17	Theoretical	20928.75
2108.14	10	21071.4	Difference	12.137
2353.19	9	21169.71	% Difference	0.058

Table 4.8: *ESI-TOF MS data of AsLOV2-Bid4.*

4.3.7 Spectroscopic analysis of AsLOV2-V416I-Bid1-4

*As*LOV2-V183I-Bid1-4 (*As*LOV2-Bid1-4) produced UV/Vis absorption maxima at 447 nm and isosbestic points at 330 nm, 380 nm and 407 nm as observed with the spectra of the parent protein. The half-lives ($t_{1/2}$) of cysteinyl-FMN adducts were determined using the absorption at 447 nm (Table 4.9) and the difference in half-life times of Hisact-*As*LOV2-V416I-Bid (8.85 ± 0.10 min) and *As*LOV2-Bid1 (10.4 ± 0.05 min), indicates that the presence of the N-terminal hisactophilin has an effect on the FMN-adduct relaxation, a trend also observed for Hisact-*As*LOV2-V416I and *As*LOV2-V416I. However, the light states of *As*LOV2-Bid2-4 were found to relax at very similar rates ($t_{1/2}$ = 7-9 min) to the parent proteins (Hisact-*As*LOV2-V416I-Bid) featuring V416I (V183I) mutation.

Protein	Half-life (min)	
	UV/Vis	CD
Hisact-*As*LOV2	0.99 ± 0.05	0.66 ± 0.02
Hisact-*As*LOV2-V416I	7.69 ± 0.10	11.1 ± 2.70
Hisact-*As*LOV2-V416I-Bid	8.85 ± 0.10	11.3 ± 3.23
*As*LOV2-V183I	11.4 ± 0.12	13.0 ± 2.80
*As*LOV2-V183I-Bid1	10.4 ± 0.05	12.3 ± 2.40
*As*LOV2-V183I-Bid2	8.60 ± 0.05	10.3 ± 3.05
*As*LOV2-V183I-Bid3	7.50 ± 0.17	7.50 ± 1.00
*As*LOV2-V183I-Bid4	7.80 ± 0.75	7.80 ± 0.80

Table 4.9: *Half-lives of hybrid proteins at 20 °C comparing by UV/Vis observation of adduct reversion at 447 nm and mean residue ellipticity at 222 nm.*

Complementary measurements using CD spectroscopy at 222 nm were conducted, which reports on the photo adduct reversion and protein secondary structural rearrangements (Figure 4.37). The CD half-life values were compared to UV/Vis half-life values (Table 4.9) revealing that *As*LOV-Bid3 and *As*LOV-Bid4 relaxed at the same rate for both UV/Vis and CD average measurements whereas, both *As*LOV-Bid1 and *As*LOV-Bid2 cofactor adduct reversions (average values) were faster by approximately 2 minutes. However, they all fall within error so no overall change between the UV/Vis and CD half-lives can be assumed.

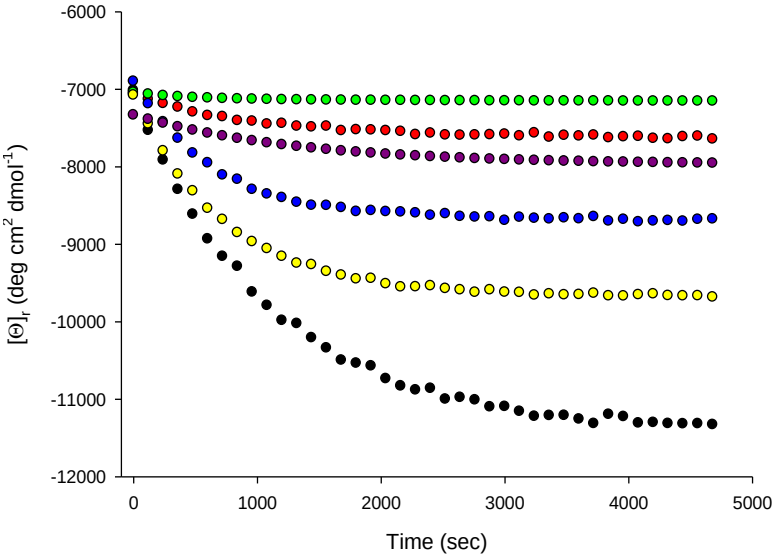

Figure 4.37: *Mean residue ellipticity at 222 nm for relaxing light state AsLOV2-V183I (black), Hisact-AsLOV-Bid1 (purple), AsLOV-Bid1 (red) AsLOV-Bid2 (green) AsLOV-Bid3 (blue) and AsLOV-Bid4 (yellow).*

Circular dichroism spectroscopy was used to analyse the proteins in the far-UV region, where negative signals at 208 nm and 222 nm indicated primarily α-helical structures, as expected (Figure 3.38). However, once irradiated a decrease in the negative signal can be seen for all proteins, except *As*LOV2-Bid2. The percentage-change in switching between the dark and the light state was calculated from the mean residue ellipticity (MRE) at 222 nm. A change in MRE at 222 nm was expected, as a result of the undocking and/or unfolding[124] of the Jα-helix (Section 3.3.4) as seen with the *As*LOV2-V416I. As expected, *As*LOV2-Bid4 resulted in the largest change in α-helical content with 28.4 % change (Table 4.10) as its Jα-helix has the least number of residue changes, as well as being longer than *As*LOV2-Bid1-3 (Figure 4.19). However, the magnitude of the change is 10 % less than for the wild-type LOV2 domain (Table 4.10), indicating that either the hybrid Jα-helices may not completely dock or undock from the LOV core, or that they are not fully helical in the docked state. *As*LOV2-Bid2 shows less than 2 % change in ellipticity at 222 nm, suggesting that the photo-activation has been disturbed in this design. Once again, interpretation of this data is complicated by the uncertainty of the structure in both extended and undocked helices. While BH3 peptides are typically unstructured in the absence of constraints,[137] the most

likely interpretation of the data overall is that the presence of residues from the Jα-helix have a helix-nucleating effect.

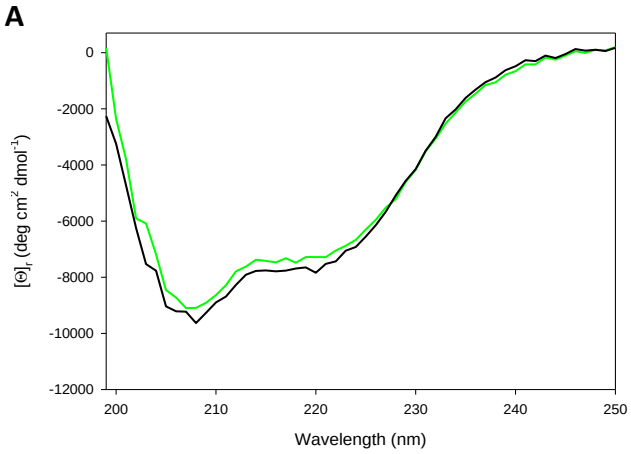

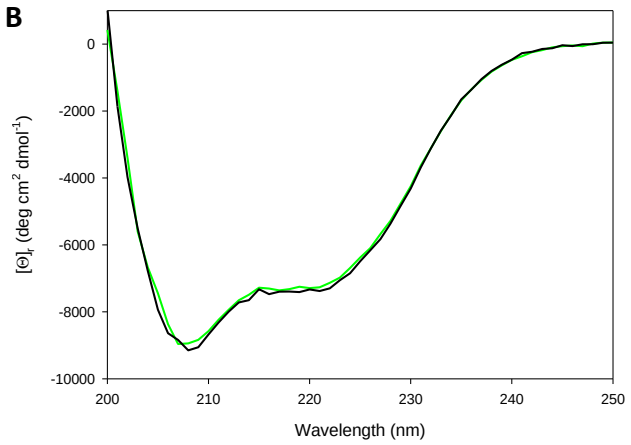

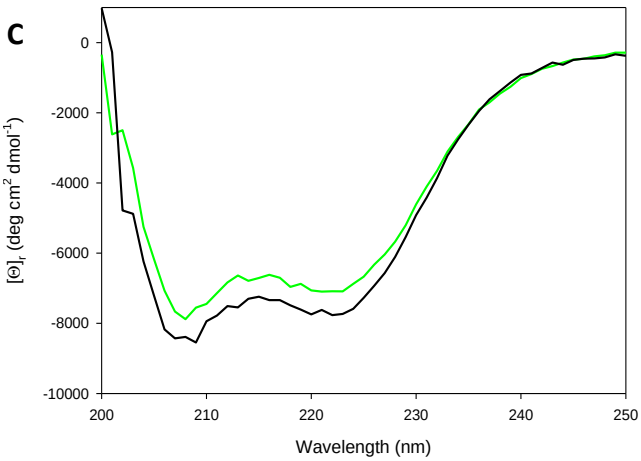

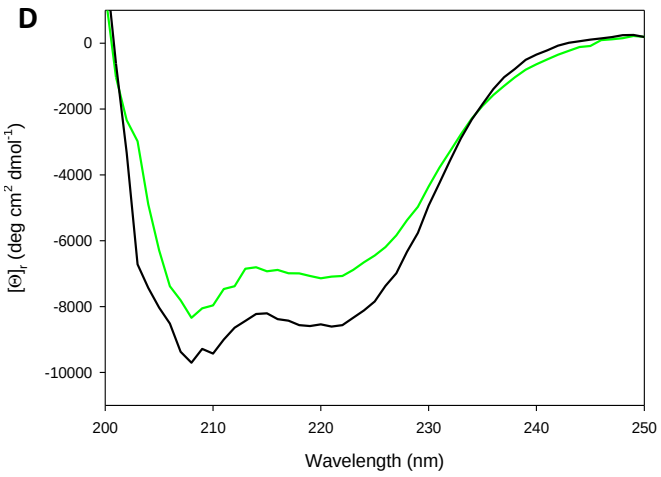

Figure 4.38: *CD measurements showing proteins in the dark (black) and light (green) states: A) AsLOV2-Bid1 B) AsLOV2-Bid2 C) AsLOV2-Bid3 D) AsLOV2-Bid4.*

Protein	% Change in $[\Theta]_r$ at 222 nm
Hisact-*As*LOV2 [a]	39.2
Hisact-*As*LOV2-V416I [a]	38.1
Hisact-*As*LOV2-V416I-Bid1 [a]	7.96
*As*LOV2-V416I [b]	38.5
*As*LOV2- V416I-Bid1 [c]	7.30
*As*LOV2- V416I-Bid2 [d]	1.90
*As*LOV2- V416I-Bid3 [e]	18.9
*As*LOV2- V416I-Bid4 [f]	28.4

Table 4.10: *Length of Jα and Jα hybrid helices according to the number of amino acid residues: [a] 288 [b] 160 [c] 178 [d] 173 [e] 176 [f] 179.*

Melting curves obtained from CD measurements at increasing temperatures reported *As*LOV2-Bid1 to be the most stable variant with a melting point at 54 °C and *As*LOV2-Bid2-4 to be the less stable since unfolding starts as low as 40 °C (Figure 4.39). A possible explanation for this may be that, as the helix is extended further in length the protein becomes structured less like the parent protein, therefore its thermal stability decreases. *As*LOV2-Bid1 is exactly the same length as *As*LOV2-V416I, therefore its melting point is the same, (54 °C; Section 3.3.4.2).

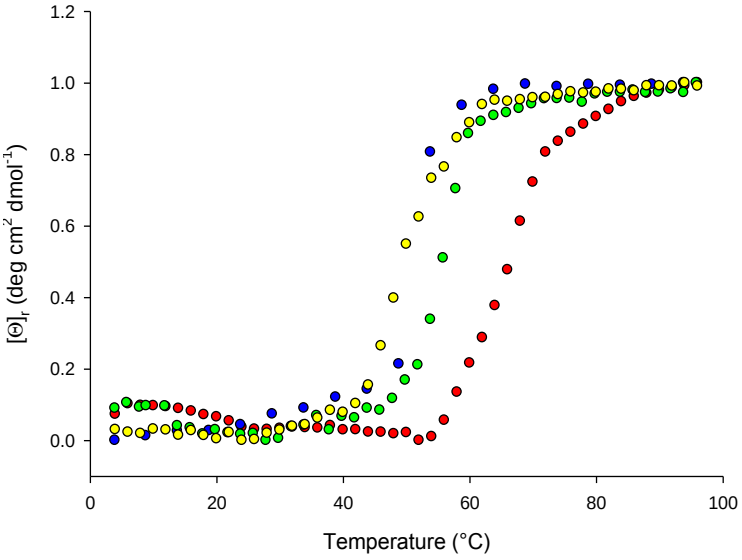

Figure 4.39: *Normalised plots of mean residue ellipticity 222 nm of AsLOV2-Bid1 (red) AsLOV2-Bid2 (green) AsLOV2-Bid3 (blue) and AsLOV2-Bid4 (yellow) over a range of temperatures (4-96 °C).*

4.3.8 Fluorescence anisotropy measurements of AsLOV-Bid1-4

Initial fluorescent anisotropy measurements carried out using Hisact-*As*LOV2-Bid-PD547C(TMR) (Hisact-*As*LOV2-Bid) gave K_D values of less than 1 μM in the light and dark state (Section 4.3.3.1) although, it was expected that caging of the helix in the absence of light would not allow binding to Bcl-x_L in the dark state. CD time-course measurements showed a low (7.96 %) change in MRE at 222 nm in comparison to *As*LOV2-V183I (Figure: 4.37, Table: 4.10), indicating that the hybrid-Jα may not completely dock to the LOV core in the dark state, as a result of the steric hindrance caused by the TMR dye at the C-terminal end of Jα-hybrid. To avoid any such factors affecting the photo-switching mechanism of the *As*LOV2-Bid proteins, the Bcl-x_L protein was labelled instead. A cysteine residue was incorporated at the N-terminus of Bcl-x_L by site-directed mutagenesis at the second amino acid (S2C) from the methionine start codon, this was confirmed by sequencing (Appendix H). Native Bcl-x_L contains a cysteine residue whose side chain is buried in the folded protein, whereas the mutational cysteine (S2C) is far from the binding site and is located on the exterior of the protein (Figure: 4.40) allowing easy access for TMR to react with the cysteine thiolate.

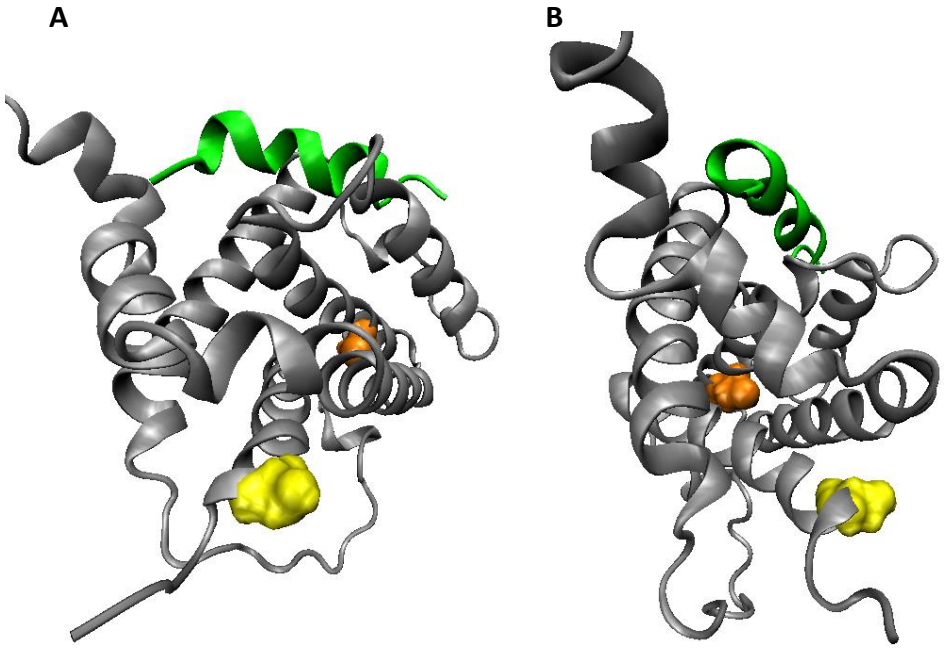

Figure 4.40: *Structure of Bcl-x_L (gray) and interacting Bak peptide (green): showing internal native cysteine (orange) and solvent exposed cysteine (S2C) inserted via mutation (yellow). A) Front view and B) side view. (PDB: 1BXL).*

Bcl-x_L-S2C was expressed and purified (Figure 4.41) using the same procedure as used for wild-type protein. The labelling procedure for Bcl-x_L was carried out as previously described for Hiscat-*As*LOV2-V416I-Bid and an approximate extinction co-efficient of 91,000 $M^{-1}cm^{-1}$ at 551 nm (Section 4.3.3) was used to estimate the concentration of labelled protein. Bcl-x_L-TMR conjugation was quantified by comparing the labelled Bcl-x_L-S2C(TMR) concentration with the total Bcl-x_L-S2C concentration before reaction (extinction co-efficient of 41,940 $M^{-1}cm^{-1}$ at 280 nm, Figure 4.42). Protein samples that were ≥75 % labelled were prepared for fluorescent anisotropy measurements. Prior to measuring protein concentrations, excess TMR dye was removed by size-exclusion chromatography (Figure 4.43) eluting in 50 mM sodium phosphate buffer containing 100 mM sodium chloride and 5 mM β-mercaptoethanol (SEC buffer B).

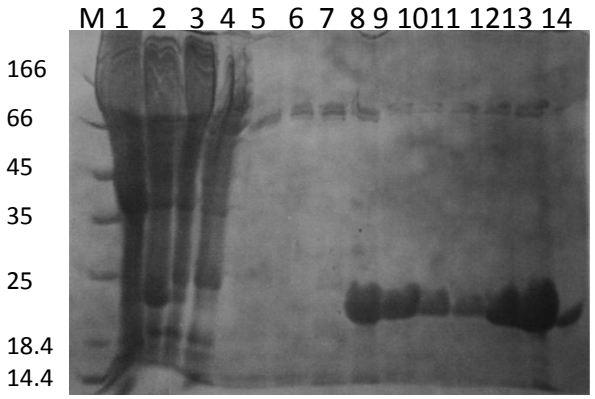

Figure 4.41: 12 % *SDS-PAGE gel of Bcl-x_L-S2C purification. M: protein marker, lane 1: cell pellet, lane 2: cell lysate, lane 3: Ni-NTA column flow-through, lane 4-7: wash, lane 8-13: eluted fractions and lane 14: TMR labelled Bcl-x_L-S2C.*

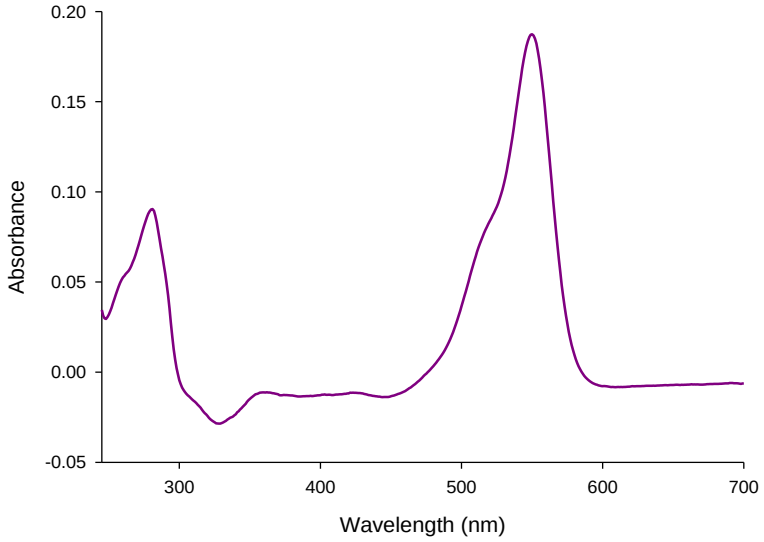

Figure 4.42: *UV/Vis absorption spectra of Bcl-x_L-S2C(TMR).*

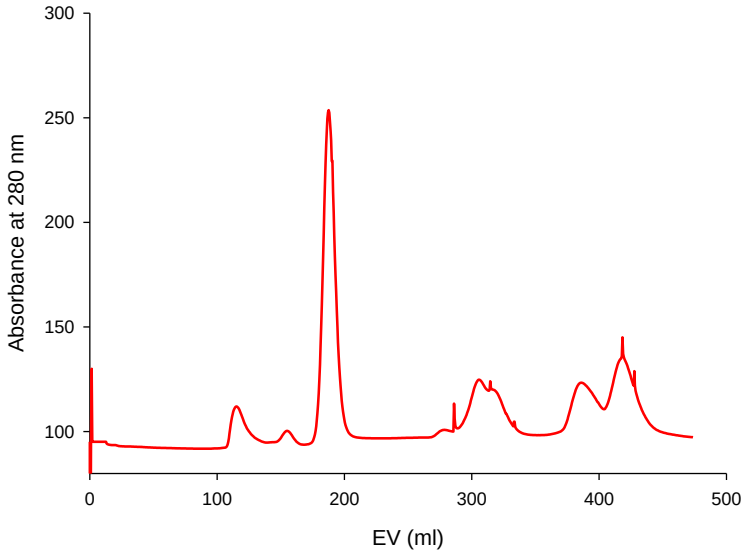

Figure 4.43: *Size-exclusion chromatogram of Bcl-x_L-S2C(TMR) (190 mL) and excess TMR (after 290 ml).*

Fluorescence anisotropy measurements between the *As*LOV2-Bid domains and TMR-labelled Bcl-x_L were carried out at a reduced temperature (15 ^{o}C) to minimise reversion to dark state during the recording of individual data points. Titrations were repeated at least in triplicate and the data for both dark and light states were normalised and plotted on one graph to allow accurate comparison (Figure 4.44).

Bcl-x_L is specific to BH3 sequences only,[103-107,153] so no binding should be observed with the LOV2 wild-type. No change in anisotropy was evident with wild-type *As*LOV2 protein in either it's dark or light states (Figure 4.44A).

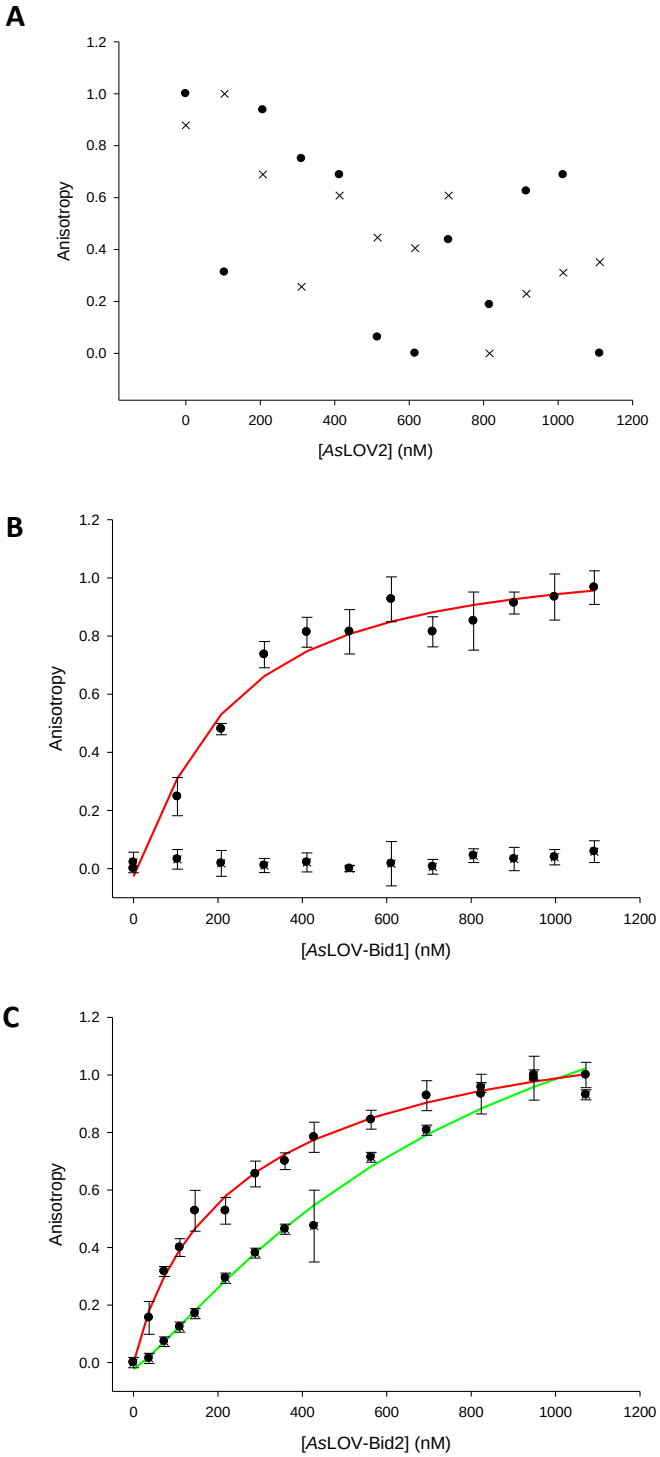

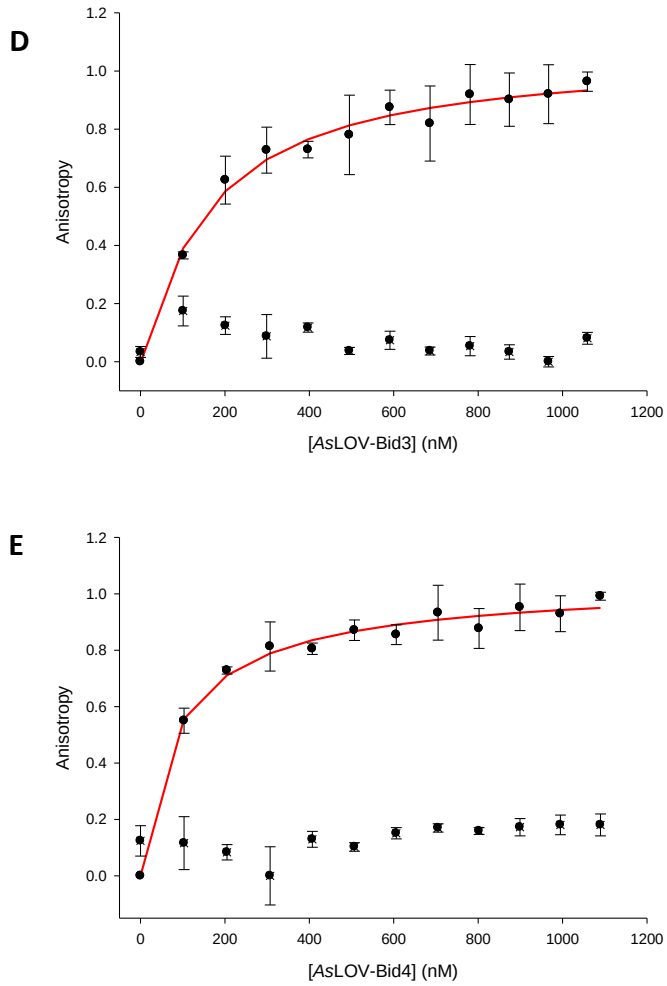

Figure 4.44: *Normalised fluorescent anisotropy binding curves of AsLOV-Bid proteins to Bcl-x_L-S2C(TMR) in the dark (green or no line) and light (red) states. A) AsLOV2 B) AsLOV-Bid1 C) AsLOV-Bid2 D) AsLOV-Bid3 E) AsLOV-Bid4.*

In contrast, light state samples of each of the *As*LOV2-Bid hybrids caused significant increases in anisotropy suggestive of binding to Bcl-x_L with apparent dissociation constants between 80 and 300 nM, higher than those observed for the LOV2-Bid peptide. The dissociation constants decreased slightly as the length of hybrid Jα-helix increased (Table 4.11) in agreement with the prediction that these sequences would possess less sterically hindered BH3 regions in the photo-activated state and would therefore possess a stronger binding affinity for Bcl-x_L. *As*LOV2-Bid1, *As*LOV2-Bid3 and *As*LOV2-Bid4 show no binding to Bcl-x_L in the dark adapted form (Figure 4.44 and Table 4.11). Following the theory adopted and proved by Strickland *et al.,*[51,57] sequence overlap with Jα-helix, may have resulted in part of the Bid BH3 sequence adopting a sterically blocked or 'caged' conformation in the

dark state, thereby restricting binding to Bcl-x_L. As discussed earlier, residue I86 is vital for binding to Bcl-x_L,[153] and in *As*LOV2-Bid1-4 it is overlapped with Jα-helix to prevent dark state binding.

However, increased light-state affinity correlated with dark-state affinity for *As*LOV-Bid2, reporting binding in both light (271 nM) and dark (998 nM) states. The CD data for *As*LOV2-Bid2, reporting less than 2 % change in protein secondary structural rearrangement, is in agreement with the binding data and implicates that the hybrid Jα-helix does not properly dock to the LOV core, in the dark state. Formation and stability of alpha-helices are dependent on intrinsic helix-forming propensities of adjacent amino acids.[6,169,170] Residues with charged side chains are known to affect helix formation through helix-propensity and coloumbic forces.[169,170] It is anticipated that replacement acidic residues, glutamate 537 and 541 (negatively charged in physiological pH) with positively charged arginine (E537R, E541R), and basic lysine 543 with acidic aspartate (K543D), may have an effect on helix formation and therefore be partially undocked, allowing the Bid BH3 sequence to interact with Bcl-x_L in the light and dark state.

Protein	K_D (Dark state)	K_D (Light State)
*As*LOV-Bid1	N/A	216 ± 16.3 nM
*As*LOV-Bid2	998 ± 111 nM	271 ± 13.7 nM
*As*LOV-Bid3	N/A	167 ± 2.5 nM
*As*LOV-Bid4	N/A	89 ± 4.9 nM

Table 4.11: *Dissociation constants for binding of hybrid AsLOV-Bid proteins to TMR-Bcl-x_L (10 nM).*

4.4 Conclusion

Four photo-responsive *Avena sativa* LOV2 Jα fusions have been designed and synthesised based on the pro-apoptotic BH3 domain of Bid. A LOV2-Bid BH3 peptide was tested first in order to ensure the modifications made to create the *As*LOV2-Bid1 sequence did not abolish affinity to Bcl-x_L. As expected, the peptide showed strong binding affinity for Bcl-x_L with a relatively small increase in dissociation constant compared to the wild-type Bid BH3 sequence. Using the same hybrid design as the LOV2-Bid peptide, Hisact-LOV-V416I-Bid was engineered successfully using recombinant DNA technology and the protein expressed and purified using the same procedure as wild-type *As*LOV2. UV/Vis and CD derived half-life values were within the same range calculated for the parent protein (Hisact-*As*LOV2-V416I), however the changes in the MRE at 222 nm using CD spectroscopy reported that the protein showed minimal changes in its secondary structure compared to Hisact-*As*LOV2-V416I. This tied in with the fluorescence anisotropy data which revealed binding with Bcl-x_L in both the dark and light adapted states, thus indicating that the hybrid Jα may be partially undocked as a result of steric hindrance between modified residues in the Jα, the hisactophilin or the TMR dye attached to the Jα C-terminus. Although Hisact-*As*LOV2-Bid demonstrated significant binding affinity to Bcl-x_L, it failed to act as an optogenetics switch.

To further improve the *As*LOV2-Bid hybrid, removal of the hisactophilin domain and varying the point of fusion between the LOV Jα-helix and the Bid BH3 sequence generated derivatives with a range of switching properties. UV/Vis and CD characterisation of *As*LOV2-Bid1-4 allowed comparison of their rates of cysteinyl-FMN adduct reversion and protein structural rearrangements. *As*LOV2-Bid2 showed a diminutive change in α-helical content between the dark and light states, with *As*LOV2-Bid4 reporting the largest change. These data broadly correlated with the fluorescence anisotropy data (in this case Bcl-x_L was labelled instead of *As*LOV2-Bid proteins), where *As*LOV-Bid2 showed significant binding to Bcl-x_L protein in the light and dark states and *As*LOV2-Bid4 gave the strongest binding affinity to Bcl-x_L. No dark state binding was observed with *As*LOV2-Bid1, indicating that dark state binding of Hisact-*As*LOV2-V416I-Bid was as a result to either, the hisactophilin or the TMR dye as opposed to modified residues in the Jα.

Chapter 5:

Bacillus subtilis

YtvA

5.1 Introduction

Following the broadly successful approach for engineering photoreceptors to control cellular pathways, as studied so far with the LOV2-Bid hybrid (Chapter 4), we aim to study and develop possible fusions using the YtvA photoreceptor (261 amino acids) from *Bacillus subtilis* which has a slow photocycling LOV domain with a half-life of 3600 sec.[116] Its longer-lived light-state is potentially advantageous for creating photo-switchable fusion proteins that will allow longer duration for signalling *in vivo*, in this case to control apoptosis.

The LOV domain of YtvA is similar to those of plant phototropins (Figure 5.1) and has a high sequence homology with LOV2 domains and the Jα linker.[45,119] Residue Q123 aligns with Q513 of *As*LOV2 and has a similar role in forming initial interactions with FMN through hydrogen bonding.[37,45,115] Residues V29 (Aβ), M111 (Hβ) and Y118 (Iβ) align with *As*LOV2 residues V416, M499 and Y508[117,118] (Figure 5.1).

```
O49003   ---------------- TTLERIEKNFVITDPRLPDNPIIFASDSFLQLTEYSREEILGR  448  O49003_AVESA
O34627   MASFQSFGIPGQLEVIKKALDHVRVGVVITDPALEDNPIVYVNQGFVQMTGYETEEILGK  60   PHOT_BACSU

O49003   NCRFLQGPETDRATVRKIRDAIDNQTEVTVQLINYTKSGKKFWNLFHLQPMRDQKGDVQY  508  O49003_AVESA
O34627   NCRFLQGKHTDPAEVDNIRTALQNKEPVTVQIQNYKKDGTMFWNELNIDPM--EIEDKTY  118  PHOT_BACSU

O49003   FIGVQLDGTEH-----------------------VRD-----------------------  522  O49003_AVESA
O34627   FVGIQNDITKQKEYEKLLEDSLTEITALSTPIVPIRNGISALPLVGNLTEERFNSIVCTL  178  PHOT_BACSU

O49003   ----AAEREGVMLIKKT--AENIDEAAKELP-----------------------------  547  O49003_AVESA
O34627   TNILSTSKDDYLIIDLSGLAQVNEQTADQIFKLSHLLKLTGTELIITGIKPELAMKMNKL  238  PHOT_BACSU

O49003   DANLRPEDLWA----------  558  O49003_AVESA
O34627   DANFSSLKTYSNVKDAVKVLPIM  261  PHOT_BACSU
```

Figure 5.1: *ClustalW alignment of AsLOV2 (O49003_AVESA) and YtvA-LOV (PHOT_BACSU), residues that match are highlighted in grey.*

YtvA-LOV has been reported to be dimeric in solution based on gel filtration experiments.[119] As discussed previously (Section 1.4.5), the crystal structure of the dark-state YtvA-LOV domain reveals a head-to-head dimer with the Jα helix undocked from the core domain (Figure 5.2).[45] A shorter loop between Iβ and the Jα in YtvA-LOV may prevent the Jα from folding against the central β-sheet, as observed in *Avena sativa* LOV2 (Figure 5.3).[45] The exposed hydrophobic face of the β-sheet is able to promote dimerisation of the YtvA-LOV.

Therefore, it will be ideal to study the hydrophobic surface in greater detail through creating point mutations on important hydrophobic amino acids, before any LOV-BH3 fusions are designed and implemented.

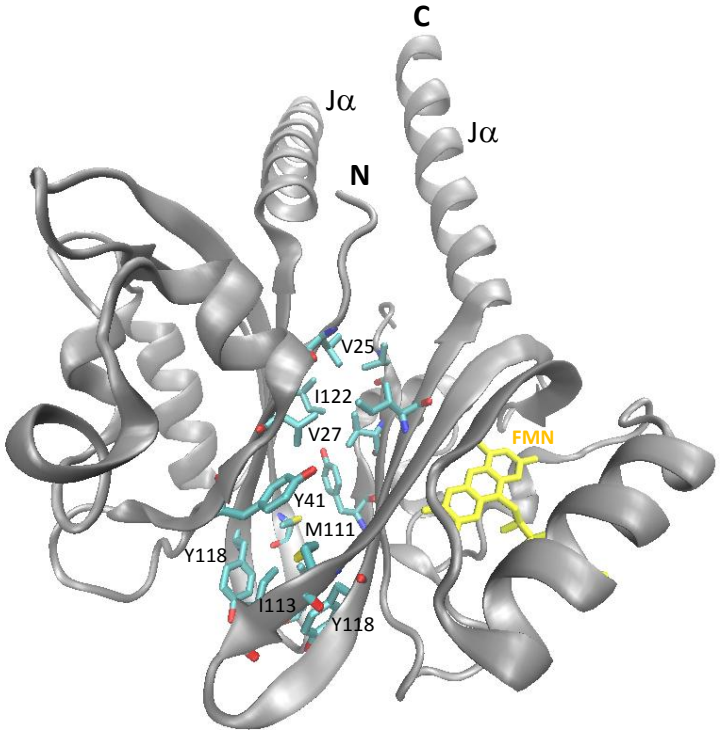

Figure 5.2: *Structure of dark state YtvA-LOV showing undocked Jα helices and the key residues in the hydrophobic dimer interface (PDB: 2PR5).*

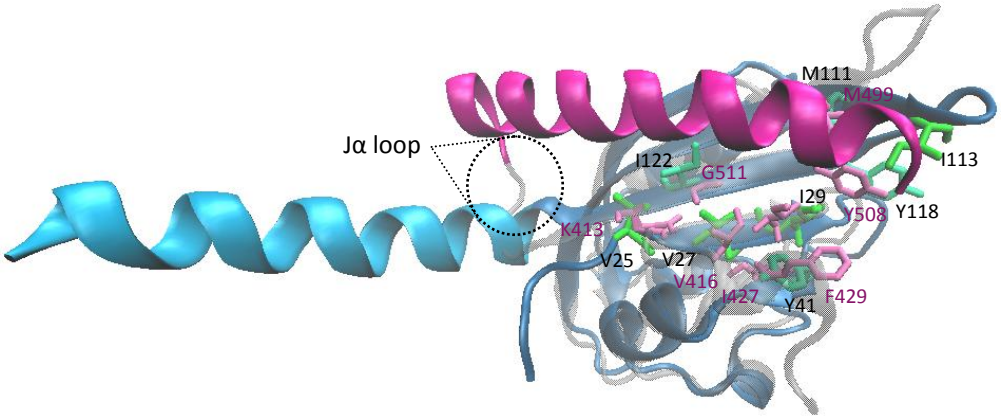

Figure 5.3 *Structure overlay of AsLOV2 (gray) and YtvA-LOV (blue), where the Jα of AsLOV2 (pink) is folded on to the core and the Jα of YtvA-LOV is open (cyan). (PDB: 2V1B and 2PR5).*

Moglich and Moffat, irradiated YtvA-LOV dark state crystals in order to get a pseudo light-state structures.[45] The results show the Jα-helices do not unfold in the light state, rather a 4-

5° rotation relative to each dimer was observed. However, to fully acknowledge its conformation and that there is no unfolding of the Jα a light state solution structure is indeed required. It is also noted that hydrophobic LOV core (β Sheet) is more extended than in *As*LOV2,[45] thereby possibly promoting dimerisation. However, residue I113 corresponds to D501 in *As*LOV2, but here forms part of Hβ rather than the loop connecting Hβ to Iβ therefore, limiting the flexibility of the loop and perhaps preventing the Jα from docking to the core and allowing the formation of dimers.

Residues on the Aβ (V25, V27), Bβ (Y41), Hβ (M111, I113) and Iβ (Y118, V120, I122) strands mediate dimer interactions (Figure 5.2). The hydrophobic residue V25 at the start of the Aβ strand in YtvA-LOV replaces a polar amino acid denoted as K413 in *As*LOV2, and V27 replaces the less hydrophobic F415 suggesting that these residues may play a role in creating the hydrophobic dimer interface (Figure 5.1 and 5.3). These residues were therefore selected for mutational studies to provide more information on the driving force for dimerisation of YtvA-LOV.

5.2 Results and Discussion

5.2.1 YtvA-LOV-STAS and YtvA-LOV modification and characterisation

The gene encoding YtvA-LOV-STAS (786 bp; Section 1.4.5) was isolated from *Bacillus subtilis* chromosomal DNA using PCR. The YtvA-LOV-STAS gene was cut with *Nde*I and *BamH*I restriction endonucleases, which were initially incorporated on to the gene by specifically designed PCR primers that were used to isolate YtvA-LOV-STAS. A pET19b vector was cut also using *Nde*I and *BamH*I restriction endonucleases and run on an agarose gel. The migration speed of the DNA band corresponded to the calculated size (5717 bp) of the cut plasmid (Figure 5.4). The vector sample was purified with the QIAquick PCR purification kit using a microcentrifuge, which removed all enzymes and residual buffers. Both the vector and insert were ligated using T4 DNA ligase (NEB protocol) and *E. coli* XL1-blue cells were transformed with the ligation mixture. The resulting colonies were picked and the DNA was isolated for a digestion test with restriction enzymes *NdeI* and *BamHI,* to detect colonies whose plasmids contained an insert (Figure 5.5). Ligation of the correct gene was confirmed by DNA sequencing. The YtvA-LOV-STAS domain was further modified by insertion of a stop

codon after the YtvA-LOV domain via site-directed mutagenesis, removing the STAS domain from the translated full length protein (Figure 5.6).

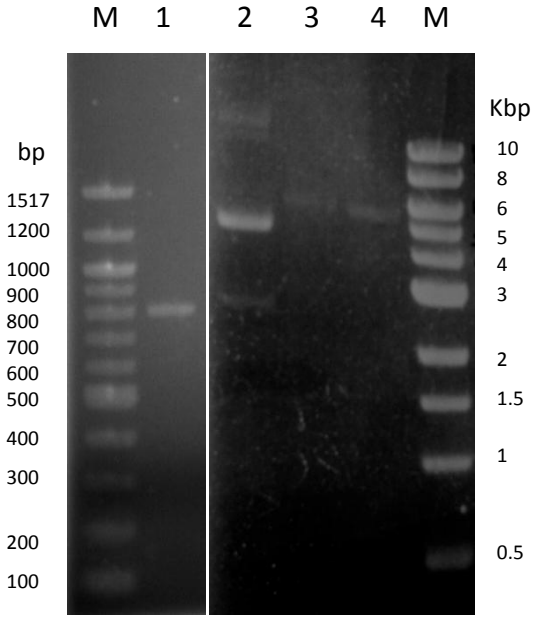

Figure 5.4: *Agarose gel showing: lane M: DNA marker, lane 1: YtvA-LOV-STAS (~800 bp). pET19b vector (5.7 kbp): lane 2: uncut, lane 3: cut with NdeI and lane 4: cut with NdeI and BamHI.*

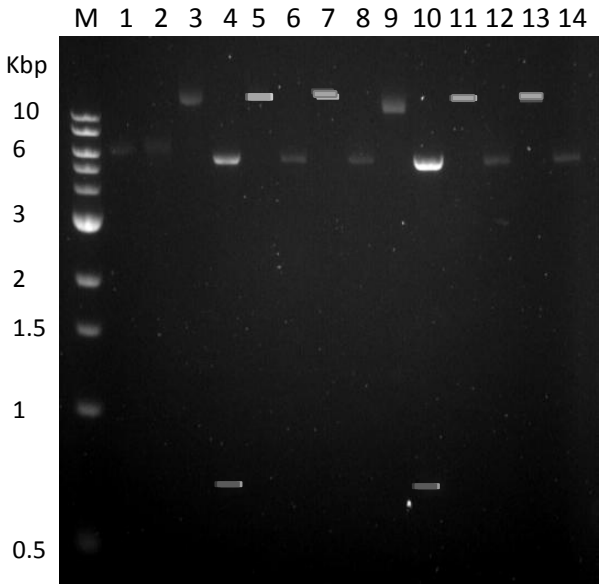

Figure 5.5: *Agarose gel of digestion tests on ligated pET19b-YtvA-LOV samples using NdeI and BamHI: uncut (lanes 1, 3, 5, 7, 9 11 and 13) and cut (lanes 2, 4, 6, 8, 10, 12 and 14). With visible YtvA-LOV-STAS (~800 bp) bands in sample 2 (Lane 4) and sample 5 (Lane 10).*

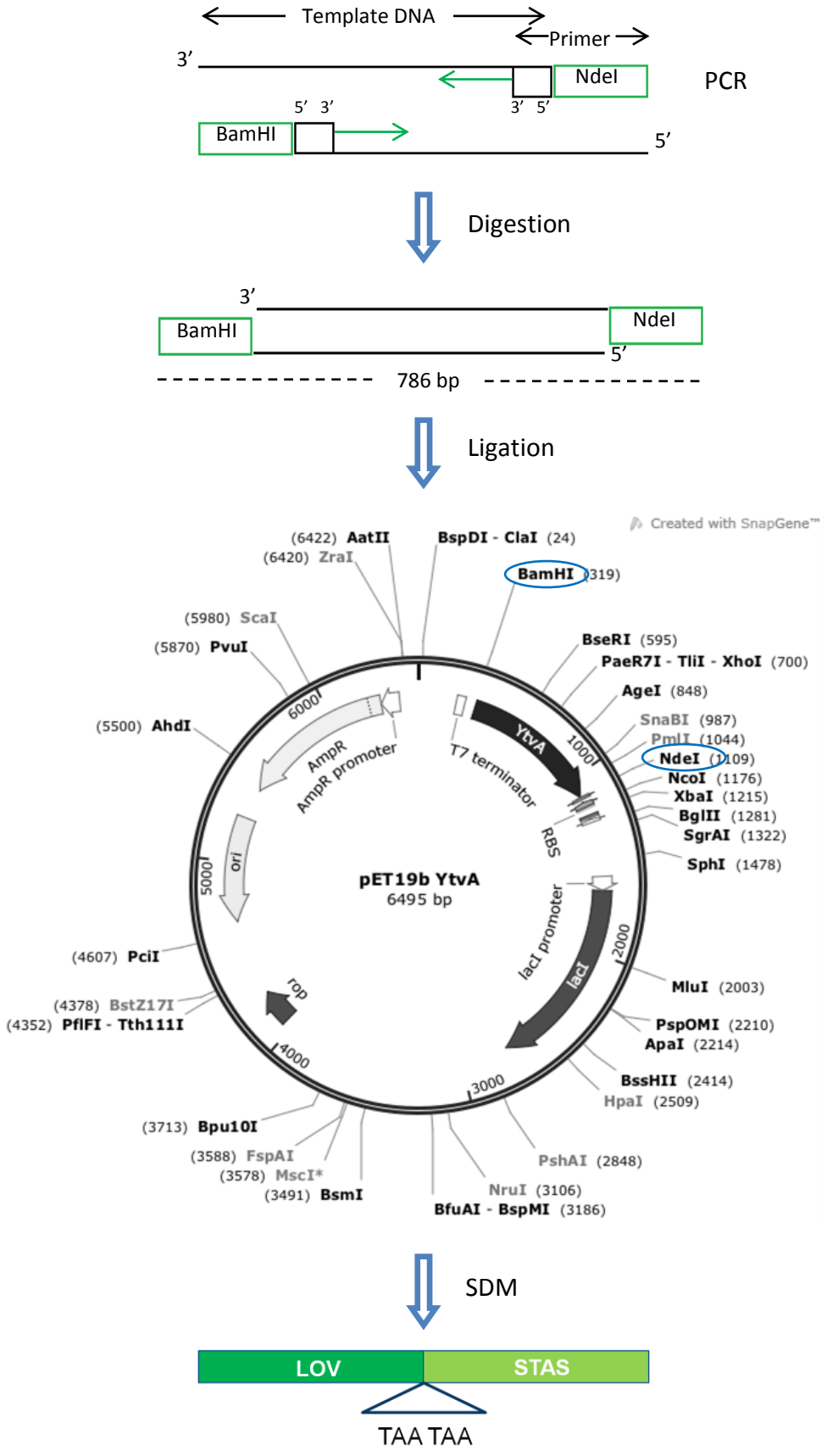

Figure 5.6: *Diagram representing the cloning steps and modifications on YtvA-LOV-STAS to acquire the single YtvA-LOV domain without STAS; NdeI and BamHI sites were incorporated on gene via PCR, which was then ligated into the pET19b vector, and stop codons were introduced after the LOV domain by SDM.*

The proteins were expressed and purified by adapting the procedure of Kay *et al.*;[39] *E. coli* cells harbouring a pET19b plasmid containing the gene encoding YtvA-LOV-STAS (32 kDa) or YtvA-LOV (19.6 kDa) over-expressed proteins corresponding to the sizes of the desired proteins upon induction at OD_{600} 0.7-0.8, and incubation overnight at 20 °C. The pET19b vector includes an N-terminal His-tag which allowed purification by nickel-nitrilotriacetic acid (Ni-NTA) affinity chromatography. Fractions were analysed using SDS-PAGE (Figure 5.7 and 5.8) and followed further purification using size-exclusion chromatography. An m/z ratio of 19696 was observed using MALDI-TOF mass spectrometry (Figure 5.9) which corresponded reasonably to the theoretical mass of YtvA-LOV at 19623.

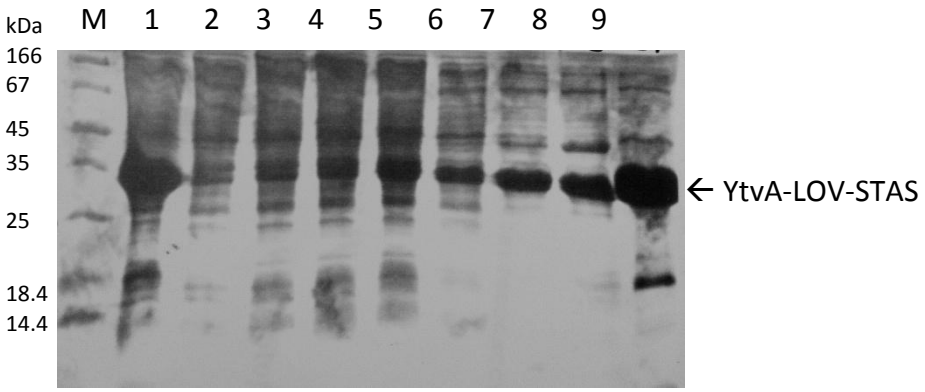

Figure 5.7: *SDS-PAGE analysis of YtvA-LOV-STAS through the stages of purification using affinity chromatography. M: protein marker, lane 1: lysate, Lane 2: flow through fraction off the affinity column (10 mM imidazole), lane 3 to 5: wash with buffer (40 mM imidazole), lane 6 to 9: elution fractions (500 mM imidazole).*

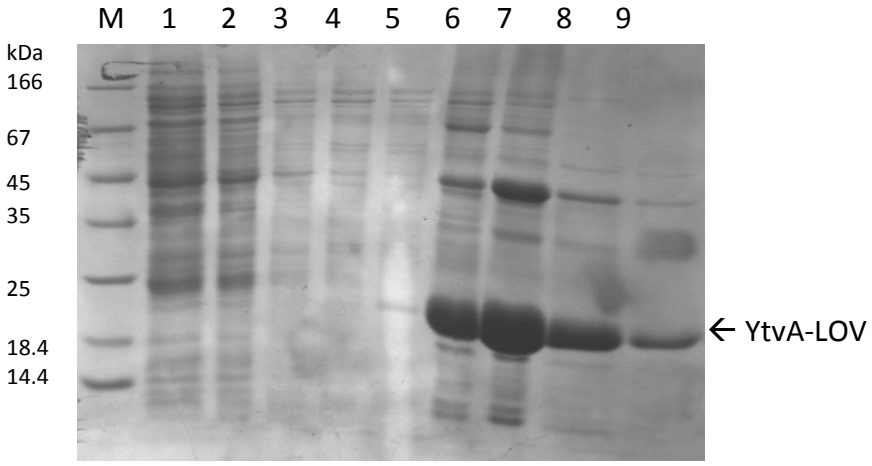

Figure 5.8: *SDS-PAGE analysis of YtvA-LOV through the stages of purification using affinity chromatography. M: protein marker, lane 1: lysate, Lane 2: flow through fraction off the affinity column (10 mM imidazole), lane 3 to 5: wash with buffer (40 mM imidazole), lane 6 to 9: elution fractions (500 mM imidazole).*

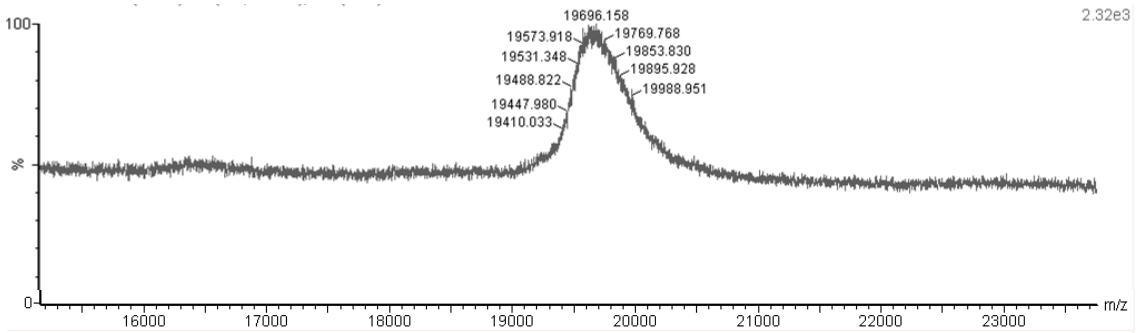

Figure 5.9: *MALDI-TOF spectrum of YtvA-LOV.*

5.2.2 Spectroscopic characterisation of YtvA-LOV-STAS and YtvA-LOV

As expected both YtvA proteins showed an absorption maximum at 447 nm with vibronic coupling (triplet peak) indicative of association with folded protein and conversion of the FMN from light state to dark state[45,125] (Figure 5.10). As previously observed for *As*LOV2 (Figure 3.13), the YtvA-LOV domain has 3 isosbestic points at 330 nm, 380 nm and 407 nm (Figure 5.10) upon photoswitching.

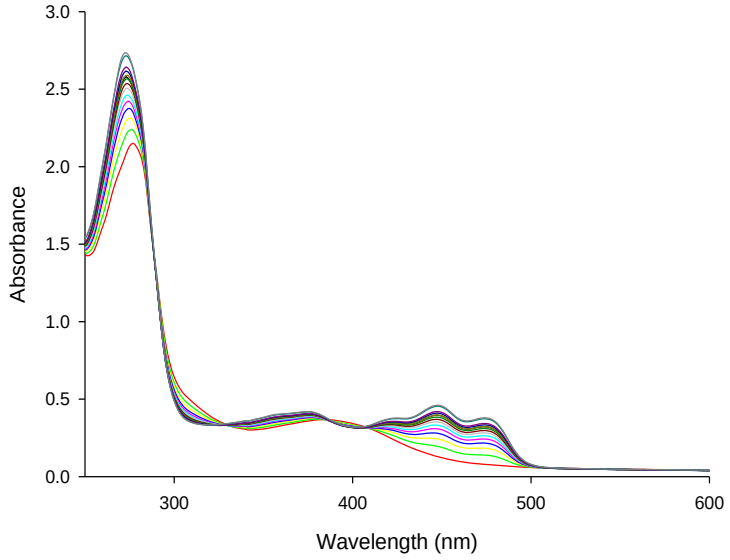

Figure 5.10: *UV/ Vis absorption spectra of YtvA-LOV (reading at every 5 min) showing the relaxation from light state (red) to dark state (black), the FMN absorption maximum visible at 447 nm and three isosbestic points are seen at 330 nm, 380 nm and 407 nm.*

The half-life of YtvA-LOV-STAS has been determined as 3600 sec by Zoltwoski *et al.*[116] In this investigation the half-life of the light state was measured by recovery of absorbance at 447 nm (20 °C). As expected, YtvA-LOV has a slower recovery rate than the *As*LOV2 domains.[118,19,45] It was calculated that YtvA-LOV-STAS has a longer relaxation half-life than the smaller YtvA-LOV domain (Figure 5.11, Table 5.1) resulting a difference of 2274 sec (37.9 min) (Table 5.1). Moglich and Moffat have determined the half-life of YtvA-STAS at 3880 ± 20 sec and YtvA-LOV with a faster recovery rate of 2000 ± 400 sec using single crystal microspectrophotometry measurements at the FMN absorption maxima.[45] A more recent study has also revealed that the YtvA-LOV-STAS has a slower photo-recovery than isolated YtvA-LOV, 46.1 ± 1.7 min and 42.4 ± 0.3 min.[131] This is opposite to the half-life change that was observed for phot1 *As*LOV2 in the absence Hisact, however structural features for autophosphorylation proposed for phot1[20,62] are different from the direct interaction of the STAS domain with the LOV core, thereby perhaps a longer half-life is observed as the STAS is likely to compete for the dimerisation surface.[119]

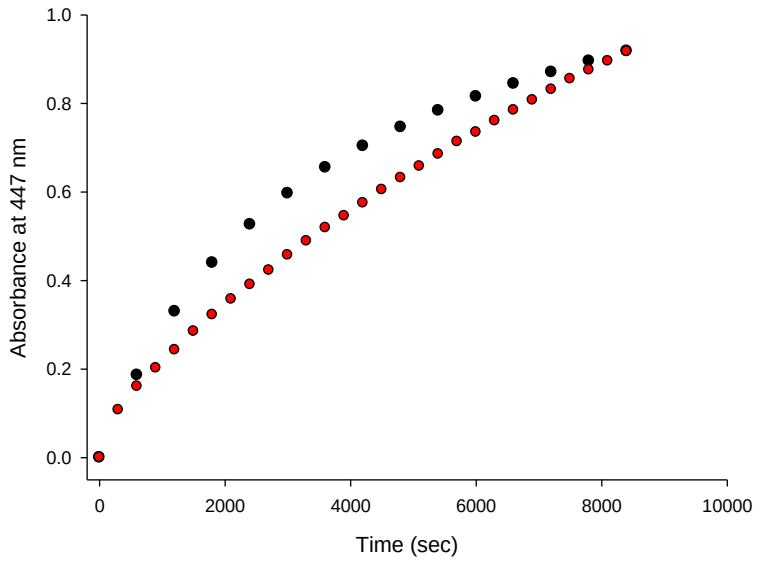

Figure 5.11: *UV/Vis absorption time-course measurements at 447 nm of YtvA-LOV-STAS (black), and YtvA-LOV (red).*

Protein	Half-life (sec)
YtvA-LOV-STAS	4788 ± 60
YtvA-LOV	2514 ± 60

Table 5.1: *Half-lives of YtvA-LOV-STAS and YtvA-LOV, listing the average of three measurements and their standard deviation.*

CD spectroscopy was carried out on purified proteins to assess the change in secondary structure upon photo-adduct formation. YtvA-LOV-STAS has a larger α-helical content (Figure 5.12A) than YtvA-LOV (Figure 5.12B) as the STAS domain contains a helix-turn-helix (HTH) motif,[44] also observed in previous studies where CD spectroscopy was used for secondary structural characterisation.[119] Moglich and Moffat observed a 10 % decrease in α-helical content of YtvA-LOV upon switching from dark to light state.[131] Although, it is complicated to quantitatively evaluate CD spectra, the change in mean residue ellipticity at 222 nm switching between dark and light states were calculated to be less than 8 % change for YtvA-LOV-STAS and 3.8 % change for YtvA-LOV. This is an exceptionally small change in comparison to *As*LOV2 and implies that the Jα helix remains relatively ordered in the light state, which relates to proceedings in the litrature.[45]

A

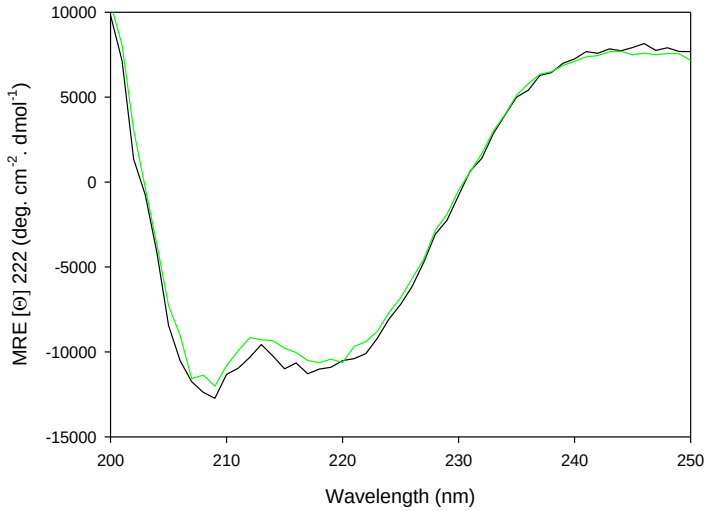

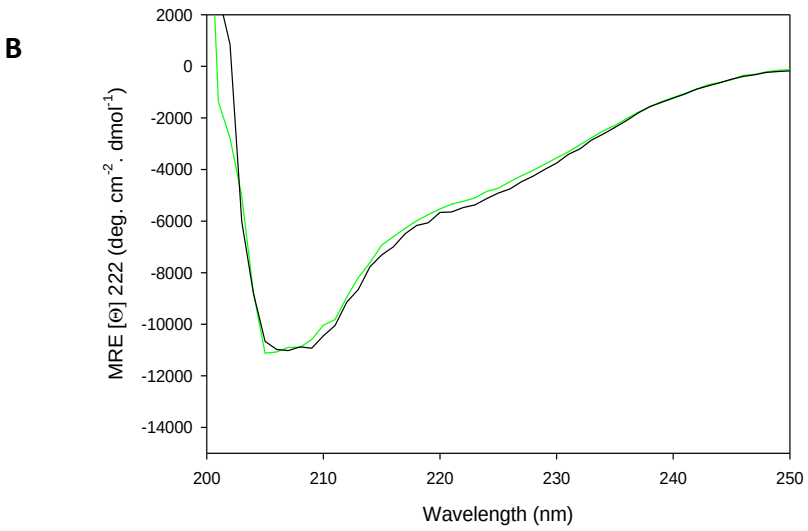

Figure 5.12: *Circular dichroism spectra of A) YtvA-LOV-STAS and B) YtvA-LOV in the dark-state (black) and light state (green).*

5.2.3 YtvA-LOV mutants

Site-directed mutagenesis using Pfu polymerase was performed to generate V27D and I113D alterations in YtvA-LOV. Both pET19b-YtvA-LOV-V27D and pET19b-YtvA-LOV-I113D were confirmed by sequencing (Appendix E and F). The proteins were expressed in *E. coli* BL21 (DE3) cells (Figure 5.13) using the same conditions as wild-type YtvA-LOV protein. Both proteins were purified by affinity chromatography using a Ni-NTA resin and eluted fractions were analysed using SDS-PAGE (Figure 5.14).

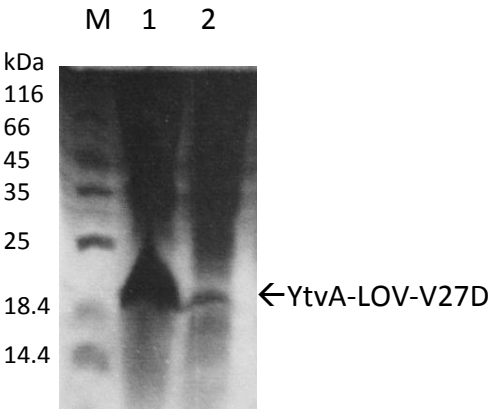

Figure 5.13: *SDS-PAGE analysis of the cell lysate of pET19b-YtvA-LOV-V27D (lane 1) pET-19b-YtvA-LOV-I113D (lane 2).*

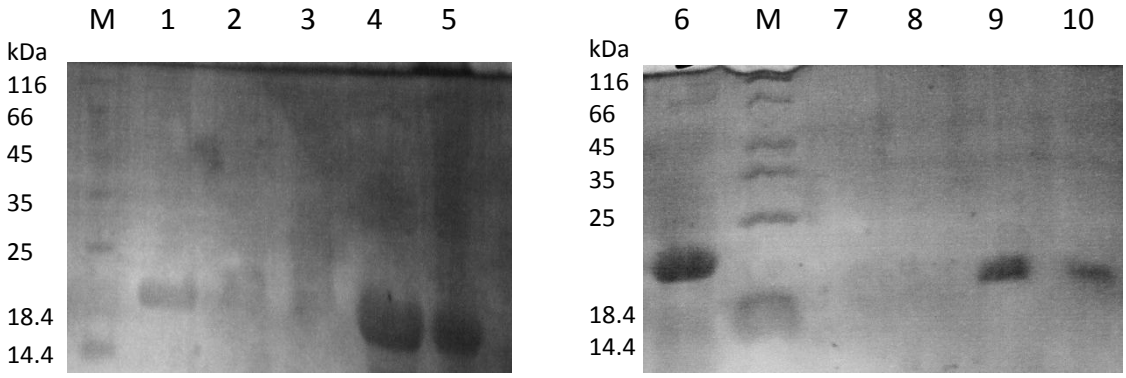

Figure 5.14: *SDS-PAGE analysis through the stages of purification using affinity chromatography of YtvA-LOV-V27D: M: protein marker, lane 1: cell lysate, lane 2: flow through fraction off the affinity column, lane 3: wash with buffer, lane 4 and 5: elution fractions. YtvA-LOV-I113D: lane 6: cell lysate, lane 7: flow through fraction off the affinity column, lane 8: wash with buffer, lane 9 and 10: elution fractions.*

5.2.4 Size-exclusion chromatography of YtvA-LOV and mutants

Size-exclusion chromatography can be used to measure the approximate masses of globular proteins under non-denaturing conditions. In this case size-exclusion chromatography was used to determine the solution state of YtvA-LOV. A predominantly dimeric form would suggest that the adjacent monomer would prevent the Jα from docking on to the β sheet and prevent effective use of the domain to mask the Jα.[20] To calibrate the elution volume a series of standards were injected onto an analytical Superdex-75 size exclusion column (Figure 5.15 and Table 5.2).

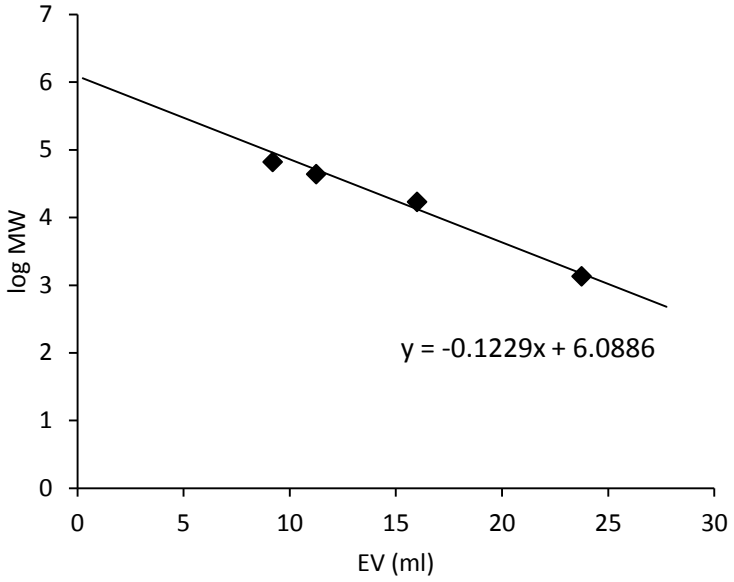

Figure 5.15: *Protein standards run on a Superdex 75 size-exclusion column and plotted using log molecular weight of each protein against the eluted volume.*

Protein	Elution Volume (mL)	Log_{10} Mass	Mass (Da)
BSA	9.2	4.82	66340
Ovalbumin	11.25	4.64	44000
Myoglobin	16	4.23	17000
Vitamin B12	23.75	3.13	1350

Table 5.2: *Proteins standards run on a Superdex-75 size-exclusion column.*

The molecular masses of each known protein were used to linearly relate the logarithm (Log_{10}) of the mass to the elution volume, to derive an equation (y = -0.1229x + 6.0886) to estimate molecular masses from elution volumes (Figure 5.16). The elution volume of YtvA-LOV suggests that the protein exists as a dimer (11.8 mL, calculated mass 44000); this is also the case for the YtvA-LOV-V27D mutant which has a calculated mass of exactly two monomer units (39200) although the peak is broader and has a pronounced tail. However, a small peak (circled in Figure 5.16) was also seen for the YtvA-LOV that suggests some monomer may be present in solution. YtvA-LOV-I113D, however gave a calculated mass (19800) very close to that expected for a monomer (19600). SDS-PAGE was used confirm that the eluted proteins corresponded to YtvA-LOV (Figure 5.17).

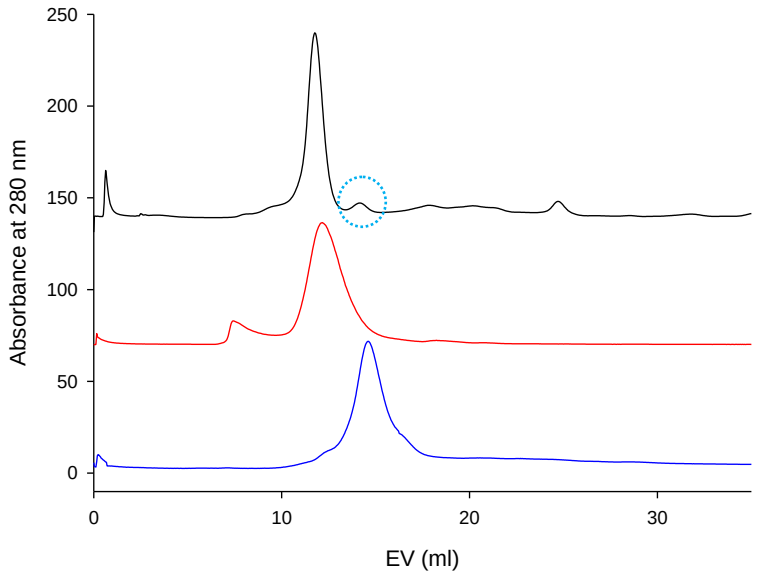

Figure 5.16: *Chromatogram of YtvA-LOV (black) with circle indicating a monomer peak, YtvA-LOV-V27D (red) and YtvA-LOV-I113D (blue) run on analytical superdex-75 size-exclusion column.*

Protein	Elution Volume (mL)	Log_{10} mass	Calculated mass (Da)
YtvA-LOV[a]	11.77	4.64	43872
YtvA-LOV[b]	14.15	4.35	22365
YtvA-LOV-V27D	12.17	4.59	39203
YtvA-LOV-I113D	14.59	4.30	19746

Table 5.3: *Each maximum peak (protein elution volume) was used to determine the log_{10} mass using the equation (y = -0.1229x + 6.0886) from the standard plot (Figure 3.36). YtvA-LOV has two peaks: [a] peak 1 and [b] peak 2 (blue circle).*

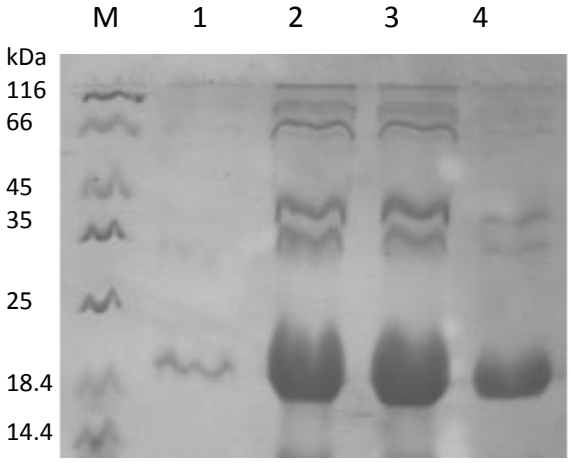

Figure 5.17: *SDS-PAGE gel of eluted fractions from size-exclusion chromatography to confirm that eluted fractions denature to molecules with the same migration speed. M: protein marker, lane 1: YtvA-LOV monomer peak, lane 2: YtvA-LOV dimer peak, lane 3: YtvA-LOV-V27D and lane 4: YtvA-LOV-I113D.*

From this it can be implied that the mutation of uncharged hydrophobic isoleucine 113 to a negatively charged aspartate (at physiological pH), may have caused a strong enough repulsion (steric clash) with the same residue from the interacting monomer, to prevent the formation of dimer (intermolecular contacts) at first instance. From the dark state crystal structure[45] (PDB 2PR5, Figure 5.18) it can be seen that I113 is more likely to form initial intermolecular contacts as it is located at the outside edge of the β-sheet (strand Hβ) as opposed to being in the middle (as in the case for V27, Figure 5.18). Whereas, V27 has other hydrophobic amino acids (V25, I29, Y41 and M111)[45] adjacent (Figure 5.2 and 5.3) and its

repulsive force (from the acidic side chain) may not be strong enough to prevent dimerisation.

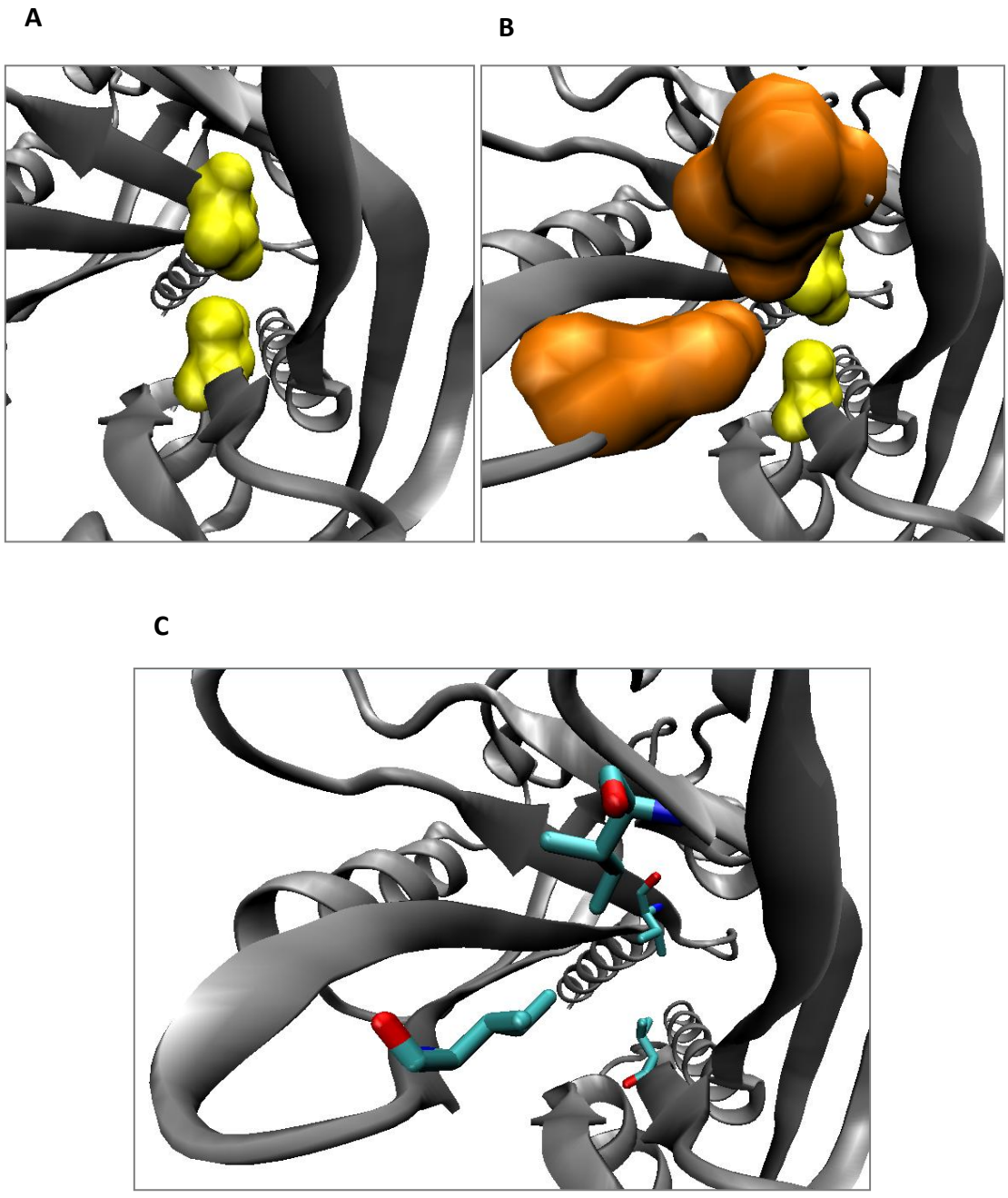

Figure 5.18: *Structure of YtvA-LOV showing hydrophobic interface between both monomers: A) V27 (yellow), B) V27 and I113 (orange) and C) V27 and I113 (Nitrogen atom in blue and oxygen in red). (PDB 2PR5).*

5.3 Conclusion

Producing LOV-Bid hybrids using the slow cycling YtvA-LOV photoreceptor still remains unaccomplished, as a result to preliminary investigations on understanding the dimeric interface of YtvA-LOV. In agreement with the literature,[131] in the absence of the STAS domain (YtvA-LOV) the photo-adduct recovery rate was significantly reduced. Circular dichroism spectroscopy was used to analyse the proteins in the far-UV region, where negative signals at 208 nm and 222 nm indicated primarily α-helical structure for YtvA-LOV-STAS and a mix of both α-helical and β-sheet was observed for YtvA-LOV, in agreement with the literature.[119] The lack of change observed in the CD signal at 222 nm between light and dark states, implies that the Jα-helices of dimeric YtvA-LOV proteins stays folded (α-helical) in the light-state. Although, a light state solution structure would achieve a clear insight in to the confirmation of Jα and the changes in the interactions observed within the hydrophobic interface, we are limited to light irradiated dark state crystals at present.[45] From this data, two hydrophobic residues found to be important for dimerisation were chosen for site-directed mutagenesis (V27D and I113D), to polar amino acids. The YtvA-LOV-V27D mutation did not show any change in quaternary structure, whereas the YtvA-LOV-I113D mutation caused a disruption to the hydrophobic β-sheet that mediates dimerisation, resulting in a protein that is monomeric in solution, observed by size-exclusion chromatography.

However, this investigation remains partial as further repeats are required to justify the change observed (dimeric to monomeric) by size-exclusion chromatography. It is also vital that the UV/Vis and CD characterisation and half-lives of these mutants are recorded which will allow comparison with the wild-type data.

Chapter 6:
General Discussion
and Future Work

Photo-sensitive protein-switches are used in dynamic researches as optogenetic tools for controlling biomolecular interactions in regulatory pathways. The ability to use non-harmful blue light to control apoptosis in a reversible manner would results in great scientific and therapeutic interest. In this work, the BH3 domain of pro-apoptotic Bid was targeted, to create fusions with LOV in order to apply an on/off mechanism of inhibiting anti-apoptotic Bcl-x_L.

The work described in this thesis demonstrates the characterisation of two LOV domains, *Avena sativa* LOV2 and *Bacillus subtilis* YtvA, using UV/Vis and CD spectroscopy to determine the photo-recovery time. Hisact-*As*LOV2 and the longer half-life Hisact-*As*LOV2-V416I mutant demonstrated temperature dependency with Hisact-*As*LOV2 relaxing with a half-life of 15.9 ± 1.3 seconds at 37 °C, whilst pH between 6.5 and 8 had minimal effect on the photo adduct reversion. Removal of the N-terminal hisactophilin from the *As*LOV2-V416I mutant resulted in an extended recovery rate, with a half-life of 137.6 ± 2.8 at 37 °C. This provides a greater cysteinyl-FMN adduct yield under reduced irradiation intervals, which will reduce damage or shock to cells used for *in vivo* testing. Therefore *As*LOV2-V416I was selected to produce hybrid proteins engineered with fusions at the Jα helix to control cellular apoptotic signalling, which will benefit from the longer undocked period of Jα to allow interactions to Bcl-x_L.

YtvA-LOV has a 10-fold longer photo-recovery than LOV2, making it advantageous for creating photo-switchable fusions, as demonstrated by Moglich *et al,* with the bacterial haem-binding PAS-histidine kinase, FixL/YF1 variants.[60] Although YtvA-LOV will allow longer signalling duration for protein-protein interactions, fusions with the BH3 domains of pro-apoptotic proteins would be complicated by the switching limitations of the YtvA Jα-helix, as the protein exists in a homodimeric form in solution.[45] Therefore, mutational studies were conducted to further understand which amino acid residues were key to the dimeric interface of YtvA-LOV. Using size-exclusion chromatography, it was demonstrated that mutant YtvA-LOV-I113D exists as a monomer in solution. However, it is yet to be examined by UV/Vis and CD spectroscopy to determine the photo-recovery time. To further confirm this result, ultracentrifugation (density gradient) studies with purified wild-type and mutant protein can be used, as both differ in molecular weight and should appear at different sediments after centrifugation. It would be interesting to generate NMR structures of the

light state of both wild-type and mutant YtvA-LOV, to understand the switching mechanics better.

The success of an optogenetics tool is highly dependent on the design concept of the photo-switch, as seen with the success of LOV-Rac[76,54-56] and the limitations of LOV-DHFR.[53] In this case, *As*LOV2-Bid hybrid designs were optimised with the BH3 sequence incorporated fully and at different positions of the Jα-helix. Initially the fully incorporated LOV-Bid design was tested using the synthesised LOV-Bid-Jα peptide, which demonstrated that binding was not abolished and a strong binding affinity for Bcl-x_L (natural binding partner) was determined. However, Hisact-*As*LOV2-bid displayed binding to Bcl-x_L both in the dark and light states, thereby failing to act as an optogenetics switch. To further understand the factors that may have caused this, it would be helpful to obtain a crystal or NMR structure of the *As*LOV2 in the light state. This can be conducted through the reconstitution of the FMN in *As*LOV2 with an 5-deaza-FMN analogue which after blue light irradiation abolishes photo-adduct reversion to the dark state until it is irradiated with UV light (313 nm).[171] It would also be interesting to obtain a dark state structure of Hisact-*As*LOV2-Bid protein, to further understand what may be causing incomplete docking of the Jα. A 1-deaza-FMN analogue may be used in this case (unpublished work by Dr. Andrew Wood, Cardiff University) which will diminish the formation of the flavin-cysteinyl covalent adduct.

Further optimisation of the LOV-Bid design enabled four other fusions (LOV-Bid1-4) to be engineered, stably produced, purified and characterised using UV/Vis and CD spectroscopy to determine the photo-recovery times of the FMN and the protein. CD spectroscopy measurements at MRE 222 also enabled assessment of the change in protein secondary structure upon photo-adduct formation, revealing that all fusions did not switch to the same magnitude as wild-type LOV2. This correlated with binding affinities determined by fluorescence anisotropy measurements, which revealed that all four proteins bound to Bcl-x_L in the light state and all except *As*LOV2-Bid2 did not bind in the dark state. We anticipate that successful 'caging' was observed with *As*LOV2-Bid1, *As*LOV2-Bid3 and *As*LOV2-Bid4, rendering these designs competent for optogenetics testing *in vivo*.

It will be interesting to record how *As*LOV2-Bid5 would bind to Bcl-x_L, as it was predicted that the proximity of the LOV domain is likely to sterically constrain accessibility to Bcl-x_L.

However, using the knowledge from the findings in this study and previous studies[57] it is expected that lack of sequence overlap with the Jα may prevent 'caging' and will become more accessible to bind in the dark.

The light state binding affinities of *As*LOV2-Bid3 and *As*LOV2-Bid4 for Bcl-x_L, are stronger than the binding constant reported for wild-type t-Bid *in vitro*,[147] with *As*LOV2-Bid4 having less than two-fold increase in binding affinity from the LOV-Bid peptide. Therefore these two designs are promising photoswitches for controlling apoptosis. Ultimately, *in vivo* studies[145] of these *As*LOV2-Bid fusions would enable us to investigate how potent these proteins are in a live cell environment and potentially pave a way for inducing apoptosis in cancer cells using BH3 mimicry.

References

1. Wald, G. The molecular basis of visual excitation. *Nature.* 1968. 219, 800-807.
2. Jablonski, A. Über den Mechanismus der Photolumineszenz von Farbstoffphosphoren. *Z. Phys.* 1935. 94: 38-46.
3. Maverakis, E., Miyamura, Y., Bowen, M. P., Correa, G., Ono, Y., and Goodarzi, H. Light, inducing Ultraviolet. *J Autoimmun*. 2010. 34(3): J247–J257.
4. D'Orazio, J., Jarrett, S., Amaro-Ortiz, A., and Scott, T. UV radiation on the skin. *Int. J. Mol. Sci.* 2013. 14(6): 12222–12248.
5. Van Grondelle, R., Dekker, J. P., Gillbro, T., and Sundström, V. Energy-Transfer and Trapping in Photosynthesis. *Biochimica Et Biophysica Acta- Bioenergetics.* 1994. 1187: 1-65.
6. Berg, J. M., J.L.Tymoczko & L.Stryer. Biochemistry 6th edition. *W. H. Freeman*. 2006.
7. Béjà, O. Aravind, L., Koonin, E.V., Suzuki, M.T., Hadd, A., Nguyen, L.P., Jovanovich, S.B., Gates, C.M., Feldman, R.A., Spudich, J.L., Spudich, E.N., and DeLong, E.F. Bacterial rhodopsin: evidence for a new type of phototrophy in the sea. *Science.* 2000. 289: 1902-1906.
8. Mathews, S. Phytochrome-mediated development in land plants: red light sensing evolves to meet the challenges of changing light environments. *Mol. Ecol.* 2006. 15: 3483-3503.
9. Imamoto, Y., and Kataoka, M. Structure and photoreaction of photoactive yellow protein, a structural prototype of the PAS domain superfamily. *Photochem. Photobiol*. 2007. 83: 40-49.
10. Nagel, G., Szellas, T., Kateriya, S., Adeishvili, N., Hegemann, P., and Bamberg, E. Channelrhodopsins: directly light-gated cation channels. *Biochem. Soc.Trans. 2005.* 33: 863-866.
11. Christie, J.M. Phototropin blue light receptors. *Annu. Rev. Plant. Biol.* 2007. 58: 21-45
12. Briggs, W.R., and Christie, J.M. Phototropins 1 and 2; versatile blue light receptors. *Trends. Plant. Sci.* 2002. 7: 204-210.
13. Everett J. Moding, Michael B. Kastan, and David G. Kirsch. Strategies for optimizing the response of cancer and normal tissues to radiation. *Nat. Rev. Drug. Discov.* 2013. 12(7): 526-542.
14. Meesat, R., Belmouaddine, H., Allard, J., Tanguay-Renaud, C., Lemay, R., Brastaviceanu, T., Tremblay, L., Paquette, P., Wagner, R., Jay-Gerin, J., Lepage, M., Huels, M. A., Houde, D. Cancer radiotherapy based on femtosecond IR laser-beam filamentation yielding ultra-high dose rates and zero entrance dose. *Proc. Natl. Acad. Sci.* 2012. 109(38): E2508-E2513.
15. Maverakis, E., Miyamura, Y., Bowen, M. P., Correa, G., Ono, Y., and Goodarzi, H. Light, including Ultraviolet. *J. Autoimmun.* 2010. 34(3): J247-J257.
16. Ghodke, H., Wang, H., Hsieh, C.L., Woldemeskel, S., Watkins, S. C., Rapić-Otrin, V., and Van Houten, B. Single-molecule analysis reveals human UV-damaged DNA-

binding protein (UV-DDB) dimerizes on DNA via multiple kinetic intermediates. *Proc. Natl. Acad. Sci.* 2014. 111(18): E1862-E1871.

17. Zaret, M. M., Snyder, W. Z., Birenbaum, L. Cataract after exposure to non-ionizing radiant energy. *Br J Ophthalmol.* 1976. 60(9): 632–637.
18. Harper, S.M., Christie, J.M., Gardner, K. H. Disruption of the LOV-Jα helix interaction activates phototropin kinase activity. *Biochem.* 2004. 43: 16184-16192.
19. Salomon, M., Eisenreich, W., Muller, F., Bacher, A., and Richter, G. An optomechanical transducer in the blue light receptor phototropin from *Avena sativa. Proc. Natl. Acad. Sci.* 2001. 98: 12357-12361.
20. Christie, J. M., Swartz, T. E., Bogomolni, R. A., and Briggs, W. R. Phototropin LOV domains exhibit distinct roles in regulating photoreceptor function. *Plant J.* 2002. 32: 205-219.
21. Purcell, E.B., Siegal-Gaskins, D., Rawling, D.C., Fiebig, A., and Crosson, S.A. Photosensing two-component system regulates bacterial cell attachment. *Proc. Natl. Acad. Sci. U S A.* 2007. 104: 18241-18246.
22. Swartz, T. E., Tseng, T.-S., Frederickson, M. A., Paris, G., Comerci, D. J., Rajashekara, G., Kim, J.-G., Mudgett, M. B., Splitter, G. A., Ugalde, R. A., Goldbaum, F. A., Briggs, W. R., and Bogomolni, R. A. Blue-Light-Activated Histidine Kinases: Two Component Sensors in Bacteria. *Sci.* 2007. 317: 1090–1093.
23. Ballario, P., Vittorioso, P., Magrelli, A., Talora, C., Cabibbo, A., and Macino, G. White collar-1, a central regulator of blue light responses in Neurospora, is a zinc finger protein. *EMBO J.* 1996. 15: 1650–1657.
24. Kataoka, H., and Takahashi, F. AUREOCHROME: A newly found bZIP-LOV photoreceptor is a common blue light receptor of heterokonts. *Plant Cell Physiol.* 2007. 48: S14.
25. Avila-Perez, M., Hellingwerf, K. J., and Kort, R. Blue light activates the (B)-dependent stress response of Bacillus subtilis via YtvA. *J. Bacteriol.* 2006. 188: 6411–6414.
26. Jentzsch, K., Wirtz, A., Circolone, F., Drepper, T., Losi, A., Gartner, W., Jaeger, K. E., and Krauss, U. Mutual Exchange of Kinetic Properties by Extended Mutagenesis in Two Short LOV Domain Proteins from Pseudomonas putida. *Biochem*. 2009. 48: 10321– 10333.
27. Schwerdtfeger, C., and Linden, H. VIVID is a flavoprotein and serves as a fungal blue light photoreceptor for photoadaptation. *EMBO J.* 2003. 22: 4846–4855.
28. Darron R. Luesse, Stacy L. DeBlasio, Roger P. Hangarter. Integration of phot1, phot2, and PhyB signalling in light-induced chloroplast movements. *J Exp Bot.* 2010. 61(15): 4387–4397.
29. Hernán E. Boccalandro, Carla V. Giordano, Edmundo L. Ploschuk, Patricia N. Piccoli, Rubén Bottini, Jorge J. Casal. Phototropins But Not Cryptochromes Mediate the Blue Light-Specific Promotion of Stomatal Conductance, While Both Enhance Photosynthesis and Transpiration under Full Sunlight. *Plant Physiol.* 2012. 158(3): 1475–1484.

30. Alexandre, M.T.A., Arents, J.C., Grondelle, R.V., Hellingwerf, K.J. and Kennis, J.T.M. A base-catalyzed mechanism for dark state recovery in the *Avena sativa* phototropin-1 LOV2 domain. *Biochem.* 2007. 46: 3129-3137.
31. Zoltowski, B.D. and Gardner, K.H. Tripping the light fantastic: Blue light photoreceptors as examples of environmentally modulated protein-protein interaction. *Biochem.* 2011. 50: 4-16.
32. Salomon, M., Christie, J.M., Knieb, E., Lempert, U., and Briggs, W.R. Photochemical and mutational analysis of the FMN binding domains of the plant blue-light preceptor phototropin. *Biochem.* 2000. 39: 9401-9410.
33. Salomon, M., Lempert, U., and Rudiger, W. Dimerization of the plant photoreceptor phototropin is probably mediated by the LOV1 domain. *FEBS. Lett.* 2004. 572: 8-10.
34. Taylor, B. L., and Zhulin I. B. PAS Domains: Internal Sensors of Oxygen, Redox Potential, and Light. Microbio. *Mol. Biol. Rev.* 1999. 63: 479-506.
35. Swartz, T.E., Corchnoy, S.B., Christie, J.M., Lewis, J.W., Szundi, I., Briggs, W.R., and Bogomolni, R. The photocycle of a flavin-binding domain of the blue-light photoreceptor phototropin. *J. Biol. Chem.* 2001. 276: 36493-36500.
36. Kasahara, M., Swartz, T. E., Olney, M. A., Onodera, A., Mochizuki, N., Fukuzawa, H., Asamizu, E., Tabata, S., Kanegae, H., Takano, Christie, J. M., Nagatani, A. and Briggs, W. R. Photochemical Properties of the Flavin Mononucleotide-Binding Domains of the Phototropins from Arabidopsis, Rice, and Chlamydomonas reinhardtii. *Plant Physiol.* 2002. 129: 762-773.
37. Crosson, S., and Moffat, K. Structure of a flavin-binding plant photoreceptor domain: Insights into light-mediated signal transduction. *Proc. Natl. Acad. Sci.* 2001. 98: 2995-3000.
38. Kennis, J. T. M., Crosson, S., Gauden, M., van Stokkum, I. H. M., Moffat, K., and van Grondelle, R. Primary reactions of the LOV2 domain of phototropin, a plant blue-light photoreceptor. *Biochem.* 2003. 42: 3385-3392.
39. Kay, C. W. M., Schleicher, E., Kuppig, A., Hofner, H., Rudiger, W., Schleicher, M., Fischer, M., Bacher, A., Weber, S., and Richter, G. Blue light perception in plants - Detection and characterization of a light-induced neutral flavin radical in a C450A mutant of phototropin. *J. Biol. Chem*. 2003. 278: 10973-10982.
40. Kottke, T., Dick, B., Fedorov, R., Schlichting, I., Deutzmann, R., and Hegemann, P. Irreversible photoreduction of flavin in a mutated Phot-LOV1 domain. *Biochem*. 2003. 42: 9854-9862.
41. Bittl, R., Kay, C. W. M., Weber, S., and Hegemann, P. Characterization of a flavin radical product in a C57M mutant of a LOV1 domain by electron paramagnetic resonance. *Biochem.* 2003. 42: 8506-8512.
42. Schleicher, E., Kowalczyk, R. M., Kay, C. W. M., Hegemann, P., Bacher, A., Fischer, M., Bittl, R., Richter, G., and Weber, S. On the reaction mechanism of adduct formation in LOV domains of the plant blue-light receptor phototropin. *J. American Chem. Soc.* 2004. 126: 11067-11076.

43. Nakasone, Y., Eitoku, T., Matsuoka, D., Tokutomi, S., and Terazima, M. Kinetic measurement of transient dimerization and dissociation reactions of *Arabidopsis* phototropin 1 LOV2 domain. *Biophys. J.* 2006. 91: 653.
44. Akbar, S., Gaidenko, T.A., Min, K., O'reilly, M., Devine, K. M., and Price, C. W. New family of regulators in the environmental signalling pathway which activates the general stress transcription factor of *Bacillus subtilis. J. Bacteriol.* 2001. 183: 1329-1338.
45. Moglich, A. and Moffat, K. Structural basis for light-dependent signaling in the dimeric LOV domain of the photosensor YtvA. *J. Mol. Biol.* 2007. 373: 112-126.
46. Losi, A. and Gartner, W. Bacterial bilin- and flavin-binding photoreceptors. *Photochem. Photobiol. Sci.* 2008. 7: 1168-1178.
47. Avila-Perez, M. Vreede, J., Tang, T., Bende, O., Losi, A., Gartner, W., and Hellingwerf, K. In vivo mutational analysis of the Bacillus subtilis LOV-domain containing protein YtvA: mechanism of light-activation of the general stress response. *J. Biol. Chem.* 2010. 284: 24958-24964.
48. Harper, S.M., Neil, L. C., and Gardner, K. H. Structural basis of a phototropin light switch. *Sci.* 2003. 301: 1541-1544.
49. Matsuoka, D., and Tokutomi, S. Blue light-regulated molecular switch of Ser/Thr kinase in phototropin. *Proc. Nat. Sci.* 2005. 102: 13337-13342.
50. Haugh, J. M. cells see the light to bring signalling under control. *Nature*. 2011. 8 (10): 808-809.
51. Strickland, D. Moffact, K. and Sosnick, T. R. Light-activated DNA binding in a designed allosteric protein. *Proc. Nat. Sci. USA*. 2008. 105 (31): 10709-10714.
52. Strickland, D., Yao, X., Gawlak, G., Rosen, M. K., Gardner, K. H., and Sosnick, T. R. Rationally improving LOV based switches. *Nat. Methods.* 2010. 7: 623-626.
53. Lee, J., Natrajan, M., Nashine, V. C. Socolich, M., Vo, T., Russ, W. P., Benkovik, S. J., and Ranganathan, R., Surface sites for engineering allosteric control in proteins. *Sci.* 2008. 322: 438-442.
54. Wu, Y., Frey, D., Lungu, O., Jaehrig, A., Schlichting, I., Kuhlman, B. And Hahn, K. M. A genetically photoactivatable Rac controls the motility of living cells. *Nature.* 2009. 461: 104-108.
55. Yoo, S.K., Deng, Q., Cavnar, P.J., Wu, Y. I., Hahn, K. M., and Huttenlocher, A. A differential regulation of protrusion and polarity by P13K during neutrophil motility in live zebrafish. *Dev. Cell.* 2010. 18: 226-236.
56. Wang, X., He, L., Wu, Y. I., Hahn, K. M., and Montell, D. J. Light-mediated activation reveals key role for Rac in collective guidance of cell movement *in vivo. Nat. Cell. Biol.* 2010. 12: 591-597.
57. Strickland, D., Lin, Y., Wagner, E., Hope, C.M., Zayner, J., Antoniou, C., Sosnick, T.R., Weiss, E.L., Glotzer, M. TULIPs: tunable, light-controlled interacting protein tags for cell biology. *Nat. Methods.* 2012. 9 (4): 379-384.

58. Mills, E., Chen, X., Pham, E., Wong, S., and Truong, K. Engineering a photoactivated caspase-7 for rapid induction of apoptosis. *ASC. Syn. Biol.* 2012. 1(3): 75-82.
59. Moglich, A., Ayers, R. A., and Moffat, K. Design and signalling mechanism of light-regulated histidine kinases. *J. Mol. Biol.* 2009. 385: 1433-1444.
60. Moglich, A., Ayers, R. A., and Moffat, K. Addition at the molecular level: signal integration in designed Per-ARNT-Sim receptor proteins. *J. Mol. Biol.* 2010. 400: 477-486.
61. Krauss. U., Lee. J., Benkovic, S. J. and Jaeger, K., LOVely enzymes-to-wards-engineering light-controllable-biocatalysts. *Microb. Biotechnol.* 2010. 3: 15-23.
62. Christie, J. M., Salomon, M., Nozue, K., Wada, M., and Briggs, W. R. LOV (Light, oxygen, or voltage) domains of the blue-light photoreceptor phototropin (nph1): Binding sites for the chromophore flavin mononucleotide. *Proc. Natl. Acad. Sci. USA.* 1999. 96(15): 8779-8783.
63. http://hyperphysics.phy-astr.gsu.edu/hbase/biology/ligabs.html
64. Besaratinia, A., Synold, T. W., Chen, H. H., Chang, C., Xi, B., Riggs, A. D., and Pfeifer, G. P. DNA lesions induced by UV A1 and B radiation in human cells: comparative analyses in the overall genome and in the p53 tumor suppressor gene. *Proc. Natl. Acad. Sci.* 2005. 102(29): 10058-63.
65. Lambert, M. W., and Lambert, M. C. DNA repair and chromatin structure in genetic diseases. *Prog. Nucleic acid Res. Mol. Biol.* 1999. 63: 257-310.
66. Clancy, S. DNA damage & repair: mechanisms for maintaining DNA integrity. *Nature Edu.* 2008. 1(1): 103
67. Pfeifer, G. P., and Besaratinia, A. UV wavelength-dependent DNA damage and human non-melanoma and melanoma skin cancer. *Photochem Photobiol Sci.* 2012. 11(1): 90–97.
68. Rochette, P. J., Therrien, J. P., Drouin, R., Perdiz, D., Bastien, N., Drobetsky, E. A., and Sage, E. UVA-induced cyclobutane pyrimidine dimers form predominantly at thymine-thymine dipyrimidines and correlate with the mutation spectrum in rodent cells. *Nucleic Acids Res.* 2003. 1; 31(11): 2786-94.
69. Tommasi, S., Denissenko, M. F., and Pfeifer, G. P. induces pyrimidine dimers preferentially at 5-methylcytosine bases. *Cancer Res.* 1997. 1; 57 (21):4727-30.
70. Brash, D. E., Rudolph, J. A., Simon, J. A., Lin, A., McKenna, G. J., Baden, H. P., Halperin, A. J., and Pontén, J. A role for sunlight in skin cancer: UV-induced p53 mutations in squamous cell carcinoma. *Proc. Natl. Acad. Sci.* 1991. 15; 88(22): 10124-10128.
71. Yamaguchi, M. Role of carotenoid β-cryptoxanthin in bone homeostasis. *J. Biomed.* Sci. 2012. 19(1): 36.
72. Shin, H. S., Cho, M., Kim,T., Yoo, J., Kim, J., Han, Y., Song,P., Jeon, J., Bhoo, S. H., and Hahn, T. A Small GTPase Activator Protein Interacts with Cytoplasmic Phytochromes in Regulating Root Development. *J. Biol. Chem.* 2010. 285(42): 32151–32159.

73. Mathews, S. Phytochrome-mediated development in land plants: red light sensing evolves to meet the challenges of changing light environments. *Mol. Ecol.* 2006. 15: 3483-3503.
74. Harrison, S.C., and Aggarwal, A.K. DNA recognition by proteins with the helix-turn-helix motif. *Annu. Rev. biochem.* 1990. 59: 933–969.
75. Rivera-Cancel, G., Motta-Mena, L. B., and Gardner, K. H. Identification of natural and artificial DNA substrates for the light-activated LOV-HTH transcription factor EL222. *Biochem*. 2012. 51 (50): 10024–10034.
76. Ridley, A. J. Rho GTPases and actin dynamics in membrane protrusions and vesicle trafficking. *Trends. Cell. Biol.* 2006. 16 (10): 522–9.
77. Sanz-Moreno, V., Gadea, G., Ahn, J., Paterson, H., Marra, P., Pinner, S., Sahai, E., and Marshall, C.J. Rac activation and inactivation control plasticity of tumor cell movement. *Cell.* 2008. 135 (3): 510–523.
78. Yang, W.H., Lan, H.Y., Huang, C.H., Tai, S.K., Tzeng, C.H., Kao, S.Y., Wu, K.J., Hung, M.C., Yang, M.H. RAC1 activation mediates Twist1-induced cancer cell migration. *Nature cell biol.* 2012. 14 (4): 366–374.
79. Stallings-Mann, M.L., Waldmann, J., Zhang, Y., Miller, E., Gauthier, M.L., Visscher, D.W., Downey, G.P., Radisky, E.S., Fields, A.P., Radisky, D.C. Matrix metalloproteinase induction of Rac1b, a key effector of lung cancer progression. *Sci. Trans. med.* 2012. 4 142: 510–523.
80. Lockshin, R.A. and Williams, C.M. Programmed cell death. II. Endocrine potentiation of the breakdown of the intersegmental muscles of silkmoths. *J. insect. Physiol.* 1964. 10: 643-649.
81. Lockshin, R.A. and Zakeri, Z. Programmed cell death and apoptosis: origins of the theory. *Nat. Rev. Mol. Cell. Biol.* 2001. 2(7): 545-550.
82. Kerr, J. F., Wyllie, A.H., and Currie, A. R. Apoptosis: a basic biological phenomenon with wide-ranging implications in tissue kinetics. *Br. J. Cancer*. 1972. 26(4): 239-57.
83. Meier, P., Finch, A. and Evan, G. Apoptosis in development. *Nature.* 2000. 407 (6805): 796-801.
84. Horvitz, H.R. Genetic control of programmed cell death in the nematode *Caenorhabditis elegans*. *Cancer Res.* 1999. 59 (7 suppl): 1701s-1706s.
85. Reddien, P. W., Horvitz, H. R. The engulfment process of programmed cell death in *Caenorhabditis elegans*. *Annu Rev Cell Dev Biol*. 2004. 20: 193–221.
86. Reddien, P. W., Cameron, S., Horvitz, H. R. Phagocytosis promotes programmed cell death in *C. elegans*. *Nature.* 2001. 412: 198–202.
87. Yuan, J., and Horvitz, H. R. A first insight into the molecular mechanisms of apoptosis. *Cell*. 2004. 116: S53–S56.
88. Zuzarte-Luis, V., and Hurle, J. M. Programmed cell death in the developing limb. *Int. J. Dev. Biol*. 2002. 46(7): 871-6.
89. Hutchins, J. B., and Barger, S. W. Why neurons die: cell death in the nervous system. *Anat. Rec*. 1998. 253(3): 79-90.

90. Majno, G. and Joris, I. Apoptosis, oncosis and necrosis. An overview of cell death. *Am. J. Pathol.* 1995. 146(1): 3-15.
91. Trump, B. F., Berezesky, I.K., Chang, S.H. and Phelps, P. C. The pathways of cell death: oncosis, apoptosis and necrosis. *Toxicol. Pathol.* 1997. 2: 82–8.
92. Chautan, M., Chazal G., Cecconi, F., Gruss, P., Golstein, P. Interdigital cell death can occur through a necrotic, and caspase-independent pathway. *Curr. Biol.* 1999. 9: 967–970.
93. Fadeel, B., Gleiss, B., Hogstrand, K., Chandra, J., Wiedmer, T., Sims, P. J., Henter, J. I., Orrenius, S., and Samali, A. Phosphatidylserine exposure during apoptosis is a cell-type-specific event and does not correlate with plasma membrane phospholipid scramblase expression. *Biochem. Biophys. Res. Commun*. 1999a. 266(2): 504-11.
94. Ponten, F., Lindman, H., Bostrom, A., Berne, B., and Bergh, J. induction of p53 expression in skin by radiotherapy and UV radiation: a randomized study. *.J Nat. Cance.r Inst*. 2001. 93(2): 128-133.
95. Madeo, F., Herker, E., Maldener, C., Wissing, S., Lachelt, S., Herlan, M., Fehr, M., Lauber, K., Sigrist, S. J., Wesselborg, S., et al. A caspase-related protease regulates apoptosis in yeast. *Mol. Cell.* 2002. 9: 911–917.
96. Salvaseen, G. S., and Riedl, S. J. Caspase mechanisms. *Adv. Exp. Med. Biol.* 2008. 615: 13-23.
97. Denault, J. B. and Salvesen, G. S. Caspases: keys in the ignition of cell death. *Chem. Rev*. 2002. 102(12): 4489-500.
98. Wilson, N. S., Dixit, V., and Askenazi, A. Death receptor signal transducers: nodes of coordination in the immune signalling networks. *Nat. Immunol.* 2009. 10(4): 348-355).
99. Youle, R. J., and Strasser, A. The Bcl-2 family: opposing activities that mediate cell death. *Nat. Rev. Mol. Cell.* 2008. 9(1): 47-59.
100. Trapani, J. A., and smyth, M. J. Functional significance of perforin/ granzyme cell death pathway. *Nat. Rev. Immunol.* 2002. 2(10): 735-747.
101. Cullen, S. P., Brunet, M., and Martin, S. J. Granzymes in cancer and immunity. *Cell death Differ.* (2010). 17(4): 616-623
102. Eskes, R., Resagher, S., Antonsson, B., and Martinou, J. C. Bid Induces the Oligomerization and Insertion of Bax into the Outer Mitochondrial Membrane. *Mol. Cell Biol.* (2000). 20: 929-935.
103. Adams, J. M., and Cory, S. Life-or-death decisions by the Bcl-2 protein family. *Trends Biochem. Sci.* 2001. 26: 61-66.
104. Borner, C. The Bcl-2 protein family: sensors and checkpoints for life-or-death decisions. *Mol. Immunol*. 2003. 39(11): 615-47.
105. Sattler, M., Liang, H., Nettesheim, D., Meadows, R.P., Harlan, J.E., Eberstadt, M., Yoon, H.S., Shuker, S.B., Chang, B.S., Minn, A.J., Thompson, C. B., and Fesik, S. W. Structure of Bcl-xL-Bak peptide complex: Recognition between regulators of apoptosis. *Science.* 1997. 275: 983–986.

106. Liu, X., Dai, S., Zhu, Y., Marrack, P., and Kappler, J.W. The structure of a Bcl-xL/Bim fragment complex: Implications for Bim function. *Immuni.* 2003. 19(3): 341-52.
107. Wysoczanski, P., Mart, R. J., Loveridge, E. J., Williams, C., Whittaker, S. B.-M., Crump, M. P., and Allemann, R.K. NMR solution structure of a photoswitchable apoptosis activating Bak peptide bound to Bcl-x_L. *J. Am. Chem. Soc.* 2012. 124: 7644-7647.
108. D. Y. Jackson, D. S. King, J. Chmielewski, S. Singh, P. G. Schultz, *J. Am. Chem. Soc.*, 1991, 113: 9391-9392.
109. J. R. Lakowicz, *Principles of fluorescence spectroscopy*. *NY, Plenum Press.* 1999.
110. T. Heyduk, Y. Ma, H. Tang, R. H. Ebright, *Methods Enzymol.* 1996. 274: 492- 503.
111. Cornel Mulhardt. The experimenter series: Molecular biology and genomics. *Academic Press.* 2007. 122-124.
112. Christie *et al.* Steric interactions stabilize the signalling state of the LOV2 domain of phototropin 1. *Biochem.* 2007. 46: 9310-9319.
113. Nash, A. I., Ko, W. H., Harper, S.M. and Gardner, K. H. A conserved glutamine plays a central role in LOV domain signal transmission and duration. *Biochem.* 2008. 47(52): 13842-13849.
114. Freddolino, P. L., Dittrich, M. and Schulten, M. Dynamic switching mechanisms in LOV1 and LOV2 domains of plant phototropins. *Biophys.* 2006. 91: 3630-3639.
115. Crosson S. and Moffat, K. Photoexcited structure of a plant photoreceptor domain reveals a light driven molecular switch. *Plant cell.* 2002. 14: 1067-1075.
116. Zoltowski, B.D., Vaccaro, B., Crane, B.R. Mechanism-based tuning of LOV domain photoreceptor. *Nat. Chem. Biol.* 2009. 5: 827-834.
117. Losi, A., Polverrini, E., Quest, B., and Gartner, W. First evidence for phototropin related blue light eceptors in prokaryotes. *Biophys. J.* 2002. 82(5): 2627-2634.
118. Losi, A. The bacterial counterparts of plant phototropins. *Photochem. Photobiol. Sci.* 2004. 42: 2-10.
119. Buttani, V., Losi, A., Eggert, T., Krauss, U., Jaeger, K., Cao, Z., and Gartner, W. Conformational analysis of the blue light sensing protein YtvA reveals a competitive interface for LOV-LOV dimerization and interdoomain interactions. *Photochem. Photobiol. Sci.* 2007. 6: 41-49.
120. Nakasone, Y., Eitoku, T., Matsuoka, D., Tokutomi, S., and Terazima, M. Kinetic measurement of transient dimerization and dissociation reactions of *Arabidopsis* phototropin 1 LOV2 domain. *Biophys. J.* 2006. 91: 653.
121. Habazettl, J., Gondol, D., Wiltscheck, R., Otlewski, J., Schleicher, M. and Holak, T. A. Structure of hisactophilin is similar to interleukin-1b and fibroblast growth factor. *Nature.* 1992a. 359: 855-858.
122. Hanakam, F., Eckerskorn, C., Lottspeich, F., Müller-Taubenberger, A., Schäfer, W. and Gerisch, G. The pH-sensitive actin-binding protein hisactophilin of Dictyostelium discoideum exists in two isoforms which both are myristoylated and distributed between plasma membrane and cytoplasm. *J. Biol. Chem*. 1995. 270: 596-602.

123. Correa, D. H. A., and Ramos, C. H. I. The use of circular dichroism spectroscopy to study protein folding, form and function. *African J. of Biochem. Res.* 2009. 3(5): 164-173.
124. Yao, X., Rosen, M.K., and Gardner, K. H. Estimation of the available free energy in a LOV2-Jα photoswitch. *Nature Chem. Biol.* 2008. 4(8): 491-497.
125. Salzmann S, Martinez-Junza V, Zorn B, Braslavsky SE, Mansurova M, Marian CM, Gärtner W. Photophysical properties of structurally and electronically modified flavin derivatives determined by spectroscopy and theoretical calculations. *J. Phys. Chem. A.* 2009. 113: 9365–9375.
126. Salzmann S, Silva-Junior MR, Thiel W, Marian CM. Influence of the LOV domain on low-lying excited states of flavin: a combined quantum-mechanics/molecular-mechanics investigation. *J Phys Chem B.* 2009. 113: 15610–15618.
127. Raffelberg, S., Mansurova, M., Gartner, W., and Losi, A. Modulation of the photocycle of a LOV domain photoreceptor by the hydrogen-bonding network. *J. Am. Chem. Soc*. 2011. 133: 5346–5356.
128. Zoltowski, B.D., Nash, A. I., and Gardner, K. H. Variations in protein/flavin hydrogen bonding in a LOV domain produce non-Arrhenius kinetics of adduct decay. *Biochem.* 2011. 50(41): 8771-8779.
129. Corchnoy, S.B. Swartz, T. E., Lewis, J. W., Szundi, I., Briggs, W. R., and Bogomolni, R. A. Intramolecular proton transfers and structural changes during the photocycle of the LOV2 domain of phototropin 1. *J. Biol. Chem.* 2003. 278: 724–731.
130. Kottke, T., Heberle, J., Hehn, D., Dick, B. & Hegemann, P. Phot-LOV1: photocycle of a blue-light receptor domain from the green alga *Chlamydomonas reinhardtii*. *Biophys. J.* 2003. 84: 1192–1201.
131. Dorn, M., Jurk, M., Wartenberg, A., Hahn, A., and Schmieder, P. LOV Takes a Pick: Thermodynamic and Structural Aspects of the Flavin-LOV-Interaction of the Blue-Light Sensitive Photoreceptor YtvA from *Bacillus subtilis. PLoS One*. 2013. 8(11): e81268.
132. Weintraub, S. J., Manson, S. R., and Deverman, B. E. resistance to anineoplastic therapy: the oncogenic tyrosine kinase-Bclx($_L$) axis. *Cancer Cell.* 2004. 5: 3-4.
133. Tan, M. L., Ooi, J. P., Ismail, N., Moad, A. I., and Muhammad, T. S. Programmed cell death pathways and current anti-tumour targets. *Pharm. Res.* 2009. 26(7): 1547-1560.
134. Hwang J.J., Kuruvilla J., Mendelson D., Pishvaian, M.J., Deeken, J.F., Siu, L.L., Berger, M.S., Viallet, J., and Marshall, J.L. Phase I dose finding studies of obatoclax (GX15-070), a small molecule pan-BCL-2 family antagonist, in patients with advanced solid tumors or lymphoma. *Clin. Cancer Res.* 2010. 16(15): 4038-4045.
135. James, D. F., Castro, J. E., Loria, O., Prada, C. E., Aguillion, R. A., and Kipps, T. J. AT-101, a small molecule Bcl-2 antagonist, in treatment naive CLL patients (pts) with high risk features; Preliminary results from ongoing phase I trial. *J. Clin. Oncol.* 2006. 24(18): 362s

136. Balakrishnan, K., Burger, J. A., Wierda, W. G., and Gandhi, V. AT-101 induces apoptosis in CLL B cells and overcomes stromal cell-mediated Mcl-1 induction and drug resistance. *Blood.* 2009. 1;113(1): 149-53.
137. Kneissl, S., Loveridge, E. J., Williams, C., Crump, M. P., and Allemann, R. K. Photocontrollable peptide based switches target the anti-apoptotic protein Bcl-xL. *ChemBioChem.* 2008, 9(18), 3046-3054.
138. Letai, A. Pharmacological manipulation of Bcl-2 family members to control cell death. *J. Clin. Invest.* 2005. 115(10): 2648-2655.
139. Yang, B. D., Liu, D., and Huang, Z. Synthesis and helical structure of lactam bridged BH3 peptides derived from pro-apoptotiic Bcl-2 family proteins. *Bioorg. Med. Chem. Lett.* 14(6): 1403-1406.
140. Walensky, L. D., Kung, a. L., Escher, I., Malia, T.J., Barbuto, S., Wright, R.D., Wagner, G., Verdine, G.L., and Korsmeyer, S.J. Activation of apoptosis in vivo by a hydrocarbon-stapled BH3 helix. *Sci.* 2004. 305(5689): 1466-1470.
141. Saraogi, I., and Hamilton, A.D. Alpha-helix memetics as inhibitors of protein-protein interactions. *Biochem. Soc. Trans.* 2008. 36 (6): 1414-1417.
142. Mills E, Chen X, Pham E, Wong S, Truong K. Engineering a photoactivated caspase-7 for rapid induction of apoptosis. *ACS Synth. Biol.* 2012. 1(3): 75-82.
143. Letai, A., Bassik, M.C., Walensky, L.D., Sorcinelli, M.D., Weiler, S., and Korsmeyer, S.J. Distinct BH3domains either sensitize or activate mitochondrial apoptosis, serving as prototype cancer therapeutics. *Cancer Cell.* 2002 2: 183–192.
144. Harper, S. M., Neil, L. C., and Gardner, K. H. Structural basis of phototropin light switch. *Sci.* 2003. 301: 1541-1544.
145. Mart, R.J., Errington, R.J., Watkins, C. L., Chappell, S.C., Wiltshire, M., Jones, A.T., Smith, P.J., and Allemann, R.K. BH3 Helix-Derived Biophotonic Nanoswitches Regulate Cytochrome c Release in Permeabilised Cells. *Mol. Biosys*. 2013. 9: 2597-2603.
146. Bhat, V., McDonald, C.B., Mikles, D.C., Deegan, B.J., Seldeen, k. L., Bates, M.L., and Farooq, A. Ligand Binding and Membrane Insertion Compete with Oligomerization of the BclXL Apoptotic Repressor. *J Mol Biol*. (2012). 416(1): 57–77.
147. García-Sáez, A.J., Ries, J., Orzáez, M., Pérez-Payà, E., and Schwille, P. Membrane promotes tBID interaction with BCL(XL). *Nat. Struct. Mol. Biol.* 2009. 16(11): 1178-85.
148. Follis, A. V., Llambi, F., Ou, L., Baran, K., Green, D. R., and Kriwacki, R. W. The DNA-binding domain mediates both nuclear and cytosolic functions of p53. *Nature Struct & Mol Biol*. 2014. 21: 535–543.
149. Strickland, D., Yao, X., Gawlak, G., Rosen, M. K., Gardner, K. H., and Sosnick, T.R. Rationally improving LOV-based photo-switches. *Nat Methods.* 2010. 7: 623-626.
150. Lee, J., Natarajan, R., Nashine, V.C., Socolich, M., Vo, T., Russ, W.P., Benkovic, S.J., and Ranganathan, R. Surface sites for engineering allosteric control in proteins. *Sci.* 2008. 322: 438-442.

151. Lungu, O. I., Hallett, R. A., Choi, E. J., Aiken, M. J., Hahn, K. M., and Kuhlman, B. Designing photoswitchable peptides using the *As*LOV2 domain. *Chem & Biol.* 2012. 19: 507-517.
152. Harper, S. M., Christie, J. M., and Gardner, K. H. Disruption of the LOV-JR Helix Interaction Activates Phototropin Kinase Activity. *Biochem.* 2004. 43: 16184-16192.
153. Yao, Y., Bobkov, A. A., Plesniak, L. A., Marassi, F. M. Mapping the interaction of pro-apoptotic tBID with pro-survival BCL-XL. *Biochem.* 2009. 48 (36): 8704-8711.
154. Yao, X., Rosen, M.K., and Gardner, K. H. Estimation of the available free energy in a LOV2-Jα photoswitch. *Nature Chem Biol.* 2008. 4(8): 491-497.
155. Whitecross, K. F., Alsop, A.E., Cluse, L. A., Wiegmans, A., Banks, K., Coomans, C., Peart, M.J., Newbold, A., Lindemann, R.K., and Johnstone, R.W. Defining the target specificity ofABT-737 and synergistic antitumor activities in combination with histone deacetylase inhibitors. *Blood*. 2009. 113 (9): 1982-1991.
156. http://www.photobiology.info/Yocum-PRC.html
157. Toettcher, J. E., Gong, D., Lim, W. A., and Weiner, O. D. Light-based feedback for controlling intracellular signalling dynamics. *Nature.* 8 (10): 837-839.
158. Levskaya, A., Weiner, O. D., Lim, W. A., and Voigt, C. A. Spaciotemporal control of cell signalling using a light-switchable protein interaction. *Nature.* 2009. 416: 997-1001.
159. Morgan, S. A., Al-Abdul-Wahid, and Woolley, G.A. Structure based design of photocontrolled DNA-binding protein. *J. Mol. Biol.* 2010. 399: 94-112.
160. Morgan, S. A., and Woolley, G.A. A photoswitchable DNA-binding protein based on a truncated GCN4-photoactive yellow protein chimera. *Photochem. Photobiol. Sci.* 2010. 1320-1326.
161. Fan, H.Y, Morgan, S.A., Brechun, K.E., Chen, Y.Y., Jaikaran, A.S., Woolley, G.A. Improving a designed photocontrolled DNA-binding protein. *Biochem.* 2011. 50 (7): 1226-1237.
162. Tsien, R. Y. The green fluorescent protein. *Annu. Rev. Bio-chem.* 1998. 65: 509-544.
163. Shaner, N. C. Patterson, G. H. and Davidson, M. W. Advances in fluorescent protein technology. 2007. *J. Cell. Sci.* 129: 4247-4260.
164. Chapman, S., Faulkner, C., Kaiserli, E., Garcia-Mata, C., Savenkov, E.I., Roberts, A.G., Oparka, K.J., Christie, J.M. The photoreversible fluorescent protein iLOV out performs GFP as a reporter for plant virus infaction. 2008. *Proc. Natl. Acad. Sci.* 105: 20038-20043.
165. Vijay, K., Brody, M. S., Fredlund, E., and Price, C. W. A PP2C phosphatase containing a PAS domain is required to convey signals of energy stress to the sigmaB transcription factor of Bacillus subtilis. *Mol. Microbiol.* 2000. 35(1): 180-188.
166. Yang, X., Kang, C. M., Brody, M. S., and Price, C. W. Opposing pairs of serine protein kinases and phosphatases transmit signals of environmental stress to activate a bacterial transcription factor. *Genes Dev*. 1996. 10(18): 2265-75.

167. Brigulla, M., Hoffmann, T., Krisp, A., Völker, A., Bremer, E., Völker, U. Chill induction of the SigB-dependent general stress response in Bacillus subtilis and its contribution to low-temperature adaptation. *J. Bacteriol.* 2003. 185(15): 4305-14.
168. Swartz, T. E., Wenzel, P., Corchnoy, S.B. Briggs, W. R., and Bogomolni, R. A. Vibration spectroscopy reveals light-induced chromophore and protein structural changes in the LOV2 domain of the plant blue-light receptor phototropin 1. *Biochem.* 2002. 41: 7183-7189.
169. Baldwin, R. L. α-Helix formation by peptides of defined sequence. *Biophys. Chem.* 1995. 55: 127–135.
170. Padmanabhan, S., York, E. J., Stewart, J. M. and Baldwin, R. L. Helix propensities of basic amino acids increase with length of the side chain. *J. Mol. Biol.* 1996. 257: 726-734.
171. Hecht, S., Richter, G., Bacher, A., Joshi, M., Römisch, W., Greiner, G., Frank, R., Weber, S., Eisenreich, W., and Fischer, M., Photocycle of a blue light receptor LOV2 domain reconstituted with 5-deaza-FMN. Flavins and Flavoproteins 2005. *T. Nishino, R. Miura, M. Tanokura, K. Fukui (Editors), ARchiTect Inc*., *Tokyo*. 569- 574.

Appendix

```
ctcgagaaatcataaaaaatttatttgctttgtgagcggataacaattataatagattca
 L  E  K  S  -  K  I  Y  L  L  C  E  R  I  T  I  I  I  D  S
attgtgagcggataacaatttcacacagaattcattaaagaggagaaattaacc atg ggt
 I  V  S  G  -  Q  F  H  T  E  F  I  K  E  E  K  L  T  M  G
aacagagcattcaaatcacatcacggtcacttttaagcgctgaaggcgaagctgtaaag
 N  R  A  F  K  S  H  H  G  H  F  L  S  A  E  G  E  A  V  K
actcaccacggtcatcatgatcatcacacccatttccacgttgaaaaccatggtggtaaa
 T  H  H  G  H  H  D  H  H  T  H  F  H  V  E  N  H  G  G  K
gttgcattaaagacccattccggtaaatacctttcaattggtgatcataaacaagtttac
 V  A  L  K  T  H  S  G  K  Y  L  S  I  G  D  H  K  Q  V  Y
ctctcacaccacttacacggtgaccactcactcttccacttagaacatcatggcggtaaa
 L  S  H  H  L  H  G  D  H  S  L  F  H  L  E  H  H  G  G  K
gtctcaatcaaaggtcatcaccaccactacatttccgctgatcatcatggtcatgtttca
 V  S  I  K  G  H  H  H  H  Y  I  S  A  D  H  H  G  H  V  S
accaaagaacaccacgatcacgacaccacctttgaagaaattattattggttccgcggca
 T  K  E  H  H  D  H  D  T  T  F  E  E  I  I  I  G  S  A  A
tctggtctggtgccacgcggatccgaatttcttgctactacacttgaacgtattgagaag
 S  G  L  V  P  R  G  S  E  F  L  A  T  T  L  E  R  I  E  K
aactttgtcattactgacccacgtttgccagataatcccattatcttcgcgtccgatagt
 N  F  V  I  T  D  P  R  L  P  D  N  P  I  I  F  A  S  D  S
ttcttgcagttgacagaatattcgcgagaagaaattctgggtcgtaactgccgttttctt
 F  L  Q  L  T  E  Y  S  R  E  E  I  L  G  R  N  C  R  F  L
caaggtcctgaaaccgatcgcgcgacagtgcgcaaaattcgtgatgccatcgataaccaa
 Q  G  P  E  T  D  R  A  T  V  R  K  I  R  D  A  I  D  N  Q
acagaggtcactgtacagctgattaattatacaaagagtggtaaaaagttctggaacctc
 T  E  V  T  V  Q  L  I  N  Y  T  K  S  G  K  K  F  W  N  L
tttcacttgcagcctatgcgtgatcagaagggtgatgtccagtactttattggtgtccag
 F  H  L  Q  P  M  R  D  Q  K  G  D  V  Q  Y  F  I  G  V  Q
ttggatggtaccgaacatgtccgtgatgcggccgagcgtgagggtgtcatgctgattaag
 L  D  G  T  E  H  V  R  D  A  A  E  R  E  G  V  M  L  I  K
aaaactgcagaaaatattgatgaggcggcaaaagaacttccagatgctaatctgcgtcca
 K  T  A  E  N  I  D  E  A  A  K  E  L  P  D  A  N  L  R  P
gaggatttgtgggctaactaagcttaattagctgag
 E  D  L  W  A  N  -  A  -  L  A  E
```

Appendix A: *Nucleotide and amino acid sequence of pNCO-Hisact-AsLOV2.*

```
accaaagaacaccacgatcacgacaccacctttgaagaaattattattggttccgcggca
 T  K  E  H  H  D  H  D  T  T  F  E  E  I  I  I  G  S  A  A
tctggtctggtgccacgcggatccgaatttcttgctactacacttgaacgtattgagaag
 S  G  L  V  P  R  G  S  E  F  L  A  T  T  L  E  R  I  E  K
aactttattattactgacccacgtttgccagataatcccattatcttcgcgtccgatagt
 N  F  I  I  T  D  P  R  L  P  D  N  P  I  I  F  A  S  D  S
ttcttgcagttgacagaatattcgcgagaagaaattctgggtcgtaactgccgttttctt
 F  L  Q  L  T  E  Y  S  R  E  E  I  L  G  R  N  C  R  F  L
caaggtcctgaaaccgatcgcgcgacagtgcgcaaaattcgtgatgccatcgataaccaa
 Q  G  P  E  T  D  R  A  T  V  R  K  I  R  D  A  I  D  N  Q
acagaggtcactgtacagctgattaattatacaaagagtggtaaaaagttctggaacctc
 T  E  V  T  V  Q  L  I  N  Y  T  K  S  G  K  K  F  W  N  L
tttcacttgcagcctatgcgtgatcagaagggtgatgtccagtactttattggtgtccag
 F  H  L  Q  P  M  R  D  Q  K  G  D  V  Q  Y  F  I  G  V  Q
ttggatggtaccgaacatgtccgtgatgcggccgagcgtgagggtgtcatgctgattaag
 L  D  G  T  E  H  V  R  D  A  A  E  R  E  G  V  M  L  I  K
aaaactgcagaaaatattgatgaggcggcaaaagaacttccagatgctaatctgcgtcca
 K  T  A  E  N  I  D  E  A  A  K  E  L  P  D  A  N  L  R  P
gaggatttgtgggctaactaa
 E  D  L  W  A  N  -
```

Appendix B: *Nucleotide and amino acid sequence of pNCO-Hisact-AsLOV2-V416I*

ctcgcgcat**atg**gctagttttcaatcatttgggataccaggacagctggaagtcatcaaa
 L A H **M** A S F Q S F G I P G Q L E V I K
aaagcacttgatcacgtgcgagtcggtgtggtaattacagatcccgcacttgaagataat
 K A L D H V R V G V V I T D P A L E D N
cctattgtctacgtaaatcaaggctttgttcaaatgaccggctacgagaccgaggaaatt
 P I V Y V N Q G F V Q M T G Y E T E E I
ttaggaaagaactgtcgcttcttacaggggaaacacacagatcctgcagaagtggacaac
 L G K N C R F L Q G K H T D P A E V D N
atcagaaccgctttacaaaataaagaaccggtcaccgttcagatccaaaactacaaaaaa
 I R T A L Q N K E P V T V Q I Q N Y K K
gacggaacgatgttctggaatgaattaaatattgatccaatggaaatagaggataaaacg
 D G T M F W N E L N I D P M E I E D K T
tattttgtcggaattcagaatgatatcaccaagcaaaaagaatatgaaaagcttctcgag
 Y F V G I Q N D I T K Q K E Y E K L L E
gattccctcacggaaattactgcactttcaactcctattgtcccgattcgcaatggcatt
 D S L T E I T A L S T P I V P I R N G I
tcggctcttccgctagtcggaaacctgacagaggagcgatttaattccatcgtttgcaca
 S A L P L V G N L T E E R F N S I V C T
ttgacgaatatcttatcaacatccaaagatgattatttgatcattgatttatccggattg
 L T N I L S T S K D D Y L I I D L S G L
gcccaagtgaacgaacaaacggccgaccaaattttcaagctgagccatttgctgaaattg
 A Q V N E Q T A D Q I F K L S H L L K L
accggaactgagttaatcattactggcattaagcctgaattggctatgaaaatgaataaa
 T G T E L I I T G I K P E L A M K M N K
ctggatgccaatttttcgtcgctgaaaacatattcaaatgtaaaggatgccgttaaagtg
 L D A N F S S L K T Y S N V K D A V K V
cttccgattatgtaa
 L P I M -

Appendix C: *Nucleotide and amino acid sequence of YtvA-STAS.*

atgggccatcatcatcatcatcatcatcatcacagcagcggccatatcgacgacgac
 M G H H H H H H H H H H S S G H I D D D
gacaagcatatggctagttttcaatcatttgggataccaggacagctggaagtcatcaaa
 D K H M A S F Q S F G I P G Q L E V I K
aaagcacttgatcacgtgcgagtcggtgtggtaattacagatcccgcacttgaagataat
 K A L D H V R V G V V I T D P A L E D N
cctattgtctacgtaaatcaaggctttgttcaaatgaccggctacgagaccgaggaaatt
 P I V Y V N Q G F V Q M T G Y E T E E I
ttaggaaagaactgtcgcttcttacaggggaaacacacagatcctgcagaagtggacaac
 L G K N C R F L Q G K H T D P A E V D N
atcagaaccgctttacaaaataaagaaccggtcaccgttcagatccaaaactacaaaaaa
 I R T A L Q N K E P V T V Q I Q N Y K K
gacggaacgatgttctggaatgaattaaatattgatccaatggaaatagaggataaaacg
 D G T M F W N E L N I D P M E I E D K T
tattttgtcggaattcagaatgatatcaccaagcaaaaagaatatgaaaagcttctcgag
 Y F V G I Q N D I T K Q K E Y E K L L E
gattccctcacggaaattactgcactttcaact**taataa**cctattgtcccgattcgcaat
 D S L T E I T A L S T **-** **-** P I V P I R N
ggcatttcggctcttccgctagtcggaaacctgacagaggagcgatttaattccatcgtt
 G I S A L P L V G N L T E E R F N S I V
tgcacattgacgaatatcttatcaacatccaaagatgattatttgatcattgatttatcc
 C T L T N I L S T S K D D Y L I I D L S
ggattggcccaagtgaacgaacaaacggccgaccaaattttcaagctgagccatttgctg
 G L A Q V N E Q T A D Q I F K L S H L L
aaattgaccggaactgagttaatcattactggcattaagcctgaattggctatgaaaatg
 K L T G T E L I I T G I K P E L A M K M
aataaactggatgccaatttttcgtcgctgaaaacatattcaaatgtaaaggatgccgtt
 N K L D A N F S S L K T Y S N V K D A V
aaagtgcttccgattatgtaa
 K V L P I M -

Appendix D: *Nucleotide and amino acid sequence of pET19b-YtvA-LOV.*

cctctagaataattttgtttaactttaagaaggagatatacc**atg**ggccatcatcatcat
 P L E - F C L T L R R R Y T **M** G H H H H
catcatcatcatcatcacagcagcggccatatcgacgacgacgacaagcatatggctagt
 H H H H H H S S G H I D D D D K H M A S
tttcaatcatttgggataccaggacagctggaagtcatcaaaaaagcacttgatcacgtg
 F Q S F G I P G Q L E V I K K A L D H V
cgagtcggt**gat**gtaattacagatcccgcacttgaagataatcctattgtctacgtaaat
 R V G **D** V I T D P A L E D N P I V Y V N
caaggctttgttcaaatgaccggctacgagaccgaggaaattttaggaaagaactgtcgc
 Q G F V Q M T G Y E T E E I L G K N C R
ttcttacaggggaaacacacagatcctgcagaagtggacaacatcagaaccgctttacaa
 F L Q G K H T D P A E V D N I R T A L Q
aataaagaaccggtcaccgttcagatccaaaactacaaaaaagacggaacgatgttctgg
 N K E P V T V Q I Q N Y K K D G T M F W
aatgaattaaatattgatccaatggaaatagaggataaaacgtattttgtcggaattcag
 N E L N I D P M E I E D K T Y F V G I Q
aatgatatcaccaagcaaaaagaatatgaaaagcttctcgaggattccctcacggaaatt
 N D I T K Q K E Y E K L L E D S L T E I
actgcactttcaacttaataacctattgtcccgattcgcaatggcatttcggctcttccg
 T A L S T - - P I V P I R N G I S A L P
ctagtcggaaacctgacagaggagcgatttaattccatcgtttgcacattgacgaatatc
 L V G N L T E E R F N S I V C T L T N I
ttatcaacatccaaagatgattatttgatcattgatttatccggattggcccaagtgaac
 L S T S K D D Y L I I D L S G L A Q V N
gaacaaacggccgaccaaattttcaagctgagccatttgctgaaattgaccggaactgag
 E Q T A D Q I F K L S H L L K L T G T E
ttaatcattactggcattaagcctgaattggctatgaaaatgaataaactggatgccaat
 L I I T G I K P E L A M K M N K L D A N
ttttcgtcgctgaaaacatattcaaatgtaaaggatgccgttaaagtgcttccgattatg
 F S S L K T Y S N V K D A V K V L P I M
taaaggatccggctgctaacaaagcccgaaaggaagctgagttggct
 - R I R L L T K P E R K L S W

Appendix E: *Nucleotide and amino acid sequence of pET19b-YtvA-LOV-V27D.*

cctctagaataattttgtttaactttaagaaggagatatacc**atg**ggccatcatcatcat
 P L E - F C L T L R R R Y T **M** G H H H H
catcatcatcatcatcacagcagcggccatatcgacgacgacgacaagcatatggctagt
 H H H H H H S S G H I D D D D K H M A S
tttcaatcatttgggataccaggacagctggaagtcatcaaaaaagcacttgatcacgtg
 F Q S F G I P G Q L E V I K K A L D H V
cgagtcggtgatgtaattacagatcccgcacttgaagataatcctattgtctacgtaaat
 R V G D V I T D P A L E D N P I V Y V N
caaggctttgttcaaatgaccggctacgagaccgaggaaattttaggaaagaactgtcgc
 Q G F V Q M T G Y E T E E I L G K N C R
ttcttacaggggaaacacacagatcctgcagaagtggacaacatcagaaccgctttacaa
 F L Q G K H T D P A E V D N I R T A L Q
aataaagaaccggtcaccgttcagatccaaaactacaaaaaagacggaacgatgttctgg
 N K E P V T V Q I Q N Y K K D G T M F W
aatgaattaaatattgatccaatggaa**gat**gaggataaaacgtattttgtcggaattcag
 N E L N I D P M E **D** E D K T Y F V G I Q
aatgatatcaccaagcaaaaagaatatgaaaagcttctcgaggattccctcacggaaatt
 N D I T K Q K E Y E K L L E D S L T E I
actgcactttcaacttaataacctattgtc
 T A L S T - - P I V

Appendix F: *Nucleotide and amino acid sequence of pET19b-YtvA-LOV-I113D.*

```
gaaattttaacgtaattccctctagaatacttttgtttaactttaagaaggagatatacat
 K  F  -  R  N  S  L  -  N  T  F  V  -  L  -  E  G  D  I  H
atgagccagtctaaccgtgaactggtcgttgacttcctgtcctacaaactgtcccagaaa
 M  S  Q  S  N  R  E  L  V  V  D  F  L  S  Y  K  L  S  Q  K
ggctattcttggtctcagttctctgacgtggaggaaaaccgtacggaagctccagaaggt
 G  Y  S  W  S  Q  F  S  D  V  E  E  N  R  T  E  A  P  E  G
accgaaagcgaagccgtcaaacaggctctgcgtgaagctggtgatgaattcgaactgcgt
 T  E  S  E  A  V  K  Q  A  L  R  E  A  G  D  E  F  E  L  R
taccgtcgtgcgtttagcgacctgacctctcagctgcacatcactccgggtaccgcatac
 Y  R  R  A  F  S  D  L  T  S  Q  L  H  I  T  P  G  T  A  Y
cagtctttcgaacaggttgtgaacgagctgttccgtgatggtgtgaactggggtcgtatc
 Q  S  F  E  Q  V  V  N  E  L  F  R  D  G  V  N  W  G  R  I
gttgctttcttctcctttggtggtgcgctgtgcgttgaatctgtggacaaagaaatgcag
 V  A  F  F  S  F  G  G  A  L  C  V  E  S  V  D  K  E  M  Q
gttctggtatcccgtatcgcagcctggatggcgacttacctgaacgatcatctggaaccg
 V  L  V  S  R  I  A  A  W  M  A  T  Y  L  N  D  H  L  E  P
tggattcaggagaacggtggttgggataccttcgtagagctgtatggcaacaacgcagcg
 W  I  Q  E  N  G  G  W  D  T  F  V  E  L  Y  G  N  N  A  A
gcagaaagccgtaaaggtcaggaacgtctggaacaccaccaccatcaccatctcgagcac
 A  E  S  R  K  G  Q  E  R  L  E  H  H  H  H  H  H  L  E  H
caccaccaccaccactgagatccggctgctaacaaagcccgaaaggaagctgagttggct
 H  H  H  H  H  -  D  P  A  A  N  K  A  R  K  E  A  E  L  A
gctgccaccgctgagcaataactagcataaccccttggggcctctaaacgggtcttgagg
 A  A  T  A  E  Q  -  L  A  -  P  L  G  A  S  K  R  V  L  R
```

Appendix G: *Nucleotide and amino acid sequence of truncated Bcl-x_L.*

```
atttgatacgcaaaactttccccctctccaaataattttgtttaactttaagaaggagat
 I  -  Y  A  K  L  S  P  S  P  N  N  F  V  -  L  -  E  G  D
atacatatgtgccagtctaaccgtgaactggtcgttgacttcctgtcctacaaactgtcc
 I  H  M  C  Q  S  N  R  E  L  V  V  D  F  L  S  Y  K  L  S
cagaaaggctattcttggtctcagttctctgacgtggaggaaaaccgtacggaagctcca
 Q  K  G  Y  S  W  S  Q  F  S  D  V  E  E  N  R  T  E  A  P
gaaggtaccgaaagcgaagccgtcaaacaggctctgcgtgaagctggtgatgaattcgaa
 E  G  T  E  S  E  A  V  K  Q  A  L  R  E  A  G  D  E  F  E
ctgcgttaccgtcgtgcgtttagcgacctgacctctcagctgcccatcactccgggtacc
 L  R  Y  R  R  A  F  S  D  L  T  S  Q  L  P  I  T  P  G  T
gcataccagtctttcgaacaggttgtgaacgagctgttccgtgatggtgtgaactggggt
 A  Y  Q  S  F  E  Q  V  V  N  E  L  F  R  D  G  V  N  W  G
cgtatcgttgctttcttctcctttggtggtgcgctgtgcgttgaatctgtggacaaagaa
 R  I  V  A  F  F  S  F  G  G  A  L  C  V  E  S  V  D  K  E
atgcaggttctggtatcccgtatcgcatcctgcatggcgacttacctgaacgatcatctg
 M  Q  V  L  V  S  R  I  A  S  C  M  A  T  Y  L  N  D  H  L
gaaccgtggattcaggagaacggtggttgggataccttcgtagagctgtatggcaacaac
 E  P  W  I  Q  E  N  G  G  W  D  T  F  V  E  L  Y  G  N  N
gcagcggcacaaagtcgtaaaggccaggaacgtctggaacaccacctccatcaccatctc
 A  A  A  Q  S  R  K  G  Q  E  R  L  E  H  H  L  H  H  H  L
gagcactaccaccaccaccactgacatccggctgctaacaaagtccgaaaggaagcttga
 E  H  Y  H  H  H  H  -  H  P  A  A  N  K  V  R  K  E  A  -
gttggctgctgccaccgctgagcataactagcataatcccttggggcctctaccgggtcc
 V  G  C  C  H  R  -  A  -  L  A  -  S  L  G  A  S  T  G  S
tgaggggcttttgctgaaccgaacaactatctcccgattgtcgaatgggacgcaccctgt
 -  G  A  F  A  E  P  N  N  Y  L  P  I  V  E  W  D  A  P  C
accagcgcattaaacgccgcgggtgtggtggtacccgcagcgtgaccgctatcttgcccg
 T  S  A  L  N  A  A  G  V  V  V  P  A  A  -  P  L  S  C  P
cgccccagcgcccgctcctttcccttttctcccctttcctttctcgccct
 R  P  S  A  R  S  F  P  F  L  P  F  L  S  R  P
```

Appendix H: *Nucleotide and amino acid sequence of truncated Bcl-x_L-S2C.*

```
ctcgagaaatcataaaaaatttatttgctttgtgagcggataacaattataatagattca
 L  E  K  S  -  K  I  Y  L  L  C  E  R  I  T  I  I  I  D  S
attgtgagcggataacaatttcacacagaattcattaaagaggagaaattaacc**atg**ggt
 I  V  S  G  -  Q  F  H  T  E  F  I  K  E  E  K  L  T  **M**  G
aacagagcattcaaatcacatcacggtcacttttaagcgctgaaggcgaagctgtaaag
 N  R  A  F  K  S  H  H  G  H  F  L  S  A  E  G  E  A  V  K
actcaccacggtcatcatgatcatcacacccatttccacgttgaaaaccatggtggtaaa
 T  H  H  G  H  H  D  H  H  T  H  F  H  V  E  N  H  G  G  K
gttgcattaaagacccattccggtaaataccttttcaattggtgatcataaacaagtttac
 V  A  L  K  T  H  S  G  K  Y  L  S  I  G  D  H  K  Q  V  Y
ctctcacaccacttacacggtgaccactcactcttccacttagaacatcatggcggtaaa
 L  S  H  H  L  H  G  D  H  S  L  F  H  L  E  H  H  G  G  K
gtctcaatcaaaggtcatcaccaccactacatttccgctgatcatcatggtcatgtttca
 V  S  I  K  G  H  H  H  H  Y  I  S  A  D  H  H  G  H  V  S
accaaagaacaccacgatcacgacaccacctttgaagaaattattattggttccgcggca
 T  K  E  H  H  D  H  D  T  T  F  E  E  I  I  I  G  S  A  A
tctggtctggtgccacgcggatccgaatttcttgctactacacttgaacgtattgagaag
 S  G  L  V  P  R  G  S  E  F  L  A  T  T  L  E  R  I  E  K
aactttattattactgacccacgtttgccagataatcccattatcttcgcgtccgatagt
 N  F  I  I  T  D  P  R  L  P  D  N  P  I  I  F  A  S  D  S
ttcttgcagttgacagaatattcgcgagaagaaattctgggtcgtaactgccgttttctt
 F  L  Q  L  T  E  Y  S  R  E  E  I  L  G  R  N  C  R  F  L
caaggtcctgaaaccgatcgcgcgacagtgcgcaaaattcgtgatgccatcgataaccaa
 Q  G  P  E  T  D  R  A  T  V  R  K  I  R  D  A  I  D  N  Q
acagaggtcactgtacagctgattaattatacaaagagtggtaaaaagttctggaacctc
 T  E  V  T  V  Q  L  I  N  Y  T  K  S  G  K  K  F  W  N  L
tttcacttgcagcctatgcgtgatcagaagggtgatgtccagtactttattggtgtccag
 F  H  L  Q  P  M  R  D  Q  K  G  D  V  Q  Y  F  I  G  V  Q
ttggatggtaccgaacatgtccgtgattgcgccgag**gat**attggtgtcaacatcgcgcgt
 L  D  G  T  E  H  V  R  D  C  A  E  **D**  I  G  V  N  I  A  R
catctggcacaggtgggtgatagcattgatcgtagcattccagatgctaatctgcgtcca
 H  L  A  Q  V  G  D  S  I  D  R  S  I  P  D  A  N  L  R  P
gaggatttgtgggctaactaagcttaattagctgag
 E  D  L  W  A  N  -  A  -  L  A  E
```

Appendix I: *Nucleotide and amino acid sequence of Hisact-AsLOV-Bid1.*

```
agcggatcgatttcttgctactacacttgaacgtattgagaagaactttattattactgac
  A  D  R  F  L  A  T  T  L  E  R  I  E  K  N  F  I  I  T  D
ccacgtttgccagataatcccattatcttcgcgtccgatagtttcttgcagttgacagaa
  P  R  L  P  D  N  P  I  I  F  A  S  D  S  F  L  Q  L  T  E
tattcgcgagaagaaattctgggtcgtaactgccgttttcttcaaggtcctgaaaccgat
  Y  S  R  E  E  I  L  G  R  N  C  R  F  L  Q  G  P  E  T  D
cgcgcgacagtgcgcaaaattcgtgatgccatcgataaccaaacagaggtcactgtacag
  R  A  T  V  R  K  I  R  D  A  I  D  N  Q  T  E  V  T  V  Q
ctgattaattatacaaagagtggtaaaaagttctggaacctctttcacttgcagcctatg
  L  I  N  Y  T  K  S  G  K  K  F  W  N  L  F  H  L  Q  P  M
cgtgatcagaagggtgatgtccagtactttattggtgtccagttggatggtaccgaacat
  R  D  Q  K  G  D  V  Q  Y  F  I  G  V  Q  L  D  G  T  E  H
gtccgtgattgcgccgaggatattggtgtcaacatcgcgcgtcatctggcacaggtgggt
  V  R  D  C  A  E  D  I  G  V  N  I  A  R  H  L  A  Q  V  G
gatagcattgatagccgtatttgctaagctaatctgcgtccagaggatttgtgggctaac
  D  S  I  D  S  R  I  **C**  -  A  N  L  R  P  E  D  L  W  A  N
```

Appendix J: *Nucleotide and amino acid sequence of Hisact-AsLOV-Bid-cys.*

```
cctaacttaaccgctcattccctctagaataattttgtttaactttaagaaggagatatacc
   -  L  N  R  S  F  P  L  E  -  F  C  L  T  L  R  R  R  Y  T
atgggcagcagccatcatcatcatcacagcagcggcctggtgccgcgcggcagccat
 M  G  S  S  H  H  H  H  H  H  S  S  G  L  V  P  R  G  S  H
atgtttcttgctactacacttgaacgtattgagaagaactttattattactgacccacgt
 M  F  L  A  T  T  L  E  R  I  E  K  N  F  I  I  T  D  P  R
ttgccagataatcccattatcttcgcgtccgatagtttcttgcagttgacagaatattcg
 L  P  D  N  P  I  I  F  A  S  D  S  F  L  Q  L  T  E  Y  S
cgagaagaaattctgggtcgtaactgccgttttcttcaaggtcctgaaaccgatcgcgcg
 R  E  E  I  L  G  R  N  C  R  F  L  Q  G  P  E  T  D  R  A
acagtgcgcaaaattcgtgatgccatcgataaccaaacagaggtcactgtacagctgatt
 T  V  R  K  I  R  D  A  I  D  N  Q  T  E  V  T  V  Q  L  I
aattatacaaagagtggtaaaaagttctggaacctctttcacttgcagcctatgcgtgat
 N  Y  T  K  S  G  K  K  F  W  N  L  F  H  L  Q  P  M  R  D
cagaagggtgatgtccagtactttattggtgtccagttggatggtaccgaacatgtccgt
 Q  K  G  D  V  Q  Y  F  I  G  V  Q  L  D  G  T  E  H  V  R
gattgcgccgag gat attggtgtcaacatcgcgcgtcatctggcacaggtgggtgatagc
 D  C  A  E  D  I  G  V  N  I  A  R  H  L  A  Q  V  G  D  S
attgatcgtagcattccagatgctaatctgcgtccagaggatttgtgggctaactaagct
 I  D  R  S  I  P  D  A  N  L  R  P  E  D  L  W  A  N  -  A
taaggatccgaattcgagctccgtcgacaagcttgcggccgcactcgagcaccaccacca
 -  G  S  E  F  E  L  R  R  Q  A  C  G  R  T  R  A  P  P  P
ccaccactgagatccggctgctaacaaagcccgaaaggaagctga
 P  P  L  R  S  G  C  -  Q  S  P  K  G  S  -
```

Appendix K: *Nucleotide and amino acid sequence of pET-21a- AsLOV-Bid1.*

```
tagaaataattttgtttaactttaagaaggagatatacc atg gcagcagccatcatcat
 -  K  -  F  C  L  T  L  R  R  R  Y  T  M  G  S  S  H  H  H
catcatcacagcagcggcctggtgccgcgcggcagccatatgtttcttgctactacactt
 H  H  H  S  S  G  L  V  P  R  G  S  H  M  F  L  A  T  T  L
gaacgtattgagaagaactttattattactgacccacgtttgccagataatcccattatc
 E  R  I  E  K  N  F  I  I  T  D  P  R  L  P  D  N  P  I  I
ttcgcgtccgatagtttcttgcagttgacagaatattcgcgagaagaaattctgggtcgt
 F  A  S  D  S  F  L  Q  L  T  E  Y  S  R  E  E  I  L  G  R
aactgccgttttcttcaaggtcctgaaaccgatcgcgcgacagtgcgcaaaattcgtgat
 N  C  R  F  L  Q  G  P  E  T  D  R  A  T  V  R  K  I  R  D
gccatcgataaccaaacagaggtcactgtacagctgattaattatacaaagagtggtaaa
 A  I  D  N  Q  T  E  V  T  V  Q  L  I  N  Y  T  K  S  G  K
aagttctggaacctctttcacttgcagcctatgcgtgatcagaagggtgatgtccagtac
 K  F  W  N  L  F  H  L  Q  P  M  R  D  Q  K  G  D  V  Q  Y
tttattggtgtccagttggatggtaccgaacatgtccgtgatgcggccgagcgtgagggt
 F  I  G  V  Q  L  D  G  T  E  H  V  R  D  A  A  E  R  E  G
gtcatgctgattaag gat attgcacgtaatattgatcgtgcgctggcggaagtgggtgat
 V  M  L  I  K  D  I  A  R  N  I  D  R  A  L  A  E  V  G  D
agcattgatcgtagcatttaagcttgcggccgcactcgagcaccaccaccaccaccactg
 S  I  D  R  S  I  -  A  C  G  R  T  R  A  P  P  P  P  P  L
agatccggctgctaacaaagcccgaaaggaagctgagttggctgctgccaccgctgagca
 R  S  G  C  -  Q  S  P  K  G  S  -  V  G  C  C  H  R  -  A
```

Appendix L: *Nucleotide and amino acid sequence of pET-21a- AsLOV-Bid2.*

atgggcagcagccatcatcatcatcacagcagcggcctggtgccgcgcggcagccat
M G S S H H H H H H S S G L V P R G S H
atgtttcttgctactacacttgaacgtattgagaagaactttattattactgacccacgt
M F L A T T L E R I E K N F I I T D P R
ttgccagataatcccattatcttcgcgtccgatagtttcttgcagttgacagaatattcg
L P D N P I I F A S D S F L Q L T E Y S
cgagaagaaattctgggtcgtaactgccgttttcttcaaggtcctgaaaccgatcgcgcg
R E E I L G R N C R F L Q G P E T D R A
acagtgcgcaaaattcgtgatgccatcgataaccaaacagaggtcactgtacagctgatt
T V R K I R D A I D N Q T E V T V Q L I
aattatacaaagagtggtaaaaagttctggaacctctttcacttgcagcctatgcgtgat
N Y T K S G K K F W N L F H L Q P M R D
Cagaagggtgatgtccagtactttattggtgtccagttggatggtaccgaacatgtccgt
Q K G D V Q Y F I G V Q L D G T E H V R
gatgcggccgagcgtgagggtgtcatgctgattaagaaaactgca**gat**attattgataac
D A A E R E G V M L I K K T A **D** I I D N
gcggcacgtgaacttgcacaggtgggtgatagcattgatcgtagcatttta
A A R E L A Q V G D S I D R S I -

Appendix M: *Nucleotide and amino acid sequence of pET-21a- AsLOV-Bid3.*

atgggcagcagccatcatcatcatcacagcagcggcctggtgccgcgcggcagccat
M G S S H H H H H H S S G L V P R G S H
atgtttcttgctactacacttgaacgtattgagaagaactttattattactgacccacgt
M F L A T T L E R I E K N F I I T D P R
ttgccagataatcccattatcttcgcgtccgatagtttcttgcagttgacagaatattcg
L P D N P I I F A S D S F L Q L T E Y S
cgagaagaaattctgggtcgtaactgccgttttcttcaaggtcctgaaaccgatcgcgcg
R E E I L G R N C R F L Q G P E T D R A
acagtgcgcaaaattcgtgatgccatcgataaccaaacagaggtcactgtacagctgatt
T V R K I R D A I D N Q T E V T V Q L I
aattatacaaagagtggtaaaaagttctggaacctctttcacttgcagcctatgcgtgat
N Y T K S G K K F W N L F H L Q P M R D
Cagaagggtgatgtccagtactttattggtgtccagttggatggtaccgaacatgtccgt
Q K G D V Q Y F I G V Q L D G T E H V R
gatgcggccgagcgtgagggtgtcatgctgattaagaaaactgcagaaaatgatattgcg
D A A E R E G V M L I K K T A E N D I A
cgtaatatcgcgcgtcatctggcacaggtgggtgatagcattgatcgtagcatttaa
R N I A R H L A Q V G D S I D R S I -

Appendix N: *Nucleotide and amino acid sequence of pET-21a- AsLOV-Bid4.*